DOCTOR OF PHILOSOPHY

A molecular modelling study of electron trapping in polythylene

Meunier, Marc

Award date:
2000

Awarding institution:
Bangor University

Prifysgol Cymru · University of Wales
BANGOR

Department of Chemistry

A Molecular Modelling Study of Electron Trapping in Polyethylene

A thesis submitted to the University of Wales
in the candidature for the degree of
Philosophiae Doctor by

Marc Meunier

– July 2000 –

To My Family
and Claudia

Acknowledgements

I am very grateful to my supervisor Professor Nick Quirke for his advice, support, and guidance in writing this thesis.

I wish to thank Dr J.N. Mac Donald from the University of Wales, Bangor, A. Aslanides and P. Manuel from EDF (France) with whom I have had the chance to confer about theoretical and methodological problems. I also thank EDF for financial support.

I wish to express my gratitude to all colleagues and friends from the Computational Chemistry Group of the University of Wales, Bangor and of the Structural and Computational Chemistry Group of Imperial College, London.

Special thanks are owed to all the staff of the Chemistry Department for their continuous assistance.

I would also like to thank Claudia for her unconditional support, and all my friends whom I have met during my time in Bangor.

Last but by no means least, big thanks are owed to my family for all their support, understanding and advice throughout my studies.

Abstract

The presence of space charge in the polymeric insulation of high voltage cables is correlated with electric breakdown. There is a vast literature concerned with the experimental characterisation of space charge and with phenomenological models of space charge formation and discharge. However, a direct link between molecular properties, space charge formation and eventual breakdown has still to be established. In this thesis, a new scheme that constitutes a first step in linking microscopic defects to the formation of space charge is suggested. Although the goal is to understand the role of defects at the molecular level in electron trapping and the formation of space charge in polyethylene, at first a "model" material is considered: the wax tridecane (n-$C_{13}H_{28}$). It is clear that both physical (e.g. conformational defects) and chemical defects (e.g. broken bonds) may be present in insulating materials and may both trap electrons. In the present thesis, the focus is on the role of physical defects. The analysis suggests that by defining the defect energy in terms of the molecular electron affinity, a relationship is established between the electron trap and the molecular properties of the material. A methodology to accurately compute the electron affinity of a wide range of atoms and molecules has been developed. The electron affinity and its variation with wax molecule conformation have been calculated using Density Functional Theory. By performing molecular dynamics simulations of amorphous waxes, likely conformational defects can be identified, and by using *ab-initio* methods, the trapping energies can be estimated. Conformational defects in these waxy materials are predicted to produce shallow traps with energies below 0.3 eV, their density is estimated to be 3.1 10^{20} traps.cm^{-3}, and the residence time of electrons is such traps is of the order of a few picoseconds.

Table of Contents

List of Tables

List of Figures

List of Acronyms

BFGS - Broyden-Fletcher-Goldfarb-Shanno

CI – Configuration Interaction

CPU – Central Processing Unit

CVFF – Consistent Valence Forcefield

D – Self-diffusion constant

DFP - Davidson-Fletcher-Powell

DFT – Density Functional Theory

DIIS – Direct Inversion of the Interactive Space

DMol – DFT based program

DN – Double Numeric

EA – Electron Affinity

HDPE – High Density Polyethylene

HF – Hartree-Fock

HOMO – Highest Occupied Molecular Orbital

KT – Koopman Theorem

LCAO – Linear Combination of Atomic Orbitals

LDA – Local Density Approximation

LDPE – Low Density Polyethylene

LJ – Lennard Jones

LUMO – Lowest unoccupied molecular orbital

MC – Monte Carlo

MD – Molecular Dynamics

MRSD-CI – Multireference Single and Doubles Configuration Interaction

MSD – Mean Square Displacement

NLDA – Non-local Density Approximation

NMR – Nuclear Magnetic Resonance

NPT – constant Number of particles, constant Pressure and constant Temperature ensemble

NVE – constant Number of particles, constant Volume and constant Energy ensemble

NVT – constant Number of particles, constant Volume and constant Temperature ensemble

PBC – Periodic Boundary Conditions

PE - Polyethylene

PES – Potential Energy Surface

RHF – Restricted Hartree-Fock

RIS – Rotational Isomeric State

RMSD – Root Mean Square Deviation

SCF – Self-Consistent Field

SH – Surface Hopping

T_g – Glass transition temperature

UHF – Unrestricted Hartree-Fock

VWN – Vosko-Wilk-Nusair functional

XLPE – Cross-Linked Polyethylene

ZPE – Zero Point Energy

CHAPTER 1

BACKGROUND, AIMS, METHODOLOGY AND STRUCTURE OF THE STUDY

1.1 INTRODUCTION

Electrical suppliers have been using polymers as insulators for the past sixty-two years in their electrical networks. Amongst the first submarine insulator cables was a mile length polyethylene cable between the Isle of Wight and England laid by Dean's company in 1938.[1] Today, industrial dielectrics are still mostly polyethylene based (high density, low density, cross-linked, etc.) that present very good insulating properties such as a low electronic and ionic conductivity and a low dielectric constant (or permittivity). However, the very high resistivity gives the polyethylene insulator the propensity to trap electrons and ions. This well-known phenomenon referred to as space charge trapping has many undesired consequences. Firstly, these trapped charges create an electric field that can disturb the applied field. Secondly, their accumulation and transport inside the material leads to ageing and eventually to dielectric breakdown. Thirdly, the physical properties - electrical, mechanical, dielectric constant, thermal stability, etc. – are modified by the presence of these excess charges.

Many experimental studies have been undertaken to measure the nature and the quantity of space charge inside insulating materials, as well as the factors influencing this phenomenon. Amongst the (many) different techniques employed are the thermal step method[2], the pulsed electro-acoustic method[3], thermal pulse methods[4], pressure pulse methods[5], photoconductivity method[6], and the mirror image method[7]. All these methods have been reviewed (to 1997) by N.H Ahmed and N.N. Srivinas.[8]

From the results obtained via the different experimental methods, some models have been deduced[9-10] that aim to predict the lifetime of extruded cables or to link the structure (crystallinity, density, etc.) and the trapping property. The microstructure is not taken into account in these models (the highest resolution of the experimental methods is ~ 1μm).[11] As a result, space charge accumulation and the related trapping-detrapping phenomena are still poorly understood at the atomic level, indeed it is unclear whether any trapping site has been unequivocally identified in polymeric insulators.[12]

1.2 THE PROBLEM

Polymers suffer from both chemical and physical ageing. When an electric field is applied, they also present electrical degradation. Stress factors can be numerous; they include, among others, temperature and mechanical force. Moreover, water, oxygen and by-products due to manufacturing processes induce polymeric degradation. All these factors, combined together for various periods of time, make life prediction of extruded cable very difficult.[13]

1.2.1 Physical ageing

Physical ageing or structural relaxation is caused by the rearrangements of the polymer chains at temperatures above the glass transition (Tg). This rearrangement occurs because the material experiences a secondary crystallisation at temperatures above Tg, a process which goes on for several years. This induces a reduction of the free volume and therefore an increase of the local density. Microvoids and discontinuities are associated with this local increase in the density. Also, more crystalline-amorphous interfaces are created. All those factors are thought to enhance the propensity of the dielectric material for electrical degradation or space charge trapping.

1.2.2 Chemical ageing

Chemical ageing is caused by chemical changes within the dielectric material. At the molecular level, these changes are initiated essentially by low-energy electrons, which dissociate molecules of the dielectric or other impurity molecules. The released fragments can then react with surrounding atoms or molecules. In polymers such as polyethylene, this will lead to both chain scission and cross-linking. In polymers containing side-groups, this will also lead to their release. Water has a particular role in polymeric degradation, as it induces water treeing. Water trees are water-filled cavities connected by microchannels through which moisture is transmitted. These structures can easily be seen under the microscope in polyethylene.

1.2.3 Electrical ageing

When a solid dielectric sheet is subjected to an electrical field, a charge will accumulate on the surface of the layer adjacent to the electrode and additional charge will be injected into the bulk of the dielectric. The penetration depth of the charge carriers and the number of deep traps filled will increase with the application time of the electrical field and its magnitude. The charge carriers interacting with the dielectric material might, in turn, induce both thermal and higher energy chemical reactions such as ionisation. They will induce the formation of electrical trees and generate partial discharge, both phenomena, which are among the most effective agents of polymeric degradation. Treeing is an electrical pre-breakdown phenomenon. It originates from a type of damage (i.e. partial discharge) which progresses through a dielectric section under electrical stress and which path has the shape of a tree.[14] Notably, it is the field enhancement produced by the accumulation of space charge that is the important feature of electrical ageing, not the presence of trapped charges themselves.[15] The enhanced local electric field will accelerate the free electrons, increasing the probability of damage via impact ionisation.

1.2.4 Dielectric breakdown

The breakdown process is a destructive and irreversible phenomenon. In the common conception of the phenomenon, the dielectric breakdown of polymeric insulator is the result of the sum of the degradation factors (sections 1.2.1 to 1.2.3). However, in the laboratory, electrical breakdown can only be simulated with very high voltage, destroying the cable in minutes or even seconds, so that the term ageing becomes less relevant. Partial discharges occurring in polymeric insulators are localised electric breakdown leading to polymeric degradation. Other kinds of breakdown can occur, i.e. thermal and electromechanical breakdowns are the result of strong applied fields.

1.3 MOTIVATION

Electron trapping in polymeric insulators presents both industrial and theoretical challenges. A better understanding of space charge formation and transport could lead to the manufacture of cable having longer life expectancy. Space charge accumulation and the related trapping-detrapping phenomena are still poorly understood. Indeed, it is unclear whether any trapping site has been unequivocally identified in polymeric insulators.[12]

1.3.1 Industrial

All around the world, electrical supplier companies are using polymers as insulators for high-voltage electric cables. These cables, due to their intrinsic properties, can trap charge carriers, and the accumulation of these space charges leads to the ageing (degradation) of the polymer. Also, these trapped charges create local electric fields that disturb the normal condition of use of the cable. This might eventually leads to dielectric breakdown. In addition, the central problem for the development of DC cables is to determine how to prevent space charge formation in the insulation material. It is

therefore a crucial issue to understand the space charge formation in polymeric insulator.

1.3.2 Theoretical

Polymers such as polyethylene are used as insulators, due to their excellent mechanical and electrical properties. Polyethylene has a large band gap, hence no excess charge carriers should be trapped in this material. The trapping-detrapping phenomenon and its role in the ageing of polymeric insulators is still poorly understood. The degree of charge localisation inside the insulator material is still a matter of debate. The nature, extent and depth of the traps are also unknown quantities. It is known that physical and chemical traps exist. Physical defects or topological defects are thought to be the result of density variation, broken chains, entanglement regions, and crystalline-amorphous interfaces. Chemical defects originate from the various additives included in the material when manufacturing the cable and from the impurities such as water, oxygen, etc.

The problem of space charge trapping in dielectric materials has a long history in engineering science.[16] The physics of the problem can easily be described by the use of band structure theory, the concept of electron localisation, etc. In this thesis, it is the chemistry of the problem that is of interest: understanding the molecular nature of what constitutes a trap, using a 'chemical' property such as the electron affinity to comprehend the interactions between the excess charge and the material, and how this is related to the molecular conformation of the polyethylene.

1.4 AIMS

In the present work, molecular modelling methods are applied to elucidate the origin of shallow traps in polyethylene insulators; in particular those localised states (*c.f.* Mott[17]) that arise from conformational (or topological) disorder in amorphous regions of the

polymer. The behaviour of free electron moving in a condensed phase has been studied in the 70's by authors such as Mott for the semiconductors. The first aim of this study has been a deeper understanding of the problem of the trapping of an excess charge in a dielectric medium. The propensity of atoms or molecules to attach an extra electron is called the electron affinity. Therefore, the first goal has been to demonstrate the ability of molecular modelling tools, and in particular the density functional theory, to compute accurately electron affinities. The second aim was to confirm the hypothesis that conformational defects could trap electrons. Molecular dynamics simulations were used to generate model conformations, and then *ab initio* calculations were performed to evaluate the trap depth. The resulting positive trap energies (section 6.3.1) confirmed this hypothesis.

1.5 HYPOTHESES

In this section, the main hypotheses employed in this thesis are outlined. Each of them will be fully explained in the chapter in which they appear.

1.5.1 Structure of polymers

The physical and chemical structure of polymers, and more specifically the physical, chemical, and electronic structure of polyethylene are described.

1.5.1.1 Physical and chemical structure

Different polymerisation mechanisms exist to synthesise macromolecular compounds. Commercial polyethylene is usually initiated via radical polymerisation. It is the most commonly used insulating material for high-voltage electric wires. Depending on the properties desired, the manufacturing process, and of the addition of cross-linking agents, the density and crystallinity of the polyethylene (PE) can vary. This leads to the

presence of chemical residues inside the material. In addition, polymers have a chain length and molecular weight distribution.

The polyethylene has one of the simplest polymeric chemical structures. Its repeat unit, or monomer, is $-(CH_2-CH_2)-$, and the polymer is simply an assembly of n (the degree of polymerisation, usually as large as 10^5) ethylene molecules. PE can be linear (HDPE), branched (LDPE) or crosslinked (XLPE). PE is referred to as semi-crystalline: it presents two different phases simultaneously, amorphous and crystalline. Crystallinity develops as a spherical or spherulitic growth, which completely fill the volume of a crystallised polymer sample. Those spherulites are composed of many lamellas, ribbon-shaped regions where the polymeric chains fold back and forth on themselves. Due to their length, the chains go from one lamella to another, crossing amorphous regions and forming intercrystalline links.[18]

At zero Kelvin, the molecules will, if possible, adopt the lowest potential energy conformation. In vacuum, for a (short[19]) linear alkane, this global energy minimum conformation corresponds to the all-trans planar conformation. However, in a condensed phase, the potential energy surface of the molecule will be changed by interactions with its neighbours leading to a change in the conformation of minimum energy. In addition, as the chain length increases, the (favourable) interactions between the monomers will force the polymer to adopt a hairpin conformation (Figure 7.2). The cost of successive gauche defects is overcome by those favourable non-bonded interactions.[19]

1.5.1.2 Electronic structure

Energy band theory is now commonly used to describe the electronic properties of covalent and ionic crystals. It is possible, with some modifications, to apply this theory to macromolecules, and to polymers in particular. A band structure appears when isolated atoms brought together have overlapping orbitals (wave function). This is due to the lifting of the degeneracy of the orbital energy. When a large number of atoms are

brought together, the difference in energy between two consecutive energy levels becomes very small, so that the sum of all the energy levels can be see as a continuum of states in which the electrons are free to move.

Macromolecules contain a lot of irregularities (non-periodic sequences): chains have different lengths (various degree of polymerisation) in amorphous phases and chain folds in crystal phases. Also, in the case of industrially used PE, additives and impurities cause irregularities. All those defects contribute to ill-defined band edges. The band gap contains, indeed, many localised states. Charge carriers entering such states will be trapped for a time, depending on the nature and the depth of the trap.

1.5.2 Waxes used as a model of PE

A chain of polyethylene is made of a very large number of atoms (typically ~10^5). Therefore, the simulation (either by molecular dynamics or by quantum mechanics) of a complete chain, is computationally too expensive. Periodicity in an all-trans configuration can be used to enable calculations to be performed (e.g. of energy, of orbital levels) but this is not the case when one has to deal with amorphous (or simply non-periodic) chains. In such cases, a smaller molecule can be used as a model. Experimentalists commonly use waxes to model the physical or chemical properties of polyethylene; the most frequently used being the hexatriacontane wax (n-$C_{36}H_{74}$).

In order to probe the contribution of conformational disorder to electron trapping in polyethylene using molecular modelling, we consider instead the condensed phases of much smaller alkane molecules which for $n \geq 13$, where n is the number of carbon atoms, have a band structure very similar to polyethylene.[20-21] The local conformational disorder of segments of polyethylene in the amorphous regions is represented by configurations taken from computer generated glassy phases of the tridecane (n=13) wax. The present strategy is to identify the local *electron* traps in PE with the increase in the electron affinity of the more distorted C_{13} molecules, *conformationally* trapped in the glass.

1.5.3 Link between electron affinity and traps

For a solid, the electron affinity is the energy released when an electron is placed at the bottom of the conduction band from the vacuum level. In the case of molecules, the electron affinity represents the energy released when an electron is attached to the neutral parent. (Note: The definition of the electron affinity is given in chapter 3). The electron affinity of a defect is the energy required to bring the electron from the vacuum level into the defect level. Subsequently, the trap energy (E_t) is the difference between the EA of the system with and without the defect. A positive E_t signifies a potential trap for the electron, since in that case the material has a greater affinity for the electron than the 'pure' material. The depth of the traps is a function of the thermal agitation of ions around their mean position, random orientation of dipoles and molecular structure irregularities. This leads to a distribution of trap depths and, therefore, to a distribution of the residence times of the charges carrier in the traps.

Chemical defects, or impurities, can have a strong electron affinity, in which case an attached electron has a very low probability of escaping such a trap. In the case of polyethylene, physical defects have lower electron affinity. These defects have various origins: regions of space containing dipoles, free volume, crystalline-amorphous interfaces. In addition, the trapping of electrons in a specific region may lead to a polarisation of the space, rending the trapping of subsequent charges easier. In the same way, a trapped charge will induce a local deformation of the material surrounding it, increasing the local dipole moment and therefore increasing the depth of the well. This latter effect is known as self-trapping. When the charge is moving inside the material, this deformation 'follows' the charge. Such effect is known as *polaron*.

1.6 PLAN

Chapter 2 presents the different molecular modelling tools used in the present study. *Ab initio* methods are reviewed with the emphasis on the Density Functional Theory (DFT). Molecular mechanics, and in particular molecular dynamics, is also described. After recalling the theoretical background of each methodology and giving a few examples of applications, each code is described in detail.

Chapter 3 considers the definition of the electron affinity, and also presents the results obtained for the computation of the electron affinity of a wide variety of atoms and molecules using quantum mechanics tools. A comparison with experimental results found in the literature is given. Good agreement with experimental data is obtained. This validation allows us to estimate electron affinities of compounds for which only scarce experimental data were found: The alkane molecules of special interest in the present study.

Chapter 4 recalls the definition and properties of the glass phase. The methodology used to compute them using molecular modelling tools is presented. The microscopic disorder found in polyethylene is modelled via simulations of glassy phases of alkane waxes. The results obtained for the simulation of glassy phases of waxes using classical molecular dynamics are detailed and analysed. It is assumed that the microscopic disorder present in the amorphous phase of the polyethylene can be modelled via simulation of glassy phases of the tridecane wax.

Chapter 5 introduces the variation of the electron affinity with the molecular conformation. Firstly, results concerning the propane and ethane molecules are given followed by longer chain alkanes: The tridecane molecule. Using the Mulliken and Walsh model, the variation of the energy level of the frontier orbitals (HOMO and LUMO) with the molecular conformation are analysed.

Chapter 6 recalls the property and behaviour of an electron in an amorphous solid. The two-potential well model is given followed by the distribution and the trap depth obtained via simulation runs. The main result of the study, the electron trap distribution is given in this chapter.

Chapter 7 discusses the various approximations (models) employed during this study and recalls the main results obtained. In addition, the limitations due to these approximations are elucidated. The role of defects both physical or chemical is discussed.

Chapter 8 is the conclusion. It summarises the entire work performed in this thesis, and puts the emphasis on the key achievements. A discussion of the need for future work is included, as well as the uses of the work at industrial level.

1.7 REFERENCES

[1] J.A. Allen. *Studies in innovation in the steel and chemical industries.* (Manchester University Press, 1967).

[2] A. Toureille. Revue générale d'électricité **8**, 15 (1991).

[3] Y. Li, T. Takada, N. Takasu. J. Phys. D **26**, 986 (1993).

[4] R.E. Collins. Practical application of the thermal pulsing technique to the study of electrets. J. Appl. Phys. **51**, 2973 (1980).

[5] J. Lewiner. Evolution of experimental techniques for the study of the electrical properties of insulating materials. IEEE Transactions on Electrical Insulation **21**, 351 (1986).

[6] A. Dias Tavares. New method for the determination of space charge in dielectric. J. Chem. Phys. **59**, 2154 (1973).

[7] C. Le Gressus, F. Valin, M. Henriot, M. Gautier, J-P. Duraud, T.S. Sudarshan, R.G. Bommakandi, G. Blaise. J. Appl. Phys. **69**, 6325 (1991).

[8] N.H. Ahmed, N.N. Srivinas. Review of space charge measurements in dielectrics. IEEE Transactions on Dielectrics and Electrical Insulation **4**, 644 (1997).

[9] G. Blaise. J.Appl. Phys. **77**, 7 (1995).

[10] L.A. Dissado, G. Mazzanti, G.C. Montanari. The role of space charges in the electrical ageing of insulating materials. IEEE Transactions on Dielectrics and Electrical Insulation **4**, 496 (1997).

[11] G.M. Sessler, and G.M. Yang. Abstracts CSC'3 Electric charge in solid insulators, 38 (1998).

[12] H. J. Wintle. Abstracts CSC'3 Electric charge in solid insulators, 49 (1998).

[13] L. Sanche. Nanoscopic aspects of electronic ageing in dielectric. IEEE Transactions on Dielectrics and Electrical Insulation **4**, 507 (1997).

[14] R.M. Eichhorn. I.E.E.E. Transactions on Dielectrics and Electrical Insulation, **EI-12**, 2 (1977).

[15] G. Blaise, and G. Moya. Abstracts CSC'3 Electric charge in solid insulators, 160 (1998).

[16] F.W. Peek. *Dielectric phenomena in high-voltage engineering.* (McGraw Hill, 1920).

[17] N.F. Mott. Phil. Mag. **22**, 7 (1970).

[18] LA. Dissado, JC. Fothergill. *Electrical degradation and breakdown in polymers.* (Peter Peregrinus Ltd., London, 1992).

[19] G.M. Goodman. *Chemical Applications of Molecular Modelling.* (RSC, 1998).

[20] C. Laurent, C. Mayoux. Electronic Processes in Electrical Ageing. Abstracts Arpeggio Seminar, (1994).

[21] J.J. Pireaux. Phys. Rev. A **14**, 2133 (1976).

CHAPTER 2

MOLECULAR MODELLING

2.1 INTRODUCTION

The purpose of this chapter is to give an overview of molecular modelling and some of its applications. In particular, the definition of the potential energy surface and the Born-Oppenheimer approximation are given in section 2.1.2. Section 2.2 describes the conformational analysis methods, including the geometry optimisation procedure (or energy minimisation) and the various algorithms employed. Section 2.3 explores the potential functions (or forcefields) used to describe molecular interactions, as well as the different terms composing those forcefields. Molecular dynamics is described in section 2.4. Section 2.5 recalls the basic notions of quantum mechanics employed to perform *ab initio* calculations, as well as the description of the Hartree-Fock method. Finally, section 2.6 gives the full mathematical description of the density functional theory. Section 2.7 is the conclusion.

2.1.1 Overview of molecular modelling

The first drawing of chemical structures were carried out in the second half of the nineteenth century. Those early models of molecules were initially employed by organic chemists such as A.W. Hoffmann in 1865. The concept of a forcefield (a mathematical function used to described intramolecular and intermolecular interactions) appeared in the first half of the twentieth century.[1] The first forcefield was given by Hill in 1946 and

already contained a Lennard-Jones[2] 6-12 potential (see Eq.2.21) for non-bonded interactions.

The first computer simulations date back to the middle of the twentieth century. The (classical) Monte-Carlo method was amongst the very first methods employed. Arguably, a proper formulation of quantum mechanics can be dated from the Schrödinger's equation (1926). The very first widely used *ab initio* based program was the *POLYATOM* program developed at MIT[3], in which Gaussian functions were already used to form the basis set. These mathematical functions which were employed almost a decade before the first computer program[4] made its appearance are still often used as they are quick to compute. Most modern *ab initio* methods are based on the theoretical framework developed by Roothan[5] to solve Hartree-Fock Self-Consistent Field (SCF) equations. Early applications on large systems were performed by Moskowitz et al.[3] and showed that the electronic structure of polyatomic systems could be obtained quantitatively and accurately using *ab initio* methods. In the middle of the sixties, Huzinaga[6] published the first basis set with the coefficients being optimised for the first row atoms of the periodic table. Since then, many tables of optimised exponents can be found in the literature for a large range of atoms and molecules. Computer hardware and molecular modelling software have become better developed and more widely available since the seventies, and therefore molecular simulation has been transformed from an academic subject with a restricted number of users to a practical tool for modern industrial applications. Pharmaceutical companies were amongst the first in industry to foresee the use of molecular modelling for the development of new molecules of specific chemical and physical properties (in particular *drug design*). In general, simulations are cheaper and faster than experiments (e.g. fluids and simple molecules[7], drug design[8], etc.). In the late sixties, a new method, namely the Density Functional Theory (DFT), emerged as a powerful tool to study crystals using plane-waves as basis functions. Its applications have quickly increased to any systems (periodic or aperiodic, organic or inorganic). The DFT is particularly suited to the study of large systems (up to a few hundreds atoms), since the calculation scales only as the cube of the number of basis functions (which is proportional to the number of electrons), compared with a scale to the fifth or seventh power for accurate Hartree-Fock based method.

A general description of the theories and applications of molecular modelling can be found in references 9, 12, 13 and references therein. An exhaustive review of articles, books as well as the information available on the *World Wide Web* regarding molecular mechanics can be found in reference 10. *Ab initio* methods are extensively detailed in reference 11. A number of examples of industrial applications of molecular modelling tools can be found in references 12 and 13.

2.1.2 The potential energy surface

The Born-Oppenheimer[14] approximation stipulates that, as the electrons are moving very much faster than the nuclei, their movements can be considered independently of the movement of the nuclei. This is a very reasonable approximation because the mass of a proton (for the lightest nucleus) is around 2,000 times greater than the electron mass. Such an approximation is of considerable importance when using quantum mechanics as it allows the modeller to separate the nuclear from the electronic wavefunction. The electrons will adjust their position *instantly* to any change in the nuclear positions. Subsequently, the energy of the ground state of a molecule can be considered as function of the nuclear coordinates only.

The changes in nuclear positions, leading to changes in energy, are described by a many-dimensional surface called a Potential Energy Surface (PES). For a system with N atoms, the energy is a function of 3N-6 internal coordinates (where the position of each atom is described relative to other atoms in the system) and, except for trivial cases, can not be visualised. Nevertheless, the PES of molecules is usually plotted with respect to one or two coordinates of importance. Figure 2.1 below shows the energy variation as the torsion angle varies in the case of linear alkanes.

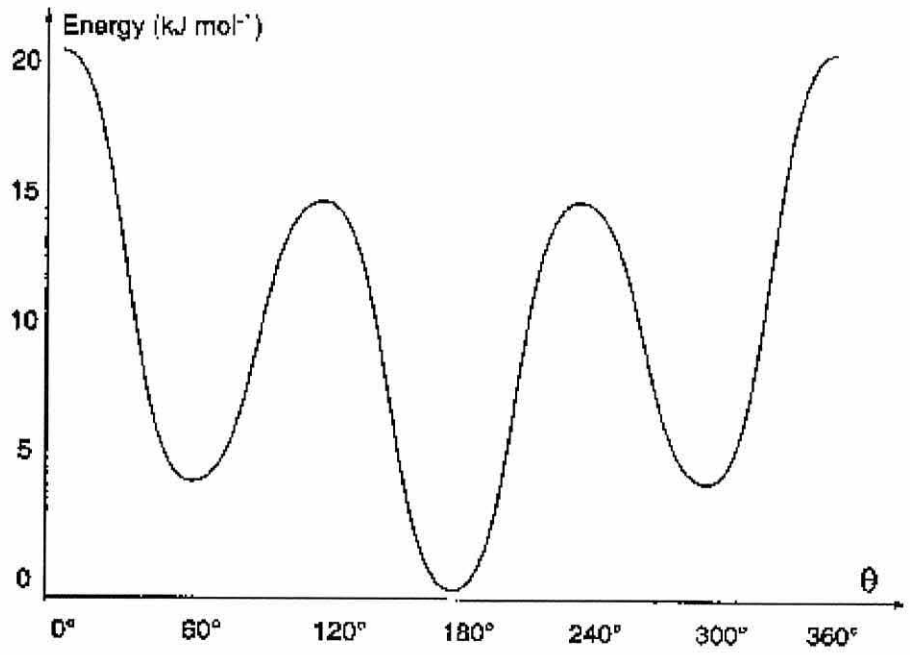

Figure 2. 1 Energy variation of unbranched alkane with –C-C-C-C- torsion angle variation. The energy minimum is found for a torsional angle of or 180°, although the penalty for twisting through 120° to 160° or 300° is small. This shows that linear unbranched alkane should adopt an all-trans planar conformation (θ = 180°).[8]

The saddle points on the energy surface, minima and maxima are of primary importance. The global energy minimum found on the surface represents the ground state of the molecule. Local minima can be found on PES, and a typical example is the chair and boat conformations of the cyclohexane molecule. Transition states are found at the maximum value on the PES, and the energy of the barrier height is related to the free energy.

The global minimum of the PES is one of the most significant points in molecular modelling, as this particular point on the PES represents the ground state of the system studied. In addition, the shape of the surface can give valuable information (such as the energy gradient) and section 2.2 describes in detail conformational analysis and minimisation techniques (e.g. molecular dynamics, simulated annealing, Monte Carlo).

2.2 CONFORMATION SEARCHING AND MINIMISATION

Conformation searching corresponds to the exploration of the potential energy surface of the system of study. In molecular modelling, the point of greatest interest is usually the global minimum. Finding this point on the hypersurface is not trivial, and numerical minimisation methods must be employed. There is a vast literature concerning this problem and typical examples are protein or polymer folding, crystal structures.

2.2.1 Conformational analysis

Conformation searching is one of the most common tasks in molecular modelling. When looking for the global minimum on the PES, different methods are available[9] (see below) but none of them gives absolute confidence that the conformation of lowest energy is found (except in trivial cases).[10] In addition, molecules are not well described by a single low energy conformation: it is a fact that molecules *exist* in different conformations, and many chemical reactions are conformation-dependent. The ratio between the different conformers can be calculated using Boltzmann factors:

$$\text{Boltzmann factor} = \exp(-E_0 / RT) \qquad (2.1)$$

where E_0 represents the energy of the conformer (relative to the zero vibrational energy level), R the gas constant, 8.314 $JK^{-1}mol^{-1}$, and T the temperature, in Kelvin. Boltzmann factors give the relative probability of finding each conformer at a given temperature. Amongst the most common methods employed to perform conformational analysis are the systematic search, molecular dynamics (described in section 2.4) and the Monte-Carlo search. Genetic algorithms and rule-based methods can also be employed. Systematic search is probably the most reliable method to identify the global energy minimum, but at a very high computational cost. This method can not be employed on large systems, but is routinely employed either for small molecules or to scan the PES of larger system with respect to one single molecular coordinate. The simulated

annealing[15] technique can also be employed with the purpose of finding the global energy minimum. In this procedure, the energy of the system is gradually removed. In chapter 4, simulated annealing combined with molecular dynamics will be used.

2.2.2 Minimisation

Energy minimisation consists of exploring the potential energy surface until the global minimum is found. This procedure is also known as geometry optimisation. Because of the complexity of the PES, finding the energy minimum can be too long or even impossible. Thus, it will be necessary to use simplifications in the minimisation algorithm. Specifically, numerical methods will be employed, that gradually vary the molecular coordinates until a minimum is found and no lower minimum can be obtained. Minimisation methods are divided into two main categories: non-derivative and derivative methods.

By definition, non-derivative methods do not require the computation of the energy derivative (i.e. the slope of the PES). These methods are usually quite easy to program but are rather less efficient than derivative methods. The most common non-derivative methods are the simplex method and the sequential univariate method. For more details see reference 22.

2.2.2.1 Derivative methods

Derivative methods compute the first, and in some cases the second derivative of the energy with respect to the coordinates. The first derivative of the energy is called the gradient. It gives information about the direction to follow in order to find the minimum energy. The magnitude of the gradient gives the steepness of the local slope. A saddle point is found when this gradient is zero. The second derivative tells us when an extremum (usually a minimum) is located, that is when $\partial E/\partial x = 0$.

2.2.2.2.1 *Steepest descent and line search algorithm*

In the steepest descent methd[16], the direction to follow is the one of the steepest slope and this is done by computing the gradient of the slope. A line searching method is used to locate the minimum on this line. Then, the gradient is again computed at this new minimum, and the procedure is repeated until a (global) minimum is found.

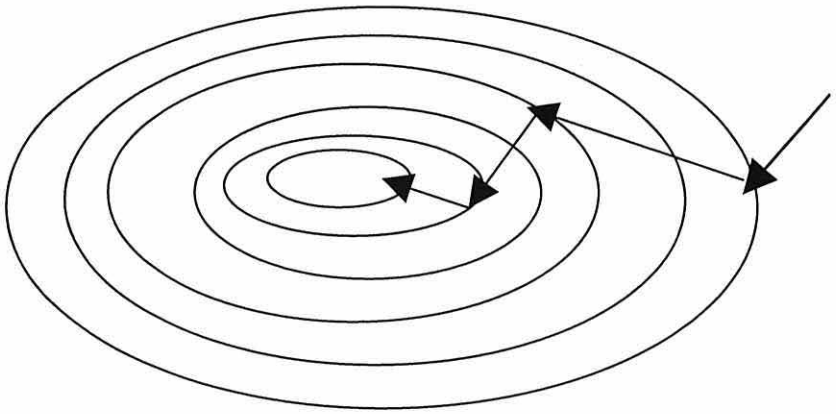

Figure 2.2 Two-dimensional minimisation using the steepest descent method. The direction to follow is the one of the steepest slope, but the best path to the minimum is constantly overshot, resulting in an inefficient, oscillating trajectory.

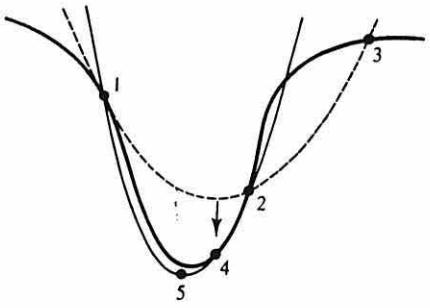

Figure 2.3 Line search method. The minimum in a line search may be found by fitting an analytical function such as a quadratic function to the initial set of three points (1, 2 and 3). A better estimate of the minimum can then be found by fitting a new function to the points 1, 2 and 4 and finding its minimum.[16]

In the line search algorithm[16], the new set of coordinates (x_1, y_1) is computed using:

$$(x_1, y_1) = \left[x_0 + \alpha \frac{\partial E}{\partial x}\bigg|_{x_0, y_0}, y_0 + \alpha \frac{\partial E}{\partial x}\bigg|_{x_0, y_0} \right] \tag{2.2}$$

The steepest descent method, followed by a line search, is ideal when starting far from the equilibrium geometry, as it is robust. The problem with this procedure is that it can be very time-consuming. In addition, convergence might be difficult to achieve in a long narrow valley. In the present work this method has always be employed as the first step (in a multi-steps minimisation algorithm) of any minimisation.

2.2.2.2.2 Conjugate gradients

The conjugate gradient method is a first derivative method based on an algorithm initially proposed by Fletcher.[17] It is an improvement to the steepest descent method in the sense that the information (gradient) computed at the i^{th} step is used at the next $(i+1)^{th}$ step for faster convergence:

$$h_{(i+1)} = g_{(i+1)} + \gamma_{(i+1)} h_i \tag{2.3}$$

with

$$\gamma_{(i+1)} = (g_{(i+1)})^2 / g_i^2 \tag{2.4}$$

where h_i is the vector direction at point M_i, and g_i is the gradient at M_i (Figure 2.4):

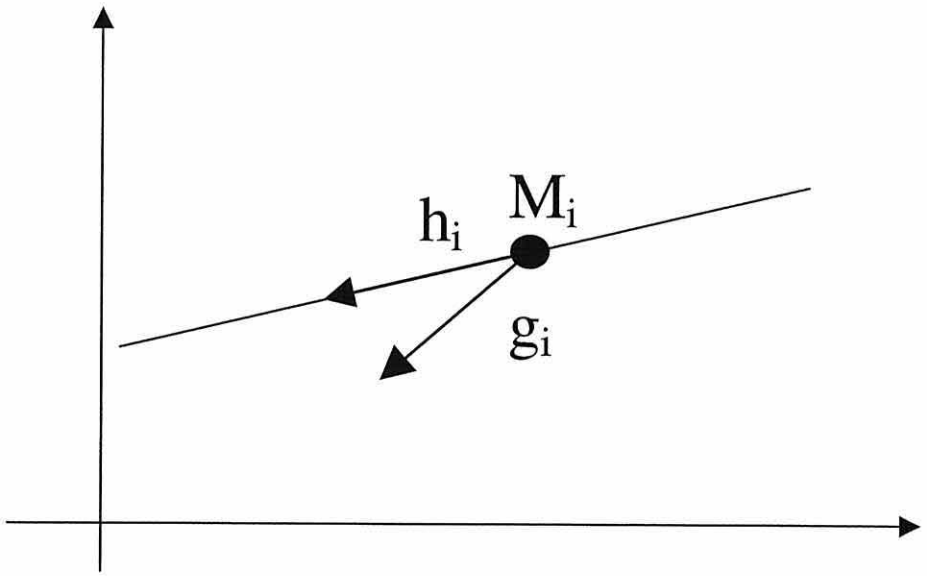

Figure 2.4 The Conjugate Gradient method. The conjugate gradient algorithm constructs and follows a set of directions that produces a complete basis set of mutually conjugate directions such that each successive step continually refines the direction toward the minimum.[18]

The gradient of the previous step has to be stored in order to compute the following step, which is memory intensive, but the conjugate gradient algorithm does not present the oscillatory behaviour of the steepest descents method in narrow valleys.[22] The Polak-Ribiere[19] method is a common variant of the Fletcher-Reeves[17] algorithm, and uses:

$$\gamma_{k+1} = \frac{(g_{k+1} - g_k).g_{k+1}}{(g_k)^2} \tag{2.5}$$

Once the gradient is computed, a line search method is performed to obtain the new set of coordinates (Eq. 2.2). The $(i+1)^{th}$ gradient is orthogonal to all previous gradients, and the new direction (h_{i+1}) is conjugate to all previous directions. A set of conjugate

directions has the property that for a quadratic function of M variables the minimum will be reached in M steps.[22]

2.2.2.2.3 *Newton-Raphson method*

The Newton-Raphson method is a second derivative method. The first and the second derivative of the energy are computed at each step. The second derivative provides information about the curvature of the surface. The minimum is located by computing the inverse of the hessian matrix (i.e. the second derivative of the energy with respect to the coordinates):

$$R_{min}=R_0-A_0^{-1}.\nabla V(R_0) \qquad (2.6)$$

where A_0^{-1} is the inverse hessian matrix and $\nabla V(R_0)$ is the gradient at R_0.
The algorithm is applied iteratively:

$$R_i=R_{i-1}-A^{-1}(R_{i-1}).\nabla V(R_0) \qquad (2.7)$$

This method is very fast, for a purely quadratic function the minimum is located in one step only. The Newton-Raphson method is not robust and is better used after the steepest descent method when starting far away from equilibrium geometry. Variants of the Newton-Raphson method exist (called Quasi-Newton methods), that aim to simplify (or partially avoid) the calculation of the inverse hessian matrix that can be computationally expensive. The inverse hessian matrix can be computed gradually, and only the gradient is computed every step. The Broyden-Fletcher-Goldfarb-Shanno (BFGS) and the Davidson-Fletcher-Powell (DFP) belong to those Quasi-Newton methods. Their description can be found in reference 22.

There is no straightforward way of choosing an appropriate minimisation algorithm. As previously mentioned, robust methods (that converge even when starting far from the equilibrium geometry) should be employed first, followed by derivative methods. These

in turn can be chosen according to computational resources available. Conjugate gradients, except the Newton-Raphson method, can be used for up to thousands of atoms with actual standard workstations. The minimisation procedure stops when the absolute minimum is obtained, but this is rarely the case. Instead, convergence criteria (eg energy, gradient, maximum value of the gradient) are used, and the procedure is stopped when those criteria are met. The role of the initial conformation when performing a geometry optimisation is crucial. It is very common to end the minimisation in a local minimum, as the algorithm does not allow the overcoming of energy barrier (going uphill on the PES, instead of down). It is therefore common to perform the geometry optimisation many times, starting with different conformation. The Monte Carlo approach is the preferred method to locate the global minimum, as it does not pose this problem.

2.3 MOLECULAR MECHANICS

Molecular mechanics is an approach to modelling the behaviour of matter. Molecular mechanics calculates the internal energy by adding up the strain energy in all the chemical bonds plus all the non-bonded interactions (e.g. van Der Waals and Coulombic). Electrons are not directly involved is those calculations, and forcefields are always employed. Forcefields use many parameters to compute molecular energies (i.e equilibrium bond distances, force constant, etc.), therefore their transferability is an important issue in molecular mechanics. Forcefields can be general (in the way that they can compute reasonably well the energy of any molecules) or specific (i.e. organic, metals, etc. compounds only). Modern forcefields (so-called Class II forcefields) use parameters derived from ab-initio calculations. It is important to note that forcefields are empirical and that there is no exact analytical function to compute the energy.

The most common energy terms in a forcefield are the bond stretching, angle bending, bond rotation (torsion), electrostatic (Coulombic) and the van der Waals term. Out-of-plane terms constraining double bond substituants in a plane can be added. Hydrogen bonds are also included in some specific forcefields such as Amber.[20] Off-diagonal (or

cross) terms, that describe the coupling between stretching of adjacent bonds can also be added for a better precision but at a higher computational cost.

The simulations that will be carried out in the present research (see chapter 4) are based on the Consistent Valence Force Field (CVFF[21]). This forcefield was originally designed for amino acids (for the study of proteins) and is particularly suitable for organic systems. Figure 2.5 illustrates the CVFF terms, containing all the traditional energy terms plus some cross terms that make it more realistic. Specifically the CVFF forcefield employs a 12-6 Lennard-Jones potential for van der Waals interactions. Bond stretching is simulated via a Morse potential that has the disadvantage of allowing the bonded atoms to drift unrealistically far apart when the simulation is performed at (very) high temperature. But for the temperatures considered in this study, the bottom of the potential well is more correctly described using a Morse potential than using a quadratic potential. The CVFF forcefield is available in the code Discover[18] used in the present work.

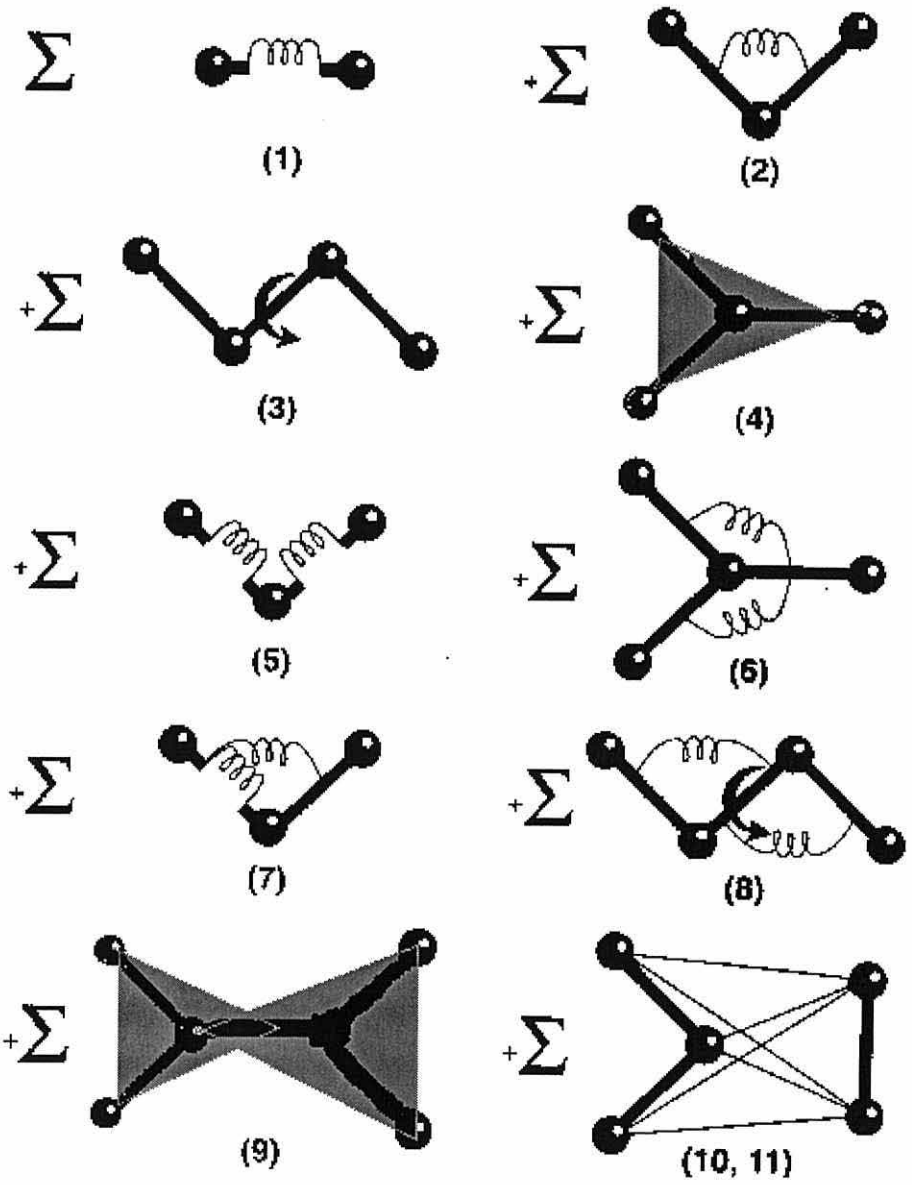

Figure 2.5 Graphic illustration of the CVFF[21] terms. Terms 1 to 4 are the diagonal terms of the forcefield and describe successively bond stretching, angle bending, torsion, and out-of-plan interactions. Terms 5 to 9 are the cross terms (see text) and represent the coupling between terms 1 to 4. Terms 10 and 11 represent the non-bonded interactions.[18]

The analytical function of the CVFF forcefield is:

$$E_{POT} = \sum_{b} D_b\left[1-e^{-\alpha(b-b_0)}\right]^2 + \sum_{\theta} H_\theta(\theta-\theta_0)^2 + \sum_{\phi} H_\phi[1+s\cos(n\phi)]$$
$$+ \sum_{\chi} H_\chi \chi^2 + \sum_{b}\sum_{b'} F_{bb'}(b-b_0)(b'-b'_0) + \sum_{\theta}\sum_{\theta'} F_{\theta\theta'}(\theta-\theta_0)(\theta'-\theta'_0)$$
$$+ \sum_{b}\sum_{\theta} F_{b\theta}(b-b_0)(\theta-\theta_0) + \sum_{\phi} F_{\phi\theta\theta'}\cos\phi(\theta-\theta_0)(\theta'-\theta'_0) + \sum_{\chi}\sum_{\chi'} F_{\chi\chi'}\chi\chi'$$
$$+ \sum \varepsilon[(r^*/r)^{12} - 2(r^*/r)^6] + \sum q_i q_j / \varepsilon r_{ij} \qquad (2.8)$$

As shown in Eq. 2.8 there are 4 valence terms (namely (1) bond stretching, (2) bond angle, (3) torsional, (4) out-of-plan), 5 cross-terms, and 2 non-bonded terms. These terms are detailed below:

(1) Bond stretching:

In the CVFF forcefield[21], the bond stretching term is represented by a Morse potential (first term in Eq. 2.8):

$$\sum_{b} D_b\left[1-e^{-\alpha(b-b_0)}\right]^2 \qquad (2.9)$$

where D_b is the depth of the potential energy minimum, b_0 is the equilibrium bond length, b is the bond distance, and α is given by:

$$\alpha = \omega\sqrt{\frac{\mu}{2D_b}} \qquad (2.10)$$

where μ is the reduced mass, and ω is related to the stretching constant of the bond k by:

$$\omega = \sqrt{\frac{k}{\mu}} \tag{2.11}$$

More commonly, a Hooke's law formula is used and has the following form:

$$E_{bond} = \frac{1}{2}k(l - l_0)^2 \tag{2.12}$$

where, l_0 is the equilibrium bond length and k the force constant. Typical force constants are in the range of a few hundreds kcal.mol^{-1}.Å^{-2}. The Hooke's law is valid only at the bottom of the potential well (near equilibrium). To remedy this problem, cubic and higher order terms are added:

$$E_{bond} = \frac{1}{2}[k_1(l - l_0)^2 + k_2(l - l_0)^3 + k_3(l - l_0)^4 + ...] \tag{2.13}$$

(2) Angle bending:

Again, a Hooke's law is routinely used.

$$E_{angle} = \frac{1}{2}k(\Theta - \Theta_0)^2 \tag{2.14}$$

Angle force constants are several order of magnitudes smaller than their 'bond' counterpart: this is because it is much easier for a molecule to bend than it is to stretch or compress.

Once more, cubic and higher terms can be added to increase the precision (at higher computational cost) in a similar way to the bond stretching.

(3) Torsional term:

This term represents the energy cost to the free rotation of molecules around single bonds. A truncated Fourier serie is generally used to describe this term:

$$E_{torsion} = \frac{V_1}{2}(1+\cos\Phi) + \frac{V_2}{2}(1-\cos 2\Phi) + \frac{V_3}{2}(1+\cos 3\Phi) \qquad (2.15)$$

Rotation barriers can be measured by microwave spectroscopy and by NMR experiments.[22] Their value is usually in the range 0-30 kJ/mol. Torsional terms are intimately linked to van der Waals terms and the choice of one set of torsional parameters will influence the choice of non-bonded parameters. This shows that there is a limit to the transferability of the forcefield parameters.

(4) Out-of plane angle bending term (or improper torsion term):

This term ensures the planarity of sp^2 atoms. It is of particular importance when studying unsaturated molecules, where carbon double bonds must be kept planar during the simulation. There exist different functional form of representing this term.

Figure 2.6 below shows two ways to model the out-of-plan term.

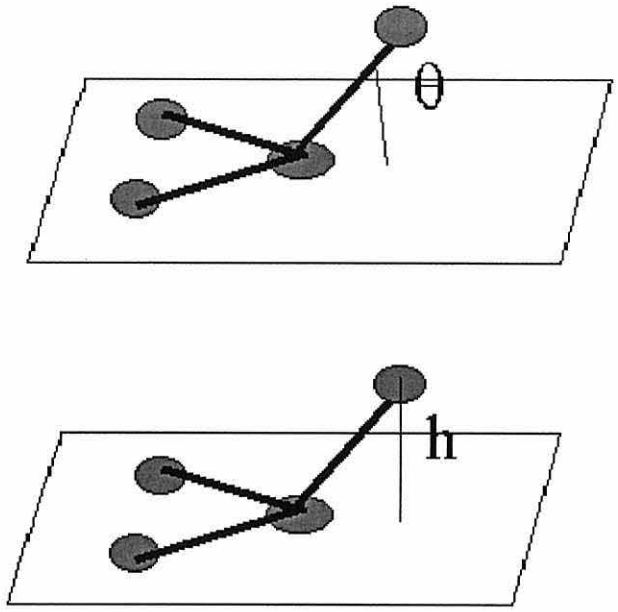

Figure 2.6 Two different representation of the out-of-plan term.[22]

The out-of-plan term can be written as:

$$E_{oop} = \frac{1}{2} k\Theta^2 \text{ or } E_{oop} = \frac{1}{2} kh^2 \qquad (2.16)\ (2.17)$$

The out-of-plan term is not always included in forcefields but they are particularly important when computing vibrational frequencies.[10,18,22]

(4-8) Cross terms:

Cross terms represent the coupling between geometric features. Greater accuracy is obtained when using those terms. As for the out-of-plan term, they are also important in vibrational frequency calculations. [10-18-22] Commonly used cross terms are the bond-angle, the angle-angle, and the torsion-angle terms:

$$E_{bond-angle} = \sum\sum k_{l\Theta}(l - l_0)(\Theta - \Theta_0) \qquad (2.18)$$

$$E_{angle-angle} = \sum\sum k_{\Theta\Theta'}(\Theta - \Theta_0)(\Theta' - \Theta_0') \qquad (2.19)$$

$$E_{torsio-angle} = \sum\sum k_{\Theta\Theta'\omega}(\Theta - \Theta_0)(\Theta' - \Theta_0')\cos\omega \qquad (2.20)$$

In some cases, research has also shown that the cross terms are important in accounting for possible structural deformations. Those terms are included in the CVFF forcefield (Eq.2.8), in addition to a bond-bond cross term and an out-of-plan – out-of-plan cross term.

(9) Non-bonded terms:

Terms 1 to 5 described 'bonded' interactions in the sense that they are defined by the connectivity of the molecule. The distant dependent non-bonded terms regroup the van der Waals and the Coulombic (or electrostatic) interactions. The van der Waals term accounts for instantaneous dipole-dipole interactions, whereas the electrostatic term accounts for polarity interactions. Interactions are computed for atoms with a 1-4 or greater separation. A cutoff is usually employed to limit the number of interactions to compute (see section 2.4.8). Non-bonded terms are especially important when dealing with polar molecules. Term 10 of the CVFF forcefield[21] (Figure 2.5 and Eq. 2.8) represents a 12-6 Lennard-Jones type of potential describing the van der Waals interactions:

$$U(r) = 4\varepsilon\left[\left(\frac{\sigma}{r}\right)^{12} - \left(\frac{\sigma}{r}\right)^{6}\right] \qquad (2.21)$$

where ε is the magnitude of the potential at the minimum ($r=2^{1/6}\sigma$) and σ is the separation at which U is zero.

Van der Waals atomic radii belong to the set of empirical parameters included in the forcefield. 9-6 Lennard-Jones potential is also commonly used to describe non-bonded interactions. In polyatomic systems, heterogeneous van de Waals radii are generally calculated using the Lorentz-Berthelot mixing rules, where cross interactions are computed using the pure atomic parameters. Electrostatic interactions are computed using Coulomb's law:

$$E_{electrostatic} = \sum_{ij} \frac{q_i q_j}{\varepsilon \, r_{ij}} \tag{2.22}$$

where ε represents the dielectric constant and q_i the atomic charge.

Modelling solvation (see below) implies the use of specific dielectric constant (e.g. 1 in vacuum, 80 for water). This value can also be made distance dependent in the expression of the forcefield. The determination of the partial atomic charges is another difficult task in molecular simulation. Electronegativity is usually employed to this end. Validation with experiment is made via the computation of the molecular dipole moment, which is relatively easy to perform. The values chosen for partial charges vary widely between forcefields.[8]

(10) Solvation:

Classical molecular mechanics calculations are generally performed in the gas phase. This may cause some errors especially when modelling biological systems as modifying the dielectric constant is not always satisfactory.[10] To remedy this problem two models are commonly employed: the explicit solvent model and the solvent continuum model. In the former, solvent molecules are added into the system and non-bond interactions computed with the appropriate parameters. Few hundred of molecules are usually added, depending on the size and the chemical nature of the solute studied. This adds to the computational cost. In the solvent continuum model, the medium is calculated as a

statistical continuum, and therefore solvent molecules are not directly included. An example of the solvent continuum model can be found in reference 23.

2.4 MOLECULAR DYNAMICS

This section investigates the methods based on molecular dynamics. The Verlet algorithm is detailed as well as one of its variant (The Leap-Frog algorithm). Computation of thermodynamic factors (such as temperature and pressure) is also explained in sections 2.4.4. and 2.4.5. Finally, the definitions (and uses) of the periodic boundary conditions and cutoff are given (section 2.4.7).

2.4.1 Definition

Molecular dynamics can be defined as the simulation of the motions of a system of particles (atoms and/or molecules) with respect to the forces that are present. The simulation starts by giving some kinetic energy to each atom. Then Newton' second law of motion (eq.2.23) is employed to obtain the trajectory of each atom.

$$\frac{d^2 x_i}{dt^2} = \frac{F_{x_i}}{m_i} \tag{2.23}$$

where x_i is the position of the i^{th} atom, F_{xi} the force applied to the i^{th} atom, and m_i the mass of the i^{th} atom.

Eq.2.23 is solved for every particle in the system and its integration over time leads to:

$$\frac{dx_i}{dt} = (\frac{F_{x_i}}{m_i})t + C \tag{2.24}$$

The initial velocity v_i is given by the constant C, at t = 0. Therefore, at time t we have

$$\frac{dx_i}{dt} = \frac{d^2x_i}{dt^2}t + v_i \tag{2.25}$$

Using ($a_i = d^2x_i/dt^2$) we obtain:

$$dx_i/dt = a_i t + v_i \tag{2.26}$$

Integrating Eq.2.26 over t leads to:

$$x_i = v_i t + \tfrac{1}{2} a_i t^2 + C' \tag{2.27}$$

The position at t is therefore deduced from the initial (t = 0) position, and from velocity and acceleration. A truncated Taylor series for displacement is used for computing the position at (t+Δt):

$$x(t+\Delta t) = x(t) + (\delta x/\delta t)\Delta t + (\delta^2 x/\delta^2 t)\Delta t^2/2 + \ldots \tag{2.28}$$

The timestep Δt varies depending of the system of study. It should be large enough to minimise computational cost (less iteration to obtain the same trajectory), but it must be much smaller than the highest vibration frequency of the system (to avoid atom overlapping or bonds being too stretched apart). All the simulations in this work applied to hydrocarbons have been performed using a 1 femtosecond (1 fs = 10^{-15} s) timestep as it is 10 times smaller than typical C-H vibrational frequency in hydrocarbons (10^{14} Hz).[24]

2.4.2 The Verlet algorithm

There exist many different integration algorithms for integrating the equation of motions. The Verlet[25] algorithm is the probably the most common, and will be used for performing glass simulations (chapter 4). Using the positions and accelerations at a time t, as well as the previous step positions, the new positions are deduced from:

$$x(t+\Delta t) = x(t) + (\delta x/\delta t)\Delta t + (\delta^2 x/\delta^2 t)\Delta t^2/2 + \ldots \quad (2.29)$$

and,

$$x(t-\Delta t) = x(t) - (\delta x/\delta t)\Delta t + (\delta^2 x/\delta^2 t)\Delta t^2/2 - \ldots \quad (2.30)$$

Adding Eq.2.29 and Eq.2.30 gives:

$$x(t+\Delta t) = 2x(t) - x(t-\Delta t) + (\delta^2 x/\delta^2 t)\Delta t^2 \quad (2.31)$$

Assuming that the velocity varies linearly during Δt (constant acceleration), and using:

$$\langle v \rangle = v(t + \Delta t/2) \quad (2.32)$$

where $\langle v \rangle$ is the average velocity, and $v(t) = (\delta x/\delta t)$ the velocity at t and using:

$$\langle a \rangle = a(t) = (\delta^2 x/\delta^2 t) \text{ (Constant)} \quad (2.33)$$

and we obtain, by dividing by $2\delta t$ the difference in position between $(t + \delta t)$ and $(t - \delta t)$:

$$v(t) = [x(t + \delta t) - x(t-\delta t)]/2\delta t \tag{2.34}$$

A drawback of the Verlet algorithm is that in order to evaluate the velocities at t, the position a (t + Δt) must be computed. Also, initial velocities can not be evaluated and a Maxwell-Boltzmann distribution (Eq.2.35) is generally used to acquire them. The Maxwell-Boltzmann distribution gives the probability f(v) that a molecule of mass m has a velocity of v at a temperature T:

$$f(v)dv = (\frac{m}{2\pi kt})^{3/2} e^{-\frac{mv^2}{2kT}} 4\pi v^2 dv \tag{2.35}$$

2.4.3 Leap-frog algorithm

The Leap-frog algorithm[26] is commonly used as a variant of the Verlet integrator. Using the position, velocity and acceleration at times t and (t - Δt/2) we have:

$$r(t + \Delta t) = r(t) + \Delta t v(t + \Delta t/2) \tag{2.36}$$

and,

$$v(t + \Delta t/2) = v(t - \Delta t/2) + \Delta t a(t) \tag{2.37}$$

From the acceleration at t and the velocities at (t-Δt/2), the velocities at (t+Δt/2) are computed, and the positions at (t+Δt/2) deduced. Therefore, the velocities at t are calculated from:

$$v(t)=1/2[v(t+\Delta t/2)+v(t-\Delta t/2)] \tag{2.38}$$

The disadvantage of this method is that the positions and the velocities calculated are $\Delta t/2$ out of synchronisation, but has the advantage of explicitly including the velocities, and does not require the calculation of the differences of large numbers (in contrast to the Verlet algorithm).[22]

The starting structure must be close to a local minimum for molecular dynamics to be performed adequately. Before the data (energy, pressure, etc.) can be collected, an equilibration stage is performed. This initial stage allows the redistribution of the system's energy to ensure stability. Also, the temperature can take many timesteps to equilibrate to the desired value.

2.4.4 Temperature

The temperature is calculated using the equipartition principle which stipulates that every degree of freedom has an average energy of ½ kT, and the average total kinetic energy, <K>, is equal to the sum over all momenta p_i:

$$< K > = \left\langle \sum_{i}^{N} \frac{p_i^2}{2m} \right\rangle \tag{2.39}$$

and

$$< K > = \frac{N_f k_b T}{2} \tag{2.40}$$

where N_f represents the number of degree of freedom, k_b is the Boltzmann constant and T the temperature. The thermodynamic temperature is obtained by the average of the instantaneous temperature T_{instan}, with:

$$T_{ins\tan} = \frac{2K}{N_f k_b T} \tag{2.41}$$

N_f is equal to (3N-6) for non-periodic systems and (3N-3) for periodic systems. During the molecular dynamics simulations, while converging toward an equilibrium structure, kinetic energy is converted into potential energy, and the temperature also changes. Therefore, the temperature needs to be monitored and corrected during the run. Velocity scaling[18], Berendsen's method[27] and Nosé dynamics[28] are amongst the most common methods to control the temperature. The direct velocity scaling method uniformly scales the atom velocities as follows:

$$\left(\frac{v_{new}}{v_{old}}\right)^2 = \frac{T_{target}}{T_{system}} \tag{2.42}$$

This method will be used in the glassy phase simulations performed in chapter 4, as well as during the equilibration stages of the simulated annealing runs. The Berendsen method will also be used for the data collection stage in our simulated annealing simulations. This method changes the atomic velocities in a smoother way that the velocity scaling method. Indeed, using Berendsen's method[27], each atomic velocity is multiplied by a factor λ equal to:

$$\lambda = \left[1 + \frac{\Delta t}{\tau}(T - T_0)\right]^{1/2} \tag{2.43}$$

where Δt is the timestep, τ a characteristic relaxation time, T_0 the target temperature and T the instantaneous temperature. The temperature is subsequently controlled by modifying T_0 and τ.

2.4.5 Pressure

Like the temperature, the pressure has to be controlled during constant-pressure (NPT) simulations. Discover[18] employs the Virial theorem[29] to compute the pressure via the following relation:

$$PV = Nk_bT + \frac{2}{3} < W > \tag{2.44}$$

where the work function W is defined as half the sum (over all atoms) of the product of the force f_i and the displacement r_i:

$$< W > = \frac{1}{2} \sum_{i=1}^{N} r_i . f_i \tag{2.45}$$

Identically to the instantaneous temperature, an instantaneous pressure (P_{instan}) defined as:

$$P_{ins\,tan} = \frac{Nk_bT}{V} + \frac{2}{3}\frac{W}{V} \tag{2.46}$$

where

$$T = \frac{2}{3Nk_b} K \tag{2.47}$$

and K is the instantaneous kinetic energy. Substituting Eq.2.47 in Eq.2.46 we have:

$$P_{ins\tan} = \frac{2}{3V}(K + W) \tag{2.48}$$

A number of methods exist to control the pressure during the simulations such as Berendsen's method[27], Anderson's method[30] and the Parrinello-Rahman[31] method.

2.4.6 Statistical ensembles

Three different ensembles are commonly used in periodic simulations: the NVT ensemble, the NVE ensemble and the NPT ensemble. In all those three ensembles, the number of particles in the system, N, is kept constant. When using the NVT ensemble, the volume also is kept constant and the temperature is controlled via one of the method previously described. The NVT or canonical ensemble, is probably the most ordinarily used. It is also suitable for non-periodic simulations. The micro-canonical ensemble NVE solves Newton's second law of motion without controlling the temperature or the pressure, as the energy is kept constant. The problem with this method is that the target temperature (equilibration) can not be predicted except by experience. This ensemble will be used in our glass simulation data collection stages to explore the conformational surface of the tridecane molecule (Chapter 4). The third type of ensemble is the NPT (constant-temperature and constant-pressure) ensemble, where the pressure is controlled by changes in the volume.

2.4.7 Periodic boundary conditions

Periodic boundary conditions are often employed to simulate the influence of bulk solvent or crystalline environment. Using this methodology, the number of atoms

included in the simulation can be reduced while maintaining bulk effects. Calculations are performed using the central cell (Figure 2.7) and the 8 surrounding cells are images of this cell. When a molecule (or atom) leaves the central cell, its image re-enters the cell via the opposite side, with the same velocity. Therefore, the number of particles in the cell remains constant during the simulation.

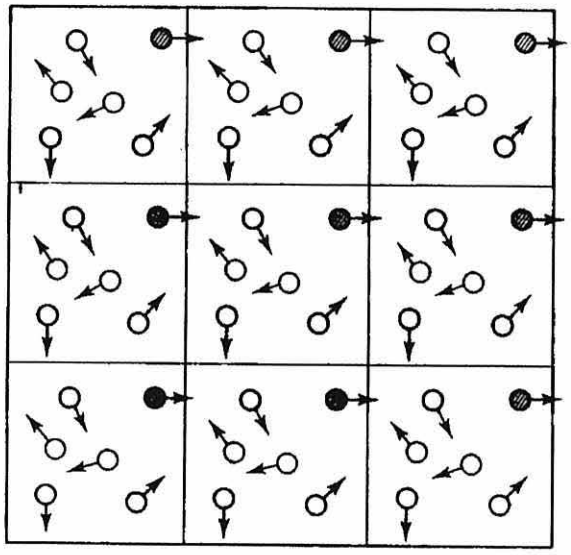

Figure 2.7 Periodic Boundary Conditions in two dimensions.[22]

Each replica of the central cell contains the same number of particles in identical position and orientation. When a particle moves through a boundary, it is automatically replaced by a particle moving into the sample through the opposite side of the central cell. Molecules closed to the edge of the real box can interact with the image molecules in the surrounding boxes, minimising edge effects. Usually a cubic cell is employed with such simulations, but other cells can also be used (hexagonal prism, parallelepiped, etc.).

2.4.8 Cutoff distances

The computational cost of the valence terms of the forcefield grows linearly with the number of atoms. By contrast, non-bonded interactions have a quadratic dependence on

the number of atoms in the simulation. To reduce the computational cost of those terms, it is a current practice to neglect interactions between atoms separated by certain distances, namely the cutoff. Cutoff distances of 8-10 Å are usually employed for computational limitations, but this can lead to errors in the calculations because non-bonded interactions are known to be still significant up to 15 Å and beyond.

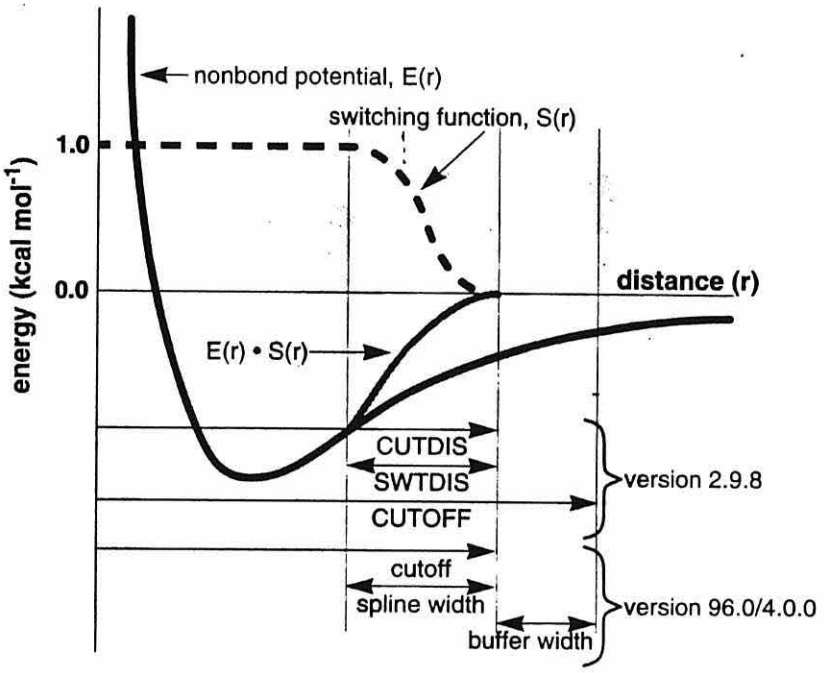

Figure 2.8 Cutoff and switching function.[18]

The true potential energy function E(r) is replaced by the product of E(r) by S(r), the switching function. Its role is to nullify E(r) for large r (greater than the cutoff value), but to do so in a smooth way. (Note: the version 2.9.8 of the Discover code has been used in the simulated annealing procedure and the version 96.0/4.0.0 has been used in the glass simulations. See Chapter 4).

In the Discover[18] program, a switching function S(r) is employed together with a cutoff to smoothly turn off the interactions. This avoids discontinuities in the non-bond energy when simply cutting the non-bond interactions off at a given value. In our simulations, a cutoff value of 9.5 Å was employed in the glass simulations and a value of 7.5 Å in the simulated annealing runs. Hydrocarbon molecules (such as the tridecane wax) are non-

polar molecules and therefore their non-bonded interactions are weak. Subsequently, the values used are a good compromise between computational limitation and accuracy.

2.5 QUANTUM MECHANICS

In the next section, the Schrödinger equation (section 2.5.2) and the variational principle (section 2.5.3) are explained. The mathematical representation of atomic and molecular orbitals (wavefunctions 2.5.4) is also given through the use of Slater determinant (section 2.5.5) and the LCAO (Linear Combination of Atomic Orbitals, section 2.5.9) theory. The Hartree-Fock theory is described in section 2.5.7, though it has not been used in this work, for comparison with the density functional theory, detailed in the next section 2.6. The SCF (Self Consistent Field) technique is described in section 2.5.8, and the RHF (Restricted Hartree-Fock) and UHF (Unrestricted Hartree-Fock) methods in section 2.5.10. Basis sets are covered in 2.5.11 as well as the electron correlation (section 2.5.12). Finally, semi-empirical methods are briefly investigated in section 2.5.13.

In contrast to methods using classical mechanics, electrons are fully taken into account in quantum mechanics-based simulation methods. The term *ab initio* is usually employed to refer to those methods, as, in theory, no parameters should be used. In practice, this is not possible and some approximations are generally utilised (i.e. time independence, Born-Oppenheimer). All *ab initio* methods are based on the solution of the Schrödinger equation. A Hamiltonian (mathematical operator) is employed to describe the model and include the electronic kinetic energy as well as the potential energy originating from nucleus-nucleus, electron-electron and electron-nucleus interactions. The size of the system that can be studied is considerably smaller than in classical dynamics (typically of the order tens of atoms). Periodic systems can be studied, using specific basis functions (Bloch functions usually). Optical and magnetic properties can also be calculated with high accuracy, as well as chemical reactions involving bond breaking or forming. Schrödinger equation can not be solved exactly for many body problems, only for hydrogen atom.

2.5.1 The Schrödinger equation

The time-independent Schrödinger equation for an isolated N-electron system is:

$$\hat{H}\Psi = E\Psi \tag{2.49}$$

Where E is the electronic energy (using both the time independent and Born-Hoppenheimer nonrelativistic) approximations), ψ is the wavefunction $\psi = \psi(x_1, x_2, \ldots, x_n)$, and $\hat{H}$ is the (electronic) Hamiltonian operator (in atomic units):

$$\hat{H} = \sum_{i=1}^{N}(-\frac{1}{2}\nabla_i^2) - \sum_{i=1}^{N} v(r_i) + \sum_{i<j}^{N}\frac{1}{r_{ij}} \tag{2.50}$$

where, the external potential $v(r_i)$ acting on electron i due to the nuclei of charges Z_α is:

$$v(r_i) = \sum_j \frac{Z_j}{r_{ij}} \tag{2.51}$$

2.5.2 The variational principle

The variational principle states that the energy calculated from an approximation to the true (exact) wavefunction will always be greater than the energy of the ground state E_0. The energy of a system in a state ψ is given by:

$$E[\Psi] = \frac{\left\langle \Psi \mid \hat{H} \mid \Psi \right\rangle}{\langle \Psi | \Psi \rangle} \tag{2.52}$$

where

$$\left\langle \Psi \mid \hat{H} \mid \Psi \right\rangle = \int \Psi^* \hat{H} \Psi dx \tag{2.53}$$

The variational principle gives:

$$E[\Psi] \geq E_0 \tag{2.54}$$

The energy computed from a guessed ψ is an upper bound to the true ground state energy E_0. Full minimisation of the functional $E[\psi]$ with respect to all allowed N-electron wavefunctions will give the true ground state ψ_0 and energy $E[\psi_0] = E_0$; that is,[32]

$$E_0 = \min E[\Psi] \tag{2.55}$$

2.5.3 Wavefunctions

Wavefunctions (denoted Ψ) are single-valued, finite and continuous mathematical functions at any point in space. Only the square of the wavefunction has a physical meaning, and that is the probability or the electron density. The sum over all space of the square of the wavefunction has a probability of 1:

$$\int \Psi^* \Psi \, dv = 1 \tag{2.56}$$

Wavefunctions are orthonormal:

$$\int \Psi_i^* \Psi_j dv = 0 \tag{2.57}$$

In the case of the hydrogen atom, the (atomic) wavefunctions employed are well known, and represented by (in polar coordinates):

$$\Psi_{nlm}(r,\theta,\phi) = R_{nl}(r) Y_{lm}(\theta,\phi) \tag{2.58}$$

where $R_{nl}(r)$ controls the radial part of the wavefunction; n, l, m are the integral quantum numbers and $Y_{lm}(\theta,\phi)$ controls the angular variation wavefunction (see Figure 2.9).

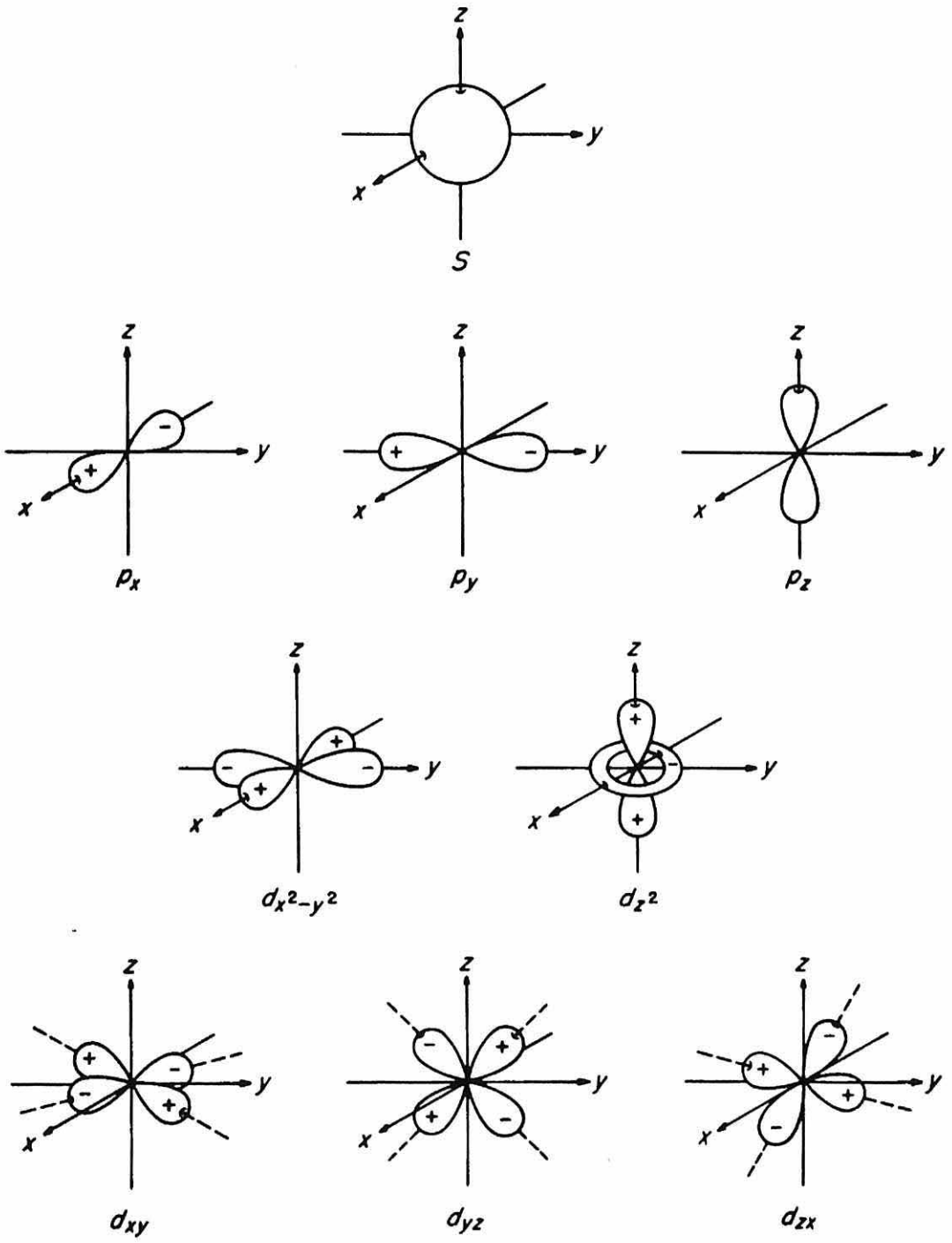

Figure 2.9 Schematic representation of s, p, and d atomic orbitals.[33] Atomic orbitals are labelled by letters according to the azimuthal quantum number ℓ (s for ℓ=0, p for ℓ=1, d for ℓ=2, etc.) and m (magnetic quantum number).

Pauli's principle implies the use of spinorbitals that are orbitals including the fourth quantum number: the electron spin. The spin angular momentum is represented by the vector operator S and has components s_x, s_y, and s_z. Spin orbitals are made of the product of a spatial function and a spin function. Thus, we have:

$$\psi(1,2,\ldots,n) = \psi_1(1)\alpha(1)\psi_2(2)\beta(2)\ldots\psi_n(n)\beta(n) \tag{2.59}$$

2.5.4 Slater determinants

Pauli's principle constrains the wavefunctions to be antisymmetric with respect to the exchange of any 2 electrons. The wavefunctions are therefore replaced by determinants that changes sign with the permutation of two electrons. These determinants are called Slater determinants and have the following formula:

$$1/\sqrt{n!}\begin{vmatrix}\phi_1(1)....\phi_i(1).....\phi_n(1)\\ \phi_1(i).....\phi_i(i).....\phi_n(i)\\ \phi_1(n)...\phi_i(n)....\phi_n(n)\end{vmatrix} \tag{2. 60}$$

A simplified notation is usually used to express the Slater determinant:

$$\text{Det} = |\phi_1\ldots\phi_i\ldots\phi_n| \tag{2.61}$$

in which the normalisation factor $(1/\sqrt{n!})$ is implicit.

2.5.5 Splitting of the electronic Hamiltonian

In a many-electrons system, the many-electrons Hamiltonian $(H)^i$ is replaced by a sum of mono-electronic Hamiltonians (h_i) (neglecting the electron correlation):

$$H = \sum_i h_i \tag{2.62}$$

It is possible to demonstrate that each eigenfunction $\psi(1\ldots n)$ of H can be transformed in a product of function $\phi(i)$:

$$\psi_i(1\ldots n) = \phi_1(i)\ldots\phi_i(i)\ldots\phi_n(i) \tag{2.63}$$

where each function $\phi(i)$ is an eigenfunction of h_i with the eigenvalue E_i.:

$$h_i\phi_i(i) = E_i\phi_i(i) \tag{2.64}$$

Therefore, the total eigenvalue of H is the sum of the eigenvalues of the h_i:

$$H\Psi(1\ldots n) = E\Psi(1\ldots n) \tag{2.65}$$

and,

$$E = \sum_{i=1}^{n} E_i \tag{2.66}$$

[i] Operators (Hamiltonian, exchange, etc.) should be written with a circumflex (^) (i.e. $\hat{H}$, $\hat{K}$ but we use a simplified way of writing (H or K) for simplicity in the text but not in the equations.

2.5.6 Hartree-Fock Theory[34,35]

The Hartree-Fock method is employed to solve the Schrödinger equation by splitting the global Hamiltonian into a sum of mono-electronic Hamiltonians (called Fock operators). The Hamiltonian used in Hartree-Fock theory is the Hartree Hamiltonian H^h:

$$H^h = \sum_i F(i) \tag{2.67}$$

where F(i) represents the Fock operators, which are mono-electronic Hamiltonians.
As we have seen previously, this approximation implies that the wavefunction is an antisymmetrised (Pauli's principle) product of mono-electronic functions ϕ_i, called spinorbitals, each of them being eigenfunction of the Hamiltonian F(i):

$$\Psi(r_1...r_i...r_n) = |\phi_1...\phi_i...\phi_n| \tag{2.68}$$

$$F\phi_i(r_i) = \varepsilon_i \phi_i(r_i) \tag{2.69}$$

In addition, this wavefunction has the form of a Slater determinant. Particles are assumed to be independent. As it will be explained later in this chapter this approximation leads to some errors in the calculations and a better treatment can be employed.
Another consequence of such wavefunctions is that the total electronic energy is the sum of mono-electronic energies:

$$E^h = \sum_i^{occ} \varepsilon_i \tag{2.70}$$

This is a sum over the occupied orbitals that are effectively present in the determinant. The approximation of independent particles assumes that the movement of an electron is

independent of the movement of the other electrons. Nevertheless, the electronic repulsion is taken into account, and F(i) becomes:

$$F(i) = h(i) + \sum_{j}^{occ} V_j \tag{2.71}$$

where the sum over V_j represents the average field exerted on the i^{th} electron by all the other electrons. This refers to the approximation of the independent particles because the influence on the i^{th} electron of all the other electrons is not taken into account. The Hartree-Fock method does not include the correlation energy (see 2.5.12). In order to find out the expression of V_j, the average energy of the i^{th} electron is defined as:

$$\langle \phi_i \mid F \mid \phi_i \rangle = \langle \phi_i \mid h_i \mid \phi_i \rangle + \sum_{j}^{occ} \mathrm{Rep}_{ij} \tag{2.72}$$

where Rep_{ij} is the average value of the operator $1/r_{12}$, corresponding to the repulsion between two electrons occupying the orbitals ϕ_i and ϕ_j. We have:

$$\mathrm{Rep_{ij}} = \mathrm{J_{ij}} - \mathrm{K_{ij}} \tag{2.73}$$

with,

$$J_{ij} = \iint \phi_i^*(1)\phi_i(1)\frac{1}{r_{12}}\phi_j^*(2)\phi_j(2)d\tau_1 d\tau_2 \tag{2.74}$$

and,

$$K_{ij} = \iint \phi_i^*(1)\phi_j(1)\frac{1}{r_{12}}\phi_i^*(2)\phi_j(2)d\tau_1 d\tau_2 \tag{2.75}$$

J_{ij} is called the Coulombic integral and correspond to the density of the i^{th} electron, multiply by the operator of repulsion electronic energy, multiply by the density of the j^{th} electron. K_{ij} is named exchange integral. In Eq.2.66, K enters with a negative sign and reduces the energy of interaction between electrons with parallel spins in different orbitals. It is a direct consequence of Pauli's principle and reflects the energy stabilisation due to the partial correlation of electrons of parallel spins.[33]
Subsequently, the operator F can be written as:

$$F = h + J + K \tag{2.76}$$

With the operators J and K defined as:

$$\int \phi_i^*(1) J \phi_i(1) d\tau_1 = \sum_j^{occ} J_{ij} \tag{2.77}$$

$$\int \phi_i^*(1) K \phi_i(1) d\tau_1 = \sum_j^{occ} K_{ij} \tag{2.78}$$

with,

$$J = \sum_j^{occ} \frac{\phi_j^*(2)\phi_j(2)d\tau_2}{r_{12}} \tag{2.79}$$

and

$$K\phi_i(1) = \sum_j^{occ} \phi_j(1) \int \frac{1}{r_{12}} \phi_i^*(2)\phi_j(2) d\tau_2 \tag{2.80}$$

A condensed notation is usually employed with those operators:

$$Jij = (ij|jj) \tag{2.81}$$

$$Kij = (ij|ij) \tag{2.82}$$

$$J = \sum_{j}^{occ} (\quad | jj) \tag{2.83}$$

$$K = \sum_{j}^{occ} (\ j |\ j) \tag{2.84}$$

(This simplified notation will be used in section 2.5.9)

2.5.7 SCF Method

In order to calculate ϕ_i, the Fock Hamiltonian H_i has to be written containing terms that can only be calculated when the other orbital ϕ_j is known. It is therefore impossible to solve each Eq.2.65 one by one. Those equations have to be solved in a coupled-system, and are named the "secular equations". In practice, a set of orbitals $\{\phi_k\}$, called a 'guessed basis set', is initially chosen. This basis set will constitute the basis in which the solutions of the ϕ_i will be expressed:

$$\phi_i = \sum_k C_{ik}\phi_k \tag{2.85}$$

And the problem is to find the C_{ik} coefficients, solving equations of type:

$$F|\phi_i\rangle = \varepsilon_i|\phi_i\rangle \tag{2.86}$$

which is equivalent to:

$$\sum_k C_{ik} F|\phi_k\rangle = \varepsilon_i \sum_k C_{ik}|\phi_k\rangle \tag{2.87}$$

Multiplying Eq.2.80 by ϕ_l and integrating we obtain:

$$\sum C_{ik}\langle\phi_l \mid F \mid \phi_k\rangle = \varepsilon_i \sum C_{ik}\langle\phi_l \mid \phi_k\rangle \tag{2.88}$$

Varying ϕ_l, we obtain as many equations as orbitals in the set, and the unknown variables are the coefficients C_{ik}. It is possible to give a vectorial form to the equations:

$$FC - \varepsilon SC = 0 \tag{2.89}$$

where F and S are matrices defined as:

$$F_{kl} = \langle\phi_k \mid F \mid \phi_l\rangle \tag{2.90}$$

$$S_{kl} = \langle\phi_k \mid \phi_l\rangle \tag{2.91}$$

and C is a column which elements are the coefficients C_{ik} of an orbital ϕ_i:

$$\begin{bmatrix} F_{11}\ldots\ldots\ldots\ldots \\ \ldots\ldots\ldots\ldots\ldots \\ \ldots\ldots F_{kl}\ldots\ldots \\ \ldots\ldots\ldots\ldots\ldots \\ \ldots\ldots\ldots\ldots F_{NN} \end{bmatrix} \times \begin{bmatrix} C_{il} \\ \ldots\ldots \\ C_{ik} \\ \ldots\ldots \\ C_{iN} \end{bmatrix} \times \begin{bmatrix} S_{11}\ldots\ldots\ldots\ldots\ldots \\ \ldots\ldots\ldots\ldots\ldots\ldots \\ \ldots\ldots\ldots S_{kl}\ldots\ldots\ldots \\ \ldots\ldots\ldots\ldots\ldots\ldots \\ \ldots\ldots\ldots\ldots\ldots S_{NN} \end{bmatrix} \times \begin{bmatrix} C_{il} \\ \ldots\ldots \\ C_{ik} \\ \ldots\ldots \\ C_{iN} \end{bmatrix} \tag{2.92}$$

This set of equations of N unknowns has non trivial solutions if the determinant $|F - \varepsilon_i S|$ is zero. As N is the number of orbitals in the basis set used, there are N possible values of ε_i that are eigenvalues of the energy of the orbitals. Once the ε_i are known it is easy to

solve Eq.2.88 and to find the corresponding eigenfunctions. Starting with any basis set, a linear combination is made that diagonalise the Fock operator. The resulting molecular orbitals are automatically orthogonal since:

$$F_{ij} - \varepsilon_i S_{ij} = 0 \quad \forall i \tag{2.93}$$

In order to be able to write these equations, the two matrix elements F_{kl} and S_{kl} have to be computed. The calculation of the S_{kl} is obvious but computing the F_{kl} suppose to know the occupied ϕ_j orbitals that can form a Slater determinant, wavefunction of the system. The problem is that it is the ϕ_j we are looking for! Therefore, an iteration procedure will be employed. The calculation starts with a basis set of orbitals $\phi j^{(0)}$ that can be either the ϕ_k or linear combination of ϕ_k. With those orbitals $\phi j^{(0)}$ the elements of the matrix of the Fock operator $F^{(0)}$ can be computed, and then the secular equations can be solved. A set of orbitals $\phi_i^{(1)}$ is obtained that will be substituted into $F^{(0)}$. If the system has p electrons, the p orbitals of lowest energy will form the new set $\phi_j^{(1)}$ with which a new Fock operator $F^{(1)}$ will be constructed. This new operator will give a new set of orbitals $\phi_j^{(2)}$, etc. This iterative process is repeated until self-consistency, that is until identity between the occupied orbitals used to build the Fock operator and the occupied eigenfunctions of this operator.

The entire process can be summarised by the following scheme:

1. Choice of the 'guessed basis set' $\{\phi_k\}$
2. ---> choice of initial occupied orbitals $\phi_j^{(0)}$
3. $\text{----->}F^{(0)} \text{----->} \phi_i^{(1)} \text{----->} F^{(1)} \text{----->} \ldots\text{----->} \phi_i^{(r)} \text{----->}F^{(r)} \text{----->} \phi_i^{(r+1)}$

The process stops when $\phi_i^{(r)} = \phi_i^{(r+1)}$ and/or $\varepsilon_i^{(r)} = \varepsilon_i^{(r+1)}$.

This approach of calculating the orbitals is called the Self Consistent Field (SCF) method. To compute the total electronic energy, E_0^{SCF}, the average value of the exact Hamiltonian is computed for the approximate wavefunction Ψ^{SCF}, using Slater rules:

$$E_0^{SCF} = \left\langle \Psi^{SCF} \mid H \mid \Psi^{SCF} \right\rangle = \sum_{i}^{occ} h_{ii} + \sum_{\substack{i,j \\ i<j}}^{occ} (J_{ij} - K_{ij}) = \sum_{i}^{occ} \varepsilon_i - \sum_{\substack{i,j \\ i<j}}^{occ} (J_{ij} - K_{ij}) \quad (2.94)$$

The initial guess of the density matrix may influence the convergence of the SCF calculation. Semi-empirical methods can be employed to form this initial guess but the results are sometimes unsatisfactory.[22] The direct inversion of the interactive space (DIIS) method developed by Pulay[36-37] is more often employed. In this technique, the coefficients of the next iteration are calculated from their values in the previous steps, and the energy is assumed to have a quadratic dependence of the basis set coefficients.

2.5.8 The LCAO approximation

In the LCAO approximation, molecular orbitals (Ψ_i) are generated by using a Linear Combination of Atomic Orbitals (ϕ_v). The LCAO method is the best approach to date for choosing the set of molecular functions. It is employed in most *ab initio* techniques.

$$\Psi_i = \sum_{v=1}^{N} C_{vi} \phi_v \quad (2.95)$$

The molecular basis set is made of the ensemble of the atomic basis set, including each atom that constitutes the molecule. The bonding interaction depends on the degree of overlap between the atomic overlaps on adjacent atoms.[38] Two conditions must be fulfilled by the atomic orbitals to combine effectively in a molecular orbital: (i) the energy difference between both atomic orbitals must be small (<10 eV) and (ii) both atomic orbitals must posses a similar symmetry with respect to the molecules. Figure 2.10 below displays the molecular orbital formed by the bonding combination of 2 σ orbitals (i.e. 1s orbital of hydrogen).

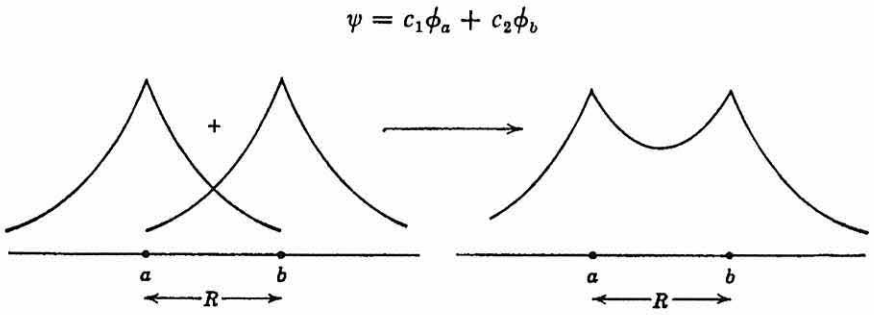

Figure 2.10 Synthesis of a LCAO variation wavefunction from atomic orbitals centred on two identical nuclei.[39] The sum of the two *atomic orbitals* ϕ_A and ϕ_B (modified by their respective C_i coefficients) gives the *molecular orbital* Ψ.

The minimum numbers of basis functions that can be used correspond to half the number of electrons (minimal basis set). Increasing the number of basis functions improves the accuracy of the calculations until the *Hartree-Fock limit* is reached, that is when the energy can not be reduced anymore. In this method, the derivative of the energy with respect to the coefficients C_{vi} is calculated and the minimum is reached when:

$$\frac{\partial E}{\partial C_{vi}} = 0 \tag{2.96}$$

In the case of a solid or a large molecule, the number of interacting atomic orbitals becomes important, and therefore a great variety of molecular orbitals can be formed. Thus, the molecular orbitals become delocalised over the entire molecule, and are very close in energy. The energy difference between subsequent molecular orbitals becomes negligible and they form continuous bands of energy. The band theory will be explained in detail in the chapter 5 (section 5.1.1) and the behaviour of electrons inside these bands in chapter 6.

2.5.9 RHF and UHF methods

Presently, only monoelectronic orbitals (spinorbitals) that comprise the product of a spatial part ($\psi_k(r)$) and a spin function ($\eta(\sigma)$) have been considered. If a molecule possesses an even number of electrons, Hartree-Fock calculations give the same orbitals (the spatial part) for α and β electrons. Therefore, the Restricted Hartree-Fock method (RHF) introduces a simplification by avoiding computing twice each equivalent spatial part of the orbitals. The constraint is that each spinorbital $\phi_k(r,\sigma)$ of spin α, has the same spatial part as the spinorbital $\bar{\phi}_k(r,\sigma)$ of spin β:

$$\phi_k(r,\sigma) = \Psi_k(r)\alpha(\sigma) \tag{2.97}$$

$$\bar{\phi}_k(r,\sigma) = \Psi_k(r)\beta(\sigma) \tag{2.98}$$

2.5.9.1 Closed-shell

Closed-shell systems are composed of an even number of electrons occupying spinorbitals by pair. Spinorbitals, thus doubly occupied, differ only by their spin counterpart. RHF equations will ignore the spin part and assume that electrons doubly occupy the spatial orbitals (using the simplified notation Eqs. 2.74-2.77):

$$F_{kl} = h_{kl} + \sum_{j}^{occ}(kl \mid jj) + \sum_{j}^{occ}(kl \mid \bar{j}\,\bar{j}) - \sum_{j}^{occ}(kj \mid lj) \tag{2.99}$$

If we sum over the spatial orbitals, we obtain:

$$F_{kl} = h_{kl} + \sum_{j}^{occ} 2(kl \mid jj) - (kj \mid kl) \tag{2.100}$$

In this RHF method, the Fock operator (F) has the expression:

$$F = h + 2J - K \tag{2.101}$$

The energy (ε_i) of an orbital is:

$$F_{ii} = \varepsilon_i = h_{ii} + \sum_{j}^{occ} (2J_{ij} - K_{ij}) \tag{2.102}$$

To each orbital correspond two spinorbitals, and the total energy is:

$$E_0^{SCF} = 2\sum_{i}^{occ} \varepsilon_i - \sum_{i}^{occ}\sum_{j}^{occ} (2J_{ij} - K_{ij}) \tag{2.103}$$

For closed-shell systems, the RHF equations (applied on spatial orbitals) or the UHF equations (applied on spinorbitals) give exactly the same solutions for the energy of the orbitals and their spatial part.

2.5.9.2 Open-shell

Open-shell systems ca either have an odd number of electrons or an even number of electrons but are high-spin systems (i.e. triplets). The problem with UHF on open-shell system is that the wavefunctions obtained are not eigenfunction of the spin operator. There is a spin contamination measured by making the difference between the average

value of S^2 (spin operator) and the determinant UHF. The calculation is valid only if this value is less than a few percent. RHF can be applied on open-shell systems, and the spin contamination can be suppressed. Each spinorbital will be forced to share the spatial part with the one of opposite spin. Only spatial orbitals will be considered as previously, but this time they will be only singly occupied. The variational principle could not be applied because it would result in a different Fock operator for α and β electrons. Other operators have been suggested (i.e. Nesbet, Davidson).

2.5.10 Basis set

Hydrogenic atomic orbitals are not computationally suitable for molecules, even for the medium-sized ones due to their complicated functional forms. Instead, Slater[40] type orbitals (STO) will be used. Their general mathematical expression is:

$$\phi_n^{l,m} = Nr^{n-1}e^{-\xi r}Y_1^m \tag{2.104}$$

In practice, a combination of Gaussian functions ($\exp[-\zeta r^2]$) will be used that mimic the Slater function. A 1s orbital will have the following expression:

$$\phi_{1s}^{'}(\zeta r) = \sum_k d_{1s,k} \exp(-\alpha_{1s,k}\zeta^2 r^2) \tag{2.105}$$

where ζ is an adjustable parameter and $d_{1s,k}$ are the contraction coefficients computed using the least-square method to ensure that the orbital φ' is similar to the true Slater orbital (φ). This is done via the minimisation of the following integral:

$$(\phi - \phi^{'})^2 d\tau \tag{2.106}$$

The basis set is called *contracted* when the coefficients $d_{1s,k}$ in Eq. 2.105 are fixed during the entire calculation procedure. Orbitals 2s, 2p, etc. are represented using equations similar to Eq.2.105, changing the coefficients ζ and $d_{nl,k}$. The number of gaussian functions used can be rather important. Usually each orbital is described using 1 to 6 gaussian functions. Many standard basis set exist in the literature, and it is becoming less and less common to optimise the best coefficients. Amongst them are the bases of Pople.[33]

Minimal basis sets are noted STO-NG where N denotes the number of gaussian functions per atomic orbital. In the double-zeta basis set the number of functions used to describe each orbital is doubled. In the split-valence basis sets, valence orbitals are doubled, and core orbitals are treated at simple-zeta level. The first number refers to the number of gaussian functions per core atomic orbital, the second number refers to the most contracted valence orbital, and the last one (usually 1) refers to the most diffuse valence orbital. Therefore the basis set 4-31G employs four gaussian functions for the 1s carbon atomic orbital, 2p and 2s orbitals are both represented by 2 orbitals, one made of 3 gaussian functions and the other orbital by only one gaussian function. The use of polarisation basis functions is noted with a *. Those functions have a higher angular momentum number (p for H, d for C, etc.). Hybrid orbitals (i.e. sp) can be described when using polarisation functions. Diffuse functions are also added (noted +) when the electronic density far from the nuclei is important. As it will be demonstrated in chapter 3, these functions can be of great importance when computing the energy of anionic species.

2.5.11 Electron correlation

The approximation of the independent particles leads to errors in the calculations. As electrons are correlated, they tend to avoid each other. The correlation energy is defined as the difference in energy between the exact energy and the Hartree-Fock energy:

$$E_{corr}^{HF} = E - E^{HF} \tag{2.107}$$

It can be of prime importance in the study of anions[41] or dispersive effects[22]. In addition, one single Slater determinant is insufficient to describe completely the wavefunction. Instead, many (up to thousands!) determinants will be employed to obtain satisfactory accuracy. In this post-Hartree-Fock method, excited states can be included in the description of an electronic state at a very high computational cost. Indeed, this treatment, when needed, greatly limits the modeller in the size of the system that can be studied. Another common way of including the electron correlation is to use the perturbation theory, as developed by Møller Plesset[42]. Again, this method is computationally very expensive.

2.5.12 Semi-empirical methods

Because ab initio calculations can be very computationally expensive (thus limiting the size of the system studied), some approximate molecular orbital theories have been developed.[33,43] These methods do not compute the entire set of orbitals but use some parameters derived from experimental data (in particular in the description of bi-electronic integrals). Amongst the most common methods used are the Hückel theory, MNDO (Modified Neglect of Differential Overlap) and CNDO (Complete Neglect of Differential Overlap). The semi-empirical methods, as they are usually referred to, have only been briefly used in the present study and therefore their mathematical description is not given.

2.6 DENSITY FUNCTIONAL THEORY

This section illustrates the main characteristics of the Density Functional Theory. After a short introduction (2.6.1), the non-local density approximation is introduced (section 2.6.2). The Kohn-Sham equations which are employed to compute the energy of the

system of study, are given together with the methodology used to solve them (section 2.6.3). Note that all equations are expressed in atomic units.

2.6.1 Introduction

In 1964, Hohenberg and Kohn[44] published the foundation of the density functional theory, foreseen in the late twenties by Thomas[45] and Fermi[46]. This theory is based on the singular property of the ground state of any quantum system: the properties of a system can be deduced solely from its electron density. Amongst those properties, the total energy can be computed using:

$$E_{TOT}[\rho] = T[\rho] + U[\rho] + E_{xc}[\rho] \tag{2.108}$$

- where ρ is the electron density:

Contrary to the Hartree-Fock method, the main variable is not the wavefunction $\psi(x_1, x_2, \ldots, x_n)$ but the electron density $\rho(r)$, that takes the expression:

$$\rho(r) = \sum_i |\phi_i(r)|^2 \tag{2.109}$$

where $\phi_i(r)$ represents a (one-electron) molecular orbital and the antisymmetrised product of all $\phi_i(r)$ form a Slater Determinant describing the wavefunction ψ:

$$\Psi = A(n)|\varphi_1(1)\phi_2(r)...\phi_n(n)| \tag{2.110}$$

where A(n) is the antisymmetrisation operator (Pauli's principle) and the $\phi_i(r)$ represent the molecular orbitals. Those molecular orbitals must be orthonormal:

$$\langle \phi_i \mid \phi_j \rangle = \delta_{ij} \tag{2.111}$$

where δ_{ij} is the Krönecker delta:

$$\delta_{ij} = \begin{cases} 1 \ if \ \ i = j \\ 0 \ if \ \ i \neq j \end{cases} \tag{2.112}$$

- T is the kinetic energy of a system of non-interacting particles of density ρ:

$$T = \left\langle \sum_i^n \phi_i \left| -\frac{\nabla^2}{2} \right| \phi_i \right\rangle \tag{2.113}$$

- U is the sum of all electrostatic energy due to the Coulombic interactions between electrons and nuclei, electrons and electrons, nuclei and nuclei:

$$\begin{aligned} U = & \sum_i^n \sum_\alpha^N \left\langle \phi_i(r) \left| \frac{-Z}{R_\alpha - r} \right| \phi_i(r) \right\rangle \\ & + \frac{1}{2} \sum_i \sum_j \left\langle \phi_i(r_1)\phi_j(r_2) \frac{1}{r_1 - r_2} \phi_i(r_1)\phi_j(r_2) \right\rangle + \sum_\alpha^N \sum_{\beta<\alpha} \frac{Z_\alpha Z_\beta}{\left| R_\alpha - R_\beta \right|} \end{aligned} \tag{2.114}$$

where, Z_α and Z_β refers to the nuclei charges. Eq.2.114 can be reformulated using Eq.2.109:

$$U \equiv \langle -\rho(r_1) V_N \rangle + \left\langle \rho(r_1) \frac{V_e(r_1)}{2} \right\rangle + V_{NN} \tag{2.115}$$

where ρV_N represents the electron-nucleus attraction, $\rho V_e/2$ represents the electron-electron repulsion, and V_{NN} represents the nucleus-nucleus repulsion.

- E_{xc} includes all many-body contributions to the total energy (exchange and correlation energies):

$$E_{xc}[\rho] \cong \int \rho(r)\varepsilon_{xc}[\rho(r)]dr \tag{2.116}$$

Eq.2.116 includes the *homogeneous gas approximation* which stipulates that the electron density varies slowly and can be represented locally by a uniform electron gas. This approximation is also called the *local density approximation.*

Similarly to the Hartree-Fock method, the electron spin will be taken into account and the orbitals $\phi_i(r)$ will be exchanged for spinorbitals $\phi_i(r,\sigma)$. Spin-restricted calculations consider only the spatial part of the spinorbitals: $\phi_i(r,\alpha) = \phi_i(r,\beta)$ that can be applied in most of the closed-shell systems (this is similar to the RHF method). Using a different spatial function for α and β electrons is called the spin-unrestricted method (used mostly with open-shell systems, similarly to the UHF method). This leads to two densities, one for α and one for β electrons, the sum being the total electron density. The difference gives the spin density.

2.6.2 Non-local density approximation

The problem of the local density approximation is that the classical Coulomb self-interaction is not properly cancelled by the local form of the exchange energy. As a consequence, the total effective potential based on the local density approximation does not exhibit the correct asymptotic (1/r) behaviour for neutral atoms or molecules.[47] Non-local density approximation (NLDA) aims to correct this abnormal behaviour by explicit inclusion of inhomogeneity corrections via gradient expansions. This can be

applied to the exchange term only or to both exchange and correlation terms, using either spin restricted or spin unrestricted methods. In this NLDA scheme, the total energy is:

$$E_{TOT}[\rho] = \sum_i \left\langle \phi_i \left| \frac{-\nabla^2}{2} \right| \phi_i \right\rangle + \left\langle \rho(r_1) \left[\varepsilon_{xc}[\rho(r_1)] + \frac{V_e(r_1)}{2} - V_N \right] \right\rangle + V_{NN} \qquad (2.117)$$

$E_{TOT}[\rho]$ is optimised with respect to variations in ρ, keeping the orbitals orthonormal:

$$\frac{\delta E_{TOT}}{\delta \rho} - \sum_i \sum_j \varepsilon_{ij} \langle \phi_i \mid \phi_j \rangle = 0 \qquad (2.118)$$

where ε_{ij} are the Lagrangian multipliers. According to Hohenberg and Kohn theorem, there exist a unique energy functional for which the variational equation $\delta E_{TOT}[\rho]=0$ yields the exact ground state density. This arises from the variational principle, applied to the electron density, similarly to the Hartree-Fock method applying the variational principle to the wave function.

2.6.3 The Kohn-Sham equations

The possible advantages of a replacement of the direct variation with respect to the density by the intermediary of an orbital picture were first emphasised by Kohn and Sham.[48] In1965, Kohn and Sham suggested a method to solve Eq.2.110, using a set of coupled equations, commonly named the Kohn-Sham equations:

$$\left\{ \frac{-\nabla^2}{2} - V_N + V_e + \mu_{XC}[\rho] \right\} \phi_i = \varepsilon_i \phi_i \qquad (2.119)$$

where μ_{XC} is the exchange-correlation potential. The resulting self consistent scheme has become a mainstay of applications of the density functional formalism.[47] The LCAO is also used in the DFT formalism. The atomic basis functions can be chosen from gaussian or Slater functions, we have:

$$\phi_i = \sum_k C_{ik}\chi_k \tag{2.120}$$

As in the HF formalism, a self consistent procedure is used to solve:

$$HC = \varepsilon SC \tag{2.121}$$

where the Hamiltonian H is:

$$H_{kl} = \left\langle \chi_k(r_1) \left| \frac{-\nabla^2}{2} - V_N + V_e + \mu_{XC}[\rho(r_1)] \right| \chi_k(r_1) \right\rangle \tag{2. 122}$$

and the overlap matrix S is:

$$S_{kl} = \left\langle \chi_k(r_1) \mid \chi_k(r_1) \right\rangle \tag{2. 123}$$

Those equations are solved iteratively using the following procedure:
An initial set of coefficients C_{ik} is chosen from which an initial set of molecular orbitals is constructed. Using Eq.2.101 the electron density ρ is calculated and using ρ, V_e and μ_{XC} are computed. It is now possible to build H_{kl} and to solve Eq.2.113 giving a new set of C_{ik}' coefficients from which a new set of molecular orbitals (and therefore a new electron density) is constructed, with which the new H_{kl}' will be built, etc. The

procedure is repeated until convergence criteria are met, that is when the difference between the electronic density from the step i and i+1 is inferior to a threshold value. When the convergence criteria are met, the total energy is computed using:

$$E_{TOT} = \sum_i \varepsilon_i + \left\langle \rho(r_1)\left[\varepsilon_{XC}[\rho] - \mu_{XC}[\rho] - \frac{V_e(r_1)}{2} \right] \right\rangle + V_{NN} \quad (2.\ 124)$$

As in the HF formalism, the convergence can be accelerated using the DIIS method developed by Pulay[36-37].

2.7 CONCLUSION

Today, molecular modelling is recognised as an important research tool in physics, chemistry, and biology. Many different methods exist that use different levels of approximation, depending on the need, the computational resources, and the time available. Methods based on molecular mechanics use the crudest approximations to describe the atoms and molecules of the system of study (using potentials) and their interactions (using a forcefield). Nevertheless, their speed and relatively good accuracy have made them very popular in all discipline of science, especially in the life sciences where the systems of study are commonly made of thousands of atoms. High accuracy is obtained using *ab initio* methods (Hartree-Fock, DFT, etc.) at high computational expense. Bond lengths or other geometric parameters obtained with those methods compete in accuracy with experiments (X-Rays, NMR, etc.). Amongst the vast variety of methods (and variants), two have been more detailed in the present chapter, namely the molecular dynamics (and in particular the CVFF forcefield as implemented in the code Discover) and the density functional theory (as implemented in the code DMol). Those two methods will be used in the following chapters to compute the electron affinity of atoms and molecules (chapter 3), to model the behaviour of the tridecane wax in the glass phase (chapter 4), and finally to examine the variation in electron affinity with the molecular conformation (chapter 5).

2.8 REFERENCES

[1] U. Burkert, N.L. Allinger. *Molecular mechanics.* (American Chemical Society, Washington, 1982).

[2] A.J. Pertsin, A.I. Kitaigorodsky. *The atom-atom potential method.* (Springer-Verlag, Berlin, 1987).

[3] I.G. Csizmadia, M.C. Harrison, J.W. Moskowitz, B.T. Sutcliffe. Theor. Chim. Acta. **6**, 191 (1966).

[4] S.F. Boys. Proc. Roy. Soc. (London), **A200**, 542 (1950).

[5] C.C.J. Roothan. Rev. Mod. Phys. **23**, 69 (1951).

[6] S. Huzinaga. J. Chem. Phys. **42**, 1293 (1965).

[7] K.E. Gubbins. *Application of molecular theory to phase equilibrium predictions. Model for thermodynamic and phase equilibrium calculations.* (Ed. S.I. Sandler, Marcel Dekker, New-York, 1994).

[8] J.M. Goodman. *Chemical applications of molecular modelling.* (RSC, 1998).

[9] K.B. Lipkowitz, D.B. Boyd. *Reviews in computational chemistry.* (Vol.1, 1991, Vol.2, 1991, Vol.3, 1992, Vol.4, 1993, Vol.5, 1994, Vol.6, 1995).

[10] M.F. Schlecht. *Molecular modelling on the PC.* (Wiley-VCH, 1998).

[11] W.J. Hehre, L. Radom, P. von R. Schleyer, J. A. Pople. *Ab initio molecular orbital theory.* (John Wiley & Sons, New-York, 1986).

[12] K.E. Gubbins, N. Quirke. *Molecular simulations and industrial processes: Methods, applications and prospects.* Current topics in molecular simulation. (Gordon Breach, 1996).

[13] N. Quirke. Molecular modelling and simulation: Tools for the modern era. Mol. Sim. In press. (2000).

[14] M. Born, J.R. Oppenheimer. Ann. Physik **84**, 457 (1927).

[15] S. Kirkpatrick, C.D. Gelatt Jr, M.P. Vecchi. Optimisation by simulated annealing. Science **220**, 671 (1983).

[16] W.H.Press, B.P. Flannery, S.A. Teukolsky, W.T. Vetterling. *Numerical recipes in Fortran.* (Cambridge University Press, 1992).

[17] R. Fletcher. *Practical methods of optimisation,* Vol. 1, *Unconstrained optimisation.* (John Wiley & Sons, 1980).

[18] Discover User Guide. (San Diego: Molecular Simulations, 1996).

[19] E. Polak. *Computational methods in optimisation: a united approach.* (Academic Press, San Diego, 1971).

[20] S.J. Weiner, P.A. Kollman, D.T. Nguyen, D.A. Case. An all atom forcefield for simulations of proteins and nucleic acid. J. Comp. Chem. **7**, 230 (1986).

[21] P. Dauber-Osguthorpe, V.A. Roberts, D.J. Osguthorpe, J. Wolff, M. Genest, A.T. Hagler. Structure and energetics of ligand binding to proteins: E. Coli dihydrofolate reductase-trimethoprim, a drug-receptor system. Protein Structure, Function and Genetics **4**, 31 (1988).

[22] A.R. Leach. *Molecular modelling, principles and applications.* (Addison Wesley Longman Ltd, 1996).

[23] W.C. Still, A. Tempczyk, R.C. Hawley, T.J. Hendrickson. J. Am. Chem. Soc. **112**, 6127 (1990).

[24] D.R. Lide. *Handbook of chemistry and physics.* (CRC Press, New-York, 1997).

[25] L. Verlet. Computer experiments on classical fluids.I. Thermodynamical properties of Lennard-Jones molecules. Phys. Rev. **159**, 98 (1967).

[26] R.W. Hockney. The potential caclculation and some applications. Methods in Computational Physics **9**, 136 (1970).

[27] H.J.C. Berendsen, J.P.M. Postma, W.F. van Guntersen, A. DiNola, J.R. Haak. Molecular dynamics with coupling to an external bath. J. Chem. Phys. **81**, 3684 (1984).

[28] S. Nosé. A molecular dynamics method for simulations in the canonical ensemble. Molec. Phys. **52**, 255 (1984).

[29] M.P. Allen, D.J. Tidelsley. *Computer simulation of liquids.* (Clarendon Press, Oxford Science Publications, 1987).

[30] H.C. Anderson. Molecular dynamics simulations at constant pressure and/or temperature. J. Comp. Physics **72**, 2384 (1980).

[31] M. Parrinello, A. Rahman. Polymorphic transitions in single crystals: A new molecular dynamics methods. J. Appl. Phys. **52**, 7182 (1981).

[32] R.G. Parr, W. Yang. *Density-functional theory of atoms and molecules.* (Oxford University Press, New-York, 1989).

[33] J.A. Pople, D.L. Beveridge. *Approximate molecular orbital theory.* (McGraw-Hill, 1970).

[34] V. Fock. Z. Physik **61**, 126 (1930).

[35] D.R. Hartree. Proc. Cambridge Phil. Soc. **24**, 89 (1928).

[36] P. Pulay. Chem. Phys. Lett. **73**, 393 (1980)

[37] P. Pulay. Improved SCF convergence acceleration. J. Comp. Chem. **3**, 556 (1982).

[38] P.A. Cox. *The electronic structure and chemistry of solids.* (Oxford University Press, 1987).

[39] F.C. Goodrich. *A primer of quantum chemistry.* (Wiley-Interscience, 1972).

[40] J.C. Slater. Atomic shielding constants. Phys. Rev. **36**, 57 (1930).

[41] M. Meunier, N. Quirke. The calculation of electron affinity of atoms and molecules. Mol. Sim. **23**, 109 (1999).

[42] C. Møller, M.S. Plesset. Note on approximate treatment for many-electron systems. Physical Review **46**, 618 (1934).

[43] M.J.S. Dewar, W. Thiel. Ground states of molecules.39. The MNDO method.Approximations and parameters. J. Am. Chem. Soc. **99**, 4899 (1977).

[44] P. Hohenberg, W. Kohn. Inhomogeneous electron gas. Phys. Rev. B **136**, 864 (1964).

[45] L.H. Thomas. The calculation of atomic fields. Proc. Camb. Phil. Soc. **23**, 542 (1927).

[46] E. Fermi. A statistical method for the determination of some atomic properties and the application of this method to the theory of the periodic system of elements. Z. Phys. **48**, 73 (1928).

[47] R.M. Dreizler, E.K.U. Gross. *Density functional theory. An approach to the quantum many-body problem.* (Springer-Verlag, Berlin, 1990).

[48] W. Kohn, L.J. Sham. Self-consistent equations including exchange and correlation effects. Phys. Rev. A **140**, 1133 (1965).

CHAPTER 3

ELECTRON AFFINITY

3.1 INTRODUCTION

Excess electrons and polarisation interactions are of great importance in physics, chemistry and biology. The electron affinity (EA) is an important molecular characteristic from both theoretical and practical points of view.[1-2] One of the fundamental notions in chemistry – electronegativity - is defined by means of electron affinity. Inductive effects in chemical bonding and electron donation properties are closely related to electron affinity. Charge-transfer complexes and their role in organic, biological, and catalytic processes represent a vast field of condensed-phase chemistry for which knowledge of electron affinities is of prime importance. The stability of the anions involved in single-electron transfer reactions, such as Birch reductions, depends both on the gas-phase electron affinity and on the solvation energy of the anion. Energy changes in redox reactions, for example ion-molecule reactions in upper layers of the atmosphere are also dependent on electron affinity.

The concept of electron affinity finds wide application in solid-state physics. For example, energies of crystalline lattices may be calculated using a Born-Haber cycle if the electron affinities of the constituent species are known. This can be seen in Figure 3.1, representing a complete cycle:

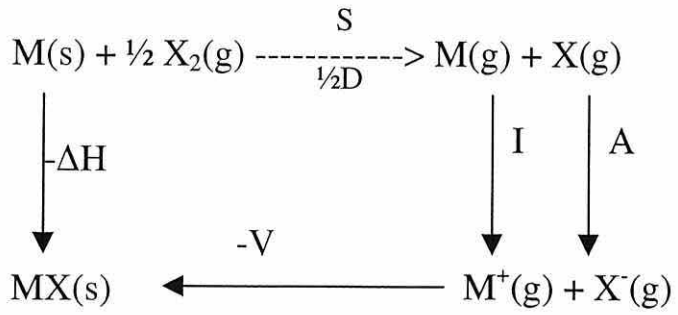

Figure 3.1 Born-Haber cycle describing the formation of one mole of solid alkali metal halide (MX) from the solid metal M(s) and ½ mole of gaseous elemental halogen $X_2(g)$.[3] ΔH is the heat of formation, V the lattice energy, I the ionisation energy and A the electron affinity.

Figure 3.1 shows that the lattice energy (V) can be obtained from the electron affinity and other energies using:

$$V = \Delta H + S + \tfrac{1}{2} D + I + A \qquad (3.1)$$

The electron affinity also plays an important role in radiation damage and light-detection technologies.[4] Bound or stable anions lie energetically below the ground state of their parent neutral form and can be studied by a variety of experimental methods (see section 3.1.2). Anions that lie energetically above the ground state of the neutral molecule (or atom) are called temporary anions since they are unstable with respect to electron detachment; moreover, their life-times are extremely short (usually less than a picosecond) and are usually measured by electron transmission spectroscopy.[1]

Despite the large number of techniques available to obtain electron affinities, the reliability of the results are still insufficient in many cases. Metastable anion lifetimes are sometimes so short that their detection by current experimental procedures is extremely difficult. Therefore, computational and theoretical treatments may serve as an alternative way of estimating electron affinities.

3.1.1 Definitions

The electron affinity of an *atom* is defined as the difference in total energy between the ground state of the neutral atom (plus the electron at rest at infinity) and its negative ion. The electron affinity of a *molecule* is defined as the difference in energy between the neutral molecule plus an electron at rest at infinity and the molecular negative ion when both the neutral molecule and the negative ion are in their ground electronic, vibrational, and rotational states. This electron affinity definition will be referred to as the *adiabatic* electron affinity:

$$EA_a = E(R_e) - E^-(R_e^-) \qquad (3.2)$$

where $E(R_e)$ is the total (ground state) energy of the neutral specie in its equilibrium geometry R_e and $E^-(R_e^-)$ is the total energy of the anion in its minimum energy geometry, R_e^-. The total energy of a molecule can be resolved into an electronic (E_{el}) and nuclear contribution, taken to be the vibrational ground state of the nuclear motion, the zero point energy (ZPE). The adiabatic electron affinity thus becomes:

$$EA_a = E_{el}(R_e) - E_{el}^-(R_e^-) + ZPE - ZPE^- \qquad (3.3)$$

The vertical attachment energy is defined as being the difference in energy between the neutral molecule in its ground state (plus an electron at rest at infinity) and its molecular negative ion formed by the addition of an electron to the neutral molecule without allowing a change in the inter-nuclear separation of the constituent nuclei.[5] This definition will be referred as the *vertical* electron affinity:

$$EA_V = E(R_e) - E^-(R_e) \qquad (3.4)$$

The total energies are calculated in the equilibrium geometry (R_e) of the neutral specie.

The vertical detachment energy (see figure 3.2) is defined as being the minimum energy required to eject the electron from the negative ion (in its ground state) without allowing the molecule to relax.

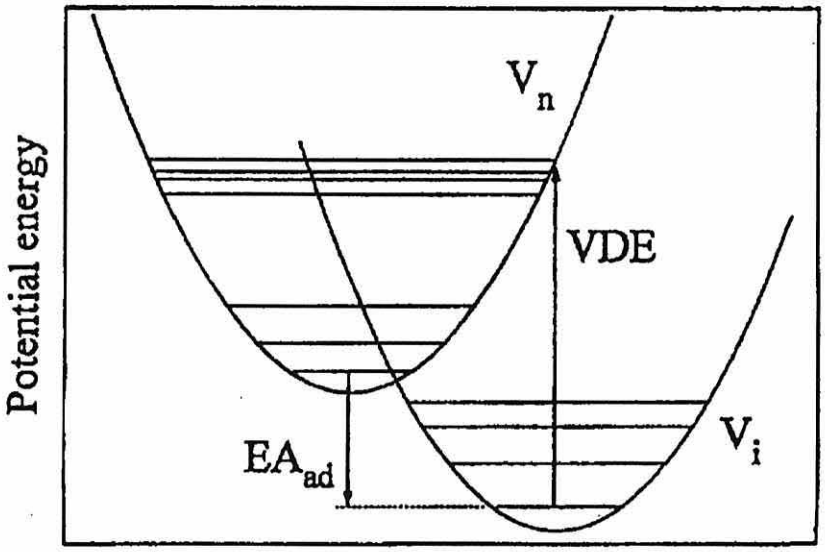

Figure 3.2 Adiabatic electron affinity and vertical detachment energy (V_n is the potential energy surface (PES) of the neutral molecule, and V_i the PES of the ionic molecule).[6]

According to Koopman's theorem, the electron affinity can also be obtained using molecular orbital energy calculations on the neutral molecule. In this case, the electron affinity is defined as being the negative of the energy of the lowest unoccupied molecular orbital (LUMO) of the neutral compound. This definition referred to as EA_{KT}, is similar to the vertical electron affinity definition:

$$EA_{KT} = -\varepsilon_{LUMO} \qquad (3.5)$$

In order to compute the adiabatic electron affinity using Koopman's theorem, the relaxation energy has to be added (as Koopman' s theorem does not take into account the electronic reorganisation due to the addition of an electron). The previous

definitions are valid not only for molecules but also for the solid state. The vertical attachment energy in this case is called the work function. The injected electron, in the case of insulator materials, goes into the conduction band. It may then, as will be demonstrated later, find a localised state inside the gap.

3.1.2 Experimental

Electron affinities can be measured (directly or indirectly) by a number of experimental techniques including laser photoelectron spectroscopy[7], electron transmission spectroscopy[8], and gas phase ion-molecule equilibrium.[9] Photon impact studies produced some of the most accurately known electron affinities for atoms, molecules, and radicals. Electron impact methods do not give as good energy resolution as photodetachment methods, but still give accurate results for most (positive) electron affinities. A complete review including thirty-one different techniques can be found in reference 5.

Despite the number of techniques available, the reliable determination of electron affinities still represents a considerable challenge, especially for large molecules where it may be difficult to use gas phase techniques. There is a particular difficulty where the electron affinity is negative and the anion is consequently short-lived (see reference 8 for a full discussion of the experimental techniques used to obtain electron affinities for temporary anions). This is the case for the alkanes discussed in section 3.3.3 where (with the exception of methane) gas phase methods such as electron transmission spectroscopy could not resolve the resonant states. There is a need for fast and reliable theoretical methods of calculating electron affinities.

3.2 METHODOLOGY

Ab initio methods of calculating electron affinities have been reviewed (to 1987) by Simons and Jordan[10] who point out the need for flexible basis sets and a careful treatment of electron correlation effects in order to obtain precise electron affinity

values. They state that 'it is extremely difficult to reliably calculate electron affinities within an accuracy of better than 0.2 eV for most classes of atoms and molecules' and call for the development of new theoretical and computational tools.

More recent ab initio work[11] using multireference configuration interaction singles and doubles (MRSD-CI) with specialised correlation-optimised and augmented basis sets applied to H, B, C, O and F obtained a root mean square deviation from recommended experimental values of the electron affinities of 0.05 eV, demonstrating that it is possible to achieve high accuracy for small atoms, albeit at considerable computational expense (see also reference 12). A detailed study of specialised exchange correlation functionals within density functional theory[13] reports average deviations of around 0.2 – 0.4 eV for atoms with atomic number less than or equal to 20.

Due to the complexity of the calculations, electron affinities for molecules are usually reported for individual species or small groups of related species. For example, electron propagator methods give excellent results[14] for the electron affinity of C_4^- (3.69eV compared to experimental results of 3.7 and 3.88 eV). For BO_2 the electron affinity is within 0.4 eV of the experimental data.[15] The use of semiempirical CNDO type calculations to explore unoccupied σ^* orbitals and hence estimate electron affinities for a number of small hydrocarbon and fluorocarbon molecules has been reported.[16] Reasonable agreement was obtained between calculated and experimental energies (see Table 3.3). There have been few assessments of the accuracy of DFT calculations of electron affinity for molecules. In 1992, Ziegler and Gutsev[17] reported non-local density approximation (NLDA, see chapter 2) calculations for 11 small molecules and found a rms deviation of ~0.3 eV (recalculated from Tables 2 and 5 of reference 17).

Although there has been a significant amount of work on both the measurement and the calculation of electron affinities for atoms, molecules, and clusters, there are not enough reliable data. The present research explores the use of density functional theory (as expressed in the widely available code DMol) to calculate electron affinities for a representative sample of small atoms and molecules having both positive and negative values of the electron affinity. The aim is to assess the accuracy of a routine DMol

calculation of electron affinity, i.e. a calculation that has not been tailored to a particular species. In addition, the electron affinity of alkanes and its variation with molecular conformation is investigated; this representing a subject little explored to date. Data on alkane electron affinities is central to new approaches to space charge and dielectric breakdown in polyethylene[18] (see section 1.5.3).

When computing electron affinities, special care has to be taken during the calculations. Firstly, the basis set must be large enough to represent the diffuse spatial extent of the outermost orbitals of the anion as the extra electron is only weakly bound in most cases. This is done by adding one or more sets of diffuse orbitals. These atomic orbitals are then able to describe properly the long-range behaviour of molecular orbitals with energies close to the ionisation limit. Because the computational cost varies as x^n (n=3-4) with the number of orbitals, these calculations are very time and CPU intensive.
Secondly, the electron correlation must be properly treated. The correlation energy of a given species is defined as the difference between the exact non-relativistic energy and the fully relaxed SCF energy. When using Hartree-Fock (HF) methods to compute electron affinities, a second step is necessary, which corrects the energy previously computed taking into account this correlation energy.[19] This is generally done by performing a configuration interaction (CI) calculation, where the excited states are included. This post-HF treatment requires both a lot of memory (storage of all the integrals in matrix form) and a lot of CPU time. This computational expense prohibits electron affinity computations for large systems using the (post) HF method. However, in the Density Functional Theory (DFT) calculations, the exchange-correlation treatment can be included in the first step of the calculation (see chapter 2). It is therefore possible to compute electron affinities of large systems whilst including correlation energies.

The third point to consider is the relativistic energies. These energies can be relatively important when dealing with heavy atoms, but one can neglect them when dealing with small organic molecules. In all the present electron affinity computations, a non-local density approximation has been used, namely the VWN[20] functional, together with the

Becke88[21] gradient-corrected exchange term and the PW91[22] gradient-corrected correlation term.

The correction to the gradient is performed on the last SCF cycle only. This has been chosen due to a software bug in DMol[23] when using the option to correct the gradient at every SCF cycle, especially in the hydrogen and chlorine cases where the computed results were in far disagreement with experimental results. This leads to less accuracy, but has the advantage of speeding up the calculations.

In DMol the basis set comprises the occupied atomic orbitals for the neutral atoms and for the +2 atomic cation, except for the hydrogen atom where a nuclear charge of +1.3 is used instead. This basis set is referred to as Double Numeric (DN). Adding a function on each atom with one angular momentum unit higher than that of its highest occupied orbital (i.e.: p for H, d for C) leads to a double numerical with polarisation function (DNP) basis set. This basis set is referred as DMol1 in the tables 3.1 and 3.2. Additional functions beyond the DNP basis set are available. A hydrogenic calculation with a nuclear charge of $+\zeta$ (variable for each system studied, see tables 3.1 and 3.2) provide additional s p and d orbitals. This basis set (DNP+) is referred to as DMol2 in tables 3.1 and 3.2. An example of an added hydrogenic function (1s) is given below:

$$\left(\frac{3}{4\pi}\right)^{\frac{1}{2}} \cos\Theta \times 2\left(\frac{\zeta}{a_0}\right)^{\frac{3}{2}} \exp\left(-\frac{1}{2}\left(\frac{2\zeta r}{a_0}\right)\right) \tag{3.6}$$

By varying ζ, the spatial extent of the orbital can be increased. This leads to diffuse functions when ζ is small compared to Z, the atomic number (e.g. less than 1 for H, less than 6 for C).

As functions are added to the basis set, they are orthogonalised with respect to those already in the set and are not included if linearly dependent. With Gaussian94 the basis sets were 6-31g**, 6-31++g** and 6-311++g**. Where appropriate post-HF treatments have also been employed. Two different numerical density grids have been used. The

XFINE (≈6000points/atom) parameter has been employed in the case of the atoms and the molecules, the FINE (≈3000points/atom) parameter for the alkanes. The SCF density convergence criteria was set to 10^{-6} (maximum density difference between two cycles), as very few change in energy results from smaller convergence criterion. The DIIS algorithm of Pulay[24] was utilised for faster convergence. The geometry optimisation convergence criteria were satisfied when the gradient was less than 10^{-4} Hartree/Bohr and when the energy change was less than 10^{-5} Hartree.

The ZINDO code[25] has been used to perform the electron affinity computation using semi-empirical techniques.

3.3 RESULTS

In this section the results of the computation of the electron affinity of atoms and molecules, including alkanes, using *ab initio* and semi-empirical methods are presented. Results for atoms are given first, followed by the results for the small organic molecules and finally, the results for the alkanes.

3.3.1 Atoms

The electron affinity of atoms from hydrogen (Z=1) to argon (Z=18) have been computed using the DFT. For comparison purposes, Table 3.1 also reports results from experimental work. The table has been divided into two parts, one for positive electron affinities and one for negative electron affinities. In the second part, results for the rare gas come from *ab initio* and semi-empirical calculations.[26]

Table 3.1 Electron affinity of atoms H to Ar, comparison with experiment

I-a. Positive electron affinities

Elements	EA$^{\partial}$	DMol 1	error	DMol 2	error	ζ parameter$^{\blacklozenge}$
H	0.75	-0.096	-0.846	0.741	-0.08	0.3*
Li	0.62	0.24	-0.38	0.42	-0.20	0.02
B	0.24	0.22	-0.02			
C	1.27	1.31	0.04			
O	1.46	1.21	-0.34	1.39	-0.07	3.0
F	3.34	3.26	-0.08			
Na	0.55	0.17	-0.38	0.41	-0.14	0.02
Al	0.46	0.40	-0.06			
Si	1.38	1.40	0.02			
P	0.74	0.47	-0.27	0.68	-0.06	1.0
S	2.08	2.00	-0.08			
Cl	3.61	3.54	-0.07			
RMSD			0.32		0.09	

I-b Negative electron affinities

Elements	EA$^{\partial}$	Dmol 1	error	DMol 2	error	ζ parameter$^{\blacklozenge}$
He	-0.22⊕	-10.78	-10.56	-0.28	-0.06	0.02*
Be	-0.19	-2.21	-2.02	-0.21	-0.02	0.02
N	-0.07	-0.75	-0.68	-0.08	-0.01	1.20
Ne	-0.3⊕	-28.02	-27.72	-0.38	-0.08	0.02
Mg	-0.22	-5.44	-5.22	-0.18	0.04	0.02
Ar	-0.36⊕	-12.86	-12.5	-0.38	-0.02	0.02
RMSD			13.3		0.05	

Note: Electron affinities in eV, $^{\partial}$ literature values taken from Ref. 27 (⊕ calculated). DMol1: VWN, B88, PW, DNP, xfine mesh, DMol 2: VWN, B88, PW, DNP++, xfine mesh, $^{\blacklozenge}$ Adjustable diffuse function orbital exponent, * Only s and p diffuse functions added.

3.3.2 Molecules

The electron affinity for twenty-six small organic molecules has been calculated, as shown on Table 3.2. In many cases the electron affinity quoted for a given molecule varied. The recommended values were taken from the most recent publications.[27-45]

Table 3.2 Adiabatic electron affinity of small molecules: comparison with experiment

II-a Positive electron affinity

Molecule	Rec. val.	reference	DMol1+ZPE	error	DMol2+ZPE	error	ΔZPE
NO	0.033±0.01	28	0.218	-0.185		-0.185	0.063
CH_3	0.08±0.03	29	0.142	-0.062		-0.062	0.062
P_2	0.23±0.23	30	0.576	-0.346		-0.346	0.016
O_2	0.451±0.007	31	0.264	0.187	0.504	-0.053	0.054
NH_2	0.744±0.022	32	0.879	-0.135		-0.135	0.099
SO_2	1.097	30	1.356	-0.259		-0.259	0.056
PH_2	1.25±0.03	32	1.158	0.092		0.092	0.028
OH	1.8276	33	2.045	-0.217		-0.217	-0.025
SH	2.319±0.01	34	2.302	0.017		0.017	0.002
CL2	2.38±0.1	35	2.782	-0.402		-0.402	0.042
BF_3	2.65	35	-0.556	3.206	2.744	-0.094	0.134
N_3	2.76±0.004	36	2.704	0.056		0.056	-0.046
F_2	3.08±0.1	35	3.569	-0.489		-0.489	0.089
NO_2	2.11±0.2	37	1.880	0.230	2.130	-0.020	0.060
HCO_2	3.498±0.015	38	3.161	0.337	3.261	0.237	0.021

Continued overleaf

(continued)

Molecule	Rec. val.	reference	DMol1+ZPE	error	DMol2+ZPE	error	ΔZPE
PO_3	3.5	39	4.349	-0.849		-0.849	-0.071
C_2	3.54	30	2.560	0.980	3.450	0.090	-0.020
OCN	3.6±0.2	40	3.430	0.170		0.170	-0.040
BO_2	4.25	41	4.020	0.230		0.230	-0.060
NO_3	3.77±0.25	39	3.325	0.445	3.405	0.365	-0.065
CN	3.821±0.004	42	3.547	0.274	3.797	0.024	0.007
RMSD				0.79		0.29	

II-b Negative electron affinity

Molecules	Rec. val.	Reference	DMol1+ZPE	error	DMol2+ZPE	error	ΔZPE
N_2	-1.9±0.1	43	-1.953	0.053		0.053	0.067
C_2H_4	-1.768	44	-1.68	-0.088		-0.088	
H_2	-0.78	44	-1.82	1.040	-1.04	0.260	0.140
CO	-1.8±0.1	45	-1.715	-0.085		-0.085	0.065
CO_2	-0.6±0.2	46	-0.712	0.112		0.112	0.088
RMSD				0.47		0.14	
						0.09°	

Note: All values in electron volts. DMol1: VWN, B88, PW, DNP. DMol2: VWN, B88, PW, DNP++, °excluding hydrogen.

3.3.3 Alkanes

Table 3.3 summarises the results for the linear alkanes (n-C_nH_{2n+2}) from methane (n=1) to hexatriacontane (n=36). The value for polyethylene (PE), which can be considered in the present study as an 'infinite' linear alkane, is also reported. Few experimental results can be found for alkanes in the literature. This is due to the difficulty of characterising the anionic form of the alkanes (see section 3.4).

Table 3.3 Alkanes (C_nH_{2n+2}): *ab initio* and semi-empirical estimates of electron affinities

n	Exp[∂]	DMol1	DMol1	INDO/2	MNDO	MNDO	CNDO[47]	Gaussian94 (Hartree-Fock)
		EA=ΔE adiabatic DNP/ VWN/ B88/PW	EA=ΔE vertical	EA=ΔE adiabatic	EA=ΔE adiabatic	EA= -LUMO vertical	EA= -LUMO vertical	EA=ΔE adiabatic 6-311G** /MP2
1 methane	-5.00	-2.87	-2.91	-7.48	-3.57	-4.38	-5.10	-3.76
2 ethane		-2.01	-2.05	-7.15	-3.07	-3.75	-4.50	-3.55
3 propane		-1.95	-1.97	-6.86	-2.72	-3.51	-4.60	-3.37
4 butane		-1.79	-1.80	-6.75	-2.68	-3.40	-4.30	
5 pentane		-1.67	-1.69	-6.66	-2.66	-3.35		
6 hexane		-1.58	-1.58	-6.54	-2.63	-3.31		
7 heptane		-1.51	-1.51	-6.52	-2.61	-3.25		
8 octane		-1.46	-1.45	-6.54	-2.60	-3.21		
9 nonane		-1.42	-1.40	-6.47	-2.61	-3.17		
10 decane		-1.37	-1.36	-6.47	-2.60	-3.15		
13 tridecane		-1.30						
15				-6.45				
20				-6.51	-2.60			
25				-6.45				
30				-6.51				
36 hexatriacontane	-0.3±0.5	-0.75	-0.75	-6.51				
PE	-0.5±0.5					-3.07		

Note: All values are in eV,∂ experimental data for methane 48, hexatriacontane 49 and polyethylene 50.

3.4 DISCUSSION

Tables 3.1 and 3.2 above show that electron affinity of atoms and small organic molecules can be computed with good precision using *ab initio* techniques, if special care concerning the basis set and the correlation are taken. Indeed, many references to the computation of electron affinity using various *ab initio* and semi-empirical techniques can be found in the literature that indicates agreement between experiment and theoretical work.[47-51-52-53] Depending on the relative energy between the neutral and anionic forms, electron affinity of atoms and molecules can be positive or negative. It can be seen from the results presented in the previous section that positive electron affinities may be computed with relatively good accuracy and without major difficulty. Problems arise whenever the electron affinity of the atom or molecule is negative. In this case the anionic system is metastable with respect to the formation of the neutral original parent plus the electron at infinity. This process is called autodetachment.

Metastable anions can be divided into two general types: shape resonance and core-excited resonance. In the former case the extra electron is attached to the molecule via a permanent induced dipole moment (examples are the ^2P anion state of Mg and the π^* states of N_2 and CO). This occurs when an incident electron with non-zero angular momentum is temporarily captured in the ground state of a molecule.[54-55] In the latter case, the electron is attached to an excited state of the neutral molecule.[56] These core-excited resonances (also referred to as two-particle one-hole[57]) can also be divided in two groups: Feschback resonances, when the energy lies below the excited neutral parent, and core-excited shape resonances, when the energy lies above their neutral excited parent (Figure 3.3).

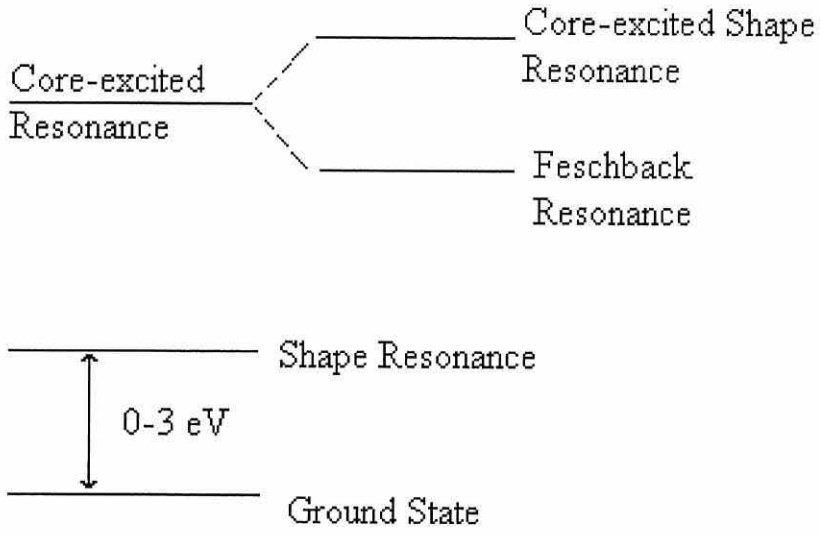

Figure 3.3 Resonances.

Experimentally, the main problem in characterising metastable anions comes from the short anion lifetime of the order of 10^{-13} to 10^{-16} second. For *ab initio* calculations, the problem lies mainly in the choice of the orbitals composing the basis set. For a molecule with a negative electron affinity, the diffuse functions monotonically lower the energy of the anion to that of the neutral molecule. This result represents the computational equivalent of electron autodetachment. However, it is possible to artificially stabilise such anion states by varying parameters in the Hamiltonian or through a judicious choice of functional and/or basis set such that *ab initio* calculations of negative electron affinities yield values consistent with experimental data.

The electron affinities of the first two rows of atoms (Z=1 to 18) and of 26 small organic molecules have been computed in the present study. Six atoms (He, Be, N, Ne, Mg and Ar) and five molecules (N_2, C_2H_4, H_2, CO and CO_2) have negative electron affinity. The energy of both the neutral and the anionic compound have been computed in each case with various basis sets. Functions, increasingly diffuse, have been added to the basis sets and the total SCF energies have been plotted (DMol2 in the tables). The energy of the neutral molecules is not largely affected by the addition of those diffuse functions. On the contrary, the SCF energy variation of the anions with the addition of those diffuse functions appears remarkable. Only slight variations are observed until the

point where the SCF energy suddenly drops and tends toward that of the neutral is reached. A typical curve representing the SCF energy variation is given below (figure 3.4):

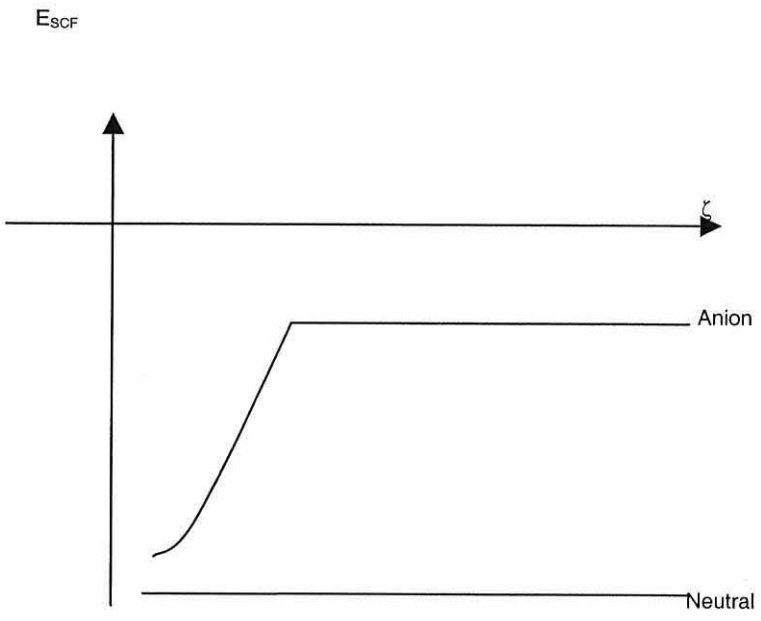

Figure 3.4 SCF energy variation, where ζ represents the diffuse character of the basis set (the smaller ζ the more diffuse the orbitals of the basis set).

Figure 3.4 shows that the energy of the anion first follows a plateau when ζ is lowered. It is this energy value which is used to compute electron affinities.

The DMol2 basis set has been used only when the error (DMol1 minus recommended value, see table 3.3-II) was greater than 0.1 eV and only when this value was negative. Indeed, when the electron affinity value computed with the DMol1 basis set, was greater than the value from the literature, this was due to the fact that the computed SCF energy of the anion is too low (too stable). In that particular case, the addition of diffuse functions could only stabilise further the anionic molecule and subsequently could only increase the error.

Being confident that this methodology could compute accurately the electron affinities (RMSD ~ 0.2 eV, in Table 3.2), the electron affinity of saturated linear alkanes (those molecules have all negative electron affinity) in their equilibrium vacuum geometry has been calculated.

Intermediate anion states of alkanes dissociate mainly via H^- elimination:

$$C_nH_{2n+2} + e^- \rightarrow (C_nH_{2n+2})^- \rightarrow C_nH_{2n+1} + H^-$$

According to Rowentree *et al.*[58] those transient anions are core-excited resonances. This means that the neutral parent molecule lying in an excited state traps the extra electron in the potential well of the ionic core. Jordan and Burrow[57] reporting unpublished work on methane and other alkanes stipulate the fact than "the extra electron must go into a Rydberg type orbital". The LUMO of the linear hydrocarbons is a σ^* orbital. These orbitals have been difficult to study by either theoretical or experimental methods.[47] They also report the absence of evidence of low-lying shape resonances due to capture of σ^* orbitals. The extra electron goes in an orbital of high energy, of the Rydberg type. Hence, this orbital is much higher in energy than the LUMO and therefore, Koopman's theorem could not be applied in this case. Or, to be more exact, the electron affinity could be linked to the negative of the energy of an orbital, but this orbital has to be the one accepting the extra electron, which in that case is not the LUMO.

In order to compute accurately the electron affinity of the alkane molecules, the excited states of these compounds should be computed first. Then, the extra electron can be added in an orbital of Rydberg type. This procedure could not be accomplished with the software used in this study. Instead, the extra electron has always been added in the LUMO of the neutral ground state of the molecule studied. Fortunately, there is a cancellation of errors in the procedure used here. The anion studied is too stable because its parent is in the ground state, but the correlation energy, due to the extra electron, is too high as the added electron is in an orbital too close from the parent core. Those two energy terms cancel partially each other, leading to a total energy value, hence an

electron affinity value, in good agreement with experiment. This is especially true for large molecules (i.e. hexatriacontane) where the energy due to the excitation or the correlation of the added electron, represents only a small percentage of the total energy. This accounts also for the difficulty, using this methodology in computing the electron affinity of small hydrocarbons like methane, where the previously cited energy terms represents a much greater percentage of the total energy.

If there is not a consensus on the dissociation attachment energy values (the results in literature show large discrepancies), the trend of decreasing resonance energy with increasing carbon chain length is well accepted. According to Dorman[59] "the degree of relaxation of the anion energy with increasing chain length is approaching an asymptote with n-butane". Both these results are confirmed in the DFT calculations which clearly show that the trend of decreasing electron affinity with increasing chain length, and that the main differences appear between the first four alkanes, after which the chain length effect seems to have reached a plateau. These results could be explained by the influence of the terminal methyl groups. As the terminal groups (e.g. CH_3) are assumed to be important in determining electron affinities, as the chain length increases the fraction of end groups in the chain becomes fractionally lower, the rate of change in electron affinity with chain length will reduce. Electron affinity calculations performed on the linear CF_3-$(CH_2)_n$-CF_3 show exactly the same tendency: that the electron affinity increases (becomes less negative) with n, proving again the lowering of the importance of the end-group (CF_3 here, CH_3 in the case of the alkanes) on the electron affinity with the chain length. Jordan and Burrow (1987) found that the alkyl-substituted ethylene anion is stabilised by large alkyl groups. They explain (quoting Dewar and Dougherty (1975)) that "as the size of the alkyl groups increases, so do their polarizabiliy, resulting in a greater stabilisation".

3.5 CONCLUSION

Electron affinity is an important molecular property in chemistry. Experimentally, the electron affinity values can be obtained via many different methods. Unfortunately, in many cases the value obtained depends on the method used. Also, the short lifetime of metastable anions makes their characterisation difficult.

Ab initio calculations can be used as an alternative way of obtaining electron affinity values. Among the *ab initio* methods available, the density functional theory appears to be a reliable tool to compute electron affinities. The results for the computation of the electron affinity of atoms and molecules (and in particular that of the alkanes) shown in the present DFT study are in fair agreement with experimental results found in the literature. Moreover, this method allows the study of large systems that could not be treated by standard Hartree-Fock methods using Gaussians atomic orbitals and a proper treatment of electron correlation.

3.6 REFERENCES

[1] P. Kebarle, S. Chowdhury. Electron affinities and electron-transfer reactions. Chem. Rev. **87**, 513 (1987).

[2] D. Pettifor. *Bonding and Structure of Molecules and Solids.* (Oxford Science Publications, Clarendon Press, 1995).

[3] N.H. March, J.F. Mucci. *Chemical Physics of Free Molecules.* (Plenum Press, New York, 1993).

[4] G.L Gutsev, L. Adamowicz. The structure of the $CF4^-$ anion and the electron affinity of the CF4 molecule. J. Chem. Phys. **102**, 9309 (1995).

[5] A.A Christodoulides, D.L McCorkle, L.G. Christophorou. *Electron molecule interactions and their applications.* (Academic Press, New York, vol. 2, 1984).

[6] Y. Bouteiller, C. Desfrancois, J.P. Schermann, Z. Latajka, B. Silvi. Calculation of electronic affinity and vertical detachment energy of the water dimer complex using the density functional theroy. J. Chem. Phys. **108**, 7967 (1998).

[7] E.H Kim, S.E. Bradforth, D.W. Arnold, R.B. Metz, D.M. Neumark. Study of HCO_2 and DCO_2 by negative ion photoelectron spectroscopy. J. Chem. Phys. **103**, 7801 (1995).

[8] K.D. Jordan, P.D. Burrow. Temporary anion states of polyatomic hydrocarbons. Chem. Rev. **87**, 557 (1987).

[9] P. Kebarle, S. Chowdhury. Electron affinities and electron-transfer reactions. Chem. Rev. **87**, 513 (1987).

[10] J. Simons, K.D. Jordan. Ab-initio electronic structure of anions. Chem. Rev. **87**, 535 (1987).

[11] R.A. Kendall, T.H. Dunning, R.J. Harrison. Electron affinities of the first-row atoms revisited. Systematic basis sets and wave functions. J. Chem. Phys. **96**, 796 (1992).

[12] J.J. Novoa, F. Mota, F. Arnau. Mono-and multireference Moller-Plesset computation of the electron affinity. A full configuration interaction analysis on first-row atoms and their hybrids. J. Phys. Chem. **95**, 3096 (1991).

[13] J.B. Krieger, J. Chen, Y. Li, G.J. Iafrate. Khon-Sham theory for orbital dependent exchange-correlation energy functionals: Application to the calculation of ionization potentials and electron affinities. Int. J. Quant. Chem. **29**, 79 (1995).

[14] J.V. Ortiz. Improved electron propagator methods: An investigation of C_4, C_4^-, and C_4^+. J. Chem. Phys. **99**, 6716 (1993).

[15] J.V. Ortiz. Electron propagator theory of BO_2 and BO_2^- electronic structure. J. Chem. Phys. **99**, 6727 (1993).

[16] E. Lindholm, L. Asbrink, S. Ljunggren. Energies of σ* orbitals. J. Phys. Chem. **95**, 3922 (1991).

[17] T. Ziegler, G.L.J. Gutsev. On the evaluation of molecular electron affinities by approximate density functional theory. Computational Chemistry **13**, 70 (1992).

[18] M. Meunier, N. Quirke, D. Binesti, G. Martic, J.M. Fourmigué. *Abstracts: Electrical Insulation and Dielectric Phenomena (CEIDP)*, Minneapolis (Oct. 1997), see also M. Meunier, N. Quirke, D. Binesti. Lecture *3rd International Conference on dielectric charge in solid insulators, CSC'3*. Tours (France) (June-July 1998).

[19] S. Baroni, E. Tucel. Exact-exchange extension of the local-spin-density approximation in atoms: Calculation of total energies and electron affinities. J. Chem. Phys. **79**, 6140 (1983).

[20] S.J. Vosko, L. Wilk, M. Nusair. Accurate spin-dependent electron liquid correlation energies for local spin density calculations: a critical analysis. Can. J. Phys. **58**, 1200 (1980).

[21] A.D. Becke. Density-functional exchange-energy approximation with correct asymptotic behaviour. J. Chem. Phys. **88**, 2547 (1988).

[22] J.P. Perdew,Y. Wang. Accurate and simple analytic representation of the electron-gas correlation-energy. Phys. Rev. **B45**, 13244 (1992).

[23] *DMol User Guide.* (Molecular Simulations Inc., San Diego, 1997).

[24] P. Pulay. Improved SCF convergence acceleration. J. Comp. Chem. **3**, 556 (1982).

[25] *ZINDO User Guide.* (Molecular Simulations Inc., San Diego, 1997).

[26] Journal of Physical Chemistry – Reference Data **14**, 731 (1985).

[27] J. Emsley. *The Elements.* (2nd edition, Oxford University Press, 1992).

[28] D.T. Alle, M.J. Brennan, S.J. Buckman. Low-energy total electron scattering cross section and electron affinity for NO. J. Phys. B: At Mol. Opt. Phys. **29**, L277 (1996).

[29] G.B. Ellison, P.C. Engelking, W.C Lineberger. An experimental determination of the geometry and electron affinity of CH3. J. Am. Chem. Soc. **100**, 2556 (1978).

[30] W. Von Niessen, L.S. Cederbaum, W. Domke. Excited States in Quantum Chemistry. (eds. Redial, Holland, 1979).

[31] M.J. Travers, D.C. Cowles, G.B. Ellison. Reinvestigation of the electron affinities of O_2 and NO. Chem. Phys. Letters **164**, 449 (1989).

[32] H.S.W. Massey. *Negatives Ions.* (3rd ed., Cambridge University, London, 1976).

[33] P.A. Schultz, R.D. Mead , P.L. Jones, W.C. Lineberger. OH^- and OD^- threshold photodetachment. J. Chem. Phys. **77**,1153 (1982).

[34] B. Steiner. Photodetachment of electrons from SH^-. J. Chem. Phys. **49**,5097 (1968).

[35] L.V. Gurvich, G.V. Karachevtsev, V.N. Kondratjev, Y.A. Lebedev, V.A. Medvedev. *Destruction Energies of Chemical Bonds. IP and Electron Affinity.* (Nauka, Moscow, 1974).

[36] E. Illenberger, P. Comita, J.I. Brauman, H.P. Fenzlaff. Experimental and theoretical investigation of the azide anion (N_3^-) in the gas phase. J. Phys. Chem. **89**,1026 (1985).

[37] K.M. Erwin, J. Ho, W.C. Lineberger. Ultraviolet photoelectron spectrum of NO_2^-. J. Chem. Phys. **92**, 5405 (1988).

[38] E.H. Kim, D.W. Arnold, S.E. Bredforth, R.B. Metz, D.M. Neumark. Study of HCO_2 and DCO_2 by negative ion photoelectron spectroscopy. J. Chem. Phys. **103**, 7801 (1995).

[39] L.N. Sidorov. Search and study of molecules with high-affinity to the electron. Uspekhi Khimii **51**, 625 (1982).

[40] J.V. Ortiz. Electron propagator theory of BO_2 and BO_2^- electronic structure. J. Chem. Phys. **99**, 6727 (1993).

[41] C.A. Wight, L.J. Beauchamps. Acidity, basicity, and ion/molecule reactions of isocyanide acid in the gas phase by ion cyclotron. J. Phys. Chem. **84**, 2503 (1980).

[42] D.W. Arnold, S.E. Bradforth, T.N. Kitsopoulos, D.M. Neumark. Vibrationally resolved spectra of C2-C-11 by anion photoelectron spectroscopy. J. Chem. Phys. **95**, 8753 (1991).

[43] A. Klein, R.P. McGinnis, S.R. Leone. Photodetachment threshold of CN- by laser optogalvanic spectroscopy. Chem. Phys. Letters **100**, 475 (1983).

[44] A.A. Christodoulides, D.L. McCorkle, L.G. Christophorou. *Electron molecule interactions and their applications.* (vol. 2, Academic Press, New York, 1984).

[45] N.S. Chu, P.D. Burrow, K.D. Jordan. Temporary anions of the fluoroethylenes. Chem. Phys. Letters **68**, 121 (1979).

[46] Y. Yoshioka, H.F. Schaefer, K.D. Jordan. Theoretical investigation of the electron affinity of CO_2. J. Chem. Phys. **75**, 1040 (1981).

[47] E. Lindholm, L. Asbrink, S. Ljunggren. Energies of σ^* orbitals. J. Phys. Chem. **95**, 3922 (1991).

[48] K. Rohr. Cross beam experiment for the scattering of low-energy electrons from methane. J. Phys. B. **13**, 4897 (1980).

[49] R. Dudde, B. Reihl. Complete electronic structure of oriented films of hexatriacontane. Chem. Phys. Letters **196**, 91 (1992).

[50] K.J. Less, E.G. Wilson. Intrinsic photoconduction and photoemission in polyethylene. J. Phys. C.: Solid State Physics **6**, 3110 (1973).

[51] R.A. Kendall, T.H. Dunning, R.J. Harrison. Electron affinities of the first-row atoms revisited. Systematic basis sets and wave functions. J. Chem. Phys. **96**, 796 (1992).

[52] J.J. Novoa, F. Mota, F. Arnau. Mono-and multireference Moller-Plesset computation of the electron affinity. A full configuration interaction analysis on first-row atoms and their hybrids. J. Phys. Chem. **95**, 3096 (1991).

[53] T. Ziegler, G.L.J. Gutsev. On the evaluation of molecular electron affinities by approximate density functional theory. Computational Chemistry **13**, 70 (1992).

[54] H.S. Taylor. Models, interpretations, and calculations concerning resonant electron scattering process in atoms and molecules. Advan. Chem. Phys. **18**, 91 (1970).

[55] L. Sanche, G.J. Schulz. Electron transmission spectroscopy: Resonances in triatomic molecules and hydrocarbons. J. Chem. Phys. **58**, 479 (1973).

[56] J. Simons, K.D. Jordan. Ab-initio electronic structure of anions. Chem. Rev. **87**, 535 (1987).

[57] K.D. Jordan, P.D. Burrow. Temporary anion states of polyatomic hydrocarbons. Chem. Rev. **87**, 557 (1987).

[58] P. Rowntree, L. Parenteau, L. Sanche. Dielectric polarisation invariance in dissociative electron attachment from condensed saturated hydrocarbons. J. Phys. Chem. **95**, 523 (1991).

[59] F.H. Dorman. Negative fragment ions from resonance capture processes. J. Chem. Phys. **44**, 3856 (1966).

CHAPTER 4

THE GLASSY WAX MODEL

4.1 INTRODUCTION

Although polyethylene (PE) has a very simple chemical composition CH_3-$(CH_2$-$CH_2)_n$-CH_3, it has a complex micro and meso structure. Polyethylene is semi-crystalline with the fraction of amorphous structure varying with the density and degree of crosslinking.[1] Crystallinity develops as spherical or spherulitic growths. The spherulites are composed of many lamellas which in turn are ribbon-shaped regions where the polymeric chains fold back and forth on themselves. Due to their length, the polymer chains go from one lamella to another, crossing amorphous regions and forming intercrystalline links. Such complexity on a range of scales is not treatable using the molecular modelling methods described in chapter 2. In order to probe the contribution of conformational disorder to electron trapping in polyethylene using molecular modelling, the condensed phases of much smaller linear alkane molecules has been considered instead, which for $n \geq 13$, where n is the number of carbon atoms, have a band structure very similar to polyethylene.[2-3]

In the present chapter, the local conformational disorder of segments of polyethylene in the amorphous regions is represented by configurations taken from computer generated glassy phases of the tridecane (n=13) wax (c.f. section 4.1.5). Glasses can be divided into four different types. The first and the most common, is the silicon glass whose composition is tetrahedral SiO_4. Other oxides such as SiO_2 or KO_2 can also be ranked in this category. The second category corresponds to the glass formed by organic molecules like alcohol or acetone. Polymers, and in particular polyethylene, belong to this category. Semi-conductors made of Ge, Se or S and their alloys (i.e. As_2Te_3)

compose the third kind of glass. Finally, ionic or partially ionic glasses such as $ZrCl_2$ compose the fourth type.
In this study, the focus will be on the second category of glass: the polymeric glasses.

4.1.1 Definitions

Cooling a liquid can lead to two different events according to the cooling rate: a low cooling rate will lead to crystallisation at a temperature T_m (temperature of melting), and a fast one to glass formation at temperatures below T_g (the glass transition temperature). Figure 4.1 below shows a typical glass volume change as the temperature is lowered. The change of slope (abrupt for crystallisation and gradual for glass formation) is noticeable. The vertical arrow illustrates the volume change accompanying the structural relaxation or stabilisation of the glass if held at temperature T_1. The temperature at which the glass transition occurs is rather ill defined and depends on the cooling rate. Indeed, this phenomenon is very complex and even now poorly understood.[4]

Glasses are amorphous materials, and as pointed out by Elliott[4] gives: "Amorphous materials do not posses the long-range translational order (periodicity) characteristic of a crystal. A glass is an amorphous solid that exhibits a glass transition." In turn, the glass transition can be defined as the change of state from the supercooled liquid to the glassy state.

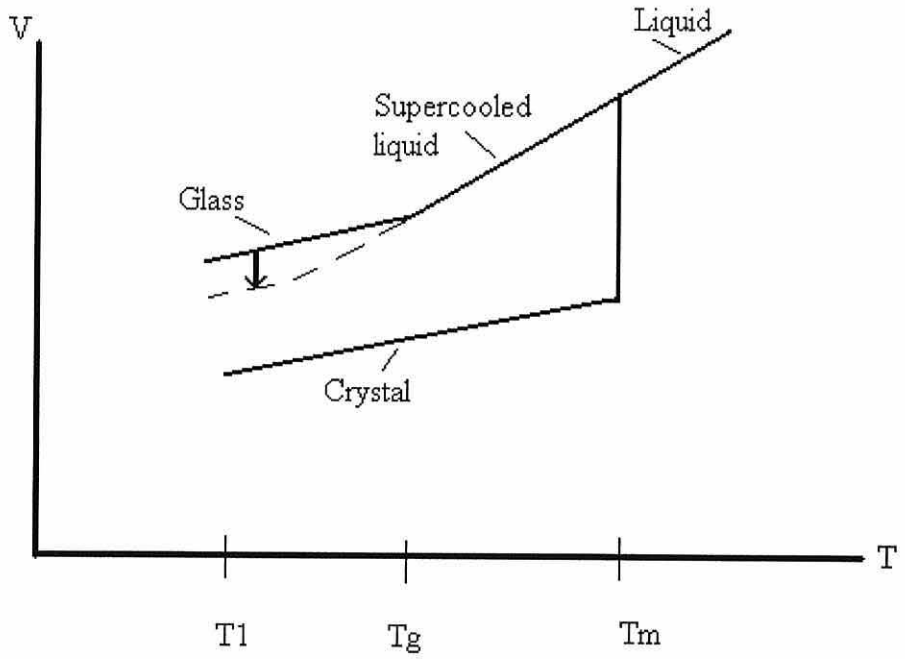

Figure 4.1 Schematic illustration of the change in glass volume with temperature as a liquid is cooled through the glass-transition temperature Tg (from ref. 4).

There exist two distinct steps during glass formation from a liquid: the kinetic glass transition and the calorimetric glass transition. Recent developments in the understanding of these processes have shown that the first step is a rather fast "freezing out" of long time-scale structural rearrangements which involves collective ("hydrodynamic"-like) motions of many molecules, over a narrow temperature range above Tg. The second step concerns more local rearrangements, involving only a few molecules jumping over potential energy barriers (an "activated" process), that are effectively quenched, on the time-scale of laboratory experiments, around Tg. This second stage leads to an incomplete exploration of available configuration space, on experimental time scales, which is reflected in the apparent discontinuities of thermodynamic properties, like the specific heat at constant pressure Cp.[5] This last point is of great importance in the present study of the particular case of polymeric glasses: as molecules (or "chains") are cooled down, they become trapped in amorphous configurations, which lead to the trapping of physical defects. One example is the *gauche defect* observed with polymeric chains; the energy barrier to relaxation to the

more stable trans conformation becomes too high to be overcome in the glassy state due to the steric constraints neighbouring molecules.

4.1.2 Polyethylene

A description of the structural properties of polyethylene has been given in Chapter 1. The reader will recall that polymeric materials such as polyethylene are defined as semi-crystalline. That is, they exhibit both crystalline and amorphous phases. Evidence can be seen from microscopic imagery as shown in Figure 4.2; the crystalline region appears in white and the amorphous in black.

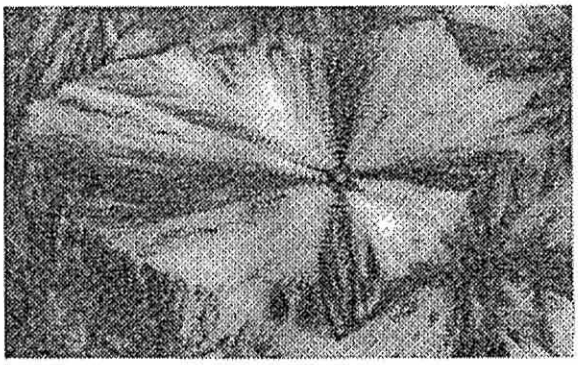

Figure 4.2 Microphotograph of the ringed spherulite texture of low-density polyethylene[6] (the crystalline region appears in white and the amorphous in black).

Polyethylene is composed largely of crystalline regions and the mechanical properties depend strongly on the degree of crystallinity. A polymer with little cristallinity is in general quite tough, but can be deformed relatively easily. As the amount of crystallinity increases, the material becomes more rigid, but also more brittle.[7]

4.1.3 Conformations

The term conformation refers to the spatial arrangement of the different parts of a chain. One conformation can be changed into another by rotating one part of a chain round the bond joining it to another.[8] This does not involve any bond breaking. The potential energy of a molecule is defined as the sum of many energy terms, including bond stretching, bond angle bending, etc. These are routinely computed using molecular mechanics tools (see Chapter 2). Plotting the potential energy values with respect to each degree of freedom of the molecules leads to a hyper-surface. Assuming that each molecule in a system studied possesses ν internal degrees of freedom, the configuration space spanned by $r_1 \ldots r_N$ will have dimension $(\nu+3)N$; (where $r_1 \ldots r_N$ are the position vectors associated with each molecule 1…N) and its possible conformations. This space contains an enormous number of local minima, each representing a mechanically stable arrangement of the molecules in three-dimensional space. General considerations[9] establish that in the thermodynamic limit the total number of local minima, Ω, grows asymptotically as follows[10]

$$\Omega \sim N!\exp(\alpha N) \tag{4.1}$$

where $\alpha > 0$, and N is the number of molecules.

It follows from the above discussion that the potential energy surface (PES) of a molecule is very complex. In the fluid phase, molecules can easily reach the region of the global minimum of this potential energy surface. In the solid phase, the packing of neighbouring molecules may prevent individual molecules from reaching their global minimum. This is particularly true for large molecules such as long polyethylene chains. In this case, molecules find themselves trapped in local potential minima.

4.1.4 Defects in polyethylene

In the crystalline region, the chains are well ordered. Nevertheless, there exist local irregularities[11-12] referred to as physical defects, dangling bonds, gauche and kink

defects or chemical defects, such as chemical impurities, industrial additives, etc. Also, the chains are so long that they usually belong to many spherulites, passing through the intervening amorphous phases. In the amorphous region, molecules can adopt many different conformations, more or less distorted. It is therefore in this part of the polymer that physical defects will occur most frequently. It is known that physical defects are partly responsible for the presence of localised states in the band structure of polyethylene[13], and it is also thought that these defects can trap electrons (*space-charges*).[14]

4.1.5 Molecular dynamics of polymeric glasses

Polyethylene crystalline morphology has been intensively studied over the past four decades. Unfortunately, though polyethylene is a rather simple and probably the best characterised polymer, many questions have not yet been adequately answered, especially the chain conformation in amorphous domains and the type of chain folding.[15]

Computer modelling, especially molecular dynamics simulation has recently emerged as a powerful new technique to complement both theoretical and experimental approaches.[16] However, the simulation of an entire amorphous phase of polyethylene is too large a system to be undertaken by molecular simulation due to limitations in computational resources available. In order to solve this problem two simplifications were deemed necessary: the first one is to reduce the size of the system studied by using waxes (the solid phase of linear alkanes) as a model of polyethylene chains. The second is to use a glass phase of those waxy materials as a model of the amorphous phase of polyethylene. This second approximation represents a large part of the work performed in the present study and is detailed in section 4.2. Indeed, polyethylene chains usually contain about 10^5 monomers of ethylene. Even the supercomputers of today cannot deal with such large molecules using first-principle methods. Fortunately, the electronic properties of polyethylene are similar to those of much smaller molecules: the alkane waxes. The tridecane (n-$C_{13}H_{28}$) wax is used as a model of polyethylene, as the

electronic properties of the two are very similar. Molecular dynamics simulations of the tridecane wax performed in this study are used to obtain the distribution of molecular conformations. The molecular modelling tools (such as energy minimisation, molecular dynamics) that have been utilised in this chapter were described in chapter 2. The results obtained will be used in Chapter 5 as inputs for *ab initio* calculations. The all-trans conformation will be employed as a reference for the state of lowest energy. Conformational distortions in the isolated tridecane molecule due to the simulation temperature, or due to neighbouring molecules in the glassy state, will also be examined. Chapter 5 explains the effects on the electron affinity of these conformational distortions. Section 4.2 describes the methodology employed to produce glassy phases of the tridecane wax.

4.2 METHODOLOGY

The crystalline region of the polyethylene is modelled by a crystalline cell of the n-$C_{13}H_{28}$ wax, and the amorphous part of the polyethylene is modelled by a glass phase of the n-$C_{13}H_{28}$ wax (figure 4.3).

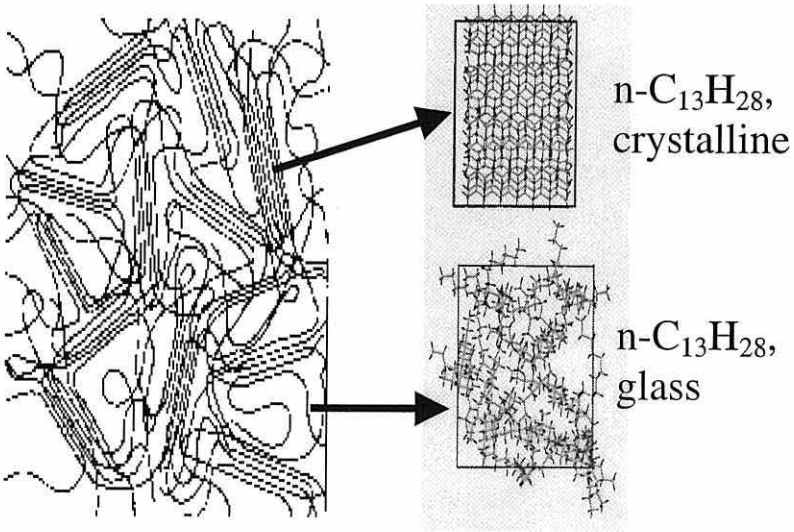

Figure 4.3 The model material. The crystalline region of the polyethylene is modelled by a crystalline cell of the n-$C_{13}H_{28}$ wax, and the amorphous part of the polyethylene is modelled by a glass phase of the n-$C_{13}H_{28}$ wax.

Reproducible disordered phases are obtained either by generating a glass phase by rapid cooling from the liquid state using molecular dynamics simulation or using a Monte Carlo procedure (Amorphous-Cell[17]) to generate an amorphous system. Results have been generated for several densities; 0.7564 g/cm^{-3}, the density of crystalline tridecane[18], 0.95 and 0.96 g/cm^{-3}, the density of high-density polyethylene and for two system sizes N=25 and 50 (N is the number of tridecane molecules in periodic boundaries). Simulation data are summarised in table 4.1.

The low-density simulations (Glasses A_1-A_5) were started from a crystalline phase of tridecane, with the cell parameters appropriate to crystalline polyethylene[19] and density 0.7564 g/cm^3. The cell contained 25 molecules in periodic boundary conditions using the CVFF forcefield[20] implemented in the code Discover.[21] CVFF represents both bonded (bond stretch, angular distortion, etc.) and non-bonded or dispersion interactions. Molecular dynamics simulations were performed in both canonical (constant N, V, T) and micro-canonical (constant N, V, E) ensembles. The canonical ensemble was used initially to fix the temperature of the system. The NVE ensemble was used for data collection so that the system is not perturbed by temperature rescaling.[22] The system was cooled from 1500 K in a sequence of four simulations at 1,200 K, 900 K, 600 K, and 300 K. The series was terminated by a simulation at 150 K (assumed to be below the T_g of tridecane or polyethylene: 184 K from simulation[23], 253 K from experiment[24]). All simulations consisted of 25 ps of NVT dynamics and 25 ps of NVE dynamics with a fixed time step of 1 fs. The radial distribution function of the carbon atoms at 150 K is shown in Figure 4.4. The first peak corresponds to the distribution of distances between covalent carbon atoms at R_{P1}=1.54 Å. The second peak corresponds to the distribution of distances between intrachain second-neighbour carbon atoms at R_{P2}=2.6 Å and the third peak to intrachain third-neighbour carbon at R_{P3}=3.8 Å. The shoulder arising just before the third peak is due to the deviation of the dihedral angle from the equilibrium value (i.e. to gauche defects) leading to shorter intrachain third-neighbour distances (see section 4.3). The interchain disorder can be seen in figure 4.4 for R> 4 Å, where the structural disorder in the glass has averaged out subsequent peaks that would be present in the crystal.

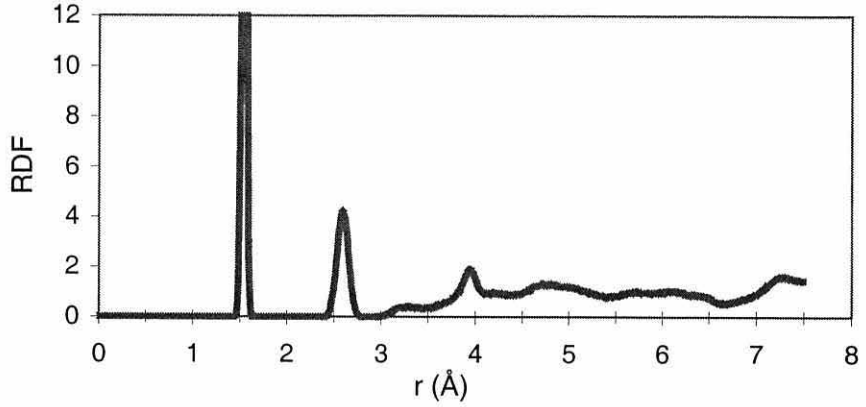

Figure 4.4 Computed Carbon-carbon radial distribution function in the low-density glass phase (A_1) at 150 K.

Figure 4.5 shows the mean square displacement (MSD) of tridecane molecules as the temperature is lowered and Table 4.2 reports the diffusion coefficient obtained from the gradient of the mean square displacement at long times.

When a molecular dynamics run is performed, the trajectory of each atom in the system can be stored. From this trajectory file, the mean square displacement can be computed as follows:

$$MSD(m) = <| r(t) - r |^2> = \frac{1}{n} \sum_{i=1}^{n} | r(m+i) - r(i) |^2 \qquad (4.2)$$

where

$0 < m+n = k$;

m is the maximum number of points allowed for the MSD calculation;

n is the number of data points used for averaging;

i represents the increments

k is the total number of snapshots read in.

The self-diffusion constant (D) was obtained from the slope of the mean square displacement in time t of the molecular centre of mass r(t) using the Einstein relation:

$$D = \frac{1}{6Nt} < | r(t) - r |^2 > \tag{4.3}$$

where

N is the number of atoms;

r is the position of the particle;

t denotes the time.

The expression within the braces is the MSD. The self-diffusion constant is obtained by calculating the slope of the MSD against time. It measures the average displacement of a given set of atoms or molecules giving an insight of the transport properties of the material.

By 150 K the diffusion coefficient is effectively zero (Table 4.2). In what follows we use the glassy conformations from the simulation at 150 K (chosen to ensure that the simulations are well below the glass transition of the model) as representative of local conformational disorder in polymeric insulators at room temperature. In the present calculations, this methodology has been applied five times to generate five different glass configurations.

In addition, high-density phases (B, C, D) of tridecane were prepared using the following methods:

(a) Glass B: A low-density configuration was compressed using NPT (constant pressure P) ensemble simulation at 4Gpa to the required density using the code Discover.[21] The simulation comprised of 125 ps of equilibration and 75 ps for data collection, at 150 K.

(b) Glasses C and D: the code Amorphous Cell[17] was employed to create amorphous tridecane configurations at 0.95 g/cm^{-3} using N=25 (Glass C) and N=50 (Glass D). Amorphous Cell generates an amorphous phase using a two-stage process. In the first stage, isolated tridecane chain configurations were generated using rotational

isomeric state (RIS)[25] probabilities. The second stage used a Monte Carlo algorithm to distribute the chosen number of molecules in a cell at a chosen density and combines both molecular dynamics and geometry optimisation to obtain a realistic configuration. The (high-density) glassy phases were obtained using the quenching methodology described previously for low-density simulations, with the difference that the initial temperature (before quenching) was set to 900 K for N=50.

(c) An orthorhombic crystalline phase of tridecane (with a density of 0.9641 g/cm^{-3} corresponding to crystalline polyethylene[19]) was simulated at T=150 K to make it possible to compare amorphous and ordered phases of n-$C_{13}H_{28}$. The simulation ran for 100 ps (NVT) to achieve equilibration and 100 ps (NVE) for data collection.

Table 4.1 Simulation data for solid alkanes.

	N	Density (g/cm^{-3})	Initial Configuration	Simulation ensembles
Glass A_1-A_5	25 (x5)	0.7564	Crystal	NVT/NVE
Glass B	25	0.9611	Glass A_1 (see text)	NPT
Glass C	25	0.9500	Amorphous	NVT/NVE
Glass D	50	0.9500	Amorphous	NVT/NVE
Crystal	25	0.9641	Crystal	NVT/NVE

Table 4.2 Variation of the diffusion coefficient ($Å^2$/ps per atom) with temperature for alkanes.

Temperature (K)	Glass A_1	Glass B	Glass C	Glass D
1500	0.1208		0.0284	
1200	0.0605		0.0095	
900	1.13E-02		3.07E-03	
600	4.43E-03		4.96E-04	
300	4.39E-04		2.77E-04	
150	2.68E-06	1.59E-05	1.16E-06	1.78E-06

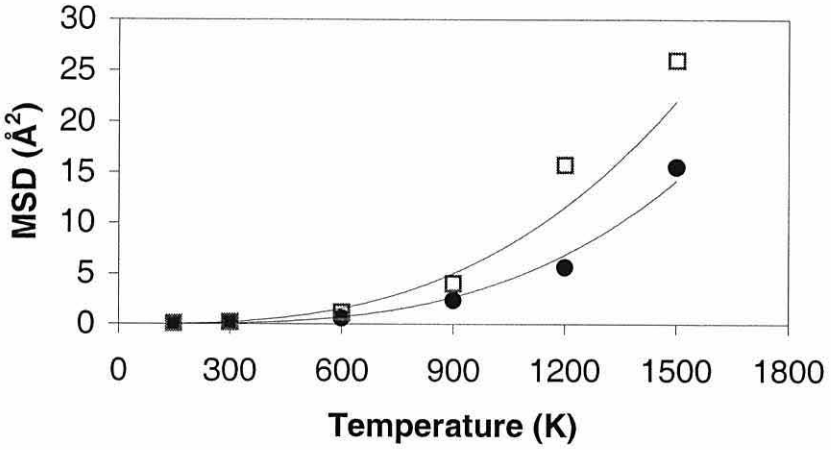

Figure 4.5 Variation of the mean-square displacement with temperature for alkane glasses (Glass A_1, • Glass C).

Two criteria are commonly applied to the results of molecular dynamics simulations to determine whether a glass has been formed: (i) the presence of liquid-like disorder and (ii) that diffusion should have effectively stopped ($D \approx 0$).[22] Visual inspection of the final configuration obtained in glasses A_1-A_5 shows that an amorphous phase is obtained (that is, the initial crystal configuration has been lost). This can also be seen in the absence of peaks in Figure 4.4 after 4 Å reflecting a disordered structure similar to that of a liquid state. Systems B, C, and D start from amorphous configuration. Diffusion coefficients at 150 K are very low (~ 1E-06, Table 4.2). Typical diffusion coefficients of small organic molecules in liquids at 298 K are ~ 0.1 $Å^2$/ps.[18] By these criteria, our simulations represent glassy phases of tridecane. For our purpose, the most important feature of these glasses is the constraint the fixed disorder imposes on the accessible conformational space of a molecule. In Chapter 5 we will use the individual molecular conformations found in the disordered states of tridecane to calculate electron affinities and finally trap energies and residence times (Chapter 6).

4.3 RESULTS AND DISCUSSION

In this section, the average structural properties of tridecane molecules in the glassy state are discussed and compared with their properties in the crystal. The equilibrium carbon-carbon bond distance used by the CVFF force field is equal to 1.526 Å. Previous molecular dynamics simulations of linear waxes have used a carbon-carbon bond distance of 1.52 Å[26,27], and 1.53 Å.[28] The experimental value (determined from x-ray studies for hexatriacontane) is 1.527±0.007Å.[29] The difference in average bond lengths in glassy and in crystalline phases determined in our simulations are reported in Table 4.3.

The distributions of dihedral angles in the glass and in the crystalline phase are compared in Figure 4.6. The glass simulations have a significant population of gauche defects (60°), the crystal (at the same temperature) has very few.[30] The high-density and the low-density simulations give similar chain dihedral angle distributions.

Table 4.3 Average bond lengths in solid alkanes.

	<d C-C> (Å)
Glass A_1-A_5	1.541
Glass B	1.537
Glass C	1.541
Glass D	1.539
Crystal	1.532

It has been suggested[31] that carbon-carbon bond lengths in alkanes expand as a function of dihedral angle due to increasing H-H repulsion (Figure 4.7). The results for the n-$C_{13}H_{28}$ wax presented in Table 4.3 are consistent with this interpretation in that the presence of gauche defects in the glass leads to average carbon-carbon bond lengths greater in the case of the amorphous phase than in the crystal phase, at 150 K (Figure 4.8).

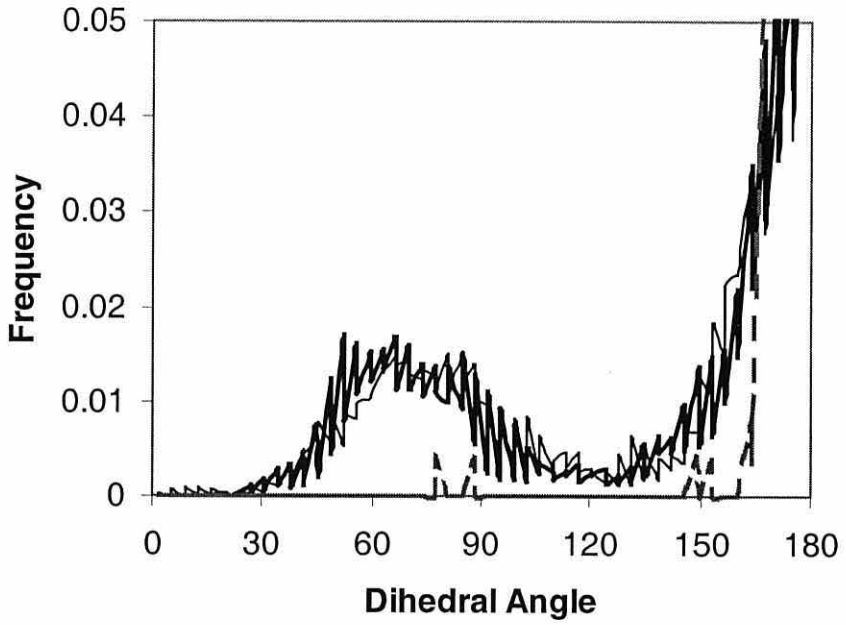

Figure 4.6 Chain dihedral angle distribution (thick line: Glass A_1, thin line: Glass C, dashed line: crystal phase). Angles in degrees.

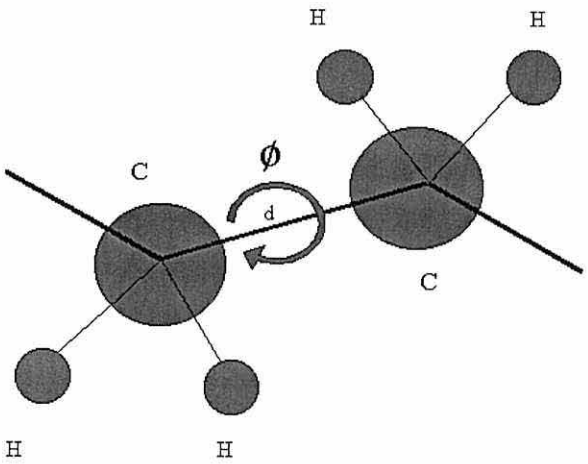

Figure 4.7 Schematic representation of a fragment of a polyethylene chain. As ϕ varies, the hydrogen-hydrogen atomic overlap increases and, therefore, d increases to reduce the bond energy.

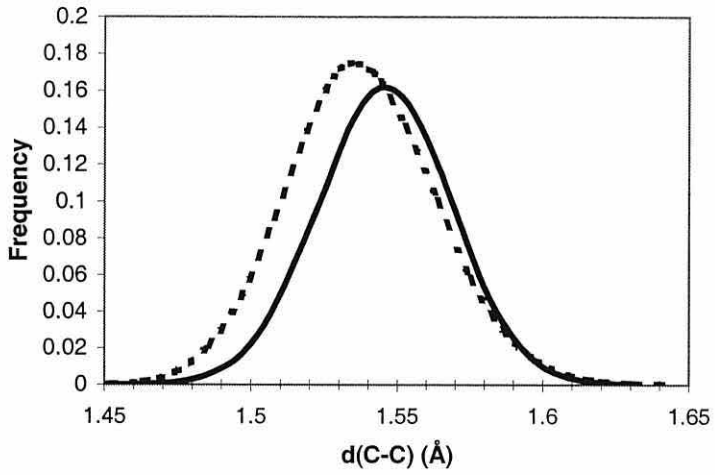

Figure 4.8 Covalent (nearest neighbour) carbon-carbon bond length distribution at 150 K in the crystal phase (dashed line) and in the glass phase (high and low density, solid line).

After the quenching procedure described above, the local energy minima of each molecule in the glassy state has been examined. The aim of the present study is to produce a set of different conformers of the tridecane molecule, treated as a model of polyethylene. The electron affinity (EA) of these conformers will be computed in the Chapter 5. When computing the electron affinity, the energy difference between the neutral molecule and the energy of the anionic molecule is performed (see Chapter 3) using:

$$EA = E^{Total}_{neutral} - E^{total}_{anionic} \qquad (4.4)$$

In order to obtain $E^{Total}_{neutral}$ from molecular dynamics simulations, one has to minimise the energy of the conformers obtained from the run. Molecules taken from molecular dynamics simulations will not have a configuration corresponding to the local minimum energy but to some thermal fluctuation about $E(R_e)$ (Eq. 3.2). Only local minima are retained for quantum mechanical calculation of vertical electron affinity. We believe that different local minima lead to different values of the vertical electron affinity (this will be demonstrated in Chapter 5). The excess electron that has the choice between different conformations of the molecules trapped in the amorphous phase will

preferentially stay where the electron affinity is the higher. (We assume that the excess electron does not stay in the vacuum but goes into the conduction band of one molecule).

The local potential minimum of each molecule was obtained using the following geometry optimisation procedure (simulated annealing): a molecular dynamics simulation at high temperature was run for 5 picoseconds, followed by a geometry optimisation (using successively the steepest descent and conjugate gradient algorithms). The lowest minimum will then be used as input for the *ab-initio* computation in the next chapter. There are two limitations with the present methodology: the first is that this procedure is very time-consuming, and the second is that one can never be certain of finding the global minimum. Nevertheless, in our case, the same minimum energy value has consistently been found many times for the conformers studied. However, in some cases, only one minimum energy has been found. A refinement of this method that has been tried on a few cases is to increase the length of time for the simulated annealing procedure. The energy minima found using these longer simulations were never lower than those in the previous calculations by more than 1 kcal/mol. It appears therefore, that the number of steps we have used in our simulated annealing procedure is a good compromise between simulation time and accuracy. Simulated annealing has been successful in finding low energy conformations for amino acid dipeptides.[32] For a complete review of the different methods used in global optimisation in chemistry, see Chapter 2 and reference 33.

As shown in figure 4.8, at 150 K, the average carbon-carbon bond length is greater in the glass phase than in the crystal phase due to the presence in the glass phase of gauche defects. It follows that the average carbon-carbon bond lengths of the tridecane wax trapped in local conformational energy minima in the glass phase is expected to be greater than the equilibrium bond length. This pattern is confirmed by the data plotted in Figure 4.9 for the bond lengths after annealing.

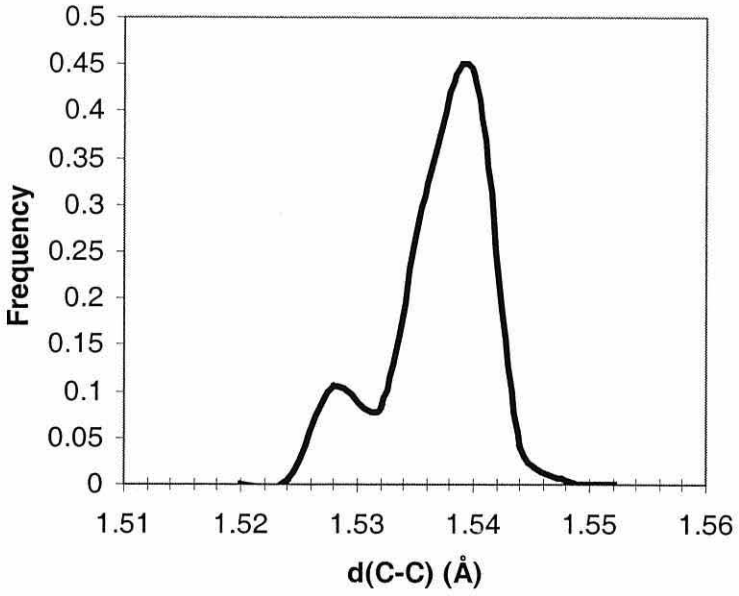

Figure 4.9 Covalent (nearest neighbour) carbon-carbon bond length distribution after the application of the simulated annealing procedure in the glass phase.

The shoulder at 1.528 Å in Figure 4.9 corresponds to $-\underline{C}H_2-\underline{C}H_3$ (end-of-chain) carbon-carbon bonds.

4.4 CONCLUSION

The results presented in this chapter demonstrate that molecular dynamics simulations allow a detailed analysis of the conformational properties of the tridecane wax. The quenching methodology applied to crystalline cells of the wax has led to the formation of a glassy state. This is demonstrated by the size of the self-diffusion constant and the radial distribution function. The glassy phase of the tridecane wax is used as a model of the amorphous phase of polyethylene. A simulated annealing procedure has been used to find the local potential minima of the tridecane chains. The waxy chains present some conformational disorder such as gauche defects. The disorder induced by the glassy state leads to an increase in the average carbon-carbon bond length. This relaxation phenomenon is explained by the increase in the hydrogen overlap when the chain

dihedral angle differs from its equilibrium value. The consequence for the electronic properties of the wax will be described in the next chapter.

4.5 REFERENCES

[1] L A. Dissado, J.C. Fothergill. *Electrical Degradation and Breakdown in Polymers,* (Peter Peregrinus Ltd., London, 1992).

[2] C. Laurent, C. Mayoux. Electronic Processes in Electrical Ageing. (Arpeggio Seminar, 1994).

[3] J.J. Pireaux. Phys. Rev. A **14**, 2133 (1976).

[4] S.R. Elliott. *Physics of amorphous materials.* (Harlow: Longman Scientific & Technical, 2nd edition, 1990).

[5] J.P. Hansen. The kinetic glass transition: what can we learn from molecular dynamics simulation? Physica A **201**, 138 (1993).

[6] D. Marsacq, P. Hourquebie, L. Olmedo, H. Janah. Effects of structural parameters of polyethylene on space charge properties. Abstratcs CSC'2 Space charge in solids dielectrics, **275**, 432 (1995).

[7] E.A. Colbourn, J. Kendrick. *Computer simulation of polymers, chapter 4: molecular modelling of crystalline polymers.* (Ed. E.A. Colbourn, 1994).

[8] P.W. Atkins. *Physical Chemistry.* (5th ed., Oxford University Press, 1994).

[9] F. H. Stillinger, T.A. Weber. Physical Review A **25**, 978 (1982).

[10] F. H. Stillinger, Interaction potentials and inherent structures in liquids, glasses, and crystals. Physica D **107**, 383 (1997).

[11] G.L. Liang, D.W. Noid, B.G. Sumpter, B. Wunderlich. Gauche defects, positional disorder, dislocations, and slip planes in crystal of long methylene sequences. J. Phys.Chem. **98**, 11739 (1994).

[12] G. Strobl, B. Ewen, E.W. Fischer, W. Piesczek. Defect structure and molecular motion in the four modifications of n-tritriacontane.I. Study of defect structure in the lamellar interfaces using small angle x-ray scattering. The Journal of Chemical Physics **61**, No. 12 (1974).

[13] N.F. Mott; Phil. Mag. **22**, 7 (1970).

[14] H.J. Wintle. *Conduction Processes in Polymers. Engineering Dielectrics volume IIA, Electrical properties of solid insulating materials: Molecular structure and electrical behaviour.* (Bartnikas/Eichhorn editors, 1983).

[15] Q. Liao, J. Xigao. Formation of segmental clusters during relaxation of a fully extended polyethylene chain at 300 K: A molecular dynamics simulation. J. Chem. Phys. **110**, 8835 (1999).

[16] H. Takeuchi, RJ. Roe. Molecular dynamics simulation of local chain motion in bulk amorphous polymers. I. Dynamics above the glass transition. J. Chem. Phys. **94**, 7446 (1991).

[17] *Amorphous-cell User Guide.* (Molecular Simulations Inc., San Diego, 1996).

[18] D.R. Lide. *Handbook of Chemistry and Physics.* (76th edition, CRC Press, 1995-1996).

[19] S. Kavesh, J.M. Schultz, J. Polymeric Science Part A-2 **8**, 243 (1970).

[20] P. Dauber-Osguthorpe, VA. Roberts, DJ. Osguthorpe, J. Wolff, M. Genest, AT. Hagler. Structure and energetics of ligand binding to proteins: E. Coli dihydrofolate reductase-trimethoprim, a drug-receptor system. Protein Structure, Function and Genetics **4**, 31 (1988).

[21] *Discover User Guide.* (Molecular Simulations Inc., San Diego, 1996).

[22] S. Gruenhut, M. Amini, D.R. Macfarlane, P. Meakin, Molecular Simulation **19**, 139 (1997).

[23] R.J. Roe, J. Chem. Phys. **100**, 1610 (1994).

[24] J.A. Brydson. *Polymer science.* (A.D. Jenkins, North Holland, 1972).

[25] R.A. Scott, H.A. Scheraga. J. Chem. Phys. **44**, 3054 (1966).

[26] D. Rigby, R.J. Roe. J. Chem. Phys. **87**, 7285 (1987).

[27] D. Rigby, R.J. Roe. J.Chem.Phys. **89,** 5280 (1988).

[28] G.D. Smith, Do.Y. Yoon. J.Chem.Phys. **100**, 649 (1994).

[29] S. Kavesh, J.M. Schultz. J. Polym. Sci. Part A-2 **8**, 243 (1970).

[30] G.L. Liang, D.W. Noid, B.G. Sumpter, B. Wunderlich. J. Phys. Chem. **98**, 11739 (1994).

[31] D. Steele. J. Chem. Soc. Faraday Trans. **2**, 1077 (1985).

[32] S.R. Wilson, W. Cui. Applications of simulated annealing to peptides. Biopolymers **29**, 225 (1990).

[33] K.B. Lipkowitz, D.B. Boyd. *Reviews in computational chemistry.* (Vol.1, 1991, Vol.2, 1991, Vol.3, 1992, Vol.4, 1993, Vol.5, 1994, Vol.6, 1995).

CHAPTER 5

EFFECT OF MOLECULAR CONFORMATION ON ELECTRON AFFINITY

5.1 INTRODUCTION

It is known that physical defects are partly responsible for the presence of localised states in the band structure of polyethylene[1], and it is also thought that these defects can trap electrons (*space-charge*).[2] In this chapter, the electron affinity of molecules trapped in conformational disorder (*physical defect*) is examined. The effect of bond length distortions in ethane and propane on the electron affinity is described. This allows a better understanding of the effect of physical disorder (modelled by glassy phases of tridecane wax) on the electron affinity of this model material. Chapter 6 is devoted to the computation of the trap energies assumed to be responsible for the presence of space charge in the material.[3-4] These trap energies are defined as the difference between the electron affinity of the constrained molecule and the electron affinity of the all-trans conformer, both in vacuum.

A unique feature of alkane molecules is their flexibility around the carbon backbone[5] and one consequence of this is that their electronic structure is dependent upon their molecular conformation. Previous theoretical and experimental work by Seki et al.[6] has demonstrated that the occupied states are similar in the extended (planar all-trans) and in the random-coil (liquid) chains whereas the unoccupied states displayed drastic changes between crystalline and molten phases. The authors have also demonstrated that in the case of the hexane molecule (n-C_6H_{14}) "the deviation of the electronic structure from that of the all-trans conformer increases with increasing number of

gauche bonds in a molecule". This effect decreases with increasing chain length, due to the relative contribution of each bond to the total electronic structure. However, if the number of gauche defect increases as well as the chain length the same effect is regained. It is known from experimental spectra (e.g. UV, IR) that amorphous and crystalline phase coexist in polyethylene, however it is difficult to separate the origin of each peak experimentally. The alkanes offer an alternative, as it is possible to obtain purely extended as well as purely entangled chains.[6]

The polyethylene polymer is a standard test case for new developments in techniques for calculating the electronic structure of polymers due to its simple chemical nature. Numerous papers report calculations on this quasi-ideal polymer. They include *ab-initio*[7-8] and semi-empirical calculations.[9-10] Comparisons between experiment and calculations on the electronic properties of the polymer can also be found in the literature.[11-12] Section 5.1.1 reports some of these comparisons (see table 5.1 and figure 5.2).

It has been shown in chapter 3 that the electron affinity of atoms and molecules in their ground state could be computed using *ab initio* techniques.[13] In chapter 4, molecular dynamics simulations have been reported for the gas phase and the condensed (glass) phase of the tridecane wax. The conformations thus obtained are analysed in this chapter, using an *ab initio* method: Density Functional Theory (DFT). The conformational defects exhibited by molecules in the simulations of amorphous tridecane are assumed to be representative of the (local) conformational defects in polyethylene as are the consequent local variations in electronic properties. Variations in the electronic band structure of polymers with conformation are reported in the literature for polyethylene[12] and for polypropylene.[14] Correlation between the conformation of polymers and the space charge phenomenon has been reported by Guarrotxena et al.[15-16] In their experimental work, the authors study the relation between the tacticity of the polymer (polypropylene) and the trapping property, to conclude whether if the space charges (trapped electrons, ions) are trapped in certain points of the material randomly or at specific well-defined structures. The authors conclude that fragments of specific tacticity (such as *mmr*) are more likely to trap space-charges.

Polyethylene shows a large temperature dependence of the position of the conduction band below the melting point, while long, linear alkane chains show a sharp change at the melting point due to the phase transition. Ueno and co-workers report that the effective bottom of the conduction band in the molten amorphous state [of polyethylene] lies below the level of conduction due to the large band tailing from the conduction band into the band gap.[17] They show that this temperature dependence is due to the increase of the specific volume of the amorphous parts upon heating.

Section 5.1.2 introduces the Mulliken and Walsh model. This model explains, in terms of molecular orbitals, the variation of the electronic structure of organic molecules with respect to their geometric parameters (bond length, bond angle, etc.).

5.1.1 Band structure of polyethylene

The electronic band structure of polyethylene can be characterised using techniques such as UPS[18] and XPS[19] (Ultraviolet and X-ray photoelectron spectroscopy, respectively), ESCA[20] (electron spectroscopy for chemical analysis), SEE[21] (secondary electron emission) and photoconduction.[22] At first in this section, the band theory, explaining the formation of band structure from LCAO (chapter 2, section 2.5.9) is recalled.

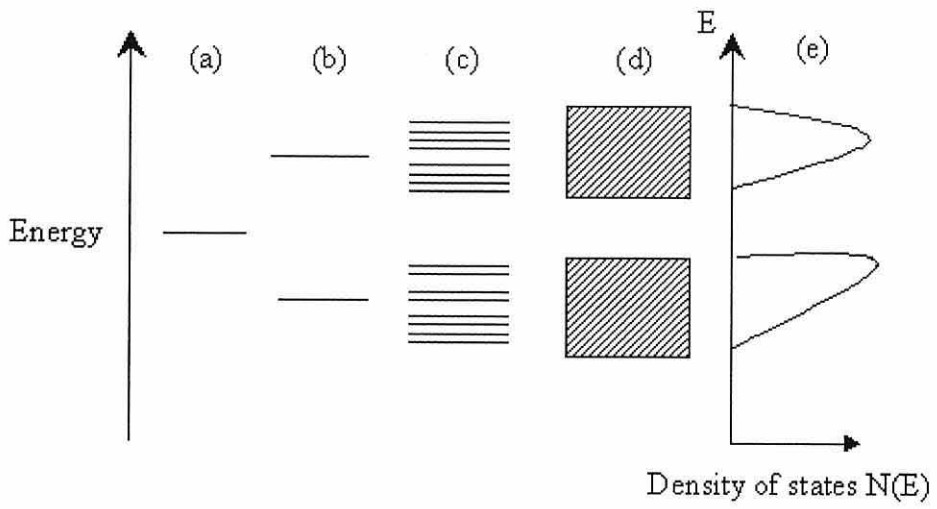

Figure 5.1 The formation of bands. Orbital energies of (a) atom, (b) small molecule, (c) large molecule, (d) solid, and (e) density of states corresponding to (d).[23]

In a periodic solid, the wavefunction must posses a periodicity. Moving the electron n times along the lattice spacing, should give the same value for the wavefunction:

$$\Psi(x+nh) = \mu^n \Psi(x) \tag{5. 1}$$

where h is the lattice spacing and μ is a complex number such that μ*μ=1.

Bloch functions are usually employed to incorporate the periodicity in the wavefunction:

$$\Psi(x) = \exp(ikx)u(x) \tag{5.2}$$

where u(x) represents any periodic function, and

$$k = \frac{2\pi p}{nh} \tag{5.3}$$

where p is an integer and h the lattice spacing. Such functions have a wave-like form with a wavelength λ defined as:

$$\lambda = 2\pi / k \tag{5.4}$$

The molecular orbital interactions of polyethylene are shown in figure 5.2 below.

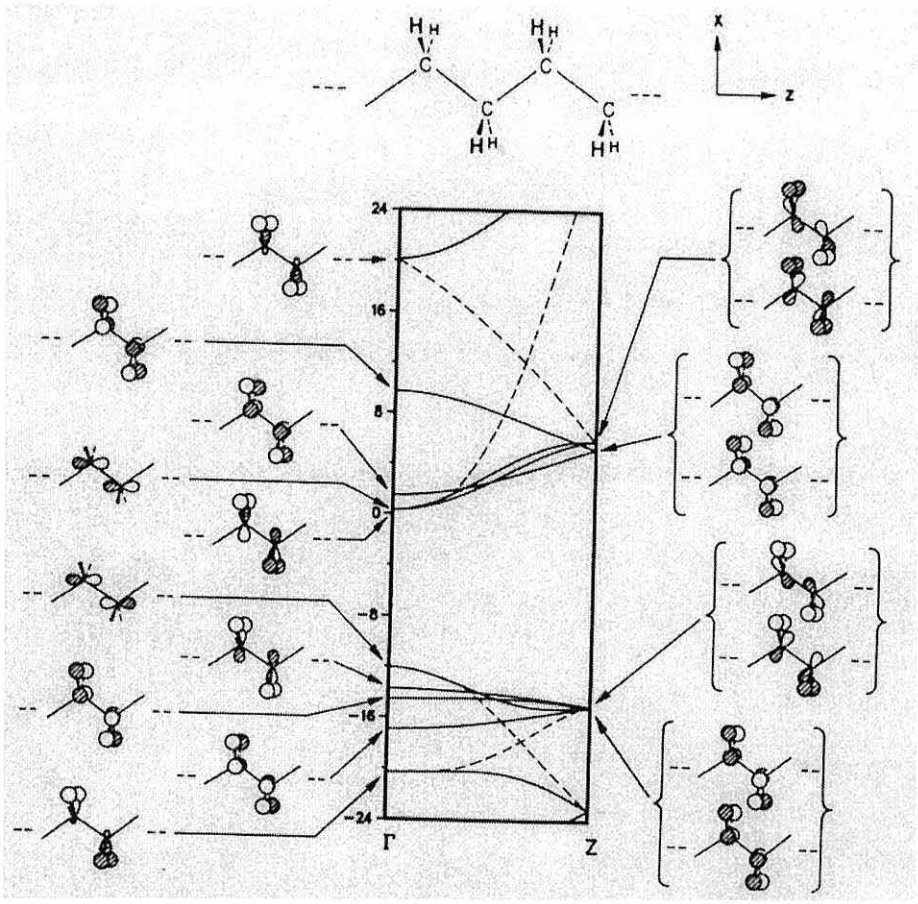

Figure 5.2 Molecular orbital interaction diagram of (crystalline) polyethylene.[24] (Valence and conduction band, the dashed lines show the forbidden crossing between bands of identical symmetry).

The valence and conduction band structures of polyethylene can be seen in figure 5.2, as well as the molecular orbitals that comprise the bands. The dashed lines show the forbidden crossing between bands of identical symmetry.

The energy gap between the valence and conduction band of a polymer is related to the lowest allowed excitation energy of its monomer units and to the bandwidth resulting from the overlap between the monomer orbitals. When computing the band gap of a solid using DFT, the so-called "band gap" problem arises, that is the computed band gap value is less than the experimental value. Salzner et al.[25] claimed that this error is caused by a discontinuity in the derivative of the exchange-correlation functional with respect to the charge density, that this discontinuity is inherent in DFT and would also

be present if the exact exchange-correlation functional was used. Nevertheless, the authors used hybrid functionals and found good agreement between experimental data and calculations for low band gap polymers.

Table 5.1 Experimental and calculated band structure parameters of PE (all values in eV).

	Electron Affinity	Ionisation Potential	Valence Bandwidth	Conduction Bandwidth	Fundamental Gap
HF/6-31G**[26]	3.2	10.2	6.2	4.3	13.4
Extended Huckel[9]	0.299	12.05	-	-	12.35
HF+MP/6-31G**[26]	1.8	8.5	5.4	3.8	10.3
Exp.[27]	- 0.6 / -1.2	7.6-8.8	6	-	8.8
PES/UV [28]	-0.5±0.5	-	-	-	8.81±0.05

Table 5.2 Geometric parameters of polyethylene - calculations versus experiment. Bond lengths are in Å and angles in degrees.

	r_{CC}	r_{CH}	α_{CCC}	α_{HCH}
Neutron Diffraction[29]	1.578±0.005	1.10±0.01	107.7±0.5	109.0±1.0
X-ray[30]	1.527±0.007	1.091	112.08	
LDA[31]	1.512	1.111	114.3	105.2
BP[31]	1.536	1.111	113.8	105.6
MNDO[32]	1.537	1.088	112.6	107
B3LYP/6-31G*[33]	1.534	1.1	113.7	106.1
SVWN/6-31G*[33]	1.511	1.11	113.6	105.4

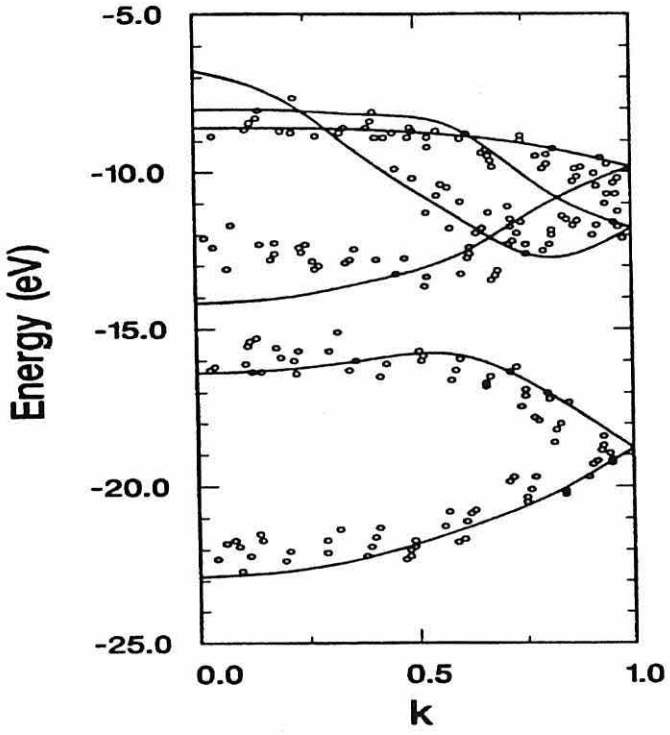

Figure 5.3 Calculated (solid curve) and experimental (circles) valence band structures of polyethylene.[34] (note: k represents the K-points used).

In addition to band structure characterisation, comparisons between experimental results and theory of geometric parameters of the crystalline phase of the polyethylene can also be found in the literature (Table 5.2). The influence of the basis set, the functional, the exchange-correlation terms etc. can be found through comparison with experiment.
The discrepancies between polyethylene carbon-carbon bond distances shown in table 5.2 are important. Although both experiment and theory are in agreement for the carbon-hydrogen bond length, both LDA and SVWN[31] give carbon-carbon bond distances that are too short when compared to the experimental value. Addition of the exchange-correlation terms (B3LYP, BP)[33] is necessary to obtain a value in a better agreement with experimental data. The semi-empirical method MNDO[32] gives a too long carbon-carbon bond distance and rather surprisingly a too short carbon-hydrogen distance.

Calculations of the band structure of polymers are necessarily based on simplified models that deal with linear polymers and assume that the polymer is in an extended

chain configuration.[35] In the particular case of the polyethylene polymer, long linear alkane chains (such as the hexatriacontane molecule n-$C_{36}H_{74}$) are commonly used as models; in the present work, the tridecane (n-$C_{13}H_{28}$) wax is used. In nature, for many polymers of great practical importance (polyethylene, polyacetylene) the presence of imperfections (vacancies, impurities, and structural disorder) is assumed to play an important role in determining their physical and chemical properties.[7] Localised states (referred to as *space charge* when filled with electrons or ions) are present in the gap (the so-called Band Gap) between the conduction band and the valence band of the polymer[36], a phenomenon called 'band tailing'.[17] These states below the conduction band can be regarded as defects, or traps (for electrons or ions). In the crystal phase, irregularities in the lattice structure due to defects or impurities are responsible for the existence of these states. In the amorphous phase, almost all the carbon atoms can be regarded as an electron trap due to the physical disorder.

5.1.2 The Mulliken and Walsh model

In 1953, Mulliken and Walsh proposed a model describing the geometrical arrangements of molecules in their ground and excited states. Their model is based on generalised orbital binding energy correlation diagrams.[37] In these diagrams, the energy of the orbitals is plotted against a geometrical parameter (i.e. the HOH angle for the water molecule, see figure 5.4 below).

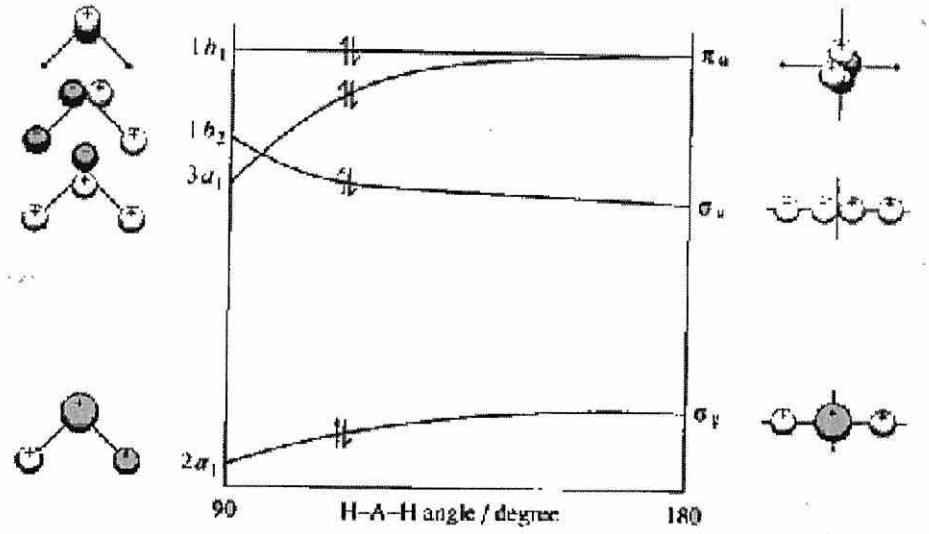

Figure 5.4 Angular correlation diagram of the water molecule.[37]

From a Walsh diagram, the lowest energy geometry of molecules can be deduced, for example if an AB_2 molecule is linear or bent. The reactivity of molecules, which can be deduced from the energies of the frontier orbitals (HOMO and LUMO), can also be predicted from these types of diagrams. The electrophilicity of the 2-butyne molecule (see figure 5.5 below) tends to that of benzyne as its dihedral angle tends to the value in benzyne.

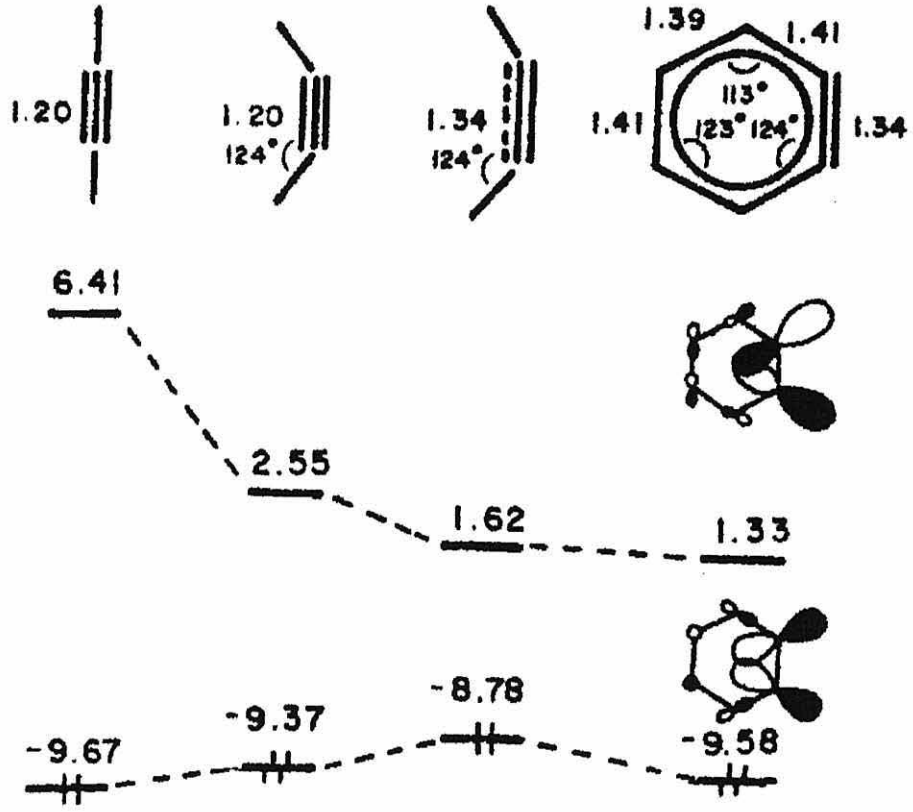

Figure 5.5 Molecular orbital energy diagram of 2-butyne and benzyne.[38]

It can be seen in figure 5.5 that the LUMO energy of the 2-butyne molecule decreases from 6.41 eV to 2.55 eV as the dihedral angle increases and decreases further from 2.55 eV to 1.62 eV as the carbon-carbon bond length changes from 1.20 Å to 1.34 Å. Applying Koopman's theorem[i], it can be concluded that the electron affinity of the 2-butyne molecule increases with an increase in either the dihedral angle or the carbon-carbon bond length.

5.2 METHODOLOGY

Using the Mulliken and Walsh model, the variation in energy of the orbitals of various alkanes has been studied with respect to their geometrical parameters. Firstly, the molecular orbitals of the ethane (C_2H_6) molecule were analysed. The variation in the

[i] see chapter 3

relative position of the frontier orbitals (HOMO and LUMO) was plotted against the carbon-carbon bond length and the corresponding values for the electron affinity were computed. Secondly, the same calculations were performed on the propane (n-C_3H_8) molecule. In addition, the effect of the (C-C-C) angle variation on the total energy of the molecule has been examined. A systematic computation of the vertical electron affinity of each conformer (distorted propane) followed. Finally, the tridecane molecule (n-$C_{13}H_{28}$) has been studied. The constrained tridecane conformations have been obtained using molecular dynamics (MD) simulations. These simulations have been extensively detailed in chapter 4. Taking the tridecane wax in its glassy phase as a model of the amorphous phase of polyethylene, an explanation for the local variations of the electron affinity of the polymer is suggested.

5.2.1 Ethane

Starting from the molecular orbitals of the CH_3 fragment, the molecular orbitals of the ethane molecule and the orbital interaction diagram were built, see the figures 5.6, 5.7 and 5.8.

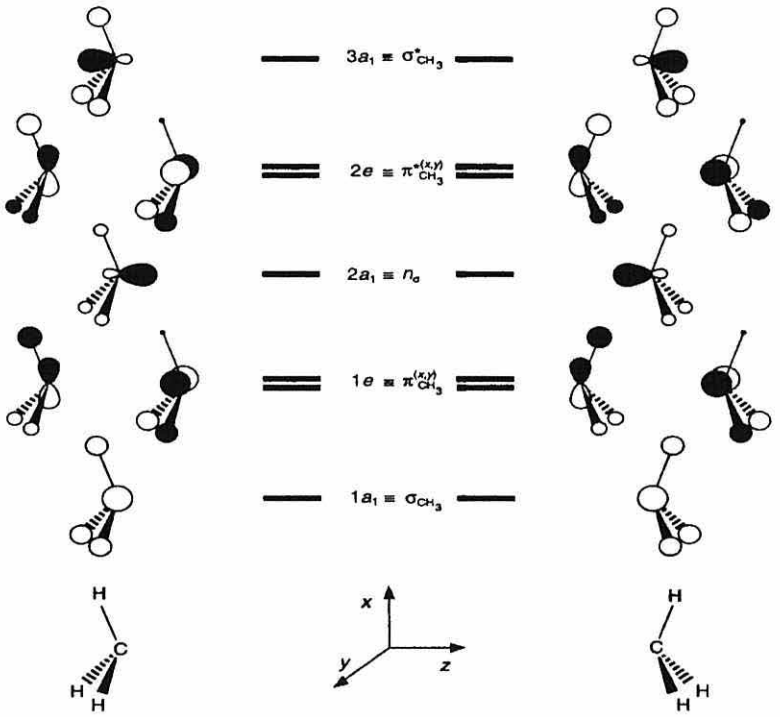

Figure 5.6 Molecular orbitals of CH_3.[39]

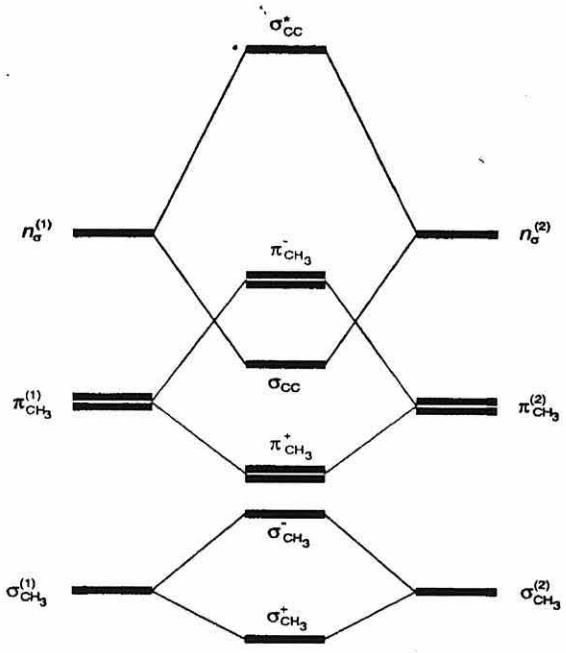

Figure 5.7 Orbital interaction for ethane, starting from two CH_3 units (all the orbitals are filled through Π^-_{CH3}).[39]

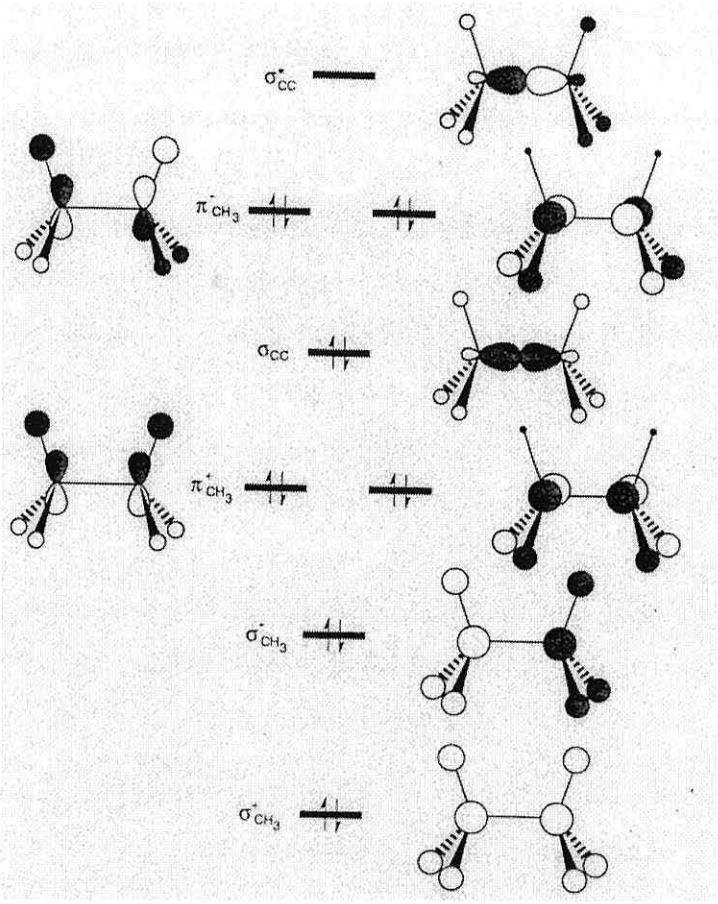

Figure 5.8 Molecular orbitals of ethane.[39]

The molecular orbitals of the ethane molecule (figure 5.6) were built from the combination of two CH_3 fragments (figure 5.7). Figure 5.8 shows the energy diagram of ethane. The Lowest Unoccupied Molecular Orbital is of particular importance in the present study; it is a σ^* orbital resulting from the combination (anti-symmetric) of the two n_σ (2 a_1) molecular orbitals of the CH_3 fragments. This orbital is displayed at the top of figure 5.8 and labelled σ^*_{CC}.

The physical significance of the orbitals obtained from density functional methods is questionable. Indeed, the Kohn-Sham orbitals and eigenvalues are not interpretable as physical observables. Nevertheless, it does not mean that they have no meaning for the total energy.[40]

In order to explain the variation of the electron affinity with molecular conformation of the polyethylene polymer, a systematic study of the electron affinity of the ethane, propane and tridecane molecules has been undertaken. The LUMO of the linear alkane molecules is an anti-bonding σ* orbital. Increasing the bond length leads to a decreasing atomic orbital overlap, and therefore to a lowering of the LUMO energy value (E_{LUMO}). The reverse is true for bond shortening. Using Koopman's theorem, which we have shown holds qualitatively but not quantitatively for alkanes[13] (see chapter 3), the electron affinity of a molecule can be defined as:

$$EA = -E_{LUMO} \tag{5.5}$$

The variation of the LUMO energy can therefore be used to explain the variation of the electron affinity (i.e. a decrease of the LUMO energy means that the molecule is more likely to trap an electron). This is clearly demonstrated in the case of the small alkane molecule in figures 5.10 and 5.15 below.

The ethane molecule has been used as a test case for the study of the electron affinity variation with respect to the geometric parameters. The carbon-carbon bond length has been varied and the energy, together with the vertical attachment energy, has been computed using DFT for each geometry. Taking the optimised geometry as a starting point, the carbon-carbon bond length has been varied from 1.3 Å to 1.7 Å in increments of 0.1 Å. For each different bond length, a constrained geometry optimisation has been performed, in which some of the geometric parameters (bond length, bond angle, etc.) are kept constant during the procedure. For computational and mathematical details of this special form of geometry optimisation, see chapter 2. The vertical electron affinity of each conformer has been computed using the methodology described earlier in chapter three. The effect of the bond length variation upon the energy of the neutral and anionic molecule of ethane is plotted below (figure 5.9), together with the electron affinity variation (figure 5.10).

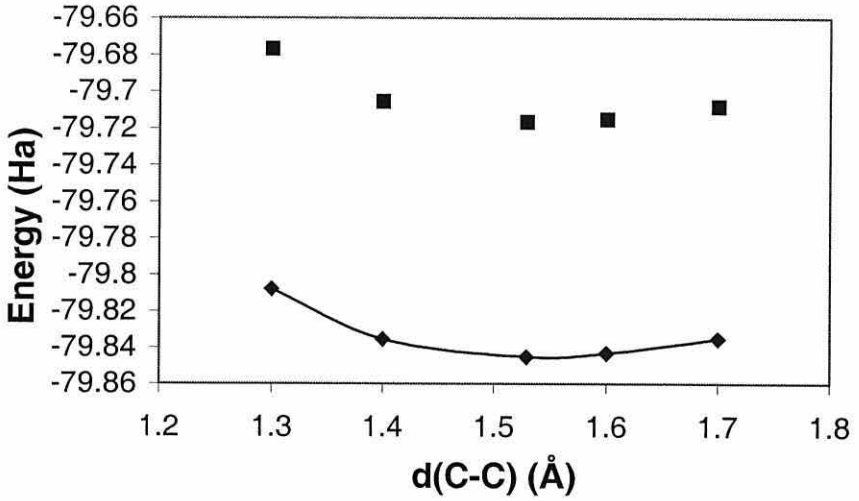

Figure 5.9 Energy variation of ethane (neutral ▲, anionic ■) with the carbon-carbon bond length.

The computed equilibrium bond distance of ethane is 1.529 Å. This value is slightly lower than the experimental value of 1.5351 Å.[41] Figure 5.10 shows that the electron affinity of the ethane molecule varies linearly with the carbon-carbon bond distance. It increases together with the carbon-carbon bond length by about 0.1 eV in 0.4 Å. At the equilibrium bond length the computed electron affinity of ethane is –3.502 eV.

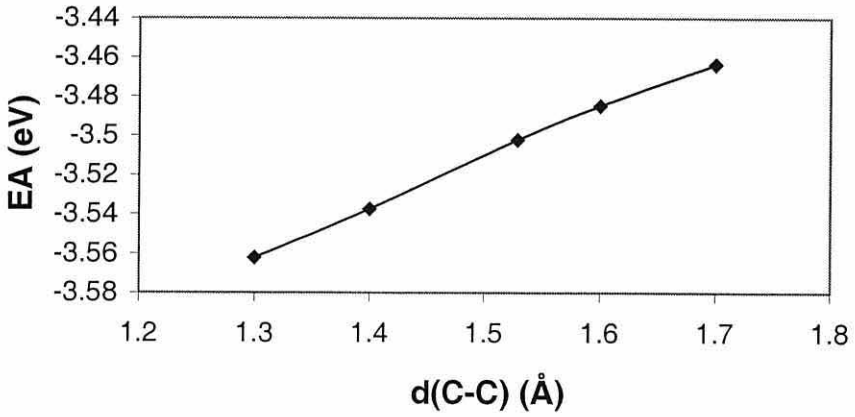

Figure 5.10 Electron affinity variation of ethane with the carbon-carbon distance.

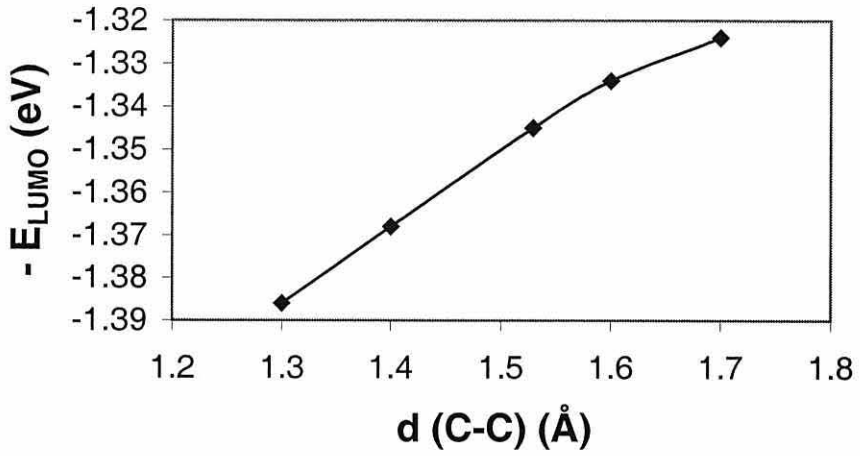

Figure 5.11 $-E_{LUMO}$ energy variation against the carbon-carbon bond distance for the ethane molecule.

The variation of $-E_{LUMO}$ the ethane molecule with respect to the carbon-carbon bond length is shown in figure 5.11. The variation is linear from 1.3 Å to 1.6 Å and the rate of increase is slower after 1.6 Å. In total, the energy has increased by 0.06 eV. At the equilibrium geometry (r_{C-C} = 1.529 Å) the energy value of the LUMO is 1.345 eV.

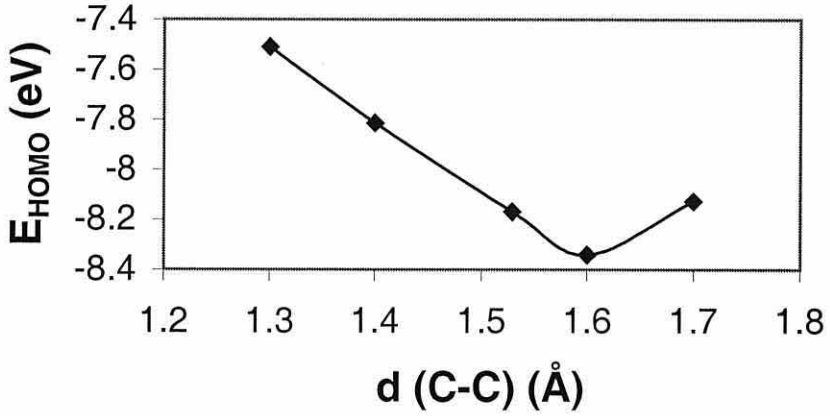

Figure 5.12 HOMO energy variation against the carbon-carbon bond distance for the ethane molecule.

The variation of the HOMO energy of ethane with respect to the carbon-carbon bond length is shown in figure 5.12. The curve decreases linearly from 1.3 Å to 1.6 Å, and

then increases between 1.6 Å and 1.7 Å. In total, the energy has decreased by 0.618 eV. At the equilibrium geometry ($r_{C\text{-}C}$ = 1.529 Å) the energy value of the HOMO is –8.168 eV. Applying Koopman's theorem, the ionisation potential is equal to the negative of the HOMO energy. Experimental ionisation potentials can easily be found in the literature[42] for the alkane molecules. The data reported in ref. 42 for the ethane molecule is 11.52±0.01 eV. The DFT computed value here of 8.168 eV is in poor agreement with the experimental data.

The study of the molecular orbital energy variation with the carbon-carbon bond length presented here indicates clearly that:

- The equilibrium carbon-carbon bond length found is in agreement with experiment results (but slightly lower).
- The energy of the highest occupied molecular orbital (HOMO) decreases with increasing bond length. The negative of the energy of the lowest unoccupied molecular orbital (LUMO) increases with increasing bond length.
- The electron affinity of the molecule increases with increasing bond length.

We have therefore demonstrated here, as expected by the Mulliken and Walsh model, and in accordance with previous theoretical studies[6], the dependence of the electronic structure of the ethane molecule on its conformation. To the best of our knowledge, this is the first time that the effect of molecular distortion on the electron affinity is given quantitatively. To confirm this dependence, and the ability to accurately compute the variation of the electron affinity upon microstructure using *ab initio* methods, similar calculations on the propane molecule are discussed in the following subsection.

5.2.2 Propane

The LUMO of propane is also a σ^* orbital. Therefore, we expect the same variation of the energy of this orbital with respect to the carbon-carbon bond length. In the case of the propane molecule, both carbon-carbon bond lengths have been varied from 1.4 Å to 1.8 Å in increments of 0.1 Å. Both carbon-carbon bond lengths have been kept at the same value when the constrained geometry optimisations have been performed. Again,

the electron affinity of each conformer has been computed using the methodology described in chapter 3. Both carbon-carbon bond lengths were varied for the propane molecule; the propane molecule reacts to this modification mainly by changing its carbon-carbon-carbon bond angle. The longer the carbon-carbon distances the smaller the bond angle and vice-versa: this is due to relaxation of the molecule. Therefore, it is also possible to deduce the energy variation with respect to the chain angle. The energy of the LUMO of each constrained conformer is also reported.

Table 5.3 Energy values, LUMO energy values, vertical electron affinity, and constraint energy of the optimised and constrained propane molecule, neutral and anionic.

r_{CC} (Å)	E_{SCF} neutral (Ha)	Constraint (eV)	α_{CCC} (Degrees)	E_{LUMO} (eV)	E_{SCF} anion (Ha)	EA (eV)
1.4	-119.145255	0.48	115.6	1.251	-119.022671	-3.336
1.5	-119.164978	0.02	113.8	1.252	-119.043159	-3.315
1.5322	-119.165967	0.00	113.2	1.250	-119.044487	-3.306
1.6	-119.162048	0.09	112.3	1.241	-119.041325	-3.285
1.7	-119.145969	0.46	110.8	1.225	-119.026327	-3.256
1.8	-119.122755	1.00	109.6	1.178	-119.004285	-3.224

The calculated equilibrium carbon-carbon bond distance is 1.5322 Å, and at this distance the LUMO energy value is 1.25 eV, the electron affinity is –3.306 eV, the dipole moment is 0.078 D and the chain angle is 113.22°. Electron Diffraction measurements report the following (gas-phase) equilibrium values: carbon-carbon bond distance 1.532 Å[41], chain angle 112°[41] and dipole moment 0.084 D.[43] Recent NLSD (GC) calculations[44] reported d (C-C) = 1.53 Å and α_{CCC}= 112.6°.

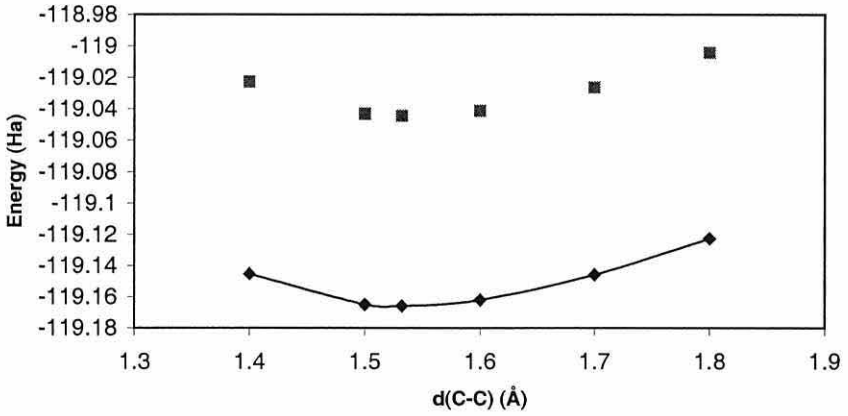

Figure 5.13 SCF energy variation of propane with the carbon-carbon bond length (ϖ anionic, -◆- neutral).

From figure 5.13, the electron affinity variation with respect to the carbon-carbon bond

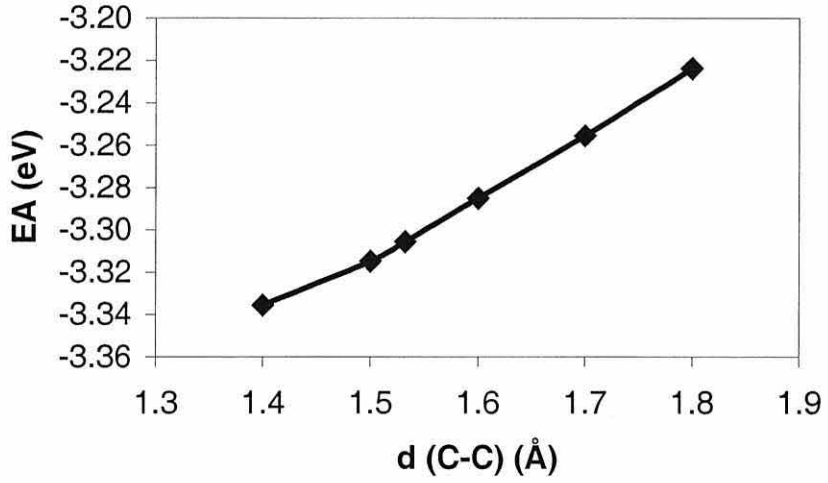

length can be plotted. This is shown in below.

Figure 5.14 Variation in the electron affinity with carbon-carbon bond length of propane.

The calculated electron affinity of the propane molecule increases linearly with the carbon-carbon bond length. In total, the electron affinity changes by 0.112 eV. As in the case of ethane, a compression of the carbon-carbon bond led to a decrease of the

electron affinity of propane, and a bond lengthening led to an increase in the electron affinity, with respect to the equilibrium value.

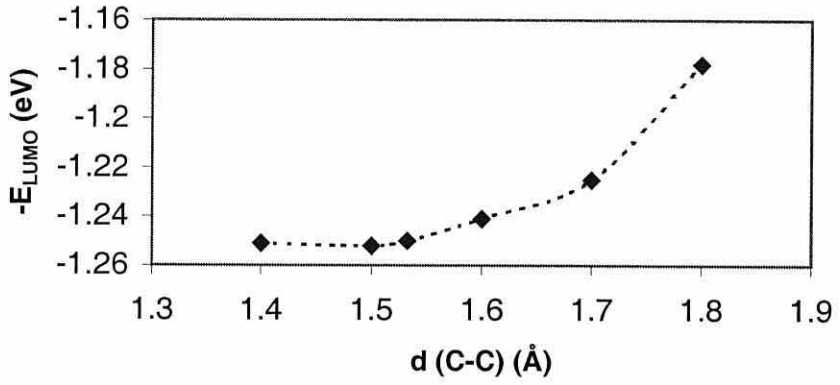

Figure 5.15 Variation of $-E_{LUMO}$ energy with carbon-carbon bond length of propane.

The negative of the LUMO energy variation of the propane molecule is shown in figure 5.15. The effect of compression of the bond length from the equilibrium value is insignificant (the value of $-E_{LUMO}$ between 1.4 Å and 1.5322 Å is invariant) whereas the effect of bond lengthening is an increase in the electron affinity.

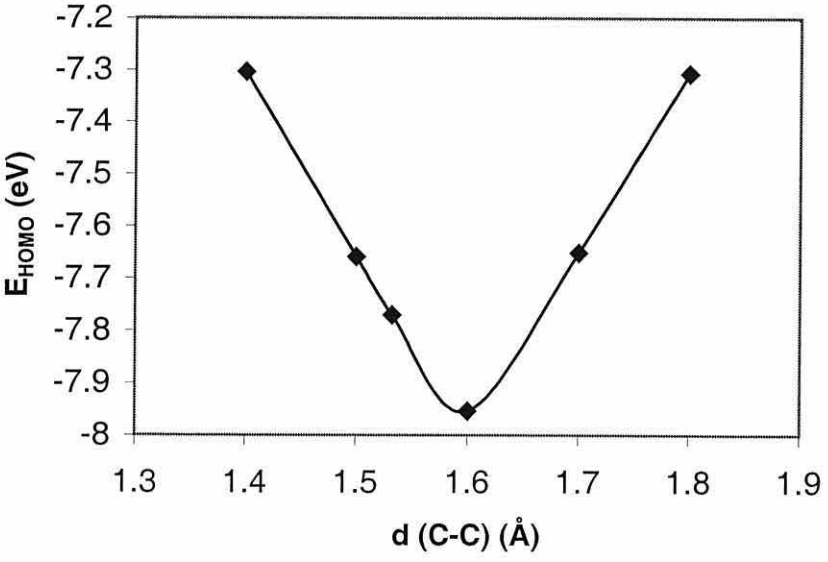

Figure 5.16 HOMO energy variation with carbon-carbon bond length of propane.

The energy of the HOMO of the propane molecule decreases with increasing carbon-carbon bond length from 1.4 Å to 1.6 Å, as in the case of the ethane molecule, the value increases. The value at equilibrium bond length is –7.77 eV, compared to the experimental ionisation potential of 10.95±0.05 eV.[42] Again, a large discrepancy between the DFT and experimental values is found.

In conclusion, the study of the electronic properties of the propane molecule have shown that:

- The calculated equilibrium geometric parameters are in close agreement with experimental data and other theoretical work.
- The frontier MOs vary linearly with the increasing carbon-carbon bond length (up to 1.6 Å).
- The electron affinity of the propane molecule increases with the increasing carbon-carbon bond length.

Overall, the study of the small ethane and propane molecules has demonstrated the capability of the DFT to investigate the electronic properties of the alkanes with respect to their conformational changes. We can therefore be confident in using our methodology to study our polyethylene model, namely the tridecane molecule.

5.2.3 Tridecane

For the tridecane molecule, molecular dynamics codes described in chapter 2 have been used to generate the distorted conformations. The results can be found in chapter 4. The constrained tridecane molecules were modelled by performing molecular dynamics simulations of glassy phases of tridecane. It has been shown that the molecular conformation of the glassy wax tridecane, used as a model of the amorphous phase of polyethylene, contained some physical defects (such as gauche defects). The molecules of tridecane lie in vibrationally excited states and the environment of the neighbouring molecules prevent them from adopting the all-trans geometry of lowest energy. From the molecular dynamics runs, local energy minima were found using a simulated annealing procedure.

The conformation of the tridecane molecules obtained in all the molecular dynamics were then used as input for the *ab-initio* computation of the electron affinity in the present study. Computing the electron affinity for each conformer led, in all simulations, to a distribution of electron affinity. The distributions are plotted for each different parameter used (densities, initial configuration, etc.). From those distributions, probability density plots could be computed. The basis set used in this section (V4.0.0) differs from the one used for the small alkanes (V3.5). Those two basis sets gave similar results except that the V4.0.0 basis set gave (incorrect) opposite tendency of the electron affinity variation (of ethane, propane) when the carbon-carbon bond length was lowered from equilibrium value. Chapters 4 shown that the carbon-carbon bond lengths of the tridecane molecules found in the glass were, on average, longer than that of the crystal phase (all-trans conformation). Therefore, we expect that this basis set error does not modify the present results significantly.

5.3 RESULTS: THE TRIDECANE WAX

In this section, the results from the computation of the electron affinity of distorted molecules of tridecane are presented. The methodology employed to obtain the various glass phases has been extensively described in chapter 4, and the methodology used to compute the electron affinity was described in chapter 3. For clarity we recall in the following table the different glasses studied:

Table 5.4 Simulation data for solid alkanes.

	N	Density (g/cm^{-3})	Initial Configuration	Simulation ensembles
Glass A_1-A_5	25 (x5)	0.7564	Crystal	NVT/NVE
Glass B	25	0.9611	Glass A_1 (see text)	NPT
Glass C	25	0.9500	Amorphous	NVT/NVE
Glass D	50	0.9500	Amorphous	NVT/NVE
Crystal	25	0.9641	Crystal	NVT/NVE

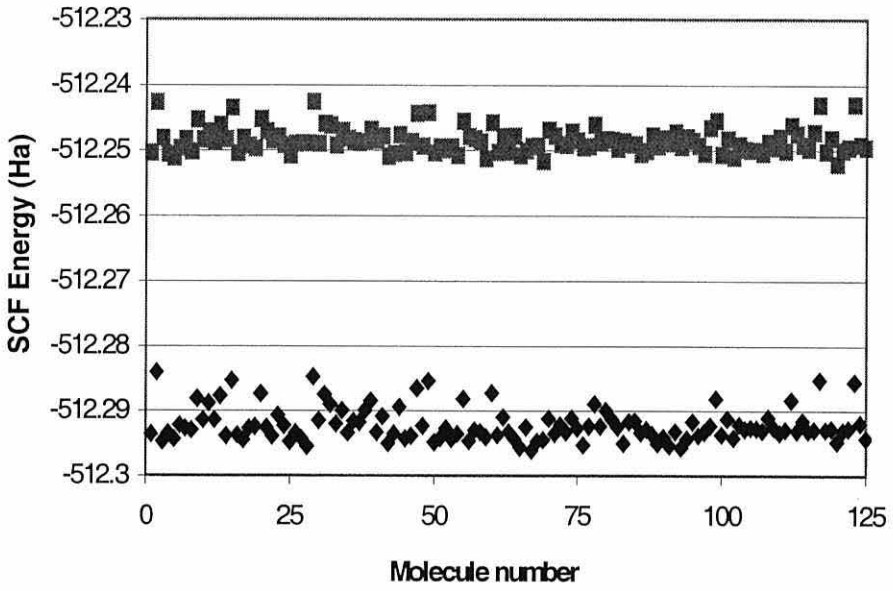

Figure 5.17 Total SCF energy of the tridecane molecule in the glass phase (A_1-A_5) (ϖ anionic, ◆ neutral).

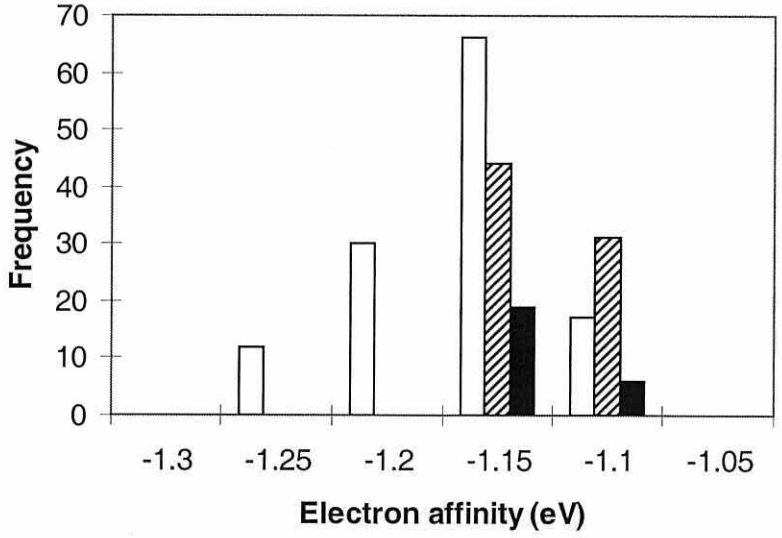

Figure 5.18 Electron affinity distribution of the tridecane molecules in the glass phase at 150 K: Blank histogram, glasses A1-A5, hashed, glasses C-D, filled, glass B.

Figure 5.17 displays the variation in the energy of the neutral and anionic tridecane in the glass phase (A_1-A_5). The energy variation is about 0.01 Ha (~6.3 kcal/mol), in both

cases. By calculating the energy difference as neutral minus anionic for each conformer, the electron affinity distribution can be obtained, so that the probability density of the electron affinity can be plotted (figure 5.18). The same procedure is applied to the glasses B, C and D.

As discussed in section 5.2, the increase in bond length leads to an increase in the electron affinity. Therefore, we expect that the electron affinity of molecules in the glass will be increased with respect to the all trans molecule. Since in our calculations for alkanes there is no significant difference between the adiabatic and vertical electron affinity[13], the vertical quantity has been used here. Figure 5.18 reports the distribution of electron trap energies obtained from the amorphous tridecane simulations described in chapter 4. The effect of trapped conformational disorder is to raise the electron affinity by between 0.1 and 0.2 eV so that an electron prefers to sit on a conformational defect rather than be in the conduction band (represented by the all trans or conformationally free molecule). It also shows that the high-density simulations (Glasses B, C, D) lead to larger average electron affinities than the low-density simulations (Glasses A_1-A_5). Due to the high density, the constraint applied by the environment is greater than in the low-density simulations, and therefore the molecules are less likely to relax (partially or totally) to the all-trans configuration when the simulating annealing procedure is applied. Consequently, more gauche defects are found in the high-density simulation compared to the low-density case.

5.4 CONCLUSION

We have shown the capability of the DFT to compute accurately the geometric and electronic properties of the small alkane molecules ethane and propane. When subject to bond length distortion, the frontier energy orbital LUMO varied inversely to the bond length alteration, as expected from the Mulliken and Walsh model. We found that the electron affinity of ethane and propane increases with the increasing carbon-carbon bond length. This is due to a decreasing atomic overlap of the anti-bonding σ^* orbital

(LUMO). Koopman's theorem (Eq. 5.5) shows that a decrease of the LUMO energy value (which occurs when the carbon-carbon bond distance increases) results in an increase in the electron affinity.

The band structure of polyethylene is a test case for *ab initio* methods as this polymer has a simple chemical structure. *Ab initio* calculations usually assume a perfect crystalline phase of the polymer, but in reality, an amorphous phase is also present in the polymer. Band theory is much more difficult to apply in the amorphous phase due to the physical disorder and consequent localised states below the level of the conduction band. Taking the conformations from the simulations of the glassy phase in previous chapter and making the approximation that the electron affinity in vacuum of the conformers is equal to the electron affinity of the conformers in the condensed phase, we have computed the electron affinity of each conformer in vacuum. The distribution obtained showed that, in the glass phase, the electron affinity of the wax is greater than in the vacuum (all-trans conformation). In following this procedure we have neglected the effect of intermolecular interactions (except for steric hindrance) and of polarisation in changing R_e (equation 3.4). However, as a first approximation we take these effects to be less important in determining the electron affinity than the facts that molecules are *conformationally* trapped.

In the next chapter, the variation of the electron affinity of the wax molecules will be used to explain the presence of electron-traps in polyethylene. The electron affinity distribution will be used to construct a trap depth probability distribution.

5.5 REFERENCES

[1] N.F. Mott. Phil. Mag. **22**, 7 (1970).

[2] H.J. Wintle. *Conduction Processes in Polymers. Engineering Dielectrics volume IIA, Electrical properties of solid insulating materials: Molecular structure and electrical behaviour.* (Bartnikas/Eichhorn editors, 1983).

[3] G. Blaise. Fields and polarisation, conduction and charge trapping in insulating materials. Abstracts CSC'3 Electric charge in solid insulators, 25 (1998).

[4] L.A. Dissado. What role is played by space charge in the breakdown and ageing of polymers? Abstracts CSC'3 Electric charge in solid insulators, 141 (1998).

[5] P.J. Flory. *Statistical mechanics of chain molecules.* (Interscience, New-York, 1969).

[6] K. Seki, N. Sato, and H. Inokuchi. Valence electronic structure of a long-chain alkane in random coil forms. Gas-phase UPS of n-C36H74 and MO calculations. Chem. Phys. **178**, 207 (1993).

[7] J. Ladik, and S. Suhai. *The electronic structure of polymers. Quantum chemistry of polymers: Solid state chemistry.* (Edition J. Ladik and J.M. André, Chapter 2, 1984).

[8] M. Springborg. Density-functional studies of electronic properties of polymers. Int. Rev. Phys. Chem. **12**, 241 (1993).

[9] J.M. André, G.S. Kapsomenos, G. Leroy. A comparison of ab-initio, extended-Huckel and CNDO band structures for polyene and polyethylene. Chem. Phys. Letters **8**, 195 (1971).

[10] A. Imamura. Electronic structures of polymers using the tight-binding approximation.I. Polyethylene by the Extended-Huckel method. J. Chem. Phys. **52**, 3168 (1970).

[11] K. Seki, N. Ueno, U.O. Karlson, R. Engelhardt, E.E. Koch. Valence bands of oriented finite linear chain molecular solids as model compounds of polyethylene studied by angle-resolved photoemission. Chem. Phys. **105**, 247 (1986).

[12] K. Seki, N. Sato, H. Inokuchi. Valence electronic structure of a long-chain alkane in random-coil forms. Gas-phase UPS of n-$C_{36}H_{74}$ and MO calculations. Chem. Phys. **178**, 207 (1993).

[13] M. Meunier, N. Quirke, and D. Binesti. The calculation of the electron affinity of atoms and molecules. Mol. Sim. **23**, 109 (1999).

[14] I. Flamant, D.H. Mosley, M. Deleuze, J.M. André, J. Delhalle. Dependence of the electronic structure on the chain geometry in stereoregular polypropylene: An exploratory theoretical study. International Journal of Quantum Chemistry: Quantum Chemistry Symposium **28**, 460 (1994).

[15] N. Guarrotxena, A. Toureille, and J.L. Millan. Relation between molecular microstructure and electrical space charges in poly(propylene). Macromol. Chem. Phys. **199**, 81 (1998).

[16] N. Vella, N. Guarrotxena, A. Toureille, J.L. Millan. Influence of the tacticity dependent microstructure on the space charge distribution of poly(vinyl chloride). Journal of Electrostatics **40&41**, 301 (1997).

[17] N. Ueno, K. Seki, K. Sugita, H. Inokuchi. Nature of the temperature dependence of conduction bands in polyethylene. Phys. Rev. B **43**, 2384 (1991).

[18] K. Seki, N. Ueno, U.O. Karlsson, R. Engelhardt, E.E. Koch. Chem. Phys. **105**, 247 (1986).

[19] J. Delhalle, J.M. André, S. Delhalle, J.J. Pireaux, R. Caudano, J.J. Verbist. J. Chem. Phys. **60**, 595 (1974).

[20] J.J. Pireaux, R. Caudano, J.J. Verbist. J. Electron spectrosc. and relat. phenom. **5**, 267 (1974).

[21] N. Ueno, K. Sugika, S. Kiyono. Chem. Phys. Letters **82**, 296 (1981).

[22] K. Less, E.G. Wilson. J. Phys. C **6**, 3110 (1973).

[23] P.A. Cox. *The electronic structure and chemistry of solids.* (Oxford University Press, 1987).

[24] R. Hoffmann, C. Janiak, C. Kollmar. A chemical approach to the orbitals of organic polymers. Macromolecules **24**, 13, 3725 (1991).

[25] U. Salzner, J.B. Lagowski, P.G. Pickup, R. A. Poirier. Design of low band gap polymers employing density functional theory-Hybrid functionals ameliorate band gap problem. J. Comp. Chem. **18**, 11943 (1997).

[26] S. Suhai. Electron correlation effects on the mechanical and optical properties of polymers. Int. Journal of Quantum Chemistry: Quantum Chemistry Symposium **18**, 161 (1984).

[27] K.J. Less, E.G. Wilson. J. Physics C **6**, 3110 (1973).

[28] D. Bloor. Correlation of experimental and theoretical electron band energies of polyethylene. Chem. Phys. Letters **40**, 2, 323 (1976).

[29] G. Avitabile, R. Napolitano, B. Pirozzi, K.D. Rouse, M.W. Thomas, B.T.M. Willis. J. Polym. Sci., Polym. Lett. D. **13**, 351 (1975).

[30] S. Kavesh, J.M. Schultz. J. Polym. Sci. Part A-2 **8**, 243 (1970).

[31] B. Montanari, P. Ballone, R.O. Jones. Density functional study of molecular crystals: Polyethylene and a crystalline analog of bisphenol-A polycarbonate. J. Chem. Phys. **108**, 6947 (1998).

[32] M.J.S. Dewar, Y. Yamaguchi, S.H. Suck. Chem. Phys. **43**, 145 (1979).

[33] S. Hirata, S. Iwata. Density functional crystal orbital study on the normal vibrations and phonon dispersion curves of all-trans polyethylene. J. Chem. Phys. **108**, 7901 (1998).

[34] M. Springborg, M. Lev. Electronic structures of polyethylene and polytetrafluoroethylene. Phys. Rev. B **40**, 3333 (1989).

[35] H.J. Wintle. Engineering Dielectrics, volume IIA, Electrical properties of solid insulating materials: Molecular structure and electrical behaviour. (R. Bartnikas, R.M. Eichhorn editors, 1983).

[36] N.F. Mott. Phil. Mag. **22**, 7 (1970).

[37] R.J. Buenker, S.D. Peyerimhoff. Molecular Geometry and the Mulliken-Walsh Molecular Orbital Model. An ab-initio Study. Chemical Review **74**, 127 (1974).

[38] N.G. Rondan, L.N. Domelsmith, K.N. Houk, A.T. Bowne, R.H. Levin. The relative rates of electron-rich and electron-deficient alkene cycloadditions to benzyne. Enhanced electrophilicity as a consequence of alkyne bending distortions. Tetrahedron Letters **35**, 3237 (1979).

[39] Y. Jean, F. Volatron, J. Burdett. *An Introduction to Molecular Orbitals*. (Oxford University Press, 1993).

[40] N. Rosch, S.B. Trickey. J. Chem. Phys. **106**, 8940 (1997).

[41] D.R. Lide. *Handbook of Chemistry and Physics.* (CRC Press, 76th edition, 1995-1996).

[42] S.G. Lias et al. Gas-phase ion and neutral thermochemistry. J. Phys. Chem., Ref. Data **17**, (1988).

[43] R.D. Nelson, D.R. Lide, A.A. Maryott. Selected values of electric dipole moments for molecule in thegas phase. Natl. Stand. Ref. Data Ser. –Natl. Bur. Stnds.10 (1967).

[44] A. Borrmann, B. Montanari, R.O. Jones. Density functional study of polypropylene and its submolecules. J. Chem. Phys. **106**, 8545 (1997).

CHAPTER 6

ELECTRON TRAPS IN POLYMERS

6.1 INTRODUCTION

The presence of space-charge in insulating polymeric materials (such as polyethylene) used by electrical companies is explained by local irregularities in the band structure of the polymer. In the first section (6.1.1), typical defects (chemical and physical defects) found in solids are enumerated, and in particular the defects found in polyethylene. Local irregularities (i.e. *physical defects*) cause the localisation (*trapping*) of the excess particle. This trapped particle is commonly called *space-charge*. Electron localisation is explained via the Anderson model.[1] Section 6.1.2 introduces the transport (*hopping*) of electrons in solids and electron tunnelling. In section 6.2, the methodology employed to compute the electron trap distribution via a relation between electron affinity and trap energy (section 6.2.1) is detailed. In addition the electron trap density calculation is given. The electron affinity of the tridecane wax has been computed in the glass phase in the previous chapter (5), the results are employed in this chapter to deduce the trapping energy of the wax used as a model of polyethylene (chapter 4). Section 6.3 presents the results.

6.1.1 Defects in polymers

All real solids, even the most perfect crystals, contain some defects and some impurities. The consequence is a loss of periodicity in the lattice and therefore a perturbation in the electronic band structure. Interestingly, it is sometimes the presence of defects that gives the properties of interest in some materials (i.e. doped semi-conductors). In crystalline materials, point defects are interstitial or substitutional.

Extended defects are also present (i.e. surface, dislocations, etc.). In polymeric materials, there exist defects originating from local conformational disorder. In addition, the presence of chemical impurities (i.e. water, methane) or industrial additives (i.e. antioxidant agents, branching agents) also increase the number of defects in the band structure. This is schematised in the figure 6.1 below:

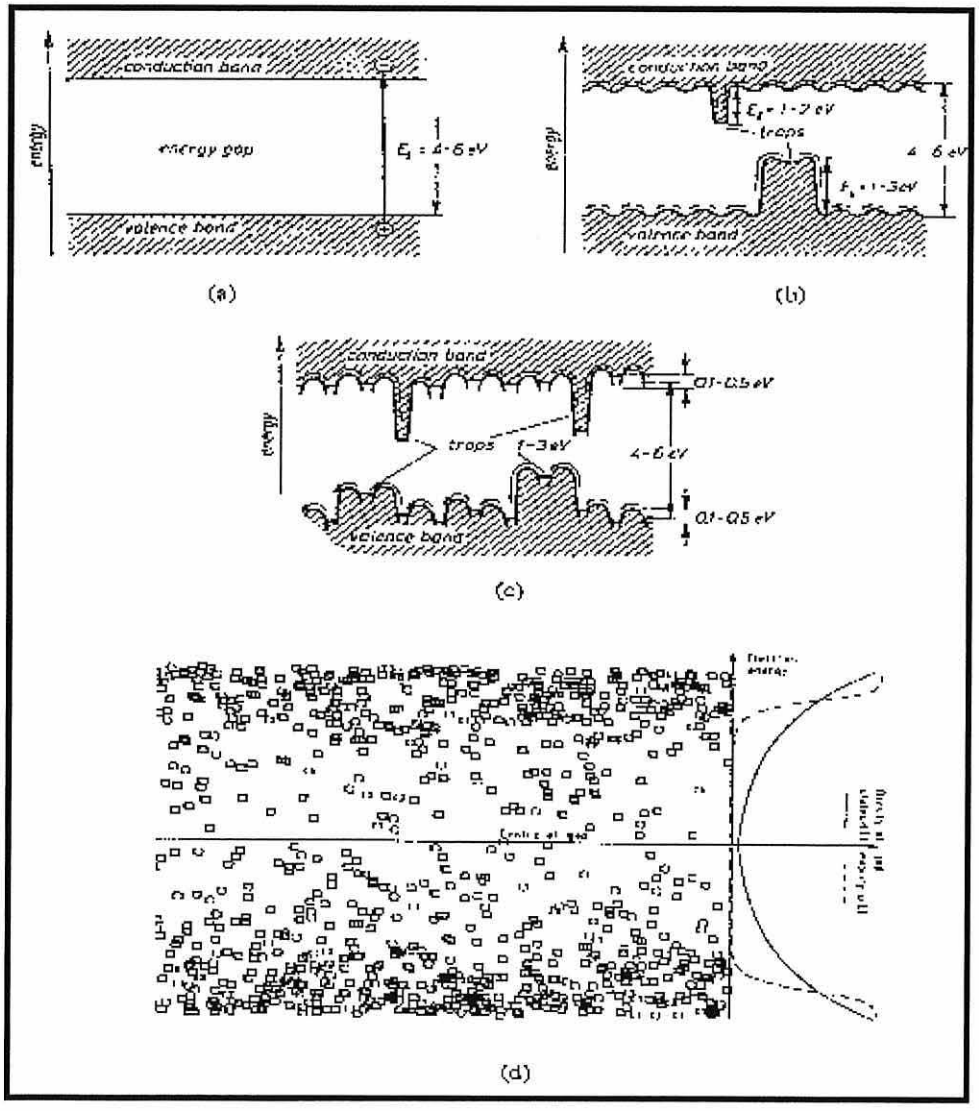

Figure 6.1 Schematic band structure of polymers. (a) Ideal dielectric. (b) Macromolecular crystal. (c) Polymer. (d) Localised states (squares), density of states and mobility as function of energy in polymers.[2]

The presence of physical and chemical defects in the material is responsible for the localised states in the band gap. Physical defects are thought to have energies of 0-0.5 eV, and chemical defects of a few eVs.[2] The results for the physical defects in the polyethylene shown in section 6.3 are in agreement with those values. Chemical defects have not been treated in the present thesis. The lack of long-range order creates the band-tail states, around the mobility edges.[3] The wavefunctions describing defect states are localised, as seen in figure 6.2 below:

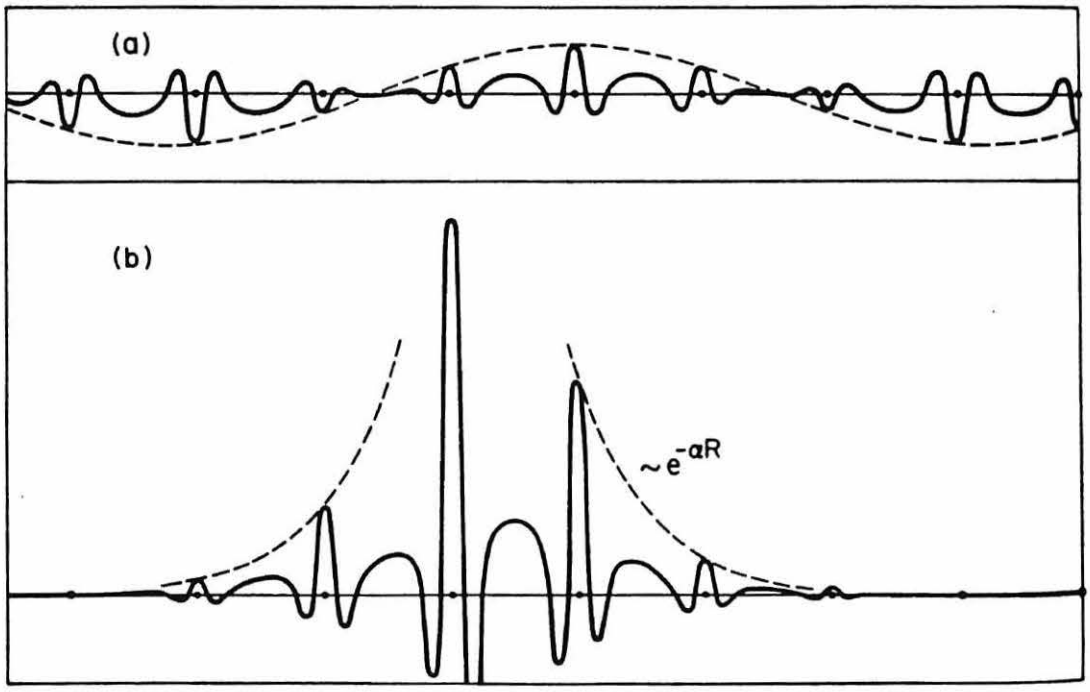

Figure 6.2 The distinction between extended and localised electron states. A Bloch-type extended-state wave function is illustrated in (a) (typical of the crystalline phase); a localised-state wave function is illustrated in (b). α is known as the *inverse localisation length.*[4]

Potential energy wells appear on the potential energy surface of the material that originate from the presence of defect states. Disorder can be introduced by either changing the distance between the wells (off-diagonal disorder, Edwards – or Lifshitz - model[5-6]) or by changing the depth of the wells within a certain width V_0 (diagonal disorder, Anderson model[1,6], see figure 6.3 below). In nature, both changes occur leading to a complex distribution of localised and extended states.

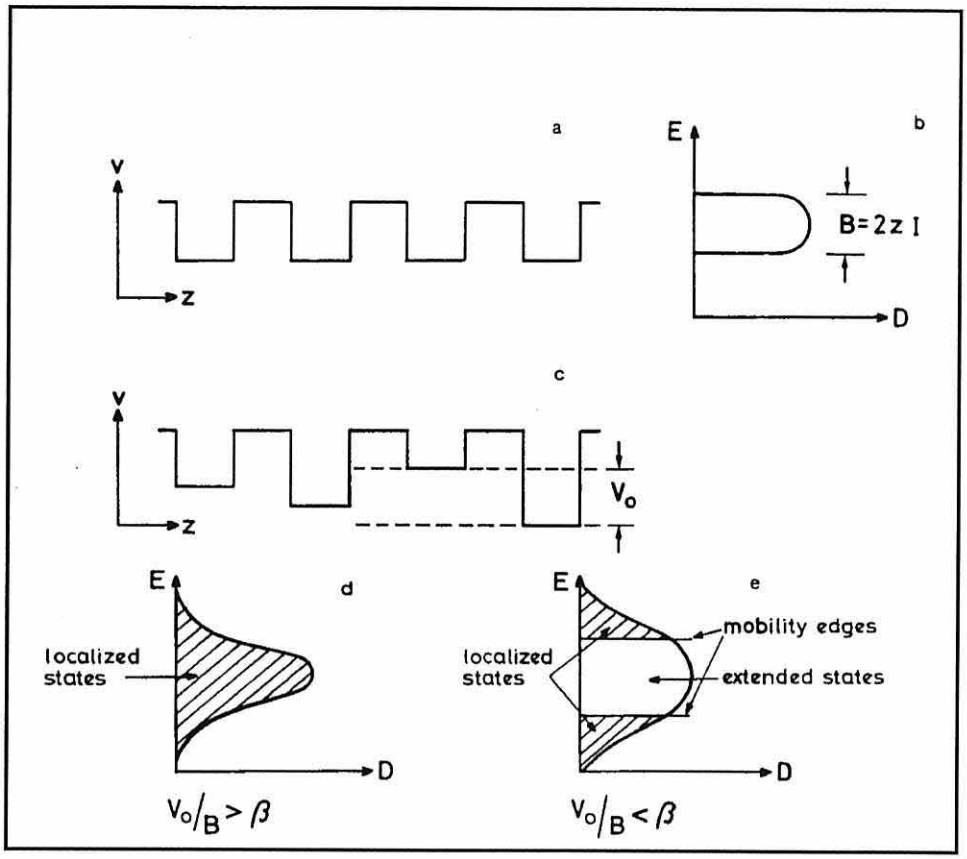

Figure 6.3 The Anderson Model a) Periodic potential of the Kronig-Penny type and (b) the resulting density of states D of the lowest band, I is the overlap-integral between neighbouring atomic wavefunctions and z is the coordination number. (c) The same potential with some fluctuations in depth within a range V_0 and (d) the resulting density of states for $V_0/B < \beta$, where β is of the order of unity, all states are localised if the fluctuations in the potential depth is large and (e) for $V_0/B > \beta$ there is both extended states in the centre of the band and localised states in the exponential tail.[7]

6.1.2 Electron transport

Conductivity in solids originates from the movement of charge carriers. Excess electrons in the dielectric media have the possibility to 'hop' (*hopping*) or to tunnel (*electron tunnelling*) between traps. In addition, thermally excited electrons can scatter (*scattering*) in the conduction band. A complete description of all the transport theories, and of the behaviour of excess electrons in solids is out of range of the present study. A complete review of those theories can be found in the references 3, 8, and 9. The two-

potential well model[10] is used (see section 6.3) to compute the residence time of electron in traps (section 6.3.3).

Tunnelling from one trap to another can occurs only if there is a certain amount of overlap between the two wavefunctions associated with the traps. The Mott criterion[11] can be used to determine whether an electron can tunnel through the energy barrier separating two traps, that is if the localised states may form a band that allows for conduction via tunnelling. Tunnelling occurs when:

$$(\bar{d})^{-1} \times a_0 \rangle\ 0.25 \tag{6.1}$$

where $\bar{d}$ is the average distance between localised states (see 6.2) and a_0 is the hydrogenic radius of the wavefunction associated to the trap, estimated using Bohr's radius formula for the hydrogen atom, including the dielectrics properties of the medium and the effective mass of conduction electrons:

$$a_0 = \frac{4\pi\varepsilon_0\varepsilon'\hbar^2}{e^2 m^*} \tag{6.2}$$

where ε' is the relative dielectric constant of the material and m* the effective mass of the conduction electrons

6.2 METHODOLOGY

In this section, the relation between electron affinity and electron traps is established. Using this relation, the depth of the electron traps present in the polymeric material is computed. In addition, the density of traps in the polyethylene is estimated. Using the two-well model, the average time spent by an electron in a trap is computed.

6.2.1 The electron affinity and electron traps

The definition of the electron affinity has been given in chapter 3, and is only briefly recalled in this section where the focus is on the 'electron affinity of a defect'. That is, the electron affinity of a molecule in a disordered state, as explain in chapter 5. The

electron affinity (EA) of a molecule is defined as the energy difference between the neutral and anionic state, where the electron is added from the vacuum.

In a solid, the electron affinity is the energy required to bring an electron from the vacuum into the conduction band. The electron affinity of a defect is the energy required to bring the electron from the vacuum level to the defect level. The trap energy (E_t) is the difference between the electron affinity of the system with and without the defect; and it can be written as follows:

$$E_t = EA_{\,defect} - EA_{\,reference} \qquad (6.3)$$

A positive E_t signifies a potential trap for the electron, since in that case the trap has a greater affinity for the electron than the 'pure' material ($EA_{\,defect} > EA_{\,reference}$ in Eq. 6.1). In our model of electron trapping in wax, using the n-$C_{13}H_{28}$ molecule, the reference electron affinity $EA_{\,reference}$ is taken to be the electron affinity of the all-trans n-$C_{13}H_{28}$ molecule, giving,

$$E_t = EA_{\,defect} - EA^{(n\text{-}C_{13}H_{28})}_{\,all\text{-}trans} \qquad (6.4)$$

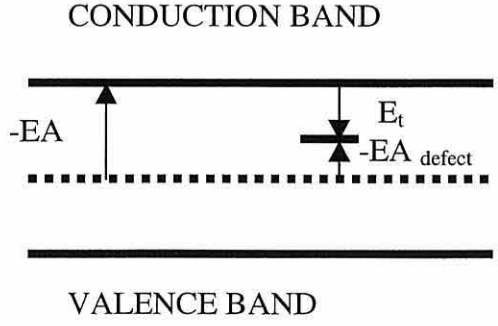

Figure 6.4 Trap energy E_t, defined as the difference between the electron affinity of the system with and without the defect.

In chapter 5, the electron affinity of the tridecane molecule has been computed for many different conformers. Each of these conformers represents a potential electron trap in the gap. Using the electron affinity distribution found in the previous chapter, and using the electron affinity value for the tridecane wax in its ground-state ($EA^{n\text{-}C_{13}H_{28}}_{all\text{-}trans}$ = -1.3 eV) computed in the chapter 3, a distribution of electron traps is obtained and the results are given in section 6.3.

6.2.2 Trap density

From the results in figure 3 we can write the electron affinity of a chain of n carbon atoms as the electron affinity of an infinite alkane chain (EA(∞)) plus a correction which we take to be an end correction, representing the influence of end CH_3 groups, $EA_{ec} = -7.7961(1/n) + 11.897(1/n)^2$.

$$EA(n) = EA(\infty) + EA_{ec}(n) \tag{6.5}$$

We now estimate the electron affinity EA_d (L) of a long chain with L carbon atoms consisting of periodic replica's of the smaller disordered n chain (but with end CH_3 groups removed, i.e. containing n-2 carbons) so that L= m(n-2), where m is an integer. For independent conformational electron traps we write that EA_d (m(n-2))= $EA_d(n) - EA_{dec}(n)$, with $EA_{dec}(n)$ the end correction for conformationally disordered alkanes. Making the approximation that

$$EA_{dec}(n) \approx EA_{ec}(n) \tag{6.6}$$

and letting L tend to ∞, the electron affinity of a long disordered chain is

$$EA_d(\infty) = EAd(n) - EA_{ec}(n) \tag{6.7}$$

From which it follows that the trap energy

$$E_t(\infty) = EA_d(\infty) - EA(\infty) = [EA_d(n) - EA_{ec}(n)] - [EA(n) - EA_{ec}(n)] = EA_d(n) - EA(n)$$

$$= E_t(n) \tag{6.8}$$

is equal to that calculated for the n=13 segment (E_t (n)). The (vertical) localisation energy does not change as n increases because the single electron only sees the local trap that is repeated along the chain. We consider the amorphous regions of polyethylene as consisting of long alkane chains each one a periodic replica of a C_{13} segment found in the wax glass.[12]

6.2.3 Electron residence times in traps

The residence times (τ, in seconds) of the electron inside the traps, estimated using a two-potential model. In this classical model, the two-well minima are separated by a barrier of height E_t, and a distance d. Under the application of an electrical field E_0 in the direction from the ion well or trap site A to that at site B, the ion located at site A will require:

$$E_t - e\frac{d}{2}E_0 \tag{6.9}$$

(where e is the elementary charge ($1.6\ 10^{-19}$ C)) of energy to surmount the barrier in moving from A to B. While the ion at site B in its attempt to move to site A, would face an energy barrier of

$$E_t + e\frac{d}{2}E_0 \tag{6.10}$$

Thus the probability Γ_{AB} of an ion moving from A to B, would be expected to be:

$$\Gamma\exp\left[-(e\frac{d}{2}E_0)/kT\right] \tag{6.11}$$

as opposed to the probability

$$\Gamma\exp\left[(e\frac{d}{2}E_0)/kT\right] \tag{6.12}$$

in moving from B to A; evidently $\Gamma_{AB}>\Gamma_{AB}$.

At zero external field, the probability Γ in moving from A to B or vice versa is equal to

$$\nu_0\exp[-Et/kT] \tag{6.13}$$

where ν_0 is the vibration frequency of the ions within the wells i.e., number of attempted ion jumps per unit time (ca. 10^{11} to 10^{12} jumps per seconds).[10]

In the case of an electron moving from one well to another, the attempt frequency ν_0 is taken in this study from the result for the infinitely deep square well[13]:

$$\nu_0 = h/8m_ed^2 = 4.168\ 10^{13}\ s^{-1} \tag{6.14}$$

where h is the Planck's constant (6.626 10^{-34} J.S) and m_e is the electron mass (9.11 10^{-31} kg).

6.3 RESULTS

In the present work all conformational traps in PE are taken to act independently, electron localisation lengths in polymeric materials are of the order of a few carbon atoms[14]. The number of (single electron) traps along a conformationally disordered PE chain is then equal to the sum of the traps obtained for segments of 13 carbons (represented by the glassy configurations of tridecane) making up the PE chain. The choice of n=13 is a compromise between the high computational cost of DMol calculations on larger molecules and the need to ensure that short chain end effects on conformational and electronic properties are small. In what follows we argue that the trap distribution in the C_{13} wax can, as a first approximation, be used for polyethylene.

6.3.1 Energy trap distribution

As discussed in chapter 5, the increase in bond length leads to an increase in the electron affinity. Therefore, we expect from Figure 4.9 that the electron affinity of molecules in the glass will be increased with respect to the all trans molecule. Since in our calculations for alkanes there is no significant difference between the adiabatic and vertical electron affinity[15], the vertical quantity has been used here. Figure 6.5 reports the distribution of electron trap energies obtained from the amorphous tridecane simulations described in chapter 4. The effect of trapped conformational disorder is to raise the electron affinity by between 0.1 and 0.2 eV so that an electron prefers to sit on a conformational defect rather than be in the conduction band (represented by the all trans or conformationally free molecule). It also shows that the high-density simulations (Glasses B, C, D) lead to larger average trap energies than the low-density simulations (Glasses A_1-A_5). Due to the high density, the constraint applied by the environment is greater than in the low-density simulations, and therefore the molecules are less likely to relax (partially or totally) to the all-trans configuration when the simulating annealing

procedure is applied. Consequently, more gauche defects are found in the high-density simulation compared to the low-density case.

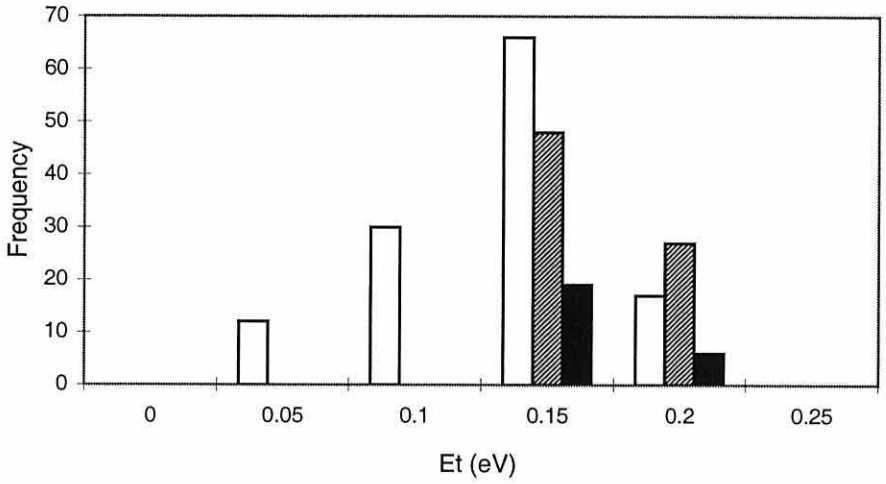

Figure 6.5 Electron trap energy distribution of the tridecane molecules in the glass phase at 150 K: blank histogram, glasses A1-A5, hashed, glasses C-D, filled, glass B).

6.3.2 Trap density

The density of traps in the wax, $f(E_t)$, may now be estimated. To calculate $f(E_t)$ the data from the high-density Glass D have been used. This system, composed of 50 molecules of tridecane, has a volume of 16112.16 $Å^3$ (the cell parameters were a=40.2 Å, b=20.04 Å, c=20.0 Å, $\alpha=\beta=\gamma=90°$). From our calculations for glass D, all the molecules give rise to traps of energy greater than kT (0.0038 eV at 300K), and hence constitute shallow traps. For *this* case, the trap density in the amorphous phase is equal to the number density $50/16112.16 \times 10^{24} \cong 3.1 \times 10^{21}$ traps/cm^{-3}. In a sample of high-density polyethylene (HDPE) where typically 10% of the volume is amorphous, we estimate the *overall* trap density in the PE sample as 10% of that of the wax *i.e.* 3.1×10^{20} traps/cm^{-3}. This value is consistent with the values reported for Anderson[16] localised states by G. Blaise[17] of 10^{19}-10^{20} cm^{-3}. Note that typical experimental space charge measurements in polyethylene report values around 1C/m^{-3} or 10^{12} trapped electrons/cm^{-3}.[18] It is difficult to compare the two numbers as the experimental apparatus only has access to the

trapped electrons (space charge) and not to the traps themselves. The polymer is very likely to suffer electric breakdown long before the complete filling of the entire set of traps. From the calculated density, the average distance between traps is:

$$d = (1/\rho_{trap})^{1/3} = 14.77 \text{ Å} \qquad (6.\ 15)$$

Tunnelling can now be ruled out, using the Mott's criterion (Eq. 6.1) as defined in section 6.1.2: Using m* = Me, ε'=2.3 (dielectric constant of PE), and d=14.77 Å we obtain a value (0.056) well below Mott's criterion of 0.25. Therefore, the tunnelling conduction is negligible in polyethylene.

6.3.3 Residence times

The calculated electron residence times in the traps are displayed in Table 6.1.

Table 6.1 Residence time of electron residence in traps (in seconds), with and without an applied electric field (taken as 10^7 V/m representing a typical cable field[19]), T=300 K.

Et (eV)	$E_0 = 0$	$E_0 = 10^7$ (V/m)
0.05	$1.6\ 10^{-13}$	$1.2\ 10^{-13}$
0.1	$1.1\ 10^{-12}$	$8.6\ 10^{-13}$
0.15	$7.9\ 10^{-12}$	$5.9\ 10^{-12}$
0.2	$5.5\ 10^{-11}$	$4.1\ 10^{-11}$
1	1510.1	1135.4

It can be seen from table 6.1 electron in conformational traps of the sort found in amorphous alkanes have residence time of the order of $10^{-11} - 10^{-13}$ s.

6.4 CONCLUSION

The disorder existing in polymeric material leads to the formation of localised states in the band gap. The disorder present in the n-$C_{13}H_{28}$ wax in the glass phase is taken as representative of the local disorder present in the amorphous phase of polyethylene. The values of the electron affinity of those disordered conformers of the wax, computed in chapter 5, are used in the present chapter to deduce trap energies. We find trap energies between 0.1 and 0.3 eV, in agreement with expectations.[2] Using the classical two-well model, the trapped electrons are found to have residence times of the order of picoseconds.

REFERENCES

[1] P.W. Anderson. Phys. Rev. **109**, 1492 (1958).

[2] L.A. Dissado, J.C. Fothergill. *Electrical degradation and breakdown in polymers.* (Peter Peregrinus Ltd., London, 1992).

[3] H. Böttger, V.V. Bryksin. *Hopping conduction in solids.* (VCH, Berlin, 1985).

[4] R. Zallen. *The physics of amorphous solids.* (John Wiley & Sons, 1983).

[5] S.F. Edwards. J. Phys. **C 3**, L 30 (1970).

[6] B.I. Shklovskii, A.L. Efros. *Electronic properties of doped semiconductors.* (Springer series in solid state sciences, 1984).

[7] C. Klingshirn. Localisation and percolation in alloy semiconductors, in *Disordered solids, structures and processes.* (Baldassare Di Bartolo, Plenum Press, 1990).

[8] S. Whitehead. *Dielectric breakdown of solids.* (Clarendon Press, Oxford, 1951).

[9] P.A. Cox. *The electronic structure and chemistry of solids.* (Oxford University Press, 1987).

[10] R. Bartnikas. IEEE Transactions on Dielectrics and Electric Insulation **4**, 544 (1997).

[11] N.F. Mott. *Conduction in non-crystalline materials.* (Clarendon Press, Oxford, 1987).

[12] M. Meunier, N. Quirke. Molecular modelling of electron trapping in polymer insulators. J. Chem. Phys. **113**, 369 (2000).

[13] P.W Atkins. *Physical Chemistry.* (Oxford University Press, 4th edition, 1990).

[14] R Zallen. *The physics of Amorphous Solids.* (John Wiley and sons, 1983)

[15] M. Meunier, N. Quirke, D. Binesti. The calculation of the electron affinity of atoms and molecules. Mol. Sim. **23**, 109 (1999).

[16] P.W. Anderson. Phys. Rev. **102**, 1008 (1958).

[17] G. Blaise. Fields and polarisation, conduction and charge trapping in insulating materials Abstracts CSC'3 Electric charge in solid insulators, 25 (1998).

[18] T.J. Lewis, Abstracts CSC'3 Electric charge in solid insulators, 16 (1998).

[19] P. Manuel (private communication).

CHAPTER 7

DISCUSSION

7.1 INTRODUCTION

When confronted with the full complexity of nature, the modeller has no option but to simplify that reality. In order to simulate a system, many simplifications and approximations are made, for example the size of the system studied – one centimetre cube of matter contains about 10^{23} atoms and therefore is not treatable by standard simulation tools (such as molecular mechanics, quantum mechanics). The length of the simulations is also short in comparison to real events: in molecular dynamics typical time steps are of the order of one femtosecond (10^{-15} second) and simulations cannot be run for much longer than ~ one nanosecond.

Electrical breakdown in a dielectric polymer is closely related to the creation of space charges in the material.[1] A model to predict the lifetime of the insulating material should include the build-up of the space charge. Several phenomenological models have been developed to explain the formation stage[2] as well as the role of the space charge in the electrical ageing.[3] Nevertheless, a clear identification of its nature, in terms of molecular arrangements, is not yet available. Experimental studies suffer from resolution limitation: even if the charge density value[4] and the mobility of the carriers can be evaluated[5], no experimental technique is currently able to determine the exact nature (at molecular level) of the traps. Molecular modelling approach offers an alternative, as it can gives insight at the atomic level.

This chapter is a critical analysis of our model. In particular, the approximations employed in the present thesis are investigated and justified. The approximations have been divided in three groups (sections 7.2.1 to 7.2.3) depending upon their nature. The first group includes the *general* approximations, due to modelling, i.e. employing a short alkane wax to model the polyethylene. The second and third groups include the approximations due to computational limitations from quantum calculations and classical simulations. Finally, the role of defects both of physical and chemical origin is explained and discussed.

7.2 APPROXIMATIONS

The different approximations employed in this study are reviewed, discussed and justified in this section.

7.2.1 General approximations

It has been demonstrated in chapter 3 that the electron affinity of a wide range of atoms and molecules could be accurately computed using DFT. In this research, the main concern is the electron affinity of alkanes, in particular tridecane and polyethylene. This will enable us to learn how the electron affinity varies with the conformation, which in turn will enable us to compute the trap energies. Measurements have been carried out for methane (-5 eV)[6], hexatriacontane n-$C_{36}H_{74}$ (-0.3 ± 0.5 eV)[7] and polyethylene (-0.5 ± 0.5 eV).[8] The value of –5 eV for methane suggests that small alkane anions are metastable and difficult to observe.[9] It has been suggested that the electron affinity increases with increasing carbon chain length and approaches an asymptote with n-butane.[10] This trend is reflected in our DFT calculations (Figure 7.1) which clearly show the increase in the electron affinity for the linear alkanes as the chain length increases and the slow variation after butane.

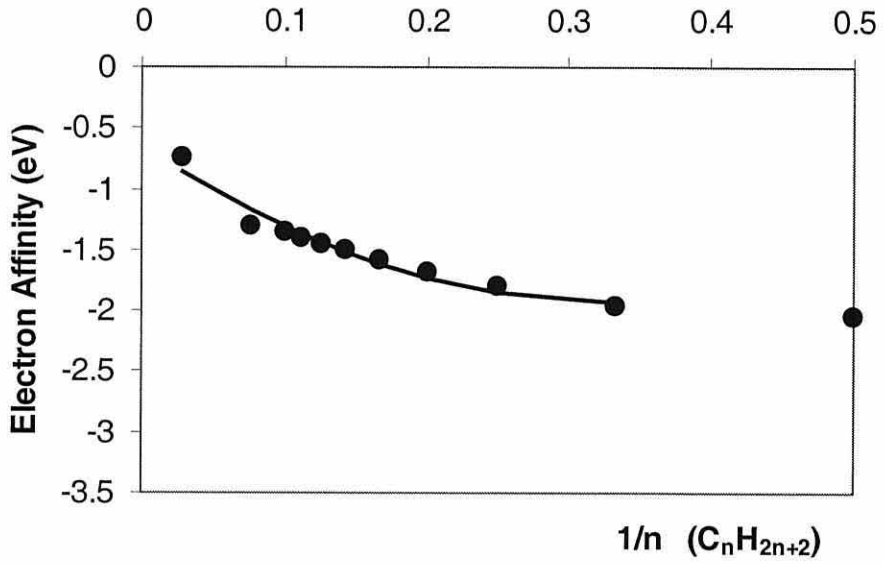

Figure 7.1 Variation of vertical electron affinity with inverse chain length for the linear alkanes (from Table 3.3). Filled circles correspond to the DMol calculations and the line to a quadratic fit [$E(n)= - 0.6499 - 7.7961(1/n)+ 11.897(1/n)^2$] to the results for $n \geq 3$.

These results can be interpreted as reflecting a reduction in the influence of the terminal methyl groups on the lowest unoccupied molecular orbital (LUMO) as the hydrocarbon chain grows. DMol, while predicting too positive an electron affinity for methane (-2.9 eV), is consistent with the experimental data for n-$C_{36}H_{74}$ (-0.75 eV) and polyethylene (-0.65 eV $n=\infty$). Estimates of the electron affinity of alkanes using DMol become better (when compared to experimental values) as the chain length increases. It follows that the methodology developed in chapter 3 can be used to predict the electron affinity of conformers of the tridecane alkane.

The linear alkane tridecane (n-$C_{13}H_{28}$) is used as a model of a short segment of a chain of polyethylene. This is justified by the similarities between the electronic band structure, and thus the electronic properties of the tridecane molecule and the polyethylene.[11-12] Despite the difference between the electron affinity of the tridecane and polyethylene, the electron affinity of the tridecane alkane could be employed when computing the trap energy as demonstrated by equations 6.5 to 6.8. The calculated

electron affinity of the tridecane molecule in the all-trans conformation is –1.3 eV.[13] The (vertical) localisation energy does not change as the number of CH_2 segment increases because the single electron only sees the local trap that is repeated along the chain. In this thesis, the amorphous regions of polyethylene are considered as long alkane chains each one being a periodic replica of a C_{13} segment found in the wax glass. It is assumed that the conformational defects displayed by molecules in the simulations of amorphous tridecane are representative of the local conformational defects in polyethylene as are the consequent local variations in electronic properties. That is to say that the microstructure of the amorphous polyethylene can be modelled by the tridecane wax in the glass phase.

A relation has been established in chapter 6 (Equation 6.4) linking the electron affinity and the trap energy in which an electron affinity of reference is employed. In the model, the excess electron has the 'choice' between the defect state (modelled by a conformationally distorted tridecane chain) and the crystalline conduction band (modelled by the all-trans tridecane conformer). Since all the electrons strive to minimise their energies by occupying the orbital with the lowest energy possible, the excess charge will end up in the defect state if the latter has an energy less than that of the all-trans conformer. In this case, the defect state represents a trap, in the common sense of the term. It can be argued that as the electron affinities of the various alkanes studied are negative, the electron should indeed escape (in the vacuum). In this case the space charge present in the material should be localised into regions (atoms, ions) of positive electron affinity. Nevertheless, the results of the (positive) trap energies suggest that, if the electron is injected inside the material in the conduction band of a polymeric chain, it will prefer to sit in those localised defect states to lower its energy.

When computing the depth and the density of traps each molecule carries a maximum of one trap. There are two assumptions in the present statement: (i) there is only one (physical) trap per 13 CH_2 segments of the polymer, and (ii) one trap is only singly occupied. In the present research all conformational traps in polyethylene are assumed to be acting independently, and the electron localisation lengths in polymeric materials are of the order of a few carbon atoms[14] (see figure 6.2). The number of (single

electron) traps along a conformationally disordered PE chain is then equal to the sum of the traps obtained for segments of 13 carbons (represented by the glassy configurations of tridecane) forming the PE chain. The choice of n=13 is a compromise between the high computational cost of DMol calculations on larger molecules and the need to ensure that short chain end effects on conformational and electronic properties are small. In addition, the probability of a second electron entering an occupied trap is certainly negligible due to the electronic repulsion. It is even likely that traps physically close to an occupied trap stays empty due to this repulsion.

The electron affinity of isolated tridecane conformers has been computed in vacuum. In following this procedure the effect of intermolecular interactions (except for steric hindrance) and of polarisation in changing R_e (see Equation 3.4) is neglected. However, as a first approximation these effects are assumed to be less important in determining the electron affinity than the fact that the molecules are *conformationally* trapped. Moreover, the polarisation effect is certainly very small because the material is non-polar. In polyethylene, the interactions between molecules are weak, and therefore the defect states are closely related to the characteristic states of the individual molecules.[15]

The type of charge carrier primarily responsible for conduction depends not only on the material's chemical and physical composition but also on the frequency of the applied field and the temperature.[1] Charge carriers can be ions, electrons, and holes. This thesis is focused on the electronic traps. The reason being that the ageing phenomena is thought to be due to the destructive interactions between the excess electrons and the dielectric.[11,15,29] Cartier and co-workers[16] have developed a method based on photo-injection of hot electrons into the conduction band of insulators and have measured their energy distributions. Results on hexatriacontane have shown that degradation was caused by hot electrons with energies as low as 3 to 4 eV and that higher energy electron could cause bond scissions, polymerisation and were increasing the trap density from 10^{-16} to 10^{-22} m^{-3}.

Ions might also be present inside the material They originate from external intrusion, or from industrial additives and by-products.

In this work, the physical defects present in the polymeric material have been studied, that is, all the fragments of PE chain which are not in the all-trans conformation. Where are the physical defects such as those studied here? Firstly, in the amorphous phase of the polyethylene where every single chain is subject to torsion, twisting, elongation, etc. Because of the neighbouring molecules, the polymeric chains are trapped in this disordered (with respect to the crystalline order) state. For long alkane molecules, the cost of having few cis (or gauche) defects (about 4 kJ mol^{-1} each) can be compensated by the attractive van der Waals potential and therefore the geometry of the lowest energy is no longer the all-trans geometry (Figure 7.2). The length of the chain at which the geometry of the lowest energy changes from all-trans to a hairpin is still a matter of debate[17] as it involves precise computation of van der Waals energy terms that are very sensitive to the computational parameters employed (forcefield, basis set, etc.). Moreover, in the crystalline phase where the chain of polyethylene whilst adopting an all-trans (planar) conformation folds back and forth inside the same crystal. In both cases, the effect of the presence of gauche (or twist) defects will be an elongating of the carbon-carbon bond distance (Chapter 4) and therefore an increasing of the electron affinity (Chapter 5) thus representing a trap (Chapter 6).

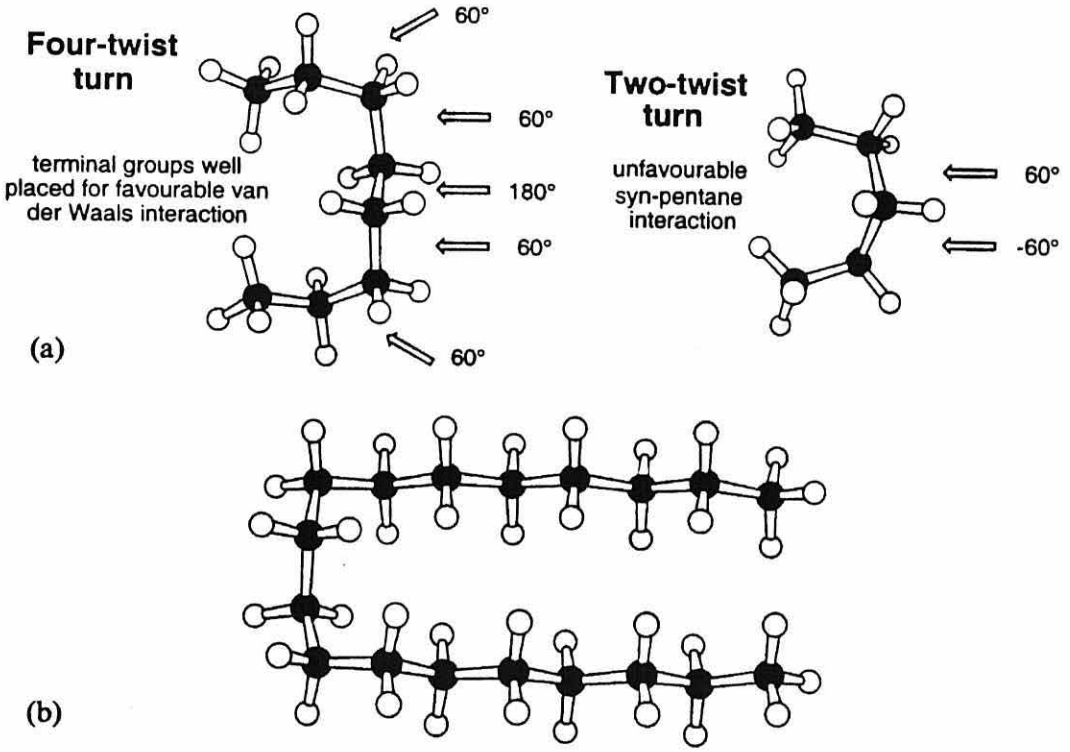

Figure 7.2 (a) Two-twist and four-twist turns in short linear alkanes. (b) Lowest energy conformation for n-$C_{18}H_{38}$.[18]

There exist two competing models to describe the re-entry of the chain in the crystal. The 'adjacent re-entry' model proposed by Keller[19] and the 'switchboard' model by Franck,[20] (Figure 7.3). None of the existing experimental techniques (i.e. x-ray scattering, NMR) have been able to chose between the two models.[21] At each lamella interface, there exist some physical defects such as those mentioned above. It is also likely that some gauche and twist defects might be present in the crystal phase.

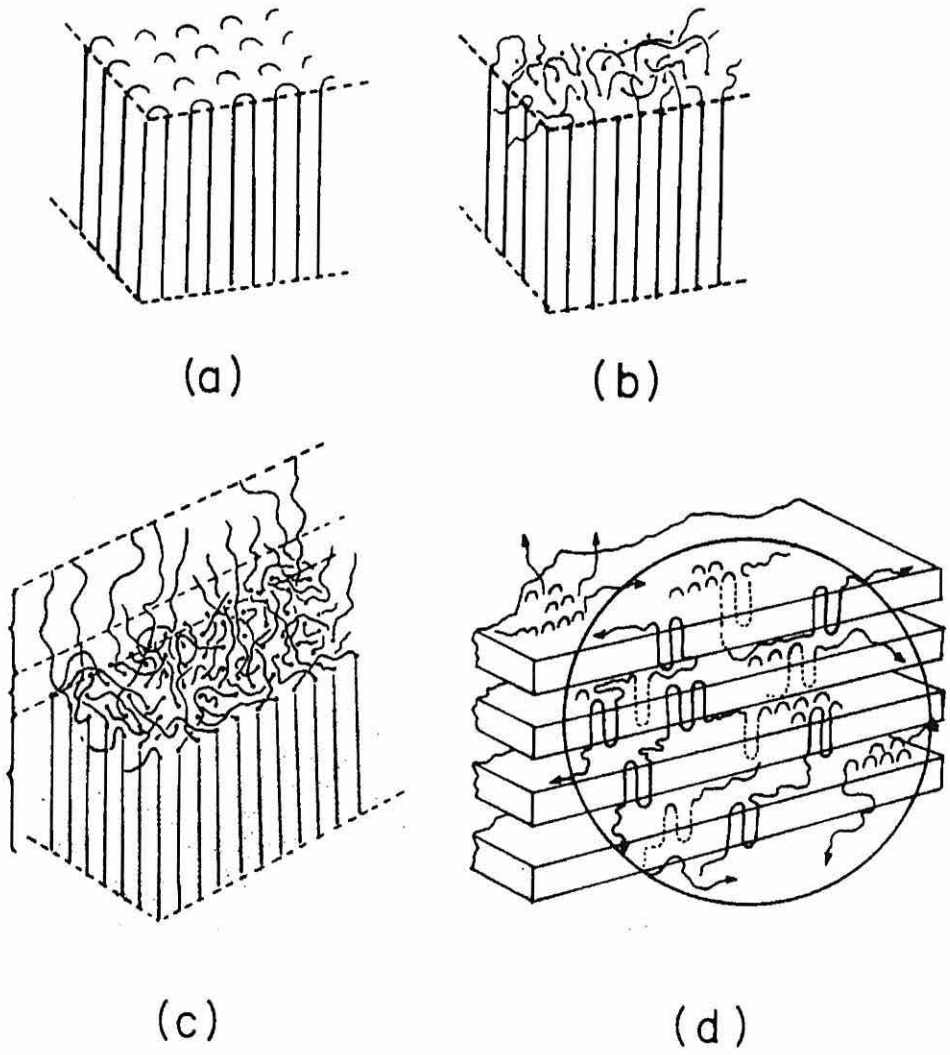

Figure 7.3 Re-entry process in polymer crystals: (a) adjacent re-entry, (b) random re-entry, (c) interzonal, (d) combined model.[22]

The second kind of defects present in polymeric material relates to the presence of chemical impurities. These may have two origins. Intrinsic defects are present on the polyethylene chain itself and include bond insaturation, 'organic' functions (alcohol, thiol, ketone, etc.). Ramification and chain ends can also be included in this category, although they do not represent a chemical impurity strictly speaking. Conversely, extrinsic defects originate either from the infiltration of external molecules (water, oxygen, methane, etc.) inside the cable, or from the addition, during the manufacture of the cable, of chemical compounds (antioxidant, branching agents, etc.). The electron

affinity of each of those species can vary a lot, and some of them can be responsible for the formation of deep traps.[23]
The role of the different defects, in terms of ageing and/or conductivity in the dielectric breakdown phenomenon is discussed in section 7.3.

7.2.2 Approximations due to quantum calculations

The second type of approximation is due to computational limitations. Within this group, the zero point energy (ZPE) corrections could not be applied in the computation of the electron affinities of the tridecane conformers. ZPE's are obtained via the calculation of all vibrational modes of the system studied, and in our case, the tridecane molecule is too large. The estimation of the value of this energy is rather difficult. Though, this value can be quite substantial, i.e. ~100kcal/mol for a six-carbon alkane.[24] However, the difference in energy between the ZPEs of the neutral and of the anion is certainly much smaller. In our calculations of the ZPE of small (organic) molecules, the sign could be either positive or negative, giving more uncertainty to this estimation. In addition, relativistic effects have also been neglected. These are important only for heavy atoms and are always neglected in the case of organic compounds.

Chapter 3 explores in detail the use of density functional theory (as expressed in the widely available code DMol) to calculate electron affinities for a representative sample of small atoms and molecules having both positive and negative values. The purpose of these calculations was to assess the accuracy of a routine DMol calculation of electron affinity i.e. a calculation that has not been tailored to a particular species. In addition, the focus was in the electron affinity of alkanes and its variation with molecular conformation: a subject little explored to date. The basis set employed successfully computed the electron affinity of a large range of molecules.[13] Nevertheless, in order to elucidate the behaviour of the total energy from DMol for metastable anions, the variation of anionic energy with respect to diffuse functions has been investigated. Diffuse functions have a well-known role in obtaining realistic energies of small anions.[25] The energy of both the neutral and the anion were computed for various basis

sets following the addition of diffuse functions. In our calculations, the energy of the neutral atom or molecule was essentially independent of the addition of extra diffuse functions as expected. In contrast, for molecules having negative electron affinities, the SCF energy of the anions with the addition of diffuse functions changes considerably. In all cases, the addition of diffuse functions stabilises the anion; only slight variations were observed on addition of further diffuse functions until a point where the SCF energy suddenly drops and tends towards that of the neutral species. At this point, there are sufficient diffuse functions to allow the electron to separate from the molecule. A typical result is given for the tridecane molecule (Figure 3.4). In the case where the electron affinity is positive, the addition of increasingly diffuse functions had little effect. Thus, one could argue that in the calculations carried out in the present research, the tridecane anion exists only due to the small size of the basis set: an 'infinite' basis set would lead to the tridecane molecule in the neutral ground state plus the (excess) electron 'free' at infinity, giving an electron affinity of zero. However, atomic and molecular negative electron affinities computed in chapter 3 (Tables 3.1 b and 3.2 b) are in agreement with experimental results. In addition, the (negative) electron affinity computed for hexatriacontane, similar to that of polyethylene, also confirms the results derived from experimental data. So, the metastable anion is represented by the plateau region of the DMol calculations (Figure 3.4).

7.2.3 Approximations due to classical calculations

The geometry optimisations of the tridecane wax in glass phase, model of amorphous segment of polyethylene, have been performed using classical molecular mechanics (a simulated annealing procedure has been used), instead of using the DFT to perform these geometry optimisations. Quantum tools could not be used due to the large system size. As well, the independence of the electron trap distribution with respect to the forcefield used was demonstrated.[26] Our results could be improved via DFT calculations to perform the geometry optimisation of a single isolated chain, and the environment (neighbouring molecules) could be described by using a solvation model, that is, a classical 'point-charges' grid, ensuring a dielectric constant equal to the experimental

value for polyethylene of 2.3.[27] However, the polarisation effect of neighbouring molecules is believed to be small (section 7.2.1).

7.3 THE ROLE OF DEFECTS

When an external electric field is applied to a dielectric such as polyethylene, there is a dielectric absorption. The resulting polarisation persists even after removal of the field, despite the fact that the material is non-polar. This polarisation is due to the localisation inside the material of charge carriers from the electrodes. Those trapped charges are known as space charge. The role of the space charge in the ageing and in the dielectric breakdown phenomena is frequently reported in the literature.[15,28,29]

Physical defects such as those presently studied are responsible for the shallow traps found in the band gap of polyethylene as demonstrated in this thesis. Their depth has been found to be of the order of a few tenths of an eV, and their residence time of the order of a few picoseconds. It is therefore unlikely that those traps are responsible for the presence of long-lived space charge in the dielectric. Nevertheless, those shallow traps will allow the conduction of the excess charges through the polymeric material via hopping conduction.

Microcavities have long been suspected for the presence of space charge in polymeric material.[28-29] Cavity traps formed by local arrangements of molecular chains seem very likely in polymer. In addition, sub-microcavities may tend to coalesce to form microcavities and eventually cavities. An electron trapped in such a cavity could gain sufficient kinetic energy from the electric field to break molecular bonds, thus leading to the ageing of the material. As well, the molecular motions are closely related to the detrapping of electrons.[29]

The interface between the amorphous phase and the crystalline is also suspected to be a strong region of trapping.[1] A heterogeneous medium exhibits frequency-dependent dielectric and conductive properties that differ from those of the constituent

components. This interfacial polarisation (or dielectric dispersion) is known as a Maxwell-Wagner polarisation.[30-31]

Chemical defects are thought to be responsible for the deep traps in polyethylene. The effect of some of those defects (those with a high electron affinity) on the trapping/detrapping phenomena is likely to be greater than that of the physical defects. Indeed, the higher the electron affinity of those compounds, the more likely they are to trap an electron present in the material (assuming a square potential well for the trap).[23] In addition, an electron trapped in such a defect will have a long residence time (section 6.2.3). The effect of the presence of this trapped charge (space charge) is to enhance the (local) electric field via polarisation of the surrounding. The energy associated with the relaxation of the material when the charge eventually escape can be sufficient to induce locally some physical damage, increasing the trapping capacity of the material.[16]

7.4 CONCLUSION

The purpose of this chapter was to discuss the main approximations employed in this thesis as well as the role of physical and chemical defects. These approximations consisted mainly of the use of the tridecane molecule in a glass phase as a model of the microstructure present in the amorphous phase of polyethylene, and a relation between the electron affinity of the molecule and the trap depth. Assumptions were made in order to describe accurately the electronic structure of the tridecane molecule in a conformational disordered state, thus allowing the computation of electron affinity.
In addition, the nature of the defects present in dielectric material has been reviewed. The results suggest that the deep traps, originating from the presence of chemical impurities, are responsible for the presence of a long-lived space charge in the material, whereas the shallow traps, originating from physical defects, change the local electrical property of the material.[1]

7.5 REFERENCES

[1] L. A. Dissado and J. C. Fothergill, *Electrical Degradation and Breakdown in Polymers*. (Peter Peregrinus Ltd., London, 1992).

[2] G. Blaise, J. Appl. Phys. **77** (7), 2916 (1995).

[3] L. A. Dissado, G. Mazzanti and G. C. Montanari, IEEE Trans. Diel. & EI **2**, 1147 (1995), ibid **4**, 496 (1997), see also G. Mazzanti, G.C. Montanari, L. Dissado, Proceedings of JICABLE'99, 707 (1999).

[4] G. C. Montanari, D. Fabiani, L. Bencivenni, B. Garros, C. Audry, Proceedings of the CEIDP, 38 (1999).

[5] N. Hozumi, Y. Muramoto, M. Nagao, Proceedings of the CEIDP, 350 (1999).

[6] K. Rohr, J. Phys. B **13**, 4897 (1980).

[7] R. Dudde, B. Reihl, Chem. Phys. Letts. **196**, 91 (1992).

[8] K. J. Less, E. G. Wilson , J. Phys. C.: Solid State Physics **6**, 3110 (1973).

[9] O. Schaefer, M. Allan, G. Szeimies, M. Sanktjohanser, J. Am. Chem. Soc. **114**, 8180 (1992).

[10] F.H. Dorman, J. Chem. Phys. **44**, 3856 (1966).

[11] C. Laurent, C. Mayoux, *Electronic Processes in Electrical Ageing*, Arpeggio Seminar, (1994).

[12] J.J. Pireaux, Phys. Rev. A **14**, 2133 (1976).

[13] M. Meunier, N. Quirke, D. Binesti. The calculation of the electron affinity of atoms and molecules. Mol. Sim. **23**, 109 (1999).

[14] R Zallen, *The physics of amorphous solids*. (John Wiley and sons, 1983).

[15] T.J. Lewis. The micro-physics of charge in dielectric. CSC'3 *Electric charge in solids insulators*, 16 (1998).

[16] E. Cartier, P. Pfluger. Phys. Rev. B, **34**, 8822 (1986).

[17] G.M. Goodman. What is the longest unbranched alkane with linear global minimum conformation? J. Chem. Inf. Comput. Sci. **37**, 876 (1997).

[18] G.M. Goodman. *Chemical Applications of Molecular Modelling*. (RSC, 1998).

[19] A. Keller. Philos. Mag. **2**, 1171 (1957).

[20] F.C. Franck. Faraday Discus. Chem. Soc. **68**, 7 (1979).

[21] S. Balijepalli, G.C. Rutledge. Molecular simulation of the intercrystalline phase of chain molecules. J. Chem. Phys. **109**, 6523 (1998).

[22] P.J. Phillips. *Morphology and molecular structure of polymers and their dielectric behaviour.* Enginering dielectrics, Vol. IIA, Chapter 2. (Bartnikas/Eichorn 1983).

[23] M. Meunier, A. Aslanides, N. Quirke. Work in progress.

[24] A.R. Leach. *Molecular modelling. Principle and applications.* (Longman, 1996).

[25] J. Simons, P.D. Burrow. Ab-initio electronic structure of anions. Chem. Rev. **87**, 535 (1987).

[26] M. Meunier, J. A. Anta, N. Quirke. EDF Program Report N°7 (June-September 1999).

[27] D.R. Lide. *Handbook of Chemistry and Physics.* (CRC Press 76th edition, 1997).

[28] J.P. Crine. A molecular model to evaluate the impact of ageing on space charges in polymer dielectrics. IEEE Transactions on Dielectric and Electrical Insulation **4**, 487 (1997).

[29] M. Ieda. Electrical conduction and carrier traps in polymeric materials. IEEE Transactions on Dielectric and Electrical Insulation **EI-19**, 162 (1984).

[30] J.C. Maxwell. *A treatise on electricity and magnetism.* (Clarendon press, Oxford, 1881).

[31] R. Pethig. *Dielectric and electronic properties of biological materials.* (John Wiley & Sons, Chichester, 1979).

CHAPTER 8

CONCLUSION

The aims of this chapter are to summarise briefly the work carried out in this thesis, to emphasise both the key achievements and what has been added to the field of space charge trapping. Finally, future work that would complete the present research is suggested as well as the uses of the results of the electron trap energy distribution in macroscopic models. As pointed out in chapter 1, there was a need for a better understanding, at the molecular level, of the phenomenon of space charge in dielectric, and in particular in the polyethylene as it is extensively used by electrical suppliers for underground high voltage cables. In chapter 2, the tools employed in this thesis were described and their capabilities to study the electronic and conformational properties of molecules established.

The electron affinity is an important molecular property in chemistry, as shown in chapter 3. In this chapter, a methodology to compute accurately the electron affinity of a wide range of atoms and molecules was described. In the literature, the difficulty of estimating electron affinities of molecules with a deviation less than 0.2 eV has been pointed out.[1] At considerable computational expense, it is possible to obtain a higher accuracy but in that case, the size of the system studied is restricted. The results of the electron affinities reported in chapter 3 have a root mean square deviation from recommended value of 0.1 eV for atoms and 0.3 eV for molecules. In addition, the same method (functional, basis set, etc.) has been employed for the 44 systems. Furthermore, the electron affinity of the alkane class (n-C_nH_{2n+2}) have been given for n=1 to 36 for the first time (only n=1 or n=36 are reported in the literature).

The microstructure of the amorphous phase of polyethylene was described in chapter 4 using glassy phases of the tridecane wax as a model. A methodology to produce glassy phases of the tridecane wax has been suggested. The simulations show that the average carbon-carbon bond length increases in the amorphous region compare to the crystalline phase. This is due to the presence of gauche defects that increase the hydrogen-hydrogen repulsion of adjacent carbon atoms (Figure 4.7) in the amorphous phase. The generation of many conformers of the tridecane molecule has given a wide sampling of the local microdisorder present in the amorphous phase of polyethylene, thus identifying the physical defects present in this material.

In chapter 5, the effect of molecular conformation on electron affinity has been explored for the alkane molecules of special interest in the present study. It is shown that the frontier energy orbital LUMO varies inversely with the bond length, as expected from the Mulliken and Walsh model. This is due to the decreasing atomic overlap of the anti-bonding σ^* orbital (LUMO). Using equation 5.5 (Koopman's theorem) a decrease of the LUMO energy value (occurring when the carbon-carbon bond distance increases) results in an increase in the electron affinity. The distribution of the electron affinity of the tridecane conformers present in the simulated glass phases has been computed. Using the relation between the electron affinity and the trap energy (equation 6.4), a distribution of trap energies has been obtained. The schematic figure 6.1 is commonly employed in the literature concerning the space charge problem. Employing the distribution obtained in chapter 6 (Figure 6.5), this representation can now be made quantitative. To the best of our knowledge, this is the first time that the depth of electron traps in polyethylene has been predicted. In addition, the trap density has been estimated to be ~3.1 10^{20} traps/cm^3 in polyethylene. This value is consistent with reported data.[2-3] The residence time of the electron in traps has been estimated to be of the order of a few picoseconds.

Further work should include the computation of the energy of the traps originating from interfacial defects, microcavities and from chemical defects. Microcavities can be studied using cluster (e.g. a fragment of a crystalline phase) calculations of alkane wax, where the central chains are removed, thus modelling a void. By computing the

difference in energy between the system with and without the void, the trap energy is deduced. Interfaces are more difficult to study with quantum mechanics tools due to the size of the system of study. Nevertheless, the present work represents a first step toward their study. Indeed, at the interface, the chains of polymer are folding back and forth inside the crystallite (see figure 7.3). The conformers present in the glassy phases such as studied in chapter 4, possess such local arrangement.

Chemical defects represent another class of defects of interest. As previously mentioned, those defects are likely to be responsible for the deep traps present in the dielectric, and therefore the residence time of the electrons in such traps is high (when compared to the residence time of electrons in traps originating from conformational defects). The study of these defects include a fine chemical analysis of the various compounds (and organic functions) present in the material. Such an analysis is not trivial. Some of the chemical defects concentration can be obtained using infrared spectroscopy (i.e. double bonds, ketone, etc.) but some of the additives present are in too small quantity inside the material to be detected (e.g. acetophenone). Therefore, their role in the space charge trapping phenomenon is much more difficult to assess. In addition, industrial engineers are very reluctant to provide such precise information for obvious reason of industrial property. Using the relation between electron affinity and trap depth established in chapter 6, the trap energy of a set of chemical defects, commonly found in polymeric insulators used for high-voltage cable insulation has been computed[4] (table 8.1).

Table 8.1 Electron affinity and trap depth for the molecules presented in figure 8.1. (All values are in electron volts).[4]

Molecule	Electron Affinity	Trap depth
tridecane	-1.30	0.00
6-tridecene	-1.14	0.16
5,7 tridecene	-0.79	0.51
6-tridecyne	-1.21	0.09
vinyl 6 dodecane	-1.07	0.23
6-tridecanone	-0.81	0.49
6-tridecanal	-0.59	0.71
6-tridecanol	-1.08	0.22
alpha-methylstyrene	0.23	1.53
Cumylalcohol	-1.02	0.28
Acetophenone	-0.40	0.90
Cumene	-1.26	0.04

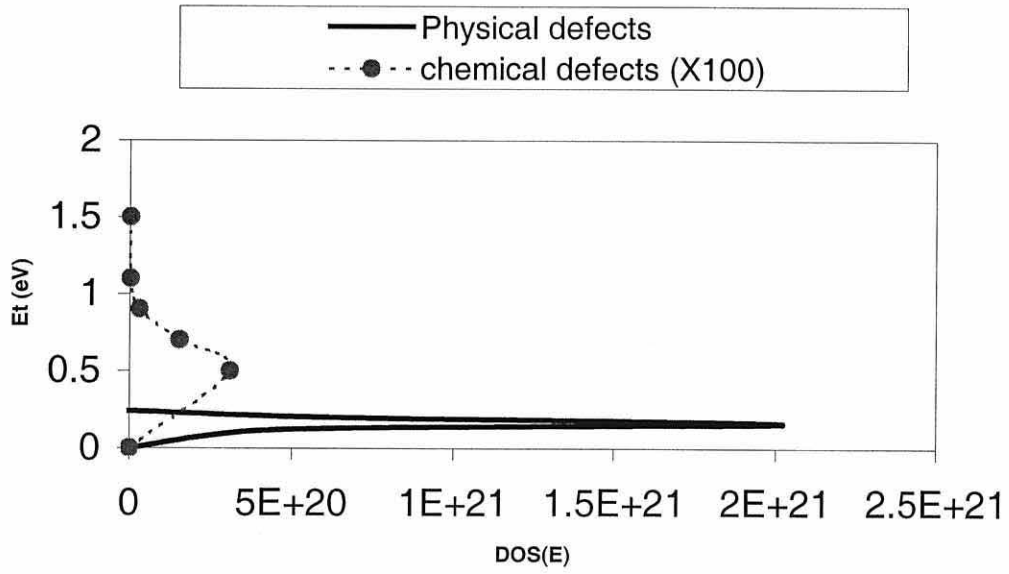

Figure 8.1 Energy trap distribution in model polyethylene.[4]

The electron trap energy distribution (figure 8.1) has been used in the simulation of the transport properties of excess electrons in polyethylene.[5] In addition, it has been used as input for a macroscopic calculation of the current-voltage characteristics of an insulation of finite geometry.[6] The aim of the macroscopic simulation being (i) the estimation of the life time of the dielectric material under the influence of a high electric field and (ii) the design of better cables.

A certain number of approximations employed in the present work could be removed using the recent progress in time-dependent quantum methods. For example, the effect of polarisation/delocalisation has been neglected.[7] The major shortcoming of the molecular dynamics approach is the complete neglect of quantum mechanical effects. The adiabatic approximation could be removed using surface hopping[8] (or similar) methods. This method originally developed by Tully and co-workers[9] has many variants. The main difference between them being the 'switch' algorithm that governs the transition probability between different quantum states. Like in the Ehrenfest approach, in the surface hopping method, the quantum character of a few selected degrees of freedom is included explicitly while the reminder of the system is treated classically, and the time-dependent Schrödinger equation is solved self-consistently. At each integration time step, a decision is made whether to switch electronic states, according to probabilistic "fewest switch" algorithm.[8] In the case of a favourable hopping event, the energy is conserved by adjusting the component of velocity in the direction of the nonadiabatic coupling vector. The transition (hop) can occur at any time step, between any coupled states, depending of the quantum mechanical probability only. In the MDQT (molecular dynamics with quantum transition) method proposed by Tully, some quantum effects are still neglected, i.e. tunnelling, and zero-point-motion.

REFERENCES

[1] J. Simons, K.D. Jordan. Ab-initio electronic structure of anions. Chem. Rev. **87**, 535 (1987).

[2] P.W. Anderson. Phys. Rev. **102**, 1008 (1958).

[3] G. Blaise. Fields and polarisation, conduction and charge trapping in insulating materials. Abstracts CSC'3 Electric charge in solid insulators, 25 (1998).

[4] M. Meunier, A. Aslanides, N. Quirke. To be submitted.

[5] J. Anta, M. Meunier, N. Quirke. To be submitted.

[6] P. Manuel, Program MASCARET, E.D.F. (1999).

[7] Preliminary estimates (M. Meunier, N. Quirke, unpublished) lead us to believe that the trap energies in polyethylene may be reduced by up to 50% due to neighbouring PE chains.

[8] J. C. Tully. Molecular dynamics with electronic transitions. J. Chem. Phys. **93**, 1061 (1990), see also S. Hammes-Schiffer, J. C. Tully. Proton transfer in solution: molecular dynamics with quantum transitions. J. Chem. Phys. **101**, 4657 (1994), D. F. Coker, L. Xiao. Methods for molecular dynamics with non-adiabatic transitions. J. Chem. Phys. **102**, 496 (1995).

[9] J.C. Tully, R.K. Preston. J. Chem. Phys. **55**, 562 (1971).

BIBLIOGRAPHY

Ahmed, N.H. Srivinas, N.N. Review of space charge measurements in dielectrics. IEEE Transactions on Dielectrics and Electrical Insulation **4**, 644 (1997).

Alle, D.T. Brennan, M.J. Buckman, S.J. Low-energy total electron scattering cross section and electron affinity for NO. J. Phys. B: At Mol. Opt. Phys. **29**, L277 (1996).

Allen, J.A. *Studies in innovation in the stell and chemical industries.* (Manchester University Press, 1967).

Allen, M.P. Tidelsley, D.J. *Computer simulation of liquids.* (Clarendon Press, Oxford Science Publications, 1987).

Amorphous-cell User Guide. (Molecular Simulations Inc. San Diego, 1996).

Anderson, H.C. Molecular dynamics simulations at constant pressure and/or temperature. J. Comp. Physics. **72**, 2384 (1980).

Anderson, P.W. Phys. Rev. **102**, 1008 (1958).

Anderson, P.W. Phys. Rev. **109**, 1492 (1958).

André, J.M. Kapsomenos, G.S. Leroy, G. A comparison of ab-initio, extended-Huckel and CNDO band structures for polyene and polyethylene. Chem. Phys. Letters **8**, 195 (1971).

Arnold, D.W. Bradforth, S.E. Kitsopoulos, T.N. Neumark, D.M. Vibrationally resolved spectra of C2-C-11 by anion photoelectron spectroscopy. J. Chem. Phys. **95**, 8753 (1991).

Atkins, P.W. *Physical Chemistry.* (Oxford University Press).

Avitabile, G. Napolitano, R. Pirozzi, B. Rouse, K.D. Thomas, M.W. Willis, B.T.M. J. Polym. Sci. Polym. Lett. D. **13**, 351 (1975).

Balijepalli, S. Rutledge, G.C. Molecular simulation of the intercrystalline phase of chain molecules. J. Chem. Phys. **109**, 6523 (1998).

Baroni, S. Tucel, E. Exact-exchange extension of the local-spin-density approximation in atoms: Calculation of total energies and electron affinities. J. Chem. Phys. **79**, 6140 (1983).

Bartnikas, R. Engineering Dielectrics, volume IIA, Electrical properties of solid insulating materials: Molecular structure and electrical behaviour. (R. Bartnikas, R.M. Eichhorn editors, 1983).

Bartnikas, R. IEEE Transactions on Dielectrics and Electric Insulation **4**, 544 (1997).

Becke, A.D. Density-functional exchange-energy approximation with correct asymptotic behaviour. J. Chem. Phys. **88**, 2547 (1988).

Berendsen, H.J.C. Postma, J.P.M. van Guntersen, W.F. DiNola, A. Haak, J.R. Molecular dynamics with coupling to an external bath. J. Chem. Phys. **81**, 3684 (1984).

Blaise, G. Moya, G. Abstracts CSC'3 Electric charge in solid insulators, 160 (1998).

Blaise, G. Fields and polarisation, conduction and charge trapping in insulating materials. Abstracts CSC'3 Electric charge in solid insulators, 25 (1998).

Blaise, G. J.Appl. Phys. **77**, 7 (1995).

Bloor, D. Correlation of experimental and theoretical electron band energies of polyethylene. Chem. Phys. Letters **40**, 323 (1976).

Born, M. Oppenheimer, J.R. Ann. Physik **84**, 457 (1927).

Borrmann, A. Montanari, B. Jones, R.O. Density functional study of polypropylene and its submolecules. J. Chem. Phys. **106**, 8545 (1997).

Böttger, H. Bryksin, V.V. *Hopping conduction in solids.* (VCH, Berlin, 1985).

Bouteiller, Y. Desfrancois, C. Schermann, J.P. Latajka, Z. Silvi, B. Calculation of electronic affinity and vertical detachment energy of the water dimer complex using the density functional theroy. J. Chem. Phys. **108**, 7967 (1998).

Boys, S.F. Proc. Roy. Soc. (London) **A200**, 542 (1950).

Brydson, J.A. *Polymer science* (A.D. Jenkins, North Holland, 1972).

Buenker, R.J. Peyerimhoff, S.D. Molecular Geometry and the Mulliken-Walsh Molecular Orbital Model. An ab-initio Study. Chemical Review **74**, 128 (1974).

Burkert, U. Allinger, N.L. *Molecular mechanics.* (American Chemical Society, Washington, 1982).

Cartier, E. Pfluger, P. Phys. Rev. B **34**, 8822 (1986).

Christodoulides, A.A. McCorkle, D.L. Christophorou, L.G. *Electron molecule interactions and their applications.* (Academic Press, New York, vol. 2, 423, 1984).

Chu, N.S. Burrow, P.D. Jordan, K.D. Temporary anions of the fluoroethylenes. Chem. Phys. Letters **68**, 121 (1979).

Coker, D.F. Xiao, L. Methods for molecular dynamics with non-adiabatic transitions. J. Chem. Phys. **102**, 496 (1995).

Colbourn, E.A. Kendrick, J. *Computer simulation of polymers, chapter 4: molecular modelling of crystalline polymers.* (Ed. E.A. Colbourn, 1994).

Collins, R.E. Practical application of the thermal pulsing technique to the study of electrets. J. Appl. Phys. **51**, 2973 (1980).

Cox, P.A. *The electronic structure and chemistry of solids.* (Oxford University Press, 1987).

Crine, J.P. A molecular model to evaluate the impact of ageing on space charges in polymer dielectrics. IEEE Trans. Dielec. and Elect. Insul. **4**, 487 (1997).

Csizmadia, I.G. Harrison, M.C. Moskowitz, J.W. Sutcliffe, B.T. Theor. Chim. Acta. **6**, 191 (1966).

Dauber-Osguthorpe, P. Roberts, V.A. Osguthorpe, D.J. Wolff, J. Genest, M. Hagler, A.T. Structure and energetics of ligand binding to proteins: E. Coli dihydrofolate reductase-trimethoprim, a drug-receptor system. Protein Structure, function and genetics, **4**, 31 (1988).

Delhalle, J. André, J.M. Delhalle, S. Pireaux, J.J. Caudano, R. Verbist, J.J. J. Chem. Phys. **60**, 595 (1974).

Dewar, M.J.S. Thiel, W. Ground states of molecules. The MNDO method.Approximations and parameters. J. Am. Chem. Soc. **99**, 4899 (1977).

Dewar, M.J.S. Yamaguchi, Y. Suck, S.H. Chem. Phys. **43**, 145 (1979).

Dias Tavares, A. New methods for the determination of space charge in dielectric. J. Chem. Phys. **59**, 2154 (1973).

Discover User Guide. (Molecular Simulations Inc., San Diego, 1996).

Dissado, L.A. Mazzanti, G. Montanari, G.C. The role of space charges in the electrical ageing of insulating materials. IEEE Transactions on Dielectrics and Electrical Insulation **4**, 496 (1997).

Dissado, L.A. What role is played by space charge in the breakdown and ageing of polymers? Abstracts CSC'3 Electric charge in solid insulators, 141 (1998).

Dissado, L A. Fothergill, J.C. *Electrical Degradation and Breakdown in Polymers,* (Peter Peregrinus Ltd. London, 1992).

DMol User Guide. (Molecular Simulations Inc., San Diego, 1997).

Dorman, F.H. Negative fragment ions from resonance capture processes. J. Chem. Phys. **44**, 3856 (1966).

Dreizler, R.M. Gross, E.K.U. *Density functional theory. An approach to the quantum many-body problem.* (Springer-Verlag, Berlin, 1990).

Dudde, R. Reihl, B. Complete electronic structure of oriented films of hexatriacontane. Chem. Phys. Letts. **196**, 91 (1992).

Edwards, S.F. J. Phys. **C 3**, L 30 (1970).

Elliott, S.R. *Physics of amorphous materials.* (Harlow: Longman Scientific & Technical, 2nd edition, 1990).

Ellison, G.B. Engelking, P.C. Lineberger, W.C. An experimental determination of the geometry and electron affinity of CH3. J. Am. Chem. Soc. **100**, 2556 (1978).

Emsley, J. *The elements.* (2nd edition, Oxford University Press, 1992).

Erwin, K.M. Ho, J. Lineberger, W.C. Ultraviolet photoelectron spectrum of NO_2^-. J. Chem. Phys. **92**, 5405 (1988).

Fermi, E. A statistical method for the determination of some atomic properties and the application of this method to the theory of the periodic system of elements. J. Phys. **48**, 73 (1928).

Flamant, I. Mosley, D.H. Deleuze, M. André, J.M. Delhalle, J. Dependence of the electronic structure on the chain geometry in stereoregular polypropylene: An exploratory theoretical study. International Journal of Quantum Chemistry: Quantum Chemistry Symposium **28**, 460 (1994).

Fletcher, R. *Practical methods of optimisation,* Vol. 1, *Unconstrained optimisation.* (John Wiley & Sons, 1980).

Flory, P.J. *Statistical mechanics of chain molecules.* (Interscience, New-York, 1969).

Fock, V. Z. Physik **61**, 126 (1930).

Franck, F.C. Faraday Discus. Chem. Soc. **68**, 7 (1979).

Goodman, G.M. *Chemical Applications of Molecular Modelling.* (RSC 1998).

Goodman, G.M. What is the longest unbranched alkane with linear global minimum conformation? J. Chem. Inf. Comput. Sci. **37**, 876 (1997).

Goodrich, F.C. *A primer of quantum chemistry.* (Wiley-Interscience, 1972).

Gruenhut, S. Amini, M. Macfarlane, D.R. Meakin, P. Molecular Simulation **19**, 139 (1997).

Guarrotxena, N. Toureille, A. Millan, J.L. Relation between molecular microstructure and electrical space charges in poly(propylene). Macromol. Chem. Phys. **199**, 81 (1998).

Gubbins, K.E. Quirke, N. *Molecular simulations and industrial processes: Methods, applications and prospects.* Current topic in molecular simulation. (Gordon Breach, 1996).

Gubbins, K.E. *Application of molecular theory to phase equilibrium predictions. Model for thermodynamic and phase equilibrium calculations.* (Ed. S.I. Sandler, Marcel Dekker, New York, 1994).

Gurvich, L.V. Karachevtsev, G.V. Kondratjev, V.N. Lebedev, Y.A. Medvedev, V.A. *Destruction Energies of Chemical Bonds. IP and Electron Affinity.* (Nauka, Moscow, 1974).

Gutsev, G.L. Adamowicz, L. The structure of the CF4- anion and the electron affinity of the CF4 molecule. J. Chem. Phys. **102**, 9309 (1995).

Hammes-Schiffer, S. Tully, J.C. Proton transfer in solution: molecular dynamics with quantum transitions. J. Chem. Phys. **101**, 4657 (1994).

Hansen, J.P. The kinetic glass transition: what can we learn from molecular dynamics simulation? Physica A **201**, 138 (1993).

Hartree, D.R. Proc. Cambridge Phil. Soc. **24**, 89 (1928).

Hehre, W.J. Radom, L. Schleyer, P. von R. Pople, J. A. *Ab initio molecular orbital theory.* (John Wiley & Sons, New York, 1986).

Hirata, S. Iwata, S. Density functional crystal orbital study on the normal vibrations and phonon dispersion curves of all-trans polyethylene. J. Chem. Phys. **108**, 7901 (1998).

Hockney, R.W. The potential calculation and some applications. Methods in Computational Physics **9**, 136 (1970).

Hoffmann, R. Janiak, C. Kollmar, C. A chemical approach to the orbitals of organic polymers. Macromolecules **24**, 13, 3725 (1991).

Hohenberg, P. Kohn, W. Inhomogeneous electron gas. Phys. Rev. B **136**, 864 (1964).

Huzinaga, S. J. Chem. Phys. **42**, 1293 (1965).

Ieda, M. Electrical conduction and carrier traps in polymeric materials. IEEE Trans. Elect. Insul. **EI-19**, 162 (1984).

Illenberger, E. Comita, P. Brauman, J.I. Fenzlaff, H.P. Experimental and theoretical investigation of the azide anion (N_3^-) in the gas phase. J. Phys. Chem. **89**,1026 (1985).

Imamura, A. Electronic structures of polymers using the tight-binding approximation.I. Polyethylene by the Extended-Huckel method. J. Chem. Phys. **52**, 3168 (1970).

Jean, Y. Volatron, F. Burdett, J. *An introduction to molecular orbitals.* (Oxford University Press, 1993).

Joffrin, J. *Ill –condensed matter.* (North-Holland Publishing Co., Oxford, 1979).

Jordan, K.D. Burrow, P.D. Temporary anion states of polyatomic hydrocarbons. Chem. Rev. **87**, 557 (1987).

Journal of Physical Chemistry – Reference Data **14**, 731 (1985).

Kavesh, S. Schultz, J.M. J. Polym. Sci. Part A-2 **8**, 243 (1970).

Kebarle, P. Chowdhury, S. Electron affinities and electron-transfer reactions. Chem. Rev. **87**, 513 (1987).

Keller, A. Philos. Mag. **2**, 1171 (1957).

Kendall, R.A. Dunning, T.H. Harrison, R.J. Electron affinities of the first-row atoms revisited. Systematic basis sets and wave functions. J. Chem. Phys. **96**, 796 (1992).

Kim, E.H. Bradforth, S.E. Arnold, D.W. Metz, R.B. Neumark, D.M. Study of HCO_2 and DCO_2 by negative ion photoelectron spectroscopy. J. Chem. Phys. **103**, 7801 (1995).

Kirkpatrick, S. Gelatt Jr, C.D. Vecchi, M.P. Optimisation by simulated annealing. Science **220**, 671 (1983).

Klein, A. McGinnis, R.P. Leone, S.R. Photodetachment threshold of CN- by laser optogalvanic spectroscopy. Chem. Phys. Letters **100**, 475 (1983).

Klingshirn, C. Localisation and percolation in alloy semiconductors, in *Disordered solids, structures and processes.* (Baldassare Di Bartolo, Plenum Press, 1990).

Kohn, W. Sham, L.J. Self-consistent equations including exchange and correlation effects. Phys. Rev. A **140**, 1133 (1965).

Krieger, J.B. Chen, J. Li, Y. Iafrate, G.J. Khon-Sham theory for orbital dependent exchange-correlation energy functionals: Application to the calculation of ionisation potentials and electron affinities. Int. J. Quant. Chem. **29**, 79 (1995).

Ladik, J. Suhai, S. *The electronic structure of polymers. Quantum chemistry of polymers: Solid state chemistry.* (Edition J. Ladik and J.M. André, Chapter 2, 1984).

Le Gressus, C. Valin, F. Henriot, M. Gautier, M. Duraud, J-P. Sudarshan, T.S. Bommakandi, R.G. Blaise, G. J. Appl. Phys. **69**, 6325 (1991).

Leach, A.R. *Molecular modelling, principles and applications.* (Addison Wesley Longman Limited, 1996).

Less, K.J. Wilson, E.G. Intrinsic photoconduction and photoemission in polyethylene. J. Phys. C.: Solid State Physics **6**, 3110 (1973).

Lewiner, J. Evolution of experimental techniques for the study of the electrical properties of insulating materials. IEEE Trans. on Elect. Insul. **21**, 351 (1986).

Lewis, T.J. The micro-physics of charge in dielectric. Abstracts CSC'3 Electric charges in solid insulators, 16 (1998).

Li, Y. Takada, T. Takasu, N. J. Phys. D **26**, 986 (1993).

Liang, G.L. Noid, D.W. Sumpter, B.G. Wunderlich, B. Gauche defects, positional disorder, dislocations, and slip planes in crystal of long methylene sequences. J. Phys. Chem. **98**, 11739 (1994).

Liao, Q. Xigao, J. Formation of segmental clusters during relaxation of a fully extended polyethylene chain at 300 K: A molecular dynamics simulation. J. Chem. Phys. **110**, 8835 (1999).

Lias, S.G. et al. Gas-phase ion and neutral thermochemistry. J. Phys. Chem. Ref. Data **17**, (1988).

Lide, D.R. *Handbook of chemistry and physics.* (CRC Press, New York, 1997).

Lindholm, E. Asbrink, L. Ljunggren, S. Energies of σ^* orbitals. J. Phys. Chem. **95**, 3922 (1991).

Lipkowitz, K.B. Boyd, D.B. *Reviews in computational chemistry.* (Vol.1, 1991, Vol.2, 1991, Vol.3, 1992, Vol.4, 1993, Vol.5, 1994, Vol.6, 1995).

Manuel, P. Program MASCARET, E.D.F. (1999).

March, N.H. Mucci, J.F. *Chemical Physics of Free Molecules.* (Plenum Press, New York, 1993).

Massey, H.S.W. *Negatives Ions.* (3rd ed. Cambridge University, London, 1976).

Maxwell, J.C. *A treatise on electricity and magnetism.* (Clarendon Press, Oxford, 1881).

Meunier, M. Aslanides, A. Quirke, N. Characterisation of charge carrier traps in polymeric insulators. IEEE Conference on Electrical Insulation and Dielectric Phenomena. Vancouver, Oct 15-18 (2000).

Meunier, M. Anta, J. A. Quirke, N. EDF Program Report N°7 (June-September 1999).

Meunier, M. Quirke, N. Binesti, D. Martic, G. Fourmigué, J.M. *Abstracts: Electrical Insulation and Dielectric Phenomena (CEIDP)*, Minneapolis (Oct. 1997)

Meunier, M. Quirke, N. Binesti, D. Lecture *3rd International Conference on dielectric charge in solid insulators, CSC'3.* Tours (France) (June-July 1998).

Meunier, M. Quirke, N. Binesti, D. The calculation of the electron affinity of atoms and molecules. Mol. Sim. **23**, 109 (1999).

Meunier, M. Quirke, N. Molecular modelling of electron trapping in polymer insulators. J. Chem. Phys. **113**, 369 (2000).

Møller, C. Plesset, M.S. Note on approximate treatment for many-electron systems. Physical Review **46**, 618 (1934).

Montanari, B. Ballone, P. Jones, R.O. Density functional study of molecular crystals: Polyethylene and a crystalline analog of bisphenol-A polycarbonate. J. Chem. Phys. **108**, 6947 (1998).

Mott, N.F. *Conduction in non-crystalline materials.* (Clarendon Press, Oxford, 1987).

Mott, N.F. Phil. Mag. **22**, 7 (1970).

Nelson, R.D. Lide, D.R. Maryott, A.A. Selected values of electric dipole moments for molecule in thegas phase. Natl. Stand. Ref. Data Ser. –Natl. Bur. Stnds.10 (1967).

Nosé, S. A molecular dynamics method for simulations in the canonical ensemble. Molec. Phys. **52**, 255 (1984).

Novoa, J.J. Mota, F. Arnau, F. Mono-and multireference Moller-Plesset computation of the electron affinity. A full configuration interaction analysis on first-row atoms and their hybrids. J. Phys. Chem. **95**, 3096 (1991).

Ortiz, J.V. Electron propagator theory of BO_2 and BO_2^- electronic structure. J. Chem. Phys. **99**, 6727 (1993).

Ortiz, J.V. Improved electron propagator methods: An investigation of C_4, C_4^-, and C_4^+. J. Chem. Phys. **99**, 6716 (1993).

Parr, R.G. Yang, W. *Density-functional theory of atoms and molecules.* (Oxford University Press, New York, 1989).

Parrinello, M. Rahman, A. Polymorphic transitions in single crystals: A new molecular dynamics methods. J. Appl. Phys. **52**, 7182 (1981).

Peek, F.W. *Dielectric phenomena in high-voltage engineering.* (McGraw Hill, 1920).

Perdew, J.P. Wang, Y. Accurate and simple analytic representation of the electron-gas correlation-energy. Phys. Rev. **B45**, 13244 (1992).

Pertsin, A.J. Kitaigorodsky, A.I. *The atom-atom potential method.* (Springer-Verlag, Berlin, 1987).

Pethig, R. *Dielectric and electronic properties of biological materials.* (John Wiley & Sons, Chichester, 1979).

Pettifor, D. *Bonding and Structure of Molecules and Solids.* (Clarendon Press Oxford, 1995).

Phillips, P.J. *Morphology and molecular structure of polymers and their dielectric behaviour.* Enginering dielectrics, Vol. IIA, Chapter 2. (Bartnikas/Eichorn, 1983).

Pireaux, J.J. Caudano, R. Verbist, J.J. J. Electron spectrosc. and relat. phenom. **5**, 267 (1974).

Pireaux, J.J. Phys. Rev. A, **14**, 2133 (1976).

Polak, E. *Computational methods in optimisation: a united approach.* (Academic Press, San Diego, 1971).

Pople, J.A. Beveridge, D.L. *Approximate molecular orbital theory.* (McGraw-Hill 1970).

Press, W.H. Flannery, B.P. Teukolsky, S.A. Vetterling, W.T. *Numerical recipes in Fortran.* (Cambridge University Press, 1992).

Pulay, P. Chem. Phys. Lett. **73**, 393 (1980)

Pulay, P. Improved SCF convergence acceleration. J. Comp. Chem. **3**, 556 (1982).

Quirke, N. Molecular modelling and simulation: Tools for the modern era. Mol. Sim. In press. (2000).

Rigby, D. Roe, R.J. J. Chem. Phys. **87**, 7285 (1987).

Rigby, D. Roe, R.J. J. Chem. Phys. **89**, 5280 (1988).

Roe, R.J. J. Chem. Phys. **100**, 1610 (1994).

Rohr, K. J. Phys. B **13**, 4897 (1980).

Rohr, K. Cross beam experiment for the scattering of low-energy electrons from methane. J. Phys. B. **13**, 4897 (1980).

Rondan, N.G. Domelsmith, L.N. Houk, K.N. Bowne, A.T. Levin, R.H. The relative rates of electron-rich and electron-deficient alkene cycloadditions to benzyne. Enhanced electrophilicity as a consequence of alkyne bending distortions. Tetrahedron Letters **35**, 3237 (1979).

Rosch, N. Trickey, S.B. J. Chem. Phys. **106**, 8940 (1997).

Roothan, C.C.J. Rev. Mod. Phys. **23**, 69 (1951).

Rowntree, P. Parenteau, L. Sanche, L. Dielectric polarisation invariance in dissociative electron attachment from condensed saturated hydrocarbons. J. Phys. Chem. **95**, 523 (1991).

Salzner, U. Lagowski, J.B. Pickup, P.G. Poirier, R. A. Design of low band gap polymers employing density functional theory-Hybrid functionals ameliorate band gap problem. J. Comp. Chem. **18**, 11943 (1997).

Sanche, L. Schulz, G.J. Electron transmission spectroscopy: Resonances in triatomic molecules and hydrocarbons. J. Chem. Phys. **58**, 479 (1973).

Sanche, L. Nanoscopic aspects of electronic ageing in dielectric. IEEE Transactions on Dielectrics and Electrical Insulation **4**, 507 (1997).

Schaefer, O. Allan, M. Szeimies, G. Sanktjohanser, M. J. Am. Chem. Soc. **114**, 8180 (1992).

Schlecht, M.F. *Molecular modelling on the PC.* (Wiley-VCH, 1998).

Schultz, P.A. Mead, R.D. Jones, P.L. Lineberger, W.C. OH^- and OD^- threshold photodetachment. J. Chem. Phys. **77**,1153 (1982).

Scott, R.A. Scheraga, H.A. J. Chem. Phys. **44**, 3054 (1966).

Seki, K. Sato, N. Inokuchi, H. Valence electronic structure of a long-chain alkane in random coil forms. Gas-phase UPS of n-C36H74 and MO calculations. Chem. Phys. **178**, 207 (1993).

Seki, K. Ueno, N. Karlson, U.O. Engelhardt, R. Koch, E.E. Valence bands of oriented finite linear chain molecular solids as model compounds of polyethylene studied by angle-resolved photoemission. Chem. Phys. **105**, 247 (1986).

Sessler, G.M. Yang, G.M. Abstracts CSC'3 Electric charge in solid insulators, 38 (1998).

Shklovskii, B.I. Efros, A.L. *Electronic properties of doped semiconductors.* (Springer series in solid state sciences, 1984).

Sidorov, L.N. Search and study of molecules with high-affinity to the electron. Uspekhi Khimii **51**, 625 (1982).

Simons, J. Jordan, K.D. Ab-initio electronic structure of anions. Chem. Rev. **87**, 535 (1987).

Slater, J.C. Atomic shielding constants. Phys. Rev. **36**, 57 (1930).

Smith, G.D. Yoon, Do.Y. J.Chem.Phys. **100**, 649 (1994).

Springborg, M. Lev, M. Electronic structures of polyethylene and polytetrafluoroethylene. Phys. Rev. B **40**, 3333 (1989).

Springborg, M. Density-functional studies of electronic properties of polymers. Int. Rev. Phys. Chem. **12**, 241 (1993).

Steele, D. J. Chem. Soc. Faraday Trans. **2**, 1077 (1985).

Steiner, B. Photodetachment of electrons from SH^-. J. Chem. Phys. **49**,5097 (1968).

Still, W.C. Tempczyk, A. Hawley, R.C. Hendrickson, T.J. J. Am. Chem. Soc. **112**, 6127 (1990).

Stillinger, F. H. Interaction potentials and inherent structures in liquids, glasses, and crystals. Physica D **107**, 383 (1997).

Stillinger, F. H. Weber, T.A. Physical Review A **25**, 978 (1982).

Strobl, G. Ewen, B. Fischer, E.W. Piesczek, W. Defect structure and molecular motion in the four modifications of n-tritriacontane.I. Study of defect structure in the lamellar interfaces using small angle x-ray scattering. The Journal of Chemical Physics **61**, No. 12 (1974).

Suhai, S. Electron correlation effects on the mechanical and optical properties of polymers. Int. Journal of Quantum Chemistry: Quantum Chemistry Symposium **18**, 161 (1984).

Takeuchi, H. Roe, R.J. Molecular dynamics simulation of local chain motion in bulk amorphous polymers. I. Dynamics above the glass transition. J. Chem. Phys. **94**, 7446 (1991).

Taylor, H.S. Models, interpretations, and calculations concerning resonant electron scattering process in atoms and molecules. Advan. Chem. Phys. **18**, 91 (1970).

Thomas, L.H. The calculation of atomic fields. Proc. Camb. Phil. Soc. **23**, 542 (1927).

Toureille, A. Revue générale d'électricité **8**, 15 (1991).

Travers, M.J. Cowles, D.C. Ellison, G.B. Reinvestigation of the electron affinities of O_2 and NO. Chem. Phys. Letters **164**, 449 (1989).

Tully, J.C. Molecular dynamics with electronic transitions. J. Chem. Phys. **93**, 1061 (1990).

Tully, J.C. Preston, R.K. J. Chem. Phys. **55**, 562 (1971).

Ueno, N. Seki, K. Sugita, K. Inokuchi, H. Nature of the temperature dependence of conduction bands in polyethylene. Phys. Rev. B **43**, 2384 (1991).

Ueno, N. Sugika, K. Kiyono, S. Chem. Phys. Letters **82**, 296 (1981).

Vella, N. Guarrotxena, N. Toureille, A. Millan, J.L. Influence of the tacticity dependent microstructure on the space charge distribution of poly(vinyl chloride). Journal of Electrostatics **40&41**, 301 (1997).

Verlet, L. Computer experiments on classical fluids.I. Thermodynamical properties of Lennard-Jones molecules. Phys. Rev. **159**, 98 (1967).

Von Niessen, W. Cederbaum, L.S. Domke, W. *Excited States in Quantum Chemistry.* (eds. Redial, Holland, 1979).

Vosko, S.J. Wilk, L. Nusair, M. Accurate spin-dependent electron liquid correlation energies for local spin density calculations: a critical analysis. Can. J. Phys. **58**, 1200 (1980).

Weiner, S.J. Kollman, P.A. Nguyen, D.T. Case, D.A. An all atom forcefield for simulations of proteins and nucleic acid. J. Comp. Chem. **7**, 230 (1986).

Whitehead, S. *Dielectric breakdown of solids.* (Clarendon Press, Oxford, 1951).

Wight, C.A. Beauchamps, L.J. Acidity, basicity, and ion/molecule reactions of isocyanide acid in the gas phase by ion cyclotron. J. Phys. Chem. **84**, 2503 (1980).

Wilson, S.R. Cui, W. Applications of simulated annealing to peptides. Biopolymers **29**, 225 (1990).

Wintle, H. J. Abstracts CSC'3 Electric charge in solid insulators, 49 (1998).

Wintle, H.J. *Conduction Processes in Polymers. Engineering Dielectrics volume IIA, Electrical properties of solid insulating materials: Molecular structure and electrical behaviour.* (Bartnikas/Eichhorn editors, 1983).

Yoshioka, Y. Schaefer, H.F. Jordan, K.D. Theoretical investigation of the electron affinity of CO_2. J. Chem. Phys. **75**, 1040 (1981).

Zallen, R. *The physics of Amorphous Solids.* (John Wiley and sons, 1983).

Ziegler, T. Gutsev, G.L.J. On the evaluation of molecular electron affinities by approximate density functional theory. Computational Chemistry **13**, 70 (1992).

ZINDO User Guide. (Molecular Simulations Inc., San Diego, 1997).

Molecular Simulation, 1999, Vol. 23, pp. 109–125
Reprints available directly from the publisher
Photocopying permitted by license only

THE CALCULATION OF THE ELECTRON AFFINITY OF ATOMS AND MOLECULES

M. MEUNIER[a], N. QUIRKE[a,*] and D. BINESTI[b]

[a] *Department of Chemistry, Imperial College of Science, Technology and Medicine, South Kensington, SW7 2AY, United Kingdom;* [b] *Electricité de France DER, Les Renardières 77818, Moret-sur-Loing Cedex, France*

(Received June 1999; accepted July 1999)

Non-local density functional theory, as implemented in the code DMol, has been used to calculate the electron affinity of a set of 44 small atoms and molecules. A judicious choice of basis sets produces a root mean square deviation from recommended values of 0.1 eV and 0.3 eV for atoms and small molecules (with positive electron affinities) respectively. Applying DMol to calculations of temporary anion states or resonances of linear alkanes to $n = 36$ (where n is the number of carbon atoms) a gradual increase in electron affinity is predicted which appears to have converged by $n = 36$ to -0.75 eV (in agreement with experimental data for C_{36} and polyethylene).

Keywords: Electron affinity; DMol; alkanes; metastable states

1. INTRODUCTION

The electron affinity, representing one half of an electron transfer process (with the ionisation potential) plays a central role in gas and condensed phase chemistry. Data on electron affinities are important [*e.g.*, 1, 2] in theories of chemical reaction and intermediate species, for biochemistry (biological redox processes, radiation damage), to our understanding of chemical bonds and in theories of electronic devices (semiconductors, dielectrics).

*Corresponding author. e-mail: N.Quirke@ic.ac.uk

An *adiabatic* electron affinity can be defined as

$$EA_a = E(R_e) - E^-(R_e^-) \tag{1}$$

where $E(R_e)$ is the total (ground state) energy of the neutral species in its equilibrium geometry R_e and $E^-(R_e^-)$ is the total energy of the anion in its minimum energy geometry. If the anion is not allowed to relax on electron attachment, a *vertical* electron affinity is defined through

$$EA_v = E(R_e) - E^-(R_e) \tag{2}$$

the total energies being calculated in the equilibrium geometry of the neutral species.

The total energy of a molecule can be resolved into an electronic (E_{el}) and nuclear contribution, taken to be the vibrational ground state of the nuclear motion, the zero point energy (ZPE). The adiabatic electron affinity then becomes (*e.g.* [3])

$$EA_a = E_{el}(R_e) - E_{el}^-(R_e^-) + ZPE - ZPE^- \tag{3}$$

The vertical affinity contains only the electronic energy

$$EA_v = E_{el}(R_e) - E_{el}^-(R_e) \tag{4}$$

There are a large number of experimental techniques, which have been applied to the determination of electron affinities including laser photoelectron spectroscopy [4], electron transmission spectroscopy [5], and gas phase ion-molecule equilibria [6]. A description of thirty-one methods for the determination of electron affinities may be found in reference seven. Despite the number of techniques available, the reliable determination of electron affinities still represents a considerable challenge, especially for large molecules where it may be difficult to use accurate gas phase techniques. There is a particular difficulty where the electron affinity is negative and the anion is consequently short lived (see [5] for a full discussion of the experimental techniques used to obtain electron affinities for temporary anions). This is the case for the alkanes discussed in the second part of the present article where (with the exception of methane) gas phase methods such as electron transmission spectroscopy cannot resolve the resonant states. There is a need for fast and reliable theoretical methods of calculating electron affinities. Data are available [43] for hexatriacontane (C_{36}) from photoemission spectroscopy of C_{36} monolayers on Cu(111) as well as for polyethylene [44].

Ab initio methods of calculating electron affinities have been reviewed (to 1987) by Simons and Jordan [8] who point out the need for flexible basis sets and a careful treatment of electron correlation effects in order to obtain accurate electron affinities. They state that 'it is extremely difficult to reliably calculate electron affinities within an accuracy of better than 0.2 eV for most classes of atoms and molecules' and call for the development of new theoretical and computational tools.

More recent *ab initio* work [9] using multireference singles and doubles configuration interaction (MRSD-CI) with specialised correlation-optimised and augmented basis sets applied to *H*, *B*, *C*, *O* and *F* obtained a root mean square deviation from recommended experimental values of the electron affinities of 0.05 eV, demonstrating that it is possible to achieve high accuracy for small atoms, albeit at considerable computational expense (see also [10]). A detailed study of specialised exchange correlation functionals within density functional theory [11] reports average deviations of around 0.2 – 0.4 eV for atoms with atomic number less than or equal to 20.

Due to the complexity of the calculations, electron affinities for molecules are usually reported for individual species or small groups of related species. For example, electron propagator methods give excellent results [12] for the electron affinity of C_4^- (3.69 eV compared to experimental results of 3.7 and 3.88 eV). For BO_2 the electron affinity is within 0.4 eV of the experimental data [13]. The use of semiempirical CNDO type calculations to explore unoccupied σ^* orbitals and hence estimate electron affinities for a number of small hydrocarbon and fluorocarbon molecules has been reported [14]. Reasonable agreement was obtained between calculated and experimental energies (see Tab. III below). There have been few assessments of the accuracy of DFT calculations of electron affinity for molecules. In a 1992 paper, Ziegler and Gutsev [15] reported non-local density functional theory (NLDFT, see Section 2 below) calculations for 11 small molecules and found a rms deviation of ~ 0.3 eV (recalculated from Tabs. II and V of Ref. [15]).

Although there has been a significant amount of work on both the measurement and the calculation of electron affinities for atoms, molecules, clusters and solids we are far from having sufficient reliable data. The present work constitutes an exploration of the use of density functional theory (as expressed in the widely available code DMol) to calculate electron affinities for a representative sample of small atoms and molecules having both positive and negative values of the electron affinity. We wish to assess the accuracy of a routine DMol calculation of electron affinity *i.e.*, a calculation that has not been tailored to a particular species. In addition, we are particularly interested in the electron affinity of alkanes and its variation

with molecular conformation: a subject little explored to date. Data on alkane electron affinities is central to new approaches to space charge and dielectric breakdown in polyethylene [47].

In the following section, we briefly review density functional theory and the code DMol. In section three we present the results of applying DMol to some 44 small atoms and molecules and make a comparison with recommended experimental results. Section four considers the alkanes and reports electron affinities for straight chain alkanes up to carbon number 36.

2. DENSITY FUNCTIONAL THEORY AND DMOL

The calculations reported in this work have been carried out using non-local density functional theory (NLDFT) as implemented in the DMol code [16]. For comparison, some calculations have been done with Hartree-Fock theory using Gaussian94 [49]. Density functional theory has been described in detail elsewhere [17] and only a very brief description is given below.

DFT starts with a theorem by Hohenberg and Kohn [18] that all ground state properties are functions of the electron density ρ. As a result, the total energy may be written as:

$$E_T[\rho] = T[\rho] + U[\rho] + E_{xc}[\rho] \tag{5}$$

Where $T[\rho]$ is the kinetic energy of a system of non-interacting particles of density ρ, $U[\rho]$ is the electrostatic interaction due to Coulomb interactions between electrons and nuclei, and $E_{xc}[\rho]$ includes all many body contributions to the total energy (exchange and correlation energies). The wavefunction ϕ is an antisymmetrised product of one-electron functions representing molecular orbitals such that the electron density is given by the sum over all occupied molecular orbitals.

$$\rho(r) = \sum |\phi_i(r)|^2 \tag{6}$$

The energy terms can then be written exactly in terms of ϕ and ρ, however the exchange-correlation term requires approximation to be tractable. The *local* density approximation assumes that the electron density varies slowly and can be represented locally by a uniform electron gas (having energy $\varepsilon_{xc}[\rho]$ at density ρ) so that

$$E_{xc}[\rho] = \int \rho(r)\varepsilon_{xc}[\rho]dr \tag{7}$$

The inhomogeneity of the electron gas can be represented by a gradient expansion (*non local* DFT) giving a gradient 'd' corrected exchange-correlation energy $E_{xc}[\rho, d(\rho)]$.

Varying the total energy with respect to each wavefunction ϕ_i yields the Kohn-Sham equations

$$(T + V(r) + \mu_{xc})\phi_i = \varepsilon_i \phi_i \tag{8}$$

where μ_{xc}, the exchange-correlation potential arises from the differentiation of E_{xc}. It is common practice to expand the molecular orbitals in terms of atomic orbitals

$$\phi_i = \sum C_{i\mu}\chi_\mu \tag{9}$$

where the χ_μ constitute the atomic basis functions. In the DMol implementation, the atomic basis functions are given numerically as values on an atomic centred spherical polar mesh. The code DMol solves the KS equations to find the electron density distribution corresponding to the lowest ground state energy.

In DMol the basis set comprises occupied atomic orbitals for the neutral atoms and for the +2 atomic cations, except for hydrogen where a nuclear charge of +1.3 is used. This basis set is referred to as Double Numeric (DN). Adding a function on each atom with one angular momentum unit higher than that of its highest occupied orbital (*i.e.*, p for H, d for C) leads to a double numerical with polarization function (DNP) basis set. This basis set is referred as DMol 1 in the tables. Additional functions beyond the DNP basis set are available. A hydrogenic calculation with a nuclear charge of $+\zeta$ (variable for each system studied, see Tabs. I and II) provide additional s p and d orbitals. This basis set (DNP+) is referred to as DMol 2 in Tables I and II. To illustrate the use of diffuse functions, the hydrogenic function ($1s$) is given below:

$$\left(\frac{3}{4\Pi}\right)^{1/2} \cos\Theta \times 2\left(\frac{\zeta}{a_0}\right)^{3/2} \exp\left(-\frac{1}{2}\left(\frac{2\zeta r}{a_0}\right)\right) \tag{10}$$

By varying ζ the spatial extent of the orbital can be increased. This leads to diffuse functions when ζ is small compared to Z, the atomic number (*e.g.*, less than 1 for H, or less than 6 for C). As functions are added to the basis set, they are orthogonalised with respect to those already in the set and are not included if linearly dependent. With Gaussian94 the basis sets were

TABLE I Electron affinity of atoms H to Ar, comparison with experiment

Elements	*EA**	*DMol* 1	*error*	*DMol* 2	*error*	*ζ parameter***
			Positive electron affinities			
H	0.75	−0.096	−0.846	0.741	−0.08	0.3***
Li	0.62	0.24	−0.38	0.42	−0.2	0.02
B	0.24	0.22	−0.02	0.25	0.01	3
C	1.27	1.31	0.04	–	–	–
O	1.46	1.21	−0.34	1.39	−0.07	3
F	3.34	3.26	−0.08	3.42	0.08	4
Na	0.55	0.17	−0.38	0.41	−0.14	0.02
Al	0.46	0.4	−0.06	0.41	−0.05	4
Si	1.38	1.4	0.02	1.41	0.03	2
P	0.74	0.47	−0.27	0.68	−0.06	1
S	2.08	2	−0.08	2	−0.08	2
Cl	3.61	3.54	−0.07	–	–	–
RMSD			0.32		0.1	
			Negative electron affinities			
He	−0.22****	−10.78	−10.56	−0.28	−0.06	0.02***
Be	−0.19	−2.21	−2.02	−0.21	−0.02	0.02
N	−0.07	−0.75	−0.68	−0.08	−0.01	1.2
Ne	−0.3****	−28.02	−27.72	−0.38	−0.08	0.02
Mg	−0.22	−5.44	−5.22	−0.18	0.04	0.02
Ar	−0.36****	−12.86	−12.5	−0.38	−0.02	0.02
RMSD			13.3		0.05	

Note: Electron affinities in eV,
* literature values taken from J. Emsley, The Elements, second edition, Oxford University Press 1992,
** adjustable diffuse function orbital exponent,
*** only *s* and *p* diffuse functions added,
**** (calculated). DMol 1, VWN, B88, PW, DNP, fine mesh, DMol 2, VWN, B88, PW, DNP++, fine mesh.

6-31G^{**}, 6-31++G^{**} and 6-311++G^{**} [50]. Where appropriate post Hartree-Fock treatments have also been employed.

3. ELECTRON AFFINITIES OF ATOMS AND SMALL MOLECULES

3.1. Atoms

Table I reports the electron affinities of atoms *H* to Ar obtained using DMol separated into two groups having positive and negative electron affinities (*EA*). For the first group DMol predicts the electron affinity to a root mean square deviation of 0.3 eV (0.2 eV if *H* is excluded), if diffuse functions are added the rms. deviation is reduced to 0.1 eV. These results compare well with those reported for *ab initio* methods (MP2, MP4, CIPSI [10], and MRSD-CI [9]) and for specialised exchange correlation functionals within DFT treatments [11] for first row atoms. For the second group of atoms

TABLE II Adiabatic electron affinity of small molecules: Comparison with experiment

Molecule	*Rec. val.*	*Reference*	*DMol 1 + ZPE*	*Error*	*DMol 2 + ZPE*	*Error*	*ΔZPE*
			Positive electron affinity				
NO	0.033 ± 0.01	25	0.218	0.185	0.257	0.224	0.063
CH3	0.08 ± 0.03	26	0.142	0.062	0.16	0.08	0.062
P2	0.23 ± 0.23	27	0.576	0.346		0.346	0.016
O2	0.451 ± 0.007	28	0.264	−0.187	0.504	0.053	0.054
NH2	0.744 ± 0.022	29	0.879	0.135		0.135	0.099
SO2	1.097	27	1.356	0.259		0.259	0.056
PH2	1.25 ± 0.03	29	1.158	−0.092	1.242	−0.008	0.028
OH	1.8276	30	2.045	0.217		0.217	−0.025
SH	2.319 ± 0.01	31	2.302	−0.017	2.333	0.014	0.002
CL2	2.38 ± 0.1	32	2.782	0.402		0.402	0.042
BF3	2.65	32	−0.556	−3.206	2.744	0.094	0.134
N3	2.76 ± 0.004	33	2.704	−0.056	2.736	−0.024	−0.046
F2	3.08 ± 0.1	32	3.569	0.489		0.489	0.089
NO2	2.11 ± 0.2	34	1.88	−0.23	2.13	0.02	0.06
HCO2	3.498 ± 0.015	35	3.161	−0.337	3.261	−0.237	0.021
PO3	3.5	36	4.349	0.849		0.849	−0.071
C2	3.54	27	2.56	−0.98	3.45	−0.09	−0.02
OCN	3.6 ± 0.2	13	3.43	−0.17		−0.17	−0.04
BO2	4.25	37	4.02	−0.23		−0.23	−0.06
NO3	3.77 ± 0.25	36	3.325	−0.445	3.405	−0.365	−0.065
CN	3.821 ± 0.004	38	3.547	−0.274	3.797	−0.024	0.007
RMSD:				0.79		0.28	
			Negative electron affinity				
N2	-1.9 ± 0.1	39	−1.953	0.053		0.053	0.067
C2H4	−1.768	7	−1.68	−0.088		−0.088	–
H2	−0.78	7	−1.82	1.04	−1.04	0.26	0.14
CO	-1.8 ± 0.1	40	−1.715	−0.085		−0.085	0.065
CO2	-0.6 ± 0.2	41	−0.712	0.112		0.112	0.088
RMSD:				0.47		0.14 0.09*	

Note: All values in electron volts. DMol 1, VWN, B88, PW, DNP. DMol 2, VWN, B88, PW, DNP++, *excluding hydrogen.

having negative electron affinities DMol gives large errors that can be reduced almost to zero using diffuse functions. Diffuse functions have a well-known role in obtaining realistic energies of small anions [22]. For molecules that have a positive affinity, the diffuse functions expand the basis set so that the anion can find its equilibrium geometry. For a molecule with a negative affinity, the diffuse functions monotonically lower the energy of the anion to that of the neutral. This result represents the computational equivalent of electron autodetachment, and as a result, the properties of these anionic states in vacuum appear to be mathematically indeterminate in variational *ab-initio* treatments [23]. However, it is possible to artificially stabilise such anion states by varying parameters in the Hamiltonian [24] or through a judicious choice of functional and/or basis set such that *ab-initio* calculations of negative electron affinities yield values consistent with experimental data. In the condensed phase, temporary anionic states may be stabilised by the environment (see for example the work of Ewig on ionic crystals [23], also [52]).

3.2. Molecules

Ziegler and Gutsev [15] reported NLDFT calculations for 11 small molecules and found a rms. deviation of ~ 0.3 eV. For the larger group studied here the same rms deviation is obtained (Tab. II, Fig. 1). However, Jursic

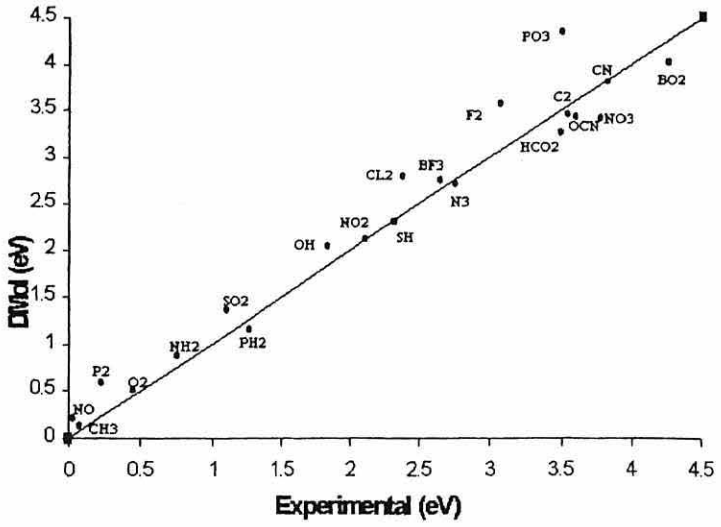

FIGURE 1 Positive electron affinity.

[48] has obtained deviations of about 0.05 eV for three small radicals using DFT. For molecules with negative electron affinities the rms deviation is 0.5 eV including H_2, and 0.1 eV excluding hydrogen (Tab. II, Fig. 2). At least for this group of molecules DMol without diffuse functions appears to produce accurate estimates of negative molecular electron affinities. In Section 4 we use DMol to study the (negative) electron affinities of alkanes.

3.3. Metastable Anions

Metastable anions can be divided into two general types: shape resonance and core-excited resonance (Fig. 3). In the former case the extra electron is attached to the molecule *via* a permanent and induced dipole moment

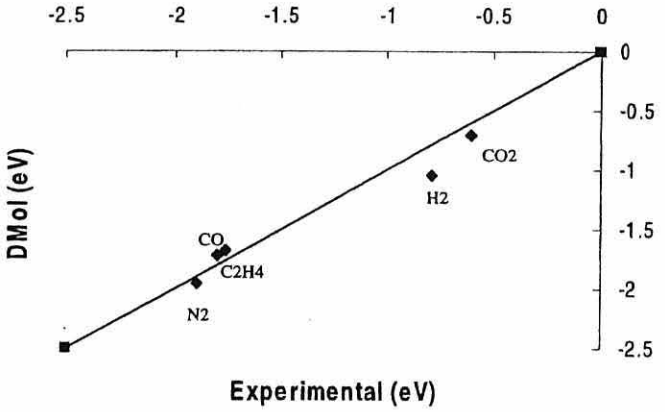

FIGURE 2 Negative electron affinities.

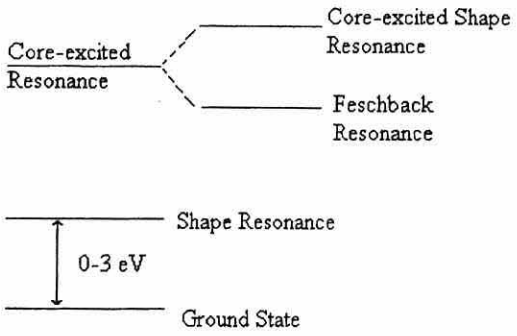

FIGURE 3 Resonances.

(examples are ^{2}P anion state of Mg, π^* states of N2, CO). This occurs when an incident electron with non-zero angular momentum is temporarily captured in the ground state of a molecule [55, 56]. In the later case the electron is attached to an excited state of the neutral molecule [8]. These core-excited resonances (also referred as two-particle one-hole, [5]) can also be divided in two groups: Feschback resonances, wherein their energy lies below the excited neutral parent, and core-excited shape resonances, wherein their energy lies above their neutral excited parent.

In order to elucidate the behaviour of the total energy from DMol for metastable anions, the variation of anionic energy with respect to diffuse functions has been investigated. The energy of both the neutral and the anion were computed for various basis sets following the addition of diffuse functions. In our calculations the energy of the neutral atom or molecule was essentially independent of the addition of extra diffuse functions as expected. The CN example is given below ($EA + 3.821$ eV) in Figure 5. In contrast for molecules having negative electron affinities, the SCF energy of the anions with the addition of diffuse functions changes considerably. In all cases the addition of diffuse functions stabilises the anion; only slight variations were observed on addition of further diffuse functions until a point where the SCF energy suddenly drops and tends toward that of the neutral species. At this point there are sufficient diffuse functions to allow the electron to separate from the molecule. A typical result is given below for the tridecane molecule (Fig. 4):

From Figures 4 and 5 we see that where the electron affinity is too negative (metastable anion) adding diffuse functions can reduce the error (at

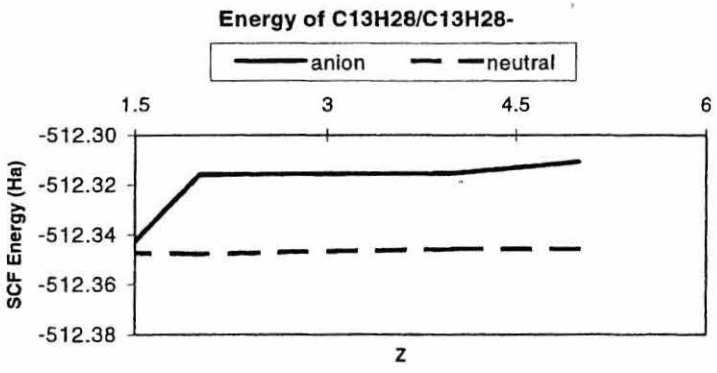

FIGURE 4 SCF energy variation of a tridecane molecule (see Section 6) with respect to added diffuse functions. Z represents the diffuse character of the basis set, the smaller Z the more diffuse the added functions in the basis set.

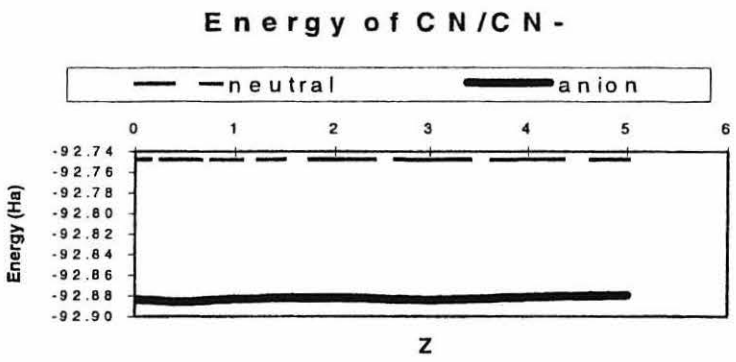

FIGURE 5 SCF energy variation of the neutral and anionic CN molecule, with respect to the diffuse functions added.

the cost of moving away from the plateau value, see Fig. 4). If the electron affinity is negative but too large then the addition of diffuse functions will not improve the result. For the case of positive electron affinities where DMol 1 provides a good estimate of the electron affinity, addition of diffuse functions does not significantly change the results (Fig. 5 and Tabs. I and II).

These calculations demonstrate that, for some molecules, DMol predicts metastable states (*cf.* plateau in Fig. 4) with respect to the electron and neutral molecule at infinity. The values of these metastable states are consistent with measured negative electron affinities. In what follows DMol without diffuse functions (DMol 1) is used to investigate the negative anions of alkanes.

4. ELECTRON AFFINITIES OF ALKANES

Very few experimental data for the electron affinity of linear alkanes can be found in the literature. Data exists for methane [42], Hexatriacontane [43] and polyethylene [44]. The value of -5 eV for methane suggests that small alkane anions are metastable and difficult to observe [see for example [45]). Intermediate anion states of alkanes dissociate mainly *via* H^- elimination:

$$C_nH_{2n+2} + e- \rightarrow (C_nH_{2n+2})^- \rightarrow C_nH_{2n+1} + H^-$$

According to P. Rowentry *et al.* [53] these transient anions are core-excited resonance states. Jordan and Burrow reporting [5] unpublished work on methane and others alkanes state that "the extra electron must go into a "Rydberg type" orbital". They also report the absence of evidence of

low-lying shape resonances due to capture by σ^* orbitals. The extra electron goes in an orbital of high energy, of the Rydberg type. Hence, this orbital is much higher in energy than the LUMO. Within Koopman's theorem, the *EA* of a molecule (atom) is related to the energy of the energy of the LUMO $\varepsilon_{\mathrm{LUMO}}$ by:

$$EA = -\varepsilon_{\mathrm{LUMO}} \tag{11}$$

Koopmans' theorem could not be applied in the present case for two reasons (1) the *EA* can be linked to minus the energy of an orbital, but this orbital has to be the one accepting the extra electron, which in that case is not the LUMO and (2) Koopmans' theorem refers to single determinant Hartree-Fock, not DFT, wave functions.

In order to obtain electron affinities the excited states should be computed. Then, the extra electron can be added in an orbital of Rydberg type. This procedure could not be followed with the software used in this study. Instead, the extra electron has been added to the LUMO of the neutral ground state of the molecule. Fortunately, there is a cancellation of errors in the procedure used here. The anion is too stable because its parent is in the ground state, but the correlation energy, due to the extra electron, is too high as the added electron is in an orbital too close to the parent core. These two energy terms partially cancel each other, leading to a total energy value, and hence an electron affinity value, in good agreement with experiment. This is especially true for large molecules (*i.e.*, hexatriacontane) where the energy due to the excitation or the correlation of the added electron, represents only a small percentage of the total energy.

Although there is no consensus on the dissociation attachment energy values, the tendency for the resonance energy to decrease with increasing carbon chain length is well known and approaches an asymptote with *n*-butane [54]. These trends are confirmed by our DFT calculations (see Tab. III below) which clearly show the decrease in the electron affinity as the chain length increases, and the small variation after butane. This could be interpreted as reflecting a reduction in the influence of the terminal methyl groups on the LUMO as the hydrocarbon chain grows. The semiempirical methods (INDO/2, MNDO, CNDO) show this tendency for the first four alkanes, but remain too negative with increasing chain length. Hartree-Fock theory, as implemented in the code Gaussian94, is too computationally expensive to extend the calculation to long chains. On the other hand, DMol, while too positive for methane is consistent with the experimental estimate for $C_{36}H_{74}$. It would appear that the DMol estimates of the electron affinity

TABLE III Alkanes: *Ab initio* and semiempirical estimates of electron affinities

C_nH_{2n+2}	*Exp**	*DMol* $EA = \Delta E$ *adiabatic* *VWN/DNP/B88/PW*	*DMol* $EA = \Delta E$ *vertical*	*INDO/2* $EA = \Delta E$ *adiabatic*	*MNDO* $EA = \Delta E$ *adiabatic*	*MNDO* $EA = -LUMO$ *vertical*	*CNDO* (17) $EA = -LUMO$ *vertical*	*Gaussian*94 $EA = \Delta E$ *adiabatic* 6-311G^{**}/*MP*2
1 methane	−5	−2.87	−2.91	−7.48	−3.57	−4.385	−5.1	−3.76
2 ethane		−2.01	−2.05	−7.15	−3.07	−3.755	−4.5	−3.55
3 propane		−1.95	−1.97	−6.86	−2.72	−3.51	−4.6	−3.37
4 butane		−1.79	−1.8	−6.75	−2.68	−3.404	−4.3	
5 pentane		−1.67	−1.69	−6.66	−2.66	−3.35		
6 hexane		−1.58	−1.58	−6.54	−2.63	−3.311		
7 heptane		−1.51	−1.51	−6.52	−2.61	−3.253		
8 octane		−1.46	−1.45	−6.54	−2.6	−3.21		
9 nonane		−1.42	−1.4	−6.47	−2.61	−3.176		
10 decane		−1.37	−1.36	−6.47	−2.6	−3.15		
13 tridecane		−1.3						
15				−6.45				
20				−6.51	−2.6			
25				−6.45				
30				−6.51				
36 hexa-triacontane	-0.3 ± 0.5	−0.75	−0.75	−6.51				
PE	-0.5 ± 0.5					−3.067		

All values are in eV, *experimental data from (methane) [42], (hexatriacontane) [43] and PE [44]; DE indicates the use of Eqs. (1) (adiabatic) and 2 (vertical).

of alkanes become better (when compared to experimental values) as the chain length increases.

In Table III the results of applying *ab initio* and semiempirical methods to the calculation of the electron affinity of alkanes in vacuum are reported. All the methods produce negative electron affinities, with the CNDO correlation naturally producing a good result for methane.

5. CONCLUSIONS

Density functional theory, as implemented in the code DMol, has been used to calculate the electron affinity of a set of 44 small atoms and molecules. By adding diffuse functions to the basis sets a root mean square deviation from recommended values of 0.1 eV for atoms and 0.3 eV for small molecules has been obtained (for positive electron affinities) in good agreement with previous work on smaller sets of molecules. For molecules with negative electron affinity, DMol (without diffuse functions) appears to produce estimates of electron affinity consistent with the experimental results. Applying DMol to calculations of temporary anion states (or resonances) of linear alkanes (to $n = 36$, where n is the number of carbon atoms) shows a gradual increase in electron affinity which appears to have converged by $n = 36$ to -0.75 eV, consistent with the experimental data for hexatriacontane and polyethylene.

From the results presented above DMol appears to be a useful tool for the calculation of molecular electron affinities. It is particularly suited for large molecules due to its computational speed (especially with respect to other *ab initio* methods). Where the electron affinity is negative DMol appears to provide a good estimate of the electron affinity which, for alkanes, improves in accuracy with increasing molecular weight.

Acknowledgements

NQ and MM would like to thank Carl Ewig and Jan Andzelm of MSI, and Pierre Manuel of EDF for useful discussions. This work was supported by Electricité de France through a studentship (to MM).

APPENDIX

The DMol version 96.0/4.0.0 (1996) was used to perform the calculations reported in this article. Parameters have been set as follows:

Functional

Non-local spin density approximation (NLSDA) with the functional of Vosko, Will and Nusair [19] together with the gradient-corrected correlation term of Perdrew-Wang [20] and the gradient-corrected exchange term of Becke [21].

Mesh

The XFINE (≈ 6000 points/atom) parameter has been employed for atoms and molecules, FINE (≈ 3000 points/atom) parameter for alkanes.

SCF Procedure and Geometry Optimization

The density tolerance for SCF was set to 10^{-6}. The DISS algorithm of Pulay was utilized for faster convergence. The geometry optimization convergence criteria were satisfied when the gradient was less than 10^{-4} Hartree/Bohr and when the energy change was less than 10^{-5} Hartree.

References

[1] Kebarle, P. and Chowdhury, S. (1987). "Electron affinities and electron-transfer reactions", *Chem. Rev.*, **87**, 513.

[2] Pettifor, D. (1995). *Bonding and Structure of Molecules and Solids*, Oxford Science Publications, Clarendon Press Oxford.

[3] Gutsev, G. L., Adamowicz, L. (1995). "The structure of the CF_4^- anion and the electron affinity of the CF_4 molecule", *J. Chem. Phys.*, **102**, 9309.

[4] Kim, E. H., Bradforth, S. E., Arnold, D. W., Metz, R. B., Neumark, D. M. (1995). "Study of HCO_2 and DCO_2 by negative ion photoelectron spectroscopy", *J. Chem. Phys.*, **103**, 7801.

[5] Jordan, K. D. and Burrow, P. D. (1987). "Temporary anion states of polyatomic hydrocarbons", *Chem. Rev.*, **87**, 557.

[6] Kebarle, P. and Chowdhury, S. (1987). "Electron affinities and electron-transfer reactions", *Chem. Rev.*, **87**, 513.

[7] Christodoulides, A. A., McCorkle, D. L. and Christophorou, L. G. (1984). *Electron Molecule Interactions and their Applications*, Academic Press N.Y., **2**, 423.

[8] Simons, J. and Jordan, K. D. (1987). "*Ab-initio* electronic structure of anions", *Chem. Rev.*, **87**, 535.

[9] Kendall, R. A., Dunning, T. H. and Harrison, R. J. (1992). "Electron affinities of the first-row atoms revisited. Systematic basis sets and wave functions", *J. Chem. Phys.*, **96**, 796.

[10] Novoa, J. J., Mota, F. and Arnau, F. (1991). "Mono-and multireference Moller-Plesset computation of the electron affinity. A full configuration interaction analysis on first-row atoms and their hybrids", *J. Phys. Chem.*, **95**, 3096.

[11] Krieger, J. B., Chen, J., Li, Y. and Iafrate, G. J. (1995). "Khon-Sham theory for orbital dependent exchange-correlation energy functionals: Application to the calculation of ionization potentials and electron affinities", *Int. J. Quant. Chem.*, **29**, 79.

[12] Ortiz, J. V. (1993). "Improved electron propagator methods: An investigation of C_4, C_4^-, and C_4^+", *J. Chem. Phys.*, **99**, 6716.

[39] Klein, A., McGinnis, R. P. and Leone, S. R. (1983). "Photodetachment threshold of CN- by laser optogalvanic spectroscopy", *Chem. Phys. Letters*, **100**, 475.
[40] Chu, N. S., Burrow, P. D. and Jordan, K. D. (1979). "Temporary anions of the fluoroethylenes", *Chem. Phys. Letters*, **68**, 121.
[41] Yoshioka, Y., Schaefer, H. F. and Jordan, K. D. (1981). "Theoretical investigation of the electron affinity of CO_2", *J. Chem. Phys.*, **75**, 1040.
[42] Rohr, K. (1980). "Cross beam experiment for the scattering of low-energy electrons from methane", *J. Phys. B.*, **13**, 4897.
[43] Dudde, R. and Reihl, B. (1992). "Complete electronic structure of oriented films of hexatriacontane", *Chem. Phys. Letts.*, **196**, 91.
[44] Less, K. J. and Wilson, E. G. (1973). "Intrinsic photoconduction and photoemission in polyethylene", *J. Phys. C.: Solid State Physics*, **6**, 3110.
[45] Schaefer, O., Allan, M., Szeimies, G. and Sanktjohanser, M. (1992). "Low-energy electron-impact spectroscopy of [1.1.1] propellane – Electron attachment energies and singlet and triplet excited-states", *J. Am. Chem. Soc.*, **114**, 8180.
[46] See for example Figure 5.1: In Sutton, A. P. *Electronic Structure of Materials*, Oxford Science Publications Clarendon Press: Oxford, 1993.
[47] Meunier, M., Quirke, N., Binesti, D., Martic, G. and Fourmigue, J. M., *Abstracts: Electrical Insulation and Dielectric Phenomena* (*CEIDP*), Minneapolis, Oct. 1997, 19; see also Meunier, M., Quirke, N. and Binesti, D., Lecture *3rd International Conference on Dielectric Charge in Solid Insulators, CSC*'3. Tours (France) June–July 1998.
[48] Jursic, B. S. (1997). "Computing electron affinities of radicals with density functional methods", *J. Mol. Stuct.* (*Theochem*), **394**, 19.
[49] Gaussian, Inc., Pittsburgh, 1994.
[50] Frisch, M. J., Polple, J. A. and Binkley, J. S. (1984). "Self-consistent molecular orbital methods 25. Supplementary functions for Gaussian basis sets", *J. Chem. Phys.*, **80**, 3265.
[51] Seki, K., Ueno, N., Karlsson, U. O., Englehardt, R. and Koch, E. E. (1986). "Valence bands of oriented finite linear-chain molecular-solids as model compounds of polyethylene studied by angle-resolved photoemission", *Chem. Phys.*, p. 105.
[52] Meunier, M. and Quirke, N., Binesti (to be submitted).
[53] Rowntree, P., Parenteau, L. and Sanche, L. (1991). "Dielectric polarization invariance in dissociative electron attachment from condensed saturated hydrocarbons", *J. Phys. Chem.*, **95**, 523.
[54] Dorman, F. H. (1966). "Negative fragment ions from resonance capture processes", *J. Chem. Phys.*, **44**, 3856.
[55] Taylor, H. S. (1970). "Models, interpretations and calculations concerning resonant electron scattering process in atoms and molecules", *Advan. Chem. Phys.*, **18**, 91.
[56] Sanche, L. and Schulz, G. J. (1973). "Electron transmission spectroscopy: Resonances in triatomic molecules and hydrocarbons", *Journal of Chemical Physics*, **58**, 479.

[13] Ortiz, J. V. (1993). "Electron propagator theory of BO_2 and BO_2^- electronic structure", *J. Chem. Phys.*, **99**, 6727.
[14] Lindholm, E., Asbrink, L. and Ljunggren, S. (1992). "Energies of σ^* orbitals", *J. Phys. Chem.*, **95**, 3922.
[15] Ziegler, T. and Gutsev, G. L. J. (1992). "On the evaluation of molecular electron affinities by approximate density functional theory", *Computational Chemistry*, **13**, 70.
[16] DMol User Guide, Molecular Simulations Inc. San Diego, 1997.
[17] Delley, B. J. (1990). "An all-electron numerical method for solving the local density functional for polyatomic molecules", *Chem. Phys.*, **92**, 508.
[18] Hohenberg, P. and Kohn, W. (1964). *Phys. Rev. B.*, **136**, 864. See also Levy, M., *Proc. Natl. Acad. Sci. USA* (1979), **76**, 6062.
[19] Vosko, S. J., Wilk, L. and Nusair, M. (1980). "Accurate spin-dependent electron liquid correlation energies for local spin density calculations: a critical analysis", *Can. J. Phys.*, **58**, 1200.
[20] Perdew, J. P. and Wang, Y. (1992). "Accurate and simple analytic representation of the electron-gas correlation-energy", *Phys. Rev.*, **B45**, 13244.
[21] Becke, A. D. (1988) "Density-functional exchange-energy approximation with correct asymptotic behaviour", *J. Chem. Phys.*, **88**, 2547.
[22] Simons, J. and Burrow, P. D. (1987). "*Ab-initio* electronic structure of anions", *Chem. Review.*, **87**, 535.
[23] Ewig, C. S. and Tellinghuisen, J. (1991). "*Ab initio* study of the electronic states of O_2^- *in vacuo* and in simulated ionic solids", *J. Chem. Phys.*, **95**, 1097. See also *Chem. Phys. Letts. 1988*, **153**, 160.
[24] Bentley, J. and Chipman, D. M. (1987). "Accurate width and position of lowest 1S resonance in H^- calculated from real-value stabilisation graphs", *J. Chem. Phys.*, **86**, 3819 and references therein.
[25] Alle, D. T., Brennan, M. J. and Buckman, S. J. (1996). "Low-energy total electron scattering cross section and electron affinity for NO", *J. Phys. B: At Mol. Opt. Phys.*, **29**, L277–L282.
[26] Ellison, G. B., Engelking, P. C. and Lineberger, W. C. (1978). *J. Am. Chem. Soc.*, **100**, 2556.
[27] Von Niessen, W., Cederbaum, L. S. and Domke, W. (1979). *Excited States in Quantum Chemistry*, Eds., Redial: Holland.
[28] Travers, M. J., Cowles, D. C. and Ellison, G. B. (1989). "Reinvestigation of the electron affinities of O_2 and NO", *Chem. Phys. Letters*, **164**, 449.
[29] Massey, H. S. W. (1976). *Negatives Ions*, 3rd edn., Cambridge University: London.
[30] Schultz, P. A., Mead, R. D., Jones, P. L. and Lineberger, W. C. (1982). "OH^- and OD^- threshold photodetachment", *J. Chem. Phys.*, **77**, 1153.
[31] Steiner, B. (1968). "Photodetachment of electrons from SH^-", *J. Chem. Phys.*, **49**, 5097.
[32] Gurvich, L. V., Karachevtsev, G. V., Kondratjev, V. N., Lebedev, Y. A. and Medvedev, V. A. (1974). *Destruction Energies of Chemical Bonds. IP and Electron Affinity*, Nauka: Moscow.
[33] Illenberger, E., Comita, P., Brauman, J. I. and Fenzlaff, H. P. (1985). "Experimental and theoretical investigation of the azide anion (N_3^-) in the gas phase", *J. Phys. Chem.*, **89**, 1026.
[34] Erwin, K. M., Ho, J. and Lineberger, W. C. (1988). "Ultraviolet photoelectron spectrum of NO_2^-", *J. Chem. Phys.*, **92**, 5405.
[35] Kim, E. H., Arnold, D. W., Bredforth, S. E., Metz, R. B. and Neumark, D. M. (1995). "Study of HCO_2 and DCO_2 by negative ion photoelectron spectroscopy", *J. Chem. Phys.*, **103**, 7801.
[36] Sidorov, L. N. (1982). "Search and study of molecules with high-affinity to the electron", *Uspekhi Khimii*, **51**, 625.
[37] Wight, C. A. and Beauchamps, L. J. (1980). "Acidity, Basicity and Ion/Molecule Reactions of Isocyanide Acid in the Gas Phase by Ion Cyclotron", *J. Phys. Chem.*, **84**, 2503.
[38] Arnold, D. W., Bradforth, S. E., Kitsopoulos, T. N. and Neumark, D. M. (1991). "Vibrationally resolved spectra of C2-C-11 by anion photoelectron spectroscopy", *J. Chem. Phys.*, **95**, 8753.

Molecular modeling of electron trapping in polymer insulators

M. Meunier and N. Quirke[a)]
Department of Chemistry, Imperial College of Science, Technology and Medicine, South Kensington, SW7 2AY United Kingdom

(Received 28 December 1999; accepted 6 March 2000)

The presence of space charge in the polymeric insulation of high-voltage cables is correlated with electric breakdown. There is a vast literature concerned with the experimental characterization of space charge and with phenomenological models of space charge formation and discharge. However, a direct link between molecular properties, space charge formation and eventual breakdown has still to be established. In this paper, we suggest a new scheme that constitutes a first step in linking microscopic defects to the formation of space charge. Although our goal is to understand the role of defects at the molecular level in electron trapping and the formation of space charge in polyethylene, we start by considering a "model" material; the wax tridecane (n-$C_{13}H_{28}$). It is clear that both physical (e.g., conformational defects) and chemical defects (e.g., broken bonds) may be present in insulating materials and may both trap electrons. In the present paper, we focus on the role of physical defects. Our analysis suggests that by defining the defect energy in terms of the molecular electron affinity, a relationship is established between the electron trap and the molecular properties of the material. The electron affinity and its variation with wax molecule conformation have been calculated using density functional theory (DFT, as implemented in the code DMol). By performing molecular-dynamics simulations of amorphous waxes, we are able to determine likely conformational defects, and by using *ab initio* methods estimate the trapping energies. Conformational defects in these waxy materials are predicted to produce shallow traps with energies below 0.3 eV. These results are used to estimate the energy, number, and residence times of electrons in conformational traps in polyethylene. © *2000 American Institute of Physics.* [S0021-9606(00)70121-8]

INTRODUCTION

Electrical supply companies use polymers as insulators r high-voltage electric cables all over the world. However, olymers suffer from chemical (e.g., free radical formation ading to cross linking or bond breaking), physical (e.g., ructural relaxation above the glass temperature), and elec- cal (e.g., partial discharges, electrical trees) aging or deg- dation. The degradation of the polymer may lead to elec- cal breakdown in the insulation of an ac (alternating rrent) or dc (direct current) cable. All of these factors, ıen combined over time make the prediction of the prob- le working life of extruded cable very difficult.[1]

Most theories relate breakdown to charge accumulation d displacement of one type or another.[1] For example in the pace charge aging model"[2] the presence of both physical d chemical defects due to aging or to the presence of ad- ives leads to the accumulation of electrons in traps form- ; a relatively immobile space charge. The traps are thought have a range of energies, from shallow (0.1–0.5 eV) to ep (a few eV) as illustrated in Fig. 1. The resulting elec- static and electromechanical forces are thought to lower energy barriers to local conformational change producing v free volume and microvoids, eventually initiating failure a variety of mechanisms such as impact ionization. An understanding of space charge accumulation and its link to dielectric breakdown would be a major scientific achievement as well as facilitating the prediction of cable lifetimes and the design of better cables. Nevertheless space charge accumulation and the related trapping–detrapping phenomena are still poorly understood, indeed it is unclear whether any trapping site has been unequivocally identified in polymeric insulators.[3]

In the present work, we apply molecular modeling methods to elucidate the origin of shallow traps in polyethylene insulators; in particular those localized states (c.f. Mott[4]) that arise from conformational disorder in amorphous regions of the polymer. The contribution of chemical and other traps will be considered elsewhere.[5] Although polyethylene has a very simple chemical structure, it has a complex micro and mesostructure. Polyethylene (PE) is semicrystalline with the fraction of amorphous structure varying with the density and degree of crosslinking.[1] Crystallinity develops as spherical or spherulitic growths. The spherulites are composed of many lamellas: Ribbon-shaped regions where the polymeric chains fold back and forth on themselves. Due to their length, the polymer chains go from one lamella to another, crossing amorphous regions and forming intercrystalline links. Such complexity on a range of scales is not treatable using our molecular modeling methods. In order to probe the contribution of conformational disorder to electron trapping in polyethylene using molecular modeling we consider instead the condensed phases of much smaller alkane molecules which

ıthor to whom correspondence should be addressed. Electronic mail: ıuirke@ic.ac.uk

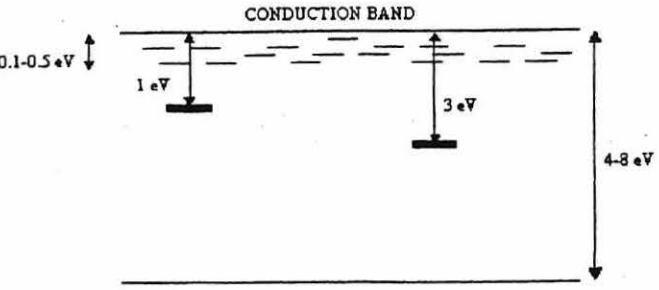

IG. 1. Representation of the band structure of an amorphous polymer. ıtraband electron traps are indicated as follows: Shallow traps (physical, ±0.5 eV), thin lines, deep traps (chemical ~ 1–3 eV), thick lines.

or $n \geqslant 13$, where n is the number of carbon atoms, have a and structure very similar to polyethylene.[6,7] We represent ıe local conformational disorder of segments of polyethyl-ne in the amorphous regions by configurations taken from omputer generated glassy phases of the tridecane ($n=13$) ax. Our strategy is to identify the local *electron* traps in PE ith the increase in the electron affinity of the more distorted $_{13}$ molecules, *conformationally* trapped in the glass.

. METHODOLOGY

Section II A describes the link between the electron af-nity of single alkane molecules and the electronic structure f the wax phase and Sec. II B, the use of density-functional ieory to calculate electron affinities. In Sec. II C, the ıethod of producing glassy wax phases is reported and re-ılts obtained for the structural and thermodynamic proper-es of these disordered phases. The following Sec. III de-cribes the calculation of electron affinities for onformational defects, which makes possible the construc-on of the electron energy trap distribution and the estima-on of residence times (Sec. IV).

. The electron affinity and electron traps

The electron affinity (EA) of a molecule is defined as the ıergy difference between the neutral and anionic state, ıere the electron is added from the vacuum. If the anion is owed to relax, an "adiabatic" electron affinity is defined

$$\mathrm{EA}_s = E(R_e) - E^-(R_e^-). \tag{1}$$

ıere $E(R_e)$ is the total energy of the neutral species in its uilibrium geometry R_e and $E^-(R_e^-)$ is the total energy of anion in its equilibrium geometry. For the case where the ion is not allowed to relax ($R_e^- = R_e$) the "vertical" elec-n affinity is defined as

$$\mathrm{EA}_v = E(R_e) - E^-(R_e). \tag{2}$$

king the total energy of a molecule as the sum of the ctronic (E_{el}) energy and the zero-point energy (ZPE the rational ground state of the nuclear motion), Eq. (1) can rewritten as

$$\mathrm{EA}_a = E_{\mathrm{el}}(R_e) - E_{\mathrm{el}}^-(R_e^-) + \mathrm{ZPE} - \mathrm{ZPE}^-. \tag{3}$$

d Eq. (2) becomes

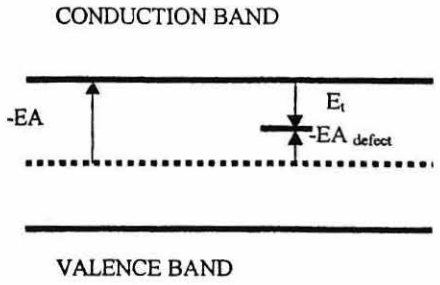

FIG. 2. Trap energy E_t, defined as the difference between the electron affinity of the system with and without the defect.

$$\mathrm{EA}_v = E_{\mathrm{el}}(R_e) - E_{\mathrm{el}}^-(R_e) + \mathrm{ZPE} - \mathrm{ZPE}^-. \tag{4}$$

From Eq. (4), the equilibrium geometry (R_e) of a molecule must be known in order to compute the (vertical) electron affinity. In vacuum, R_e corresponds to the global energy minimum, which for a (short[8]) linear alkane will be the all-trans planar conformation. However, in a condensed phase, the potential-energy surface of the molecule will be changed by interactions with its neighbors leading to a change in R_e and consequently the electron affinity.

In a solid the electron affinity is the energy required to bring an electron from the vacuum into the conduction band (in Fig. 2 the sign is a convention). The electron affinity of a defect is the energy required to bring the electron from the vacuum level to the defect level. The trap energy (E_t) is the difference between the electron affinity of the system with and without the defect; and it can be written as follows:

$$E_t = \mathrm{EA}_{\mathrm{defect}} - \mathrm{EA}_{\mathrm{reference}}. \tag{5}$$

A positive E_t signifies a potential trap for the electron, since in that case the trap has a greater affinity for the electron than the "pure" material [$\mathrm{EA}_{\mathrm{defect}} > \mathrm{EA}_{\mathrm{reference}}$ in Eq. (5)]. In our model of electron trapping in wax, using the n-$C_{13}H_{28}$ molecule, the reference electron affinity $\mathrm{EA}_{\mathrm{reference}}$ is taken to be the electron affinity of the all-trans n-$C_{13}H_{28}$ molecule, giving

$$E_t = \mathrm{EA}_{\mathrm{defect}} - \mathrm{EA}^{(n-\mathrm{C_{13}H_{2g}})}{}_{\text{all-trans}}. \tag{6}$$

B. The calculation of electron affinity

The computation of the electron affinity of atoms and molecules using *ab initio* methods is an active area of research, especially with respect to the choice of basis set. We have recently demonstrated[9] that density-functional methods[10] as implemented in the code DMol[11] predict values consistent with the experimental data for a range of atoms and small molecules having both positive and negative electron affinities. In this work our main concern is the electron affinity of alkanes, in particular, tridecane and polyethylene. There is very little experimental data for the electron affinity of linear alkanes. Measurements have been made for methane (−5 eV),[12] hexatriacontane n-$C_{36}H_{74}$ (-0.3 ± 0.5 eV)[13] and polyethylene (-0.5 ± 0.5 eV).[14] The value of −5 eV for methane suggests that small alkane anions are metastable and difficult to observe.[15] It has been suggested that the electron affinity increases with increasing carbon chain length and approaches an asymptote with n-butane.[16] This trend is

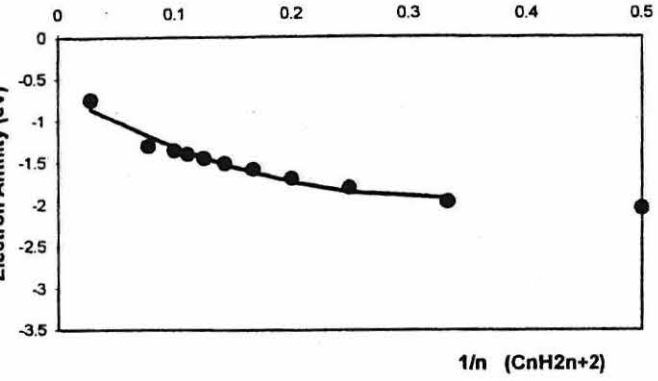

G. 3. Variation of vertical electron affinity with inverse chain length for e linear alkanes (from Table III in Ref. 9). Filled circles correspond to the Mol calculations and the line to a quadratic fit $[E(n)=-0.6499 - 7.7961(1/n)+11.897(1/n)^2]$ to the results for $n\geq 3$.

flected in our DFT calculations (Fig. 3) which clearly show e increase in the electron affinity as the chain length in-eases and the slow variation after butane.[9]

These results can be interpreted as reflecting a reduction the influence of the terminal methyl groups on the lowest ıoccupied molecular orbital (LUMO) as the hydrocarbon ıain grows. DMol, while predicting too positive an electron finity for methane (−2.9 eV), is consistent with the experi-ental data for $C_{36}H_7$ (−0.75 eV) and polyethylene -0.65 eV $n=\infty$). Estimates of the electron affinity of al-ınes using DMol become better (when compared to experi-ental values) as the chain length increases. For tridecane e calculated electron affinity in the all-trans conformation −1.3 eV.[9] The electron affinity of the tridecane molecule the glass phase is different from the all trans value only cause the glassy environment prevents the molecule from mpling the whole of the potential-energy surface. It is con-ained by neighboring molecules to only part of the surface d has a new equilibrium geometry [R_e in Eq. (1)] corre-ɔnding to the glass.

Models of conformational disorder: Preparation of ıssy waxes

In Sec. IV B, we represent the conformational disorder sent in polyethylene by configurations sampled from dis-ered tridecane waxes. Reproducible disordered phases are ained either by generating a glass phase by rapid cooling n the liquid state using molecular-dynamics simulation or ıg a Monte Carlo procedure (Amorphous-Cell[17]) to gen-e an amorphous system. Results have been generated for ɛral densities; 0.7564 g/cm^{-3}, the density of crystalline ɛcane,[18] 0.95 and 0.96 g/cm^{-3}, the density of high-sity polyethylene and for two system sizes $N=25$ and 50 s the number of tridecane molecules in periodic bound-s). Simulation data are summarized in Table I.

The low-density simulations (Glasses A_1–A_5) were ed from a crystalline phase of tridecane, with the cell meters appropriate to crystalline polyethylene[19] and den-0.7564 g/cm^3. The cell contained 25 molecules in peri-boundary conditions using the CVFF forcefield[20] imple-ted in the code Discover.[21] CVFF represents both

TABLE I. Simulation data for solid alkanes.

	N	Density (g/cm^{-3})	Initial configuration	Simulation ensembles
Glasses A_1–A_5	25(×5)	0.7564	Crystal	NVT/NVE
Glass B	25	0.9611	Glass A_1 (see text)	NPT
Glass C	25	0.9500	Amorphous	NVT/NVE
Glass D	50	0.9500	Amorphous	NVT/NVE
Crystal	25	0.9641	Crystal	NVT/NVE

bonded (bond stretch, angular distortion, etc.) and non-bonded or dispersion interactions. Molecular-dynamics simulations were performed in both canonical (constant N,V,T) and micro-canonical (constant N,V,E) ensembles. The canonical ensemble was used initially to fix the temperature of the system. The NVE ensemble was used for data collection so that the system is not perturbed by temperature rescaling.[22] The system was cooled from 1500 K in a sequence of four simulations at 1200, 900, 600, and 300 K. The series was terminated by a simulation at 150 K (assumed to be below the T_g of tridecane or polyethylene: 184 K from simulation,[23] 253 K from experiment[24]). All simulations consisted of 25 ps of NVT dynamics and 25 ps of NVE dynamics with a fixed time step of 1 fs. The radial distribution function of the carbon atoms at 150 K is shown in Fig. 4. The first peak corresponds to the distribution of distances between covalent carbon atoms at $R_{P1}=1.54$ Å. The second peak corresponds to the distribution of distances between intrachain second-neighbor carbon atoms at $R_{P2}=2.6$ Å and the third peak to intrachain third-neighbor carbon at $R_{P3}=3.8$ Å. The shoulder arising just before the third peak is due to the deviation of the dihedral angle from the equilibrium value (i.e., to gauche defects) leading to shorter intrachain third-neighbor distances (see Sec. III). The interchain disorder can be seen on the figure for $R>4$ Å where the structural disorder in the glass has averaged out subsequent peaks that would be present in the crystal.

Figure 5 shows the mean square displacement of tridecane molecules as the temperature is lowered and Table II reports the diffusion coefficient obtained from the gradient of the mean-square displacement at long times. The self-diffusion constant (D) was obtained from the slope of the mean-square displacement in time t of the molecular center of mass $r(t)$ using the Einstein relation:

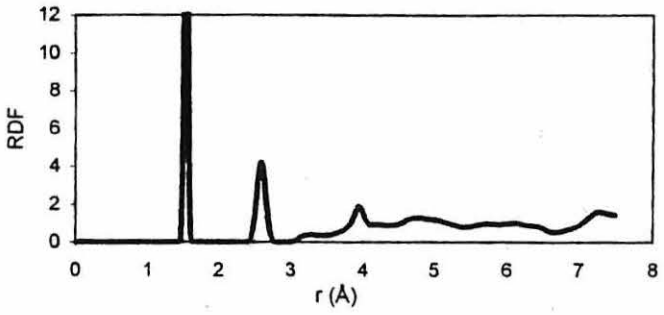

FIG. 4. Carbon–carbon radial distribution function in the low-density glass phase (A_1) at 150 K.

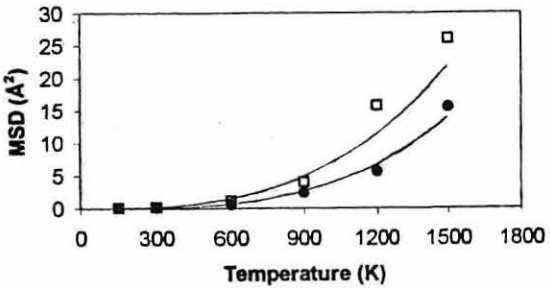

G. 5. Variation of the mean-square displacement with temperature for kane glasses (□, Glass A_1; ●, Glass C).

$$D=\frac{1}{6Nt}\langle|r(t)-r|^2\rangle. \tag{7}$$

here N is the number of atoms. By 150 K the diffusion efficient is effectively zero (Table II). In what follows we e the glassy conformations from the simulation at 150 K hosen to ensure that the simulations are well below the ass transition of the model) as representative of local conrmational disorder in polymeric insulators at room temrature. In the present calculations, this methodology has en applied five times to generate five different glass conurations. In addition, high-density phases (B,C,D) of tridene were prepared using the following methods:

) Glass B: A low-density configuration was compressed using NPT (constant pressure P) ensemble simulation at 4 Gpa to the required density using the code Discover.[21] The simulation comprised of 125 ps of equilibration and 75 ps for data collection, at 150 K.

) Glasses C and D: the code Amorphous Cell[17] was employed to create amorphous tridecane configurations at 0.95 g/cm^{-3} using $N=25$ (Glass C) and $N=50$ (Glass D). Amorphous Cell generates an amorphous phase using a two-stage process. In the first stage, isolated tridecane chain configurations were generated using rotational isomeric state (RIS)[25] probabilities. The second stage used a Monte Carlo algorithm to distribute the chosen number of molecules in a cell at a chosen density and combines both molecular dynamics and geometry optimization to obtain a realistic configuration. The (high-density) glassy phases were obtained using the quenching methodology described previously for low-density simulations, with the difference that the initial temperature (before quenching) was set to 900 K for $N=50$.

3LE II. Variation of the diffusion coefficient (Å²/ps per atom) with perature for alkanes.

mperature (K)	Glass A_1	Glass B	Glass C	Glass D
1500	0.1208		0.0284	
1200	0.0605		0.0095	
900	1.13E-02		3.07E-03	
600	4.43E-03		4.96E-04	
300	4.39E-04		2.77E-04	
150	2.68E-06	1.59E-05	1.16E-06	1.78E-06

TABLE III. Average bond lengths in solid alkanes.

	$\langle d_{(C-C)}\rangle$(Å)
Glasses A_1–A_5	1.541
Glass B	1.537
Glass C	1.541
Glass D	1.539
Crystal	1.532

(c) An orthorhombic crystalline phase of tridecane (with a density of 0.9641 g/cm^{-3} corresponding to crystalline polyethylene[19]) was simulated at $T=150$ K to make it possible to compare amorphous and ordered phases of n-$C_{13}H_{28}$. The simulation ran for 100 ps (NVT) to achieve equilibration and 100 ps (NVE) for data collection.

Two criteria are commonly applied to the results of molecular-dynamics simulations to determine whether a glass has been formed: (i) The presence of liquidlike disorder and (ii) that diffusion should have effectively stopped ($D\approx0$).[22] Visual inspection of the final configuration obtained in glasses A_1–A_5 shows that an amorphous phase is obtained (that is, the initial crystal configuration has been lost). This can also be seen in the absence of peaks in Fig. 4 after 4 Å reflecting a disordered structure similar to that of a liquid state. Systems B, C, and D start from amorphous configuration. Diffusion coefficients at 150 K are very low (~1E-06, Table II). Typical diffusion coefficients of small organic molecules in liquids at 298 K are ~0.1 Å²/ps.[18] By these criteria, our simulations represent glassy phases of tridecane. For our purpose, the most important feature of these glasses is the constraint the fixed disorder imposes on the accessible conformational space of a molecule. In the next section we will use the individual molecular conformations found in the disordered states of tridecane to calculate electron affinities and finally (Sec. IV) trap energies and residence times.

III. THE STRUCTURE OF AMORPHOUS WAXES

In this section we consider the average structural properties of tridecane molecules in the glassy state and compare with their properties in the crystal. The equilibrium carbon–carbon bond distance used by the CVFF force field is equal to 1.526 Å. Previous molecular-dynamics simulations of linear waxes have used a carbon–carbon bond distance of 1.52 Å,[26,27] and 1.53 Å.[28] The experimental value (determined from x-ray studies for hexatriacontane) is 1.527±0.007 Å.[29] The difference in average bond lengths in glassy and in crystalline phases determined in our simulations are reported in Table III.

The distributions of dihedral angles in the glass and in the crystalline phase are compared in Fig. 6. The glass simulations have a significant population of gauche defects (60°), the crystal (at the same temperature) has very few.[30] The high-density and the low-density simulations give similar chain dihedral angle distributions.

It has been suggested[31] that carbon–carbon bond lengths in alkanes expand as a function of dihedral angle due to

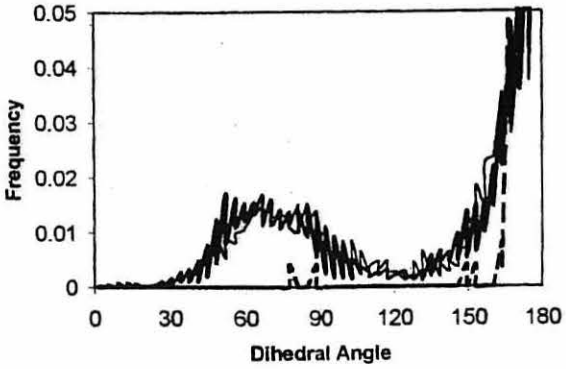

G. 6. Chain dihedral angle distribution (thick line: Glass A_1, thin line: ass C, dashed line: crystal phase). Angles in degrees.

creasing H–H repulsion (Fig. 7). Our results for the $C_{13}H_{28}$ wax presented in Table IV are consistent with this erpretation in that the presence of gauche defects in the ass leads to average carbon–carbon bond lengths greater in e case of the amorphous phase than in the crystal phase, at 0 K (Fig. 8).

In order to explore the variation of the electron affinity th the molecular conformation of n-$C_{13}H_{28}$ and in particu- the role of carbon–carbon bond lengths, a systematic dy of the electron affinity of the small alkane molecules ane and propane has been performed.[32] Our results show t the energy of the lowest unoccupied molecular orbital of ane and propane varies systematically with the carbon– bon bond length. In the linear alkanes the LUMO is an i-bonding (σ^*) orbital, hence increasing the bond length ds to a decreasing atomic orbital overlap, and therefore, to owering of the energy of the LUMO (E_{LUMO}) as is evident Fig. 9.

Using Koopman's theorem, which we have shown holds alitatively but not quantitatively for alkanes,[9] the vertical ctron affinity of a molecule is defined as:

$$\mathrm{EA} = -E_{\mathrm{LUMO}}. \tag{8}$$

e variation of the LUMO energy can, therefore, be used to lerstand the variation of the electron affinity with carbon– bon bond length. The longer the bond length the greater

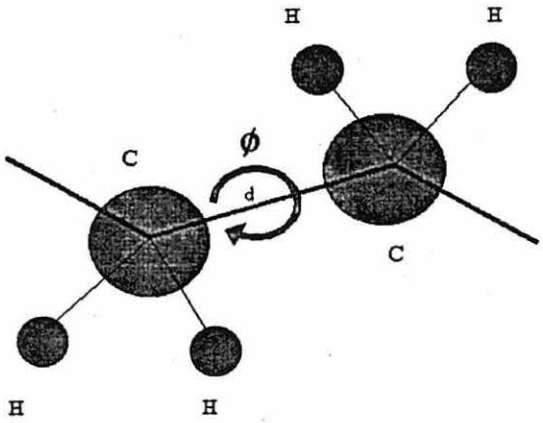

7. Schematic representation of a fragment of a polyethylene chain. As ies, the hydrogen–hydrogen atomic overlap increases and, therefore, d ases to reduce the bond energy.

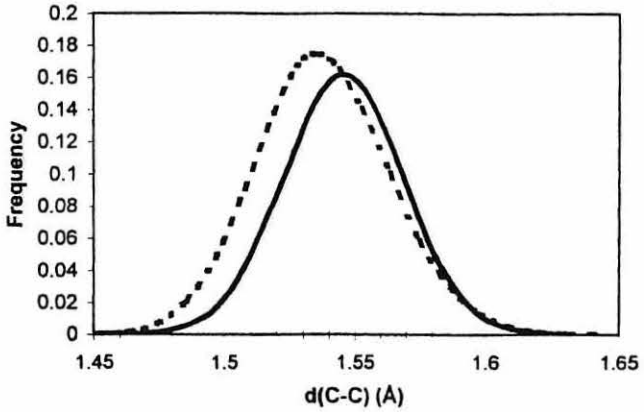

FIG. 8. Covalent (nearest neighbor) carbon–carbon bond length distribution at 150 K in the crystal phase (dashed line) and in the glass phase (high and low density, solid line).

the electron affinity. Since the distorted molecules found in our simulated glass phases, have longer (average) bond lengths than the all trans molecule (Fig. 10), we expect them to have a greater electron affinity. This is clearly demonstrated by the calculations described in the next section.

IV. RESULTS

A. The electron trap energy distribution function for a C_{13} alkane wax

In this section, we describe the construction of an electron trap energy distribution from the disordered states of tridecane whose preparation was described in Sec. III. The trap energy of a defect in a solid was defined in Eq. (5), as the difference between the electron affinity of the system with and without a defect. The trap energy due to a local conformational defect in tridecane is calculated as the difference between the electron affinities of an all-trans tridecane molecule (−1.3 eV) and a given tridecane molecule chosen from the amorphous configurations described in Sec. III (neglecting vibrational contributions). All calculations performed in vacuum. In following this procedure we have neglected the effect of intermolecular interactions (except for steric hindrance) and of polarization in changing R_e (see below). However, as a first approximation we take these effects to be less important in determining the electron affinity than the fact that the molecules are *conformationally* trapped.

The electron affinity of a molecule is computed with the molecule in its ground state[9] (Sec. II A). Molecules taken from the glass simulation will not have a configuration cor-

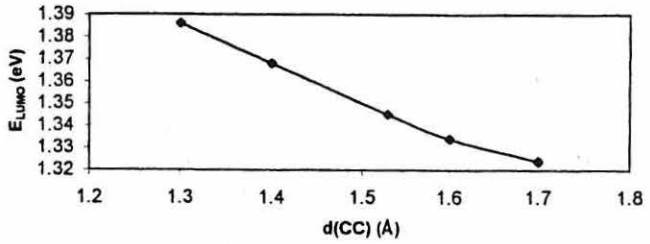

FIG. 9. LUMO energy variation with carbon–carbon bond length in the ethane molecule (Ref. 32).

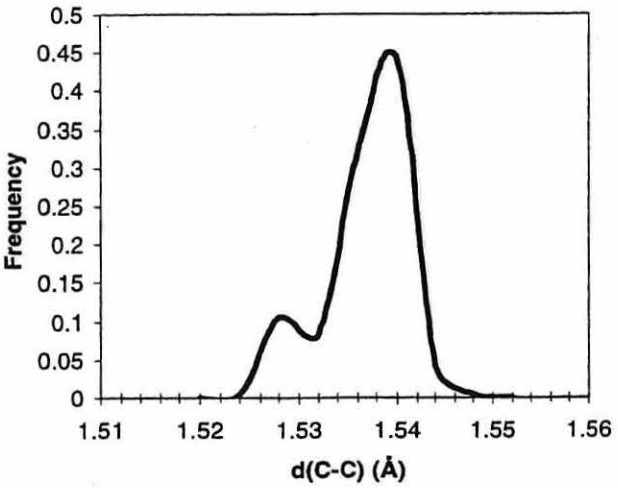

G. 10. Covalent (nearest neighbor) carbon–carbon bond length distribu-on after the application of the simulated annealing procedure in the glass ase.

sponding to the local minimum energy [i.e., to R_e used in q. (4)] but to some thermal fluctuation about R_e. Therefore, additional stage is included in our procedure that searches r the local equilibrium geometry of the molecule in the vironment of the glass. *Ab initio* tools could not be used ie to the large system size (1025 atoms for $N=25$). Instead, simulated annealing procedure has been employed with the assical forcefield. In order to estimate the local equilibrium ructure each molecule underwent a simulated annealing ocedure as follow: A molecular-dynamics simulation at gh temperature (550 K) for five picoseconds has been per-rmed, followed by geometry optimization using succes-vely the steepest descent and conjugate gradient algorithms the (fixed) environment of its neighbors. This procedure as repeated until no configuration of lower energy could be und (around one hundred times in most cases).

We have seen (cf. Fig. 8) that, at 150 K, the average rbon–carbon bond length is greater in the glass phase than the crystal phase due to the presence in the glass phase of uche defects. We, therefore, expect that the average rbon–carbon bond lengths of the tridecane wax trapped in :al conformational energy minima in the glass phase will o be greater than the equilibrium bond length and this is nfirmed by the data plotted in Fig. 10 for the bond lengths er annealing.

The shoulder at 1.528 Å in Fig. 10 corresponds to CH_2-CH_3 (end-of-chain) carbon–carbon bonds. As dis-ssed in Sec. III, the increase in bond length leads to an rease in the electron affinity. Therefore, we expect from ;. 10 that the electron affinity of molecules in the glass l be increased with respect to the all trans molecule. Since our calculations for alkanes there is no significant differ-:e between the adiabatic and vertical electron affinity,[9] the tical quantity has been used here. Figure 11 reports the tribution of electron trap energies obtained from the amor-ous tridecane simulations described in Sec. III. The effect trapped conformational disorder is to raise the electron nity by between 0.1 and 0.2 eV so that an electron prefers sit on a conformational defect rather than be in the con-

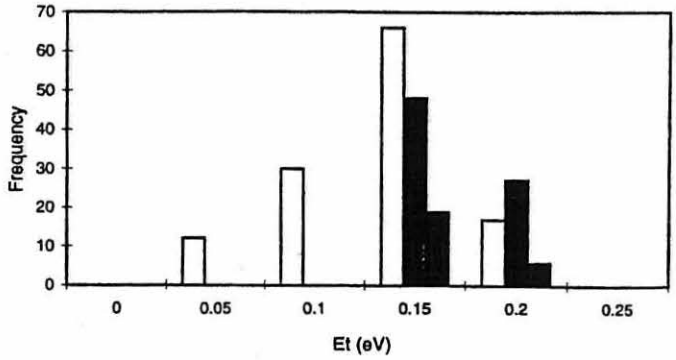

FIG. 11. Electron trap energy distribution of the tridecane molecules in the glass phase at 150 K: Blank histogram, glasses $A1-A5$, hashed, glasses $C-D$, filled, glass B.

duction band (represented by the all trans or conformationally free molecule). It also shows that the high-density simulations (Glasses B,C,D) lead to larger average trap energies than the low-density simulations (Glasses A_1-A_5). Due to the high density, the constraint applied by the environment is greater than in the low-density simulations, and therefore, the molecules are less likely to relax (partially or totally) to the all-trans configuration when the simulating annealing procedure is applied. Consequently, more gauche defects are found in the high-density simulation compared to the low-density case.

The density of traps in the wax, $f(E_t)$, may now be estimated. To calculate $f(E_t)$ we have used the data from the high-density Glass D. This system, composed of 50 molecules of tridecane, has a volume of 16 112.16 Å^3 (the cell parameters were $a=40.2$ Å, $b=20.04$ Å, $c=20.0$ Å, $\alpha=\beta=\gamma=90°$). From our calculations for glass D, *all* the molecules give rise to traps of energy greater than kT, and hence constitute shallow traps. For *this* case, the trap density in the amorphous phase is equal to the number density $50/16\,112.16\times10^{24}\cong3.1\times10^{21}$ traps cm^{-3}.

B. The electron trap energy distribution function for "polyethylene"

In order to estimate the electron trap energy distribution function in polyethylene we assume that the conformational defects displayed by molecules in the simulations of amorphous tridecane are representative of the (local) conformational defects in polyethylene (PE) as are the consequent local variations in electronic properties. In the present work all conformational traps in PE are taken to act independently, electron localization lengths in polymeric materials are of the order of a few carbon atoms.[33] The number of (single electron) traps along a conformationally disordered PE chain is then equal to the sum of the traps obtained for segments of 13 carbons (represented by the glassy configurations of tridecane) making up the PE chain. The choice of $n=13$ is a compromise between the high computational cost of DMol calculations on larger molecules and the need to ensure that short chain end effects on conformational and electronic properties are small. In what follows we show that the trap distribution in the C_{13} wax can, as a first approximation, be used for polyethylene.

From the results in Fig. 3 we can write the electron ffinity of a chain of n carbon atoms as the electron affinity f an infinite alkane chain [EA(∞)] plus a correction which ve take to be an end correction, representing the influence of nd CH_3 groups, $EA_{ec}=-7.7961(1/n)+11.897(1/n)^2$.

$$EA(n)=EA(\infty)+EA_{ec}(n). \tag{9}$$

Ve now estimate the electron affinity $EA_d(L)$ of a long hain with L carbon atoms consisting of periodic replica's of ne smaller disordered n chain (but with end CH_3 groups emoved, i.e., containing $n-2$ carbons) so that $L=m(n-2)$, where m is an integer. For independent conformational lectron traps we write that $EA_d[m(n-2)]=EA_d(n)-EA_{dec}(n)$, with $EA_{dec}(n)$ the end correction for conformaonally disordered alkanes.

Iaking the approximation that

$$EA_{dec}(n)\approx EA_{ec}(n), \tag{10}$$

nd letting L tend to ∞, the electron affinity of a long disorered chain is

$$EA_d(\infty)=EA_d(n)-EA_{ec}(n). \tag{11}$$

rom which it follows that the trap energy:

$$\begin{aligned} E_t(\infty)&=EA_d(\infty)-EA(\infty)\\ &=[EA_d(n)-EA_{ec}(n)]-[EA(n)-EA_{ec}(n)]\\ &=EA_d(n)-EA(n)=E_t(n), \end{aligned} \tag{12}$$

equal to that calculated for the $n=13$ segment $[E_t(n)]$. he (vertical) localisation energy does not change as n inreases because the single electron only sees the local trap hich is repeated along the chain. We consider the amorious regions of polyethylene as consisting of long alkane ains each one a periodic replica of a C_{13} segment found in e wax glass. In a sample of high-density polyethylene IDPE) where typically 10% of the volume is amorphous, e estimate the *overall* trap density in the PE sample as 10% that of the wax, i.e., 3.1×10^{20} traps cm^{-3}. This value is nsistent with the values reported for Anderson[34] localized ites by G. Blaise[35] of $10^{19}-10^{20}\,cm^{-3}$. Note that typical perimental space charge measurements in polyethylene port values around $1\,C\,m^{-3}$ or 10^{12} trapped ctrons cm^{-3}.[36] It is difficult to compare the two numbers the experimental apparatus only has access to the trapped ctrons (space charge) and not to the traps themselves. The lymer is very likely to suffer electric breakdown long be- e the complete filling of the entire set of traps. From the culated density, the average distance between all traps is

$$d=(1/\rho_{trap})^{1/3}=14.77\ \text{Å}. \tag{13}$$

e residence time (τ, in seconds) of the electrons in the ps, estimated using a two-potential model[37] in which the p-well minima are separated by a barrier of height E_t (corponding to the trap energy), and a distance d, is

$$\tau=1/\Gamma_{AB}, \tag{14}$$

ere

TABLE IV. Residence times (in seconds), with and without an applied electric field [taken as 10^7 V/m representing a typical cable field (Ref. 39)], $T=300$ K.

Et(eV)	$E_0=0$	$E_0=10^7$ (V/m)
0.05	$5.2\,10^{-14}$	$3.9\,10^{-14}$
0.1	$3.6\,10^{-13}$	$2.7\,10^{-13}$
0.15	$2.5\,10^{-12}$	$1.9\,10^{-12}$
0.2	$1.7\,10^{-11}$	$1.3\,10^{-11}$
1	471.6	354.4

$$\Gamma_{AB}=\Gamma\times\exp\left[e\frac{d}{2}E_0\Big/kT\right]$$

$$\text{and}\quad \Gamma=\nu_0\exp[-E_i\times e/kT]. \tag{15}$$

Γ_{AB} represents the hopping probability from well A to B,d is the average trap separation, E_0 is the electric field, ν_0 is the attempt frequency. The attempt frequency ν_0 can be taken from the result for the infinitely deep square well[38]

$$\nu_0=h/8m_ed^2=1.336\,10^{14}\ s^{-1}. \tag{16}$$

The calculated residence times are displayed in Table IV. It can be seen from the table that electrons in the physical traps of the sort found in amorphous alkanes have residence times of the order of $10^{-11}-10^{-13}$ s.

V. CONCLUSION

A general methodology for computing the distribution of electron trap energies in alkane waxes (taken as a model for polyethylene) has been developed. It has been shown that a combination of molecular dynamics (to generate representative conformational defects) and density-functional theory (to estimate the electron affinity) can produce reasonable estimates[40] of electron trap energies. Typical trap energies are of the order of 0.15 eV and all are less than 0.3 eV. From our trap distribution, the two potential well model gives residence times of the order of 10^{-12} s.

ACKNOWLEDGMENTS

The authors thank E.D.F. (France) for financial support. We are also grateful to Dr. J. N. Mac Donald (University of Wales, Bangor, UK) and Dr. P. Manuel (E.D.F., France) for their constructive comments and discussion.

[1] L. A. Dissado and J. C. Fothergill, *Electrical Degradation and Breakdown in Polymers* (Peter Peregrinus Ltd., London, UK, 1992).
[2] L. A. Dissado, G. Mazzanti, and G. C. Montanari, IEEE Trans. Dielectr. Electr. Insul. **2**, 1147 (1995); **4**, 496 (1997); See also L A. Dissado, abstracts CSC'3 Electric charge in solid insulators, 141 (1998).
[3] H. J. Wintle, abstracts CSC'3 Electric charge in solid insulators, 49 (1998).
[4] N. F. Mott, Philos. Mag. **22**, 7 (1970).
[5] Some preliminary results can be found in M. Meunier, N. Quirke, D. Binesti, G. Martic, and J. M. Fourmigue, Ann. Rep. CEIDP , 68 (1997); M. Meunier, N. Quirke, D. Binesti, abstracts CSC'3 Electric charge in solid insulators 66 (1998).

C. Laurent and C. Mayoux, *Electronic Processes in Electrical Ageing*, Arpeggio Seminar, 1994.
J. J. Pireaux, Phys. Rev. A **14**, 2133 (1976).
G. M. Goodman, *Chemical Applications of Molecular Modeling* (RSC, 1998).
M. Meunier, N. Quirke, and D. Binesti, Mol. Simul. **23**, 109 (1999).
B. J. Delley, J. Chem. Phys. **92**, 508 (1990).
DMol User Guide (Molecular Simulations Inc., San Diego, 1997).
K. Rohr, J. Phys. B **13**, 4897 (1980).
R. Dudde and B. Reihl, Chem. Phys. Lett. **196**, 91 (1992).
K. J. Less and E. G. Wilson, J. Phys. C **6**, 3110 (1973).
O. Schaefer, M. Allan, G. Szeimies, and M. Sanktjohanser, J. Am. Chem. Soc. **114**, 8180 (1992).
F. H. Dorman, J. Chem. Phys. **44**, 3856 (1966).
Amorphous-cell User Guide (Molecular Simulations Inc., San Diego, 1996).
Handbook of Chemistry and Physics, 76th ed. (1995–1996).
S. Kavesh and J. M. Schultz, J. Polym. Sci., Part A: Polym. Chem., **8**, 243 (1970).
P. Dauber-Osguthorpe, V. A. Roberts, D. J. Osguthorpe, J. Wolff, M. Genest, and A. T. Hagler, Proteins: Struct., Funct., Genet. **4**, 31 (1988).
Discover User Guide (Molecular Simulations Inc., San Diego, 1996).
S. Gruenhut, M. Amini, D. R. Macfarlane, and P. Meakin, Mol. Simul. **19**, 139 (1997).
R. J. Roe, J. Chem. Phys. **100**, 1610 (1994).
[24] J. A. Brydson, *Polymer Science*, edited by A. D. Jenkins (North Holland, Amsterdam, 1972).
[25] R. A. Scott and H. A. Scheraga, J. Chem. Phys. **44**, 3054 (1966).
[26] D. Rigby and R. J. Roe, J. Chem. Phys. **87**, 7285 (1987).
[27] D. Rigby and R. J. Roe, J. Chem. Phys. **89**, 5280 (1988).
[28] G. D. Smith and Do. Y. Yoon, J. Chem. Phys. **100**, 649 (1994).
[29] S. Kavesh and J. M. Schultz, J. Polym. Sci., Part A: Polym. Chem. **8**, 243 (1970).
[30] G. L. Liang, D. W. Noid, B. G. Sumpter, and B. Wunderlich, J. Phys. Chem. **98**, 11739 (1994).
[31] D. Steele, J. Chem. Soc., Faraday Trans. 1 **2**, 1077 (1985).
[32] M. Meunier (unpublished work).
[33] R. Zallen, *The Physics of Amorphous Solids* (Wiley, New York, 1983).
[34] P. W. Anderson, Phys. Rev. **102**, 1008 (1958).
[35] G. Blaise, Abstracts CSC'3 Electric charge in solid insulators, 25 (1998).
[36] T. J. Lewis, Abstracts CSC'3 Electric charge in solid insulators, 16 (1998).
[37] R. Bartnikas, IEEE Trans. Dielectr. Electr. Insul. **4**, 544 (1997).
[38] P. W. Atkins, *Physical Chemistry*, 4th ed. (Oxford University Press, New York, 1990).
[39] P. Manuel (private communication).
[40] We have neglected contributions to the trap energy from neighboring alkanes molecules. We estimate that neighbors may act to reduce the trap energy by up to 40% for traps of order 0.2 eV.